

**Studies on prokaryotic and eukaryotic
ribosomes and their interaction with
unfolded proteins**

*Thesis submitted for the degree of
Doctor of Philosophy (Science)
in
Biotechnology*

*By
Sehnaz Ferdosh*

*Post graduate and Research Department of Biotechnology
St.Xavier's College (Autonomous),
Affiliated to the University of Calcutta*

2021

Dedicated

To

the survivors everywhere...

Acknowledgements

I would like to express my heartfelt gratitude towards Dr. Chandana Barat, my PhD supervisor, for accepting me as her PhD student and allowing me the opportunity to work under her guidance in her laboratory. She has been a constant source of inspiration since the early years of my undergraduate course. Her simple yet sound approach towards complex problems did not just make it easier to understand the concepts but also kindled a fascination towards the problem and an urge to navigate the different aspects of it. She would patiently explain and design experiments with us even if it meant dedicating long hours in the lab after a hectic schedule of classes throughout the day. Under her tutelage I got to work with a wide variety of ribosomal particles from different sources which allowed me to learn as well as appreciate the importance of the delicate balance that exists between speed and efficiency while performing experiments. She taught me the value of persistence and precision while doing bench work. Even when experiments failed and yielded no results, she encouraged us to identify the problems and troubleshoot. Her inputs would not only help us in analyzing the results but would also provide us with the very essential boost to our morale. Even in the face of an uncertain future due to the unprecedented onset of the pandemic, I could always rely on her guidance. She has constantly stayed in touch, designing experiments and discussing different approaches addressing our work. It is all because of her that I could resume work after almost 6 months of lockdown. I would have been completely lost without her guidance and encouragement during that period of limited access to instrumentation and facilities. This period has been uncertain, difficult and tragic for so many of us and she has been nothing but supportive throughout. She has been a constant rock and has patiently taught us to overcome obstacles. Even during the process of writing my thesis, she was there by my side at every single step of the way. I could always reach out to her no matter what difficulty I faced. My years in her laboratory allowed me to be part of a work culture where no one

competed for personal credit but unitedly worked towards investigating scientific problems. It would be an understatement to say that it has been a great learning experience. It has been a blessing and a privilege to have learnt from her.

I would forever be grateful towards St. Xavier's College (Autonomous), Kolkata for always maintaining the best possible academic environment as well as the necessary infrastructure for conducting PhD research work. I sincerely acknowledge Father Principal, Rev. Dr. Dominic Savio, S.J., for constantly ensuring the advancement of the PhD curriculum as well as the PhD students, even in the face of uncertain circumstances.

I would like to thank Prof. Bertram Da Silva, Vice-Principal (Arts and Science), St. Xavier's College (Autonomous) Kolkata, Dr. Tapati Dutta, Dean of Science and Dr. Argha Banerjee, Dean of Arts, for maintaining the disciplined nature of the institution and relentlessly working towards the removal of any form of obstacle that might be encountered by the students. I would especially like to thank Dr. Tapati Dutta, the first PhD coordinator of the PhD department of St. Xavier's College (Autonomous) Kolkata. Her kind and patient guidance has helped us sail through some very difficult times. No matter what the circumstances, we could always turn to her for advice and rely on her fair support. She has always encouraged us to pursue our academic goals while also emphasizing on the importance of maintaining a healthy and positive mindset.

I would sincerely like to express my gratitude towards the PhD office of St. Xavier's College (Autonomous) Kolkata and our current PhD coordinator, Dr. Samrat Roy. He has ensured that the impact of the uncertainties imposed by the lockdown do not severely affect the PhD proceedings and that the interests of the PhD students are protected to the utmost. He has always personally addressed every single doubt that I have had regarding the submission of the documents and has made certain that the proceedings run smoothly. I will always be grateful to him for his kind guidance throughout the PhD experience.

I would like to thank all my professors of the Department of Biotechnology, St. Xavier's College (Autonomous), Kolkata, who have not only been teaching me during the coursework of my PhD, but since my admission in this college as a student of the integrated M.Sc course. Our current Head of the Department, Dr. Jhimli Dasgupta, has consistently maintained a healthy environment for research within the department for which I cannot thank her enough. I acknowledge all my professors, Dr. Chandana Barat, Dr. Uma Siddhanta, Dr. Sudipa Saha, Dr. Aniruddha Banerji, Dr. Jhimli Dasgupta, Dr. Dipankar Chakraborty, Dr. Aryadeep Roy Chowdhury, Dr. Priyanka De, Dr. Souvik Roy and Dr. Sayak Ganguli, from the bottom of my heart for teaching me all that I know and inspiring me to pursue research.

I would also like to express my heartfelt gratitude towards the support staff of the Department of Biotechnology, Abhijit da, Rajkumar da and Bidesh da. They were always there to provide any assistance that was necessary at any time. Their contribution towards maintaining an organized laboratory and departmental facilities is undeniable.

I would like to sincerely acknowledge the Central Research Facility (CRF) of St. Xavier's College (Autonomous), Kolkata, for providing all research students with the necessary provisions and equipments for conducting experiments. The facility, headed by Dr. Rina Ghosh, has allowed for the optimal utilization of the instruments while maintaining them in their best possible condition. The CRF support staff, constituted by Arup da and Pallab da, has always been there to help with the handling of the instruments which not only made our work easier but also helped to maintain the high quality performance of the equipments. I thank them from the bottom of my heart.

I would like to acknowledge the Central Library of St. Xavier's College (Autonomous), Kolkata for housing one of the largest collections of academic materials that we could access whenever we needed, during the course of our research work.

I would like to thank Science and Engineering Research Board, Department of Science and Technology, Government of India (SERB-DST) and also the Department of Higher Education, Science and Technology and Biotechnology, Government of West Bengal (DHESTBT) for providing the necessary funding to the laboratory that allowed me to conduct the experiments presented in my thesis. I would also like to especially thank DHESTBT, Government of West Bengal for providing me with fellowship during the course of my PhD.

My sincerest gratitude towards Dr. Sagarmoy Ghosh, Department of Microbiology, University of Calcutta, for not only allowing us to use the ultracentrifuge present in the central instrumentation facility of the department, but also for personally guiding us through the whole process. Most of the sucrose density gradient centrifugation studies conducted during the course of my work was performed using the ultracentrifuge present in his department. He not only allowed us to use the instrument but also welcomed us to use the other facilities in his laboratory so that we could perform our experiments on time and with precision. Even on days when his itinerary was packed with important meetings and classes, he would accommodate us and would never question the urgency of an experiment. His personal handling of the instruments with utmost care has always inspired me and demonstrated to me how careful and delicate handling of an instrument can be a factor in its efficient performance as well as in the results obtained from the experiment. He has not only helped me to conduct the experiments but has also shared his insights regarding the scientific investigations pursued in our laboratory. I always looked forward to his honest scientific feedback of my work which allowed me to work towards my objectives in a more comprehensive manner. His inputs always provided me with the incentive to think of different approaches to deal with a problem and inspired me to become a better researcher. I would also like to thank the members of his laboratory, Suparna di, Mitali and Debashish, who were always there to help out whenever we needed. Suparna di would always ensure that we could

access the ultracentrifuge rotor early in the morning, by keeping it safely stored in Sir's laboratory from a day before our scheduled spin. We could also safely store our reagents and samples in Sir's laboratory under the care of Mitali and Debashish. I will always remain indebted to them for their help and cooperation.

I would like to express my sincerest acknowledgements to Dr. Jayati Sengupta, IICB, Kolkata. Without her constant support and guidance, the work would not have been possible. She has always been extremely generous in extending the facilities of her laboratory to us whenever we needed. The preparation of ribosomes, which is imperative for our work, was conducted in her laboratory. She always made sure that we were able to schedule the preparations as per our requirement so that our work could continue without hindrance. Her scientific inputs enriched the quality of our work and provided us with the encouragement to continue further investigations. The help and cooperation from her and all her lab members, including Sayan da, Sandip da, Shirin, Priya, Rajanya di, Sayan da, Sukanya di, Krishnamoorthi and Aneek, have allowed me to conduct my work with ease. Every member has helped me to the best of their abilities. Sayan da took the time out of his work to help with cell lysis as well as with the Pymol image preparations. Shirin, Priya, Aneek and Krishnamoorthi ensured that I always found the assistance that I needed while working in their laboratory. Without the warm and welcoming presence of the "Joy Lab", the work would not have been the same.

I would like to thank Dr. Sujoy Kumar Dasgupta, Department of Microbiology, Bose Institute, for allowing me access to their central instrumentation facility in order to use the French Pressure Cell for cell lysis. He made sure that I could comfortably access their institute, abiding by the strict restrictions and regulations imposed due to the pandemic, and thus ensured that my work could proceed without obstacles. Narayan da, the operator of instruments in the central facility of Bose Institute, deserves a special note of thanks. He

diligently helped me every time I went to use the instrument and made sure that I could optimally avail the instrument.

I would sincerely like to thank Dr. Amar Nath Ghosh, National Institute of Cholera and Enteric Diseases, India, for his kind and patient help in obtaining the transmission electron microscopic images for our studies. It has been an inspiration and privilege to have got the opportunity to learn from him.

I would also like to thank Dr. Sumita Sengupta, Department of Biophysics, Molecular Biology and Bioinformatics, University of Calcutta. It is under her guidance that I had my first hands on research experience during my M.Sc dissertation and learnt many research techniques that helped me during my PhD. A warm note of thanks to Dr. Srimoyee Mukherjee, a senior scholar at the time in Dr. Sumita Sengupta's laboratory, who relentlessly and ever so kindly taught and supported me throughout my M.Sc dissertation period which inspired me to pursue PhD.

I have had the blessing of working with the most caring and warm lab mates. The two PhD alumni of this laboratory, Dr. Surojit Mondal (Surojit da) and Dr. Bani Kumar Pathak (Bani da), helped to build the foundations of this laboratory and continue to inspire me. Even though they both graduated with their PhD degrees before I joined the lab, I could still count on their advice and help whenever I needed. Bani da did not just offer advice but also actively helped me with the ribosomal preparations and functional assays during his tenure as a post-doctoral fellow in IICB. He always encouraged me to perform experiments independently and helped to mediate interactions with other institutions. I will forever be grateful to him for taking the time out of his busy schedule to offer me his steady support.

My experience in this laboratory would not have been the same, if it was not for the presence of Miss Senjuti Banerjee. Senjuti has been my long time friend and I can only be grateful that

I was fortunate enough to get her as my senior lab mate as well. I am constantly impressed by her organized and efficient way of working and her inherent ability to navigate a problem and troubleshoot. It is she who inspires me to be unapologetically uncompromising about maintaining the sanctity of an experiment. She helped me to pick up the experimental techniques and relentlessly worked with me which really allowed us to progress the work together. Working together with her made even long and arduous days of work seem extremely fun. We worked in perfect harmony that allowed us to explore multiple aspects of an experiment simultaneously. She has been there by my side through the most difficult of times and I could always blindly count on her support. Even now as she ventures into a bright future as a post-doctoral researcher, she continues to help me with every little thing, wherever and whenever I need her. I have no doubt that a great future awaits her. I wish her the very best and will miss her a lot.

I would also like to thank Miss Shirsha Saha, Miss Rituparna Bhowmick, Mr. Swapnonil Banerjee and Miss Ritaja Chattopadhyay, who all have worked with me at different times throughout the course of my PhD. They all provided me with the much-needed assistance and helped me in conducting several intense experiments.

A special note of thanks to Miss Jayshree Singh, who was my junior in the laboratory for more than a year. She has helped me through most of my work during that period. It is with her help that I could resume work after the lockdown. If not for her presence, it would have been exponentially more difficult to do so.

I would also like to thank all the scholars working in the Department of Biotechnology. I could always reach out to them whenever I needed any kind of help. All of the scholars, including Arnab da, Shreeparna di, Sanatan, Sourabh da, Sonia, Anagh, Preeti, Drishti, Saptarshi, Shubhangi, Shreshtha, Indrila, Peeali, Ojorshy, Ruchira, Aditya, Ankur, Aheli di and Anirban, deserve my heartfelt gratitude.

I must mention how fortunate I have been in having the most supportive group of friends and a loving family who have been my rock throughout this journey. I am really thankful to all my friends from school, especially Sreemoyee, Mekhola and Diya and my dearest friends from college, Arjun, Rohan and Shalini, who have stayed in touch and offered their support and encouragement, despite being busy in their respective lives.

My parents, Mr. Md. Idris Ali and Mrs. Sahin Ara Begum, have always been extremely supportive of all my endeavours. From very early on, they instilled in me a deep sense of discipline, diligence and sincerity. It continues to help me in my work to this day. Whenever I have been faced with a difficult choice in life, they have never tried to influence my opinions and respected my independent informed decisions, regardless of their personal reservations. They have gone out of their way to ensure that I have a comfortable environment which helps me to pursue my academic interests. They are my constant source of inspiration and I am grateful every day to have been blessed with parents like them. Another person who continues to be my inspiration is my brother, Dr. Md. Samim Iqbal. His calm demeanour and ability to treat success and failure alike are qualities that I have always admired and tried to imbibe. In his own serene manner, he has always encouraged me to not become perturbed by obstacles and failures and keep working towards my goals. I am fortunate to have a sibling in him. I would also like to thank all my family members and cousins who have constantly believed in me and encouraged me. Finally, I would like to thank my grandparents, Late Mr. Kayemuddin Ahmed and Mrs. Nuzera Khatun, whose selfless blessings continue to accompany me in all phases of life.

I sign off by thanking all my loved ones from the bottom of my heart. You all have been a blessing. Thank you.



(Sehnaz Ferdosh)

Contents

	Page No.
Abbreviations	1
Summary	7
Chapter 1: Review of Literature	13
Section A. Prokaryotic ribosome and unfolded proteins	14
Section A.1. Ribosome, the protein synthesis machinery of the cell	14
Section A.2. The fate of the newly synthesized polypeptides inside the cell	17
Section A.3. The ribosome associated chaperone network.....	20
Section A.4. The chaperoning ability of the ribosome.....	22
Section A.5. Dissociation of ribosomal subunits	26
Section A.6. Response to cellular stress: Expression of protein factors to modulate translation in bacterial cells	29
Section A.7. Hibernating ribosome: Formation and significance	32
Section A.8. Structure of the 100S ribosome from <i>Escherichia coli</i> and <i>Staphylococcus aureus</i>	34
Section B. Eukaryotic ribosome and aggregating proteins	37
Section B.1. Protein amyloid aggregation and Alzheimer's disease.....	37
Section B.2. Formation of A β peptides from the Amyloid Precursor Protein (APP)	39
Section B.3. Structure of A β 40 and A β 42 fibrils and mechanism of A β fibrillization	40
Section B.4. A β oligomer mediated neurotoxicity.....	44
Section B.5. Intracellular accumulation of A β oligomers and its implications.....	45
Section B.6. A β aggregation and loss of ribosomal integrity associated with Alzheimer's disease progression	47
References	50

Chapter 2: Prokaryotic hibernating ribosome and unfolded proteins	62
Introduction.....	63
Materials and Methods.....	72
Results and Discussion	83
Conclusions.....	127
References.....	131
Chapter 3: Eukaryotic ribosome and aggregating proteins.....	138
Introduction.....	139
Materials and Methods.....	146
Results and Discussion	155
Conclusions.....	206
References.....	212
Chapter 4: General Materials and Methods	221
References.....	230
Publications	232

Abbreviations

100S _{Ec}	:	100S ribosome isolated from <i>Escherichia coli</i>
100S _{Sa}	:	100S ribosome isolated from <i>Staphylococcus aureus</i>
6-AP	:	6-Aminophenanthridine
70S _{Ec}	:	70S ribosome isolated from <i>E. coli</i>
70S _{Ec} -free	:	Empty 70S ribosome isolated from <i>E. coli</i>
70S _{Ec} -HPF	:	70S _{Ec} ribosome bound to hibernation promoting factor
70S _{Sa}	:	70S ribosome isolated from <i>S. aureus</i>
A	:	Absorbance
AD	:	Alzheimer's disease
AICD	:	APP Intracellular Domain
APP	:	Amyloid precursor protein
APS	:	Ammonium persulphate
ATP	:	Adenosine triphosphate
A β 40	:	A β 1-40
A β 42	:	A β 1-42
BCA	:	Bicinchoninic acid
BCAII	:	Bovine carbonic anhydrase II
bDV RNA	:	<i>In vitro</i> transcribed bacterial domain V RNA
BLS	:	Blasticidine S
BP	:	Bound protein
bp	:	Base pair
CaCl ₂	:	Calcium chloride
CBB	:	Coomassie Brilliant Blue
conc.	:	concentration
CTD	:	C-terminal domain

DEAE	:	Diethylaminoethyl
DEPC	:	Diethyl pyrocarbonate
DNA	:	Deoxyribonucleic acid
DNase	:	Deoxyribonuclease
dNTP	:	2-deoxyribonucleoside 5-triphosphate
DTT	:	Dithiothreitol
<i>E. coli</i>	:	<i>Escherichia coli</i>
EDTA	:	Ethylene diamine tetra acetic acid
EF-G	:	Elongation Factor-G
EF-Tu	:	Elongation factor thermo unstable
EM	:	Electron microscopy
ER	:	Endoplasmic reticulum
EtBr	:	Ethidium bromide
EttA	:	Energy dependent expression throttle A
fMet	:	N- Formylmethionine
GAG	:	Glycosaminoglycan
GFP	:	Green fluorescent protein
GTP	:	Guanosine triphosphate
GuHCl	:	Guanidine hydrochloride
h26	:	helix 26
h39	:	helix 39
h40	:	helix 40
h44	:	helix 44
h69	:	helix 69
HEPES	:	4-(2-hydroxyethyl)-1-piperazineethane sulphonic acid
HPF	:	Hibernation promoting factor

HPF _{Ec}	:	Hibernation Promoting Factor expressed in <i>E.coli</i>
HPF _{Sa}	:	long form of HPF expressed in <i>Staphylococcus aureus</i>
HRP	:	Horse radish peroxidase
hrs	:	Hours
HYPK	:	Huntingtin interacting protein K
IF1	:	Initiation Factor 1
IF2	:	Initiation Factor 2
IF3	:	Initiation Factor 3
IgG	:	Immunoglobulin G
IPTG	:	Isopropyl- β -D-thiogalactopyranoside
IVT	:	<i>In vitro</i> translation
K ₂ HPO ₄	:	Potassium phosphate dibasic
Kb	:	Kilobase
KDa	:	Kilodalton
KH ₂ PO ₄	:	Potassium phosphate monobasic
KOAc	:	Potassium acetate
KOH	:	Potassium hydroxide
KV	:	Kilovolts
LB media	:	Luria Bertani medium
LiCl	:	Lithium chloride
LS	:	Light scattering
M	:	Molar
mBCAII	:	Molten globule form of bovine carbonic anhydrase II
Mg(OAc) ₂	:	Magnesium acetate
MgCl ₂	:	Magnesium chloride
MgSO ₄	:	Magnesium sulphate

min	:	minute
ml	:	milliliter
mM	:	millimolar
mRNA	:	Messenger ribonucleic acid
MW	:	Molecular weight
Myr	:	Myricetin
Na ₂ HPO ₄	:	Sodium phosphate dibasic
NAC	:	Nascent polypeptide associated complex
NaCl	:	Sodium chloride
NaH ₂ PO ₄	:	Sodium phosphate monobasic
nBCAII	:	native bovine carbonic anhydrase II
NFT	:	Neurofibrillary tangles
ng	:	nanogram
NH ₄ Cl	:	Ammonium chloride
nm	:	nanometer
NMR	:	Nuclear magnetic resonance
nt	:	Nucleotides
NTA	:	Nitriloacetic acid
NTD	:	N-terminal domain
O.D	:	Optical density
p	:	pico
PA	:	Poly(A) RNA
PAGE	:	Polyacrylamide gel electrophoresis
PBST	:	Phosphate buffered saline with Tween-20
PCR	:	Polymerase chain reaction
PFAR	:	Protein folding activity of ribosome

PNPA	:	Paranitrophenyl acetate
ppGpp	:	Guanosine tetraphosphate
PTC	:	Peptidyl transferase center
PU	:	Poly(U) RNA
PVDF	:	Polyvinylidene difluoride
R/D Lyso	:	Reduced-denatured Lysozyme
RA	:	Rosmarinic acid
RaiA	:	Ribosome associated inhibitor A
RF1	:	Release factor 1
RF2	:	Release factor 2
RF3	:	Release factor 3
RMF	:	Ribosome modulation factor
RNA	:	Ribonucleic acid
RNase	:	Ribonuclease
rNTP	:	Ribonucleoside 5-triphosphate
rpm	:	Revolutions per minute
RRF	:	Ribosome recycling factor
RRM	:	RNA recognition motif
rRNA	:	ribosomal RNA
RT	:	Room temperature
S	:	Svedberg
<i>S.aureus</i>	:	<i>Staphylococcus aureus</i>
<i>S.cerevisiae</i>	:	<i>Saccharomyces cerevisiae</i>
SDGC	:	Sucrose density gradient centrifugation
SDS	:	Sodium dodecyl sulphate
sec	:	second

TAE	:	Tris- acetate EDTA
TB	:	Terrific broth
TEM	:	Transmission electron microscopy
TEMED	:	N, N, N', N'-tetramethylethylenediamine
ThT	:	ThioflavinT
Tris	:	Tris (hydroxymethyl) aminomethane
tRNA	:	transfer RNA
TSB	:	Tryptic soy broth
U	:	unit
uBCAII	:	Unfolded bovine carbonic anhydrase II
UTP	:	Uridine 5'-triphosphate
UV	:	Ultra violet
V	:	volts
v/v	:	volume/volume
w/v	:	weight/volume
β -ME	:	2-Mercaptoethanol
μ	:	micro
μ g	:	microgram
μ l	:	microlitre
μ M	:	micromolar

SUMMARY

The interactions between nucleic acids and proteins play a key role in many significant biological processes including transcription and translation. The ability of globular proteins to bind to specific nucleic acid sequences and structures has been studied extensively. Recent studies have also reported the propensity of intrinsically unstructured proteins to bind to RNA. The ability of RNA to moonlight as chaperones and influence the aggregation of amyloid proteins, like the prion protein and the amyloid forming p53 protein has also been reported. A major proportion of the total cellular RNA is present as a constituent of the ribosome, in the form of ribosomal RNA or rRNA. Recent studies have highlighted the importance of electrostatic interactions between the highly charged ribosome exit tunnel and the translating polypeptide chain, in influencing the rate of translation as well as co-translational protein folding.

In addition to serving as the primary cellular translational machinery, the ribosome also exhibits a non-canonical chaperoning function. The center for this chaperoning activity lies in the domain V of the 23S rRNA in the 50S large ribosomal subunit, which also hosts the peptidyl transferase center. Thus, rRNA-unfolded protein interaction lies at the crux of the ability of ribosome to act as a protein folding modulator. Previous studies in our laboratory demonstrated that a P-site tRNA bound ribosome does not exhibit chaperoning, which clearly segregated the translating and non-translating ribosomal populations and indicated that chaperoning can be mediated by a non-translating ribosome only. It was also shown in previous works of our laboratory that besides assisting in protein folding, the ribosome can also suppress aggregation of protein folding intermediates like the molten globule state. Thus, the ribosome was shown to act as both foldase and holdase chaperone.

In this aspect, the importance of the relative stoichiometric concentrations of unfolded protein and ribosome is immense and essentially determines the outcome of such interactions. While the presence of stoichiometric concentrations of unfolded protein and ribosome leads to expression of the ribosomal chaperoning activity (both in assisting protein folding and suppressing protein aggregation), the presence of 5-fold excess concentration of unfolded protein results in significantly different outcomes. Previous works in the laboratory demonstrated that, in the presence of 5-fold excess concentration of unfolded protein, the ribosomal subunits are dissociated and the unfolded protein exhibits anti-association activity towards the 50S subunit. This leads to sustained dissociation of the subunits, which in turn makes them more susceptible to degradation by cellular nucleases. It has been reported in previous studies that degradation of about 50% of the ribosomal population occurs when the bacterial cells transition from their exponential phase of growth to their stationary phase of growth. The residual 50% population is maintained in a translationally silenced form due to the binding of several stress factors that are expressed in bacterial cells under different stress conditions, like those existing during the stationary phase. One such stress factor is the hibernation promoting factor (HPF) which is expressed in gram-negative bacteria like *Escherichia coli* during the stationary phase and which acts in concert with another stress factor, the ribosome modulation factor (RMF), to bind to and dimerize the 70S ribosome into the translationally silenced 100S ribosome. HPF can also bind to 70S ribosome individually and mediate its translational silencing. The formation of 100S ribosome in *Staphylococcus aureus* is mediated by a single long form of HPF. This phenomenon of preserving the ribosomal population in a translationally silent state is known as “Ribosome Hibernation” which is a predominant cellular survival strategy under stress. The stationary phase of bacterial growth is marked by the prevalence of unfavourable growth conditions like nutrient deprivation. Such stressful conditions also induce a global unfolding of proteins within the

cells. The ATP-independent chaperoning ability of the non-translating ribosome can help in cellular survival under such conditions by helping to reduce the unfolded protein load within the cells.

Our studies, discussed in **Chapter 2**, demonstrate the outcomes of unfolded protein interaction with the prokaryotic hibernating ribosome. Studies were conducted with both, the HPF-bound monomeric 70S hibernating ribosome and the dimeric 100S hibernating ribosome. It is known from previous studies that, while such ribosomal structures are present in the gram-negative *E.coli* cells only during their stationary phase of growth, these structures are present within the gram-positive *S.aureus* cells during all their phases of growth including the exponential phase. Despite no clear demonstration of any biological activity of these 100S dimers, their maintenance was shown to be crucial for the survival and virulence of *S.aureus*.

Hence, our studies were conducted with 100S ribosome isolated from both gram-negative *E.coli* and gram-positive *S.aureus*. Since formation of such hibernating ribosome is mediated by HPF binding and the binding site of HPF lies in the 30S ribosomal subunit, the chaperoning centre of such ribosome in the domain V of 23S rRNA in the 50S subunits should remain available for interaction with unfolded proteins. This prompted us to investigate (a) the effect of HPF binding to the 70S ribosome on its interaction with unfolded proteins and (b) the effect of unfolded proteins on 100S dimers.

(a) *Effect of HPF on unfolded protein-ribosome interaction*: Our studies with unfolded protein and HPF bound 70S ribosome demonstrate that HPF binding can make the ribosome resistant to unfolded protein mediated subunit dissociation and subsequent degradation by cellular nucleases. Such ribosome is also able to assist in protein folding and suppress protein aggregation. Thus our studies indicate at the ability of the HPF-bound monomeric 70S hibernating ribosome to stabilize the ribosomal population under stress by resisting unfolded protein mediated subunit dissociation and subsequent

degradation as well as the retention of its chaperoning activity which contributes towards cellular survival during stress.

(b) *Effect of unfolded proteins on the 100S dimers*: Our studies with unfolded proteins and 100S dimeric ribosome showed that these hibernating dimers, from both gram-negative and gram-positive bacteria, are also resistant towards unfolded protein mediated subunit dissociation and subsequent degradation and retain their chaperoning ability and ability to suppress protein aggregation.

These studies thus provide an understanding of the basis of the stability of hibernating ribosomal population that is maintained within the cells during stress and stationary phase. The resistance towards unfolded protein mediated subunit dissociation and subsequent degradation contributes towards such stability. The demonstration of chaperoning ability of these ribosomes also ascribed a biological function to these hibernating dimeric structures.

Previous studies in our laboratory demonstrated that the presence of super-stoichiometric concentrations of aggregating proteins, like lysozyme under reducing conditions, in the vicinity of the 70S ribosome can lead to co-aggregation of the ribosomal components. Lysozyme, under reducing conditions, tends to form amorphous aggregates. We next performed subsequent studies with aggregating proteins with a tendency to form amyloid aggregates. For this purpose, the Tau protein was chosen (both, the full length Ht40 and the 4-repeat microtubule binding subdomain of Tau protein, K18). Our studies revealed that Tau protein could associate with the rRNA-rich surface of the yeast 80S ribosome and induce the formation of large and small ribosome protein co-aggregates. These studies implied that targeting of the ribosome by Tau protein aggregates could underlie their neurotoxicity that is observed in Alzheimer's disease (AD).

The intraneuronal neurofibrillary tangles (NFTs) composed of Tau proteins, constitute one of the primary hallmarks of AD, the other hallmark being extraneuronal deposition of senile plaques composed of amyloid β ($A\beta$) peptides. $A\beta$ peptides are also reported to accumulate and oligomerize intraneuronally, which places these peptides in the vicinity of the ribosome. The studies discussed in **Chapter 3** demonstrate the effects of aggregating $A\beta$ peptides, both $A\beta$ 1-40 ($A\beta$ 40) and $A\beta$ 1-42 ($A\beta$ 42), on eukaryotic 80S ribosome. The ability of RNA to act as a modulator of $A\beta$ aggregation and the effect of polyphenolic inhibitors to influence the $A\beta$ -ribosome aggregation was also investigated. Thus, the objectives of our work with $A\beta$ peptides and eukaryotic ribosome included studies on (a) the effect of $A\beta$ aggregation on eukaryotic ribosome and (b) the effect of RNA: protein stoichiometry and polyphenolic inhibitors on $A\beta$ ribosome co-aggregation.

(a) *Effect of $A\beta$ aggregation on eukaryotic ribosome:* Our observations demonstrate that, when 80S ribosome is incubated with super-stoichiometric concentrations of aggregating $A\beta$ peptides, both $A\beta$ 40 and $A\beta$ 42, the aggregation of $A\beta$ peptides on the rRNA-rich ribosomal surface can lead to co-aggregation of the ribosomal components and thus can induce loss of physical integrity of the ribosome. Aggregating $A\beta$ peptides could also engage with RNA molecules like the total ribosomal RNA extracted from yeast 80S ribosome and small RNA molecules Poly(A) and Poly(U), resulting in stimulation of its aggregation and formation of RNA-protein co-aggregates.

(b) *Effect of RNA: protein stoichiometry and polyphenolic inhibitors on $A\beta$ -ribosome co-aggregation:* Earlier studies with the p53 protein revealed that it can undergo amyloid aggregation in the presence of RNA and the outcome of its interaction with RNA depends on their relative stoichiometries. While a low RNA: high protein stoichiometric ratio was shown to favour stimulation of aggregation, a high RNA: low protein ratio was shown to suppress aggregation stimulation. In our studies, we examined the effect of stoichiometry

on A β -ribosome aggregation as well as RNA-mediated stimulation of A β -aggregation. It was observed that the RNA-mediated stimulation of A β aggregation and formation of co-aggregates is essentially dependent on RNA: protein or ribosome: protein stoichiometry. A low ribosome or low RNA stoichiometric concentration with respect to the A β peptides was shown to favour formation of A β -ribosome or A β -rRNA co-aggregates and stimulation of A β aggregation respectively. We also examined the effect of polyphenolic inhibitors of amyloid aggregation on RNA-mediated stimulation of A β aggregation and A β -ribosome co-aggregation. Our observations demonstrated that co-aggregation of ribosomal components as well as RNA-mediated stimulation of A β aggregation could be mitigated in the presence of polyphenolic inhibitors like rosmarinic acid (RA) and myricetin (Myr).

Thus, taken together, our studies imply that the destabilization of the ribosomal population in AD-afflicted neurons might be one of the underlying modes of neurotoxicity of A β aggregates seen in this disease and that the polyphenolic inhibitors might possess therapeutic potential in abating the neuronal dysregulations associated with AD.

These studies, therefore, illustrate the diverse outcomes of unfolded protein interaction with the prokaryotic and eukaryotic ribosomes. Such outcomes are dependent on multiple factors like the relative stoichiometries of the interacting partners and the presence of co-factors and inhibitors. Our observation sets the stage for future investigations to delineate the intricacies of RNA and unfolded protein interactions and its subsequent effect on the ribosomal integrity, which might be crucial in terms of cellular survival during stress.

Chapter 1

Review of Literature

Section A

Prokaryotic ribosome and unfolded proteins

A.1. Ribosome, the protein synthesis machinery of the cell

The ribosome is the cellular translational machinery. It is a large ribonucleoprotein particle, solely entrusted with the biosynthesis of the cellular proteins that is a crucial step in the central dogma of molecular biology. Ribosomes constitute a major portion of the net dry weight of a growing cell. The 2.5 MDa bacterial prokaryotic 70S ribosome is a ribonucleoprotein complex constituted by the large ribosomal 50S subunit and the small ribosomal 30S subunit. The eukaryotic counterparts of these structures are the large 60S subunit and the small 40S subunit, together comprising the 80S ribosome. Multiple interactions between the ribosomal subunits help to maintain the intactness of the structure as well as facilitate the necessary dynamics that are crucial for its translational activity [Liu et al., 2016].

The prokaryotic 50S large ribosomal subunit is composed of 23S rRNA and 5S rRNA along with the presence of 30 ribosomal proteins whereas the 30S small ribosomal subunit is composed of the 16S rRNA and 20 ribosomal proteins. The ribosomal subunit interface is primarily composed of RNA. The 23S rRNA component of the 50S subunit consists of multiple domains including the domain V which is the residence of the catalytic centre of the ribosome for peptide bond formation, the peptidyl transferase centre (PTC). The 30S subunit houses the binding site for mRNA. The binding is governed by base pairing between the conserved nucleotide sequence, the Shine-Dalgarno sequence, located just upstream of the start codon in the mRNA and the complementary 3' end of the 16S rRNA of the 30S subunit. The mRNA binds in a cleft between the "head" and the "body" of the 30S subunit and forms the site of interaction between the mRNA codons and the tRNA anti-codons. The 70S

ribosome comprises of three tRNA binding sites spanning between the two subunits: (i) the A-site which binds the incoming aminoacyl tRNA (ii) the P-site which binds the peptidyl-tRNA attached to the nascent polypeptide chain and (iii) the E-site which marks the exit site of the deacylated tRNA after peptide bond formation. The 3' ends of both A-site and P-site tRNA remains in close proximity in the PTC of the 50S subunit. The 3' end of the E-site tRNA remains about 50 Å away from the PTC. **Figure 1A** depicts the structure of the tRNA bound *E.coli* 70S ribosome [Schmeing et al., 2009].

As discussed above, the prokaryotic translation process initiates through the binding of mRNA to the 30S ribosomal subunit. The mRNA is responsible for bringing the genetic information, to be translated into protein, to the ribosome while the tRNAs are the adapter molecules, with anticodons complementary to mRNA codons that are charged with appropriate amino acids in accordance to the genetic code. Several translation factors interact with the ribosome at different stages of protein synthesis to facilitate and assist in the process.

Bacterial translation proceeds through four stages: initiation, elongation, termination and ribosome recycling. Initiation of translation involves the recruitment of the methionine charged initiator tRNA at the start codon of mRNA positioned at the P-site as well as the three initiation factors, IF1, IF2 and IF3. IF3 initially binds to the recycled 30S subunits from previous rounds of translation. Subsequent binding of mRNA, IF1, IF2 and the initiator tRNA, results in the formation of the 30S initiation complex. The GTPase IF2 promotes subunit assembly to form the 70S initiation complex with the simultaneous release of IF3. The initiator tRNA moves into the P-site in the vicinity of the PTC, following GTP hydrolysis and phosphate release from IF2 [Schmeing et al., 2009]. The elongation step involves the interaction of factors like Elongation Factor Tu (EF-Tu) and Elongation Factor G (EF-G) and mediates the elongation of the nascent peptide chain through addition of amino acids (**Figure 1B**). The first step in elongation is the decoding step where a ternary complex

of EF-Tu, GTP and aminoacyl tRNA bind to the ribosome and mediates the recognition of the mRNA codons by the anticodons. It ensures the selection of the correct aminoacyl tRNA at the A-site as dictated by the mRNA codon. The next step involves the peptidyl transfer where a peptide bond is formed between the P-site bound peptide chain and the A-site tRNA bound amino acid. After the peptide bond formation, the mRNA-tRNA complex translocates to shift position by one codon and the elongation cycle continues until a stop codon is encountered at the A-site which signals the termination of translation. **Figure 1B** includes a schematic representation of the elongation cycle of translation [Frank, 2004].

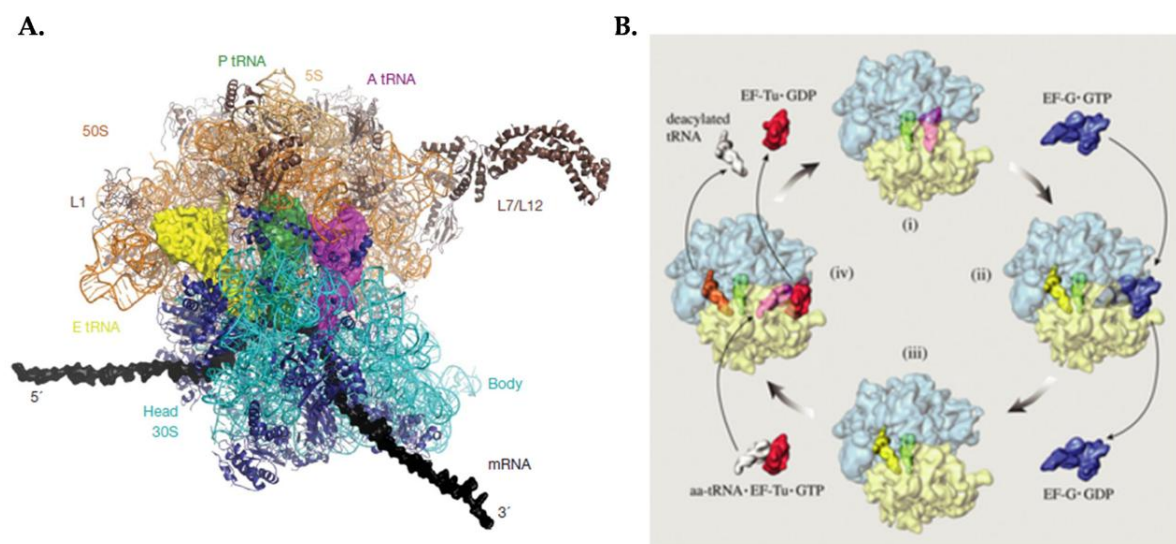


Figure 1: Structure of a translating 70S ribosome and elongation cycle of translation

A. Structural representation of the “top view” of the 70S ribosome with the mRNA (depicted in black) and the A-, P- and E-site bound tRNAs (depicted in purple, green and yellow respectively). The 30S subunit and 50S subunit are represented in blue and light orange respectively [Figure prepared using Pymol (Delano Scientific) and Adobe Photoshop] [Figure adapted from Schmeing et al., 2009]. **B.** Schematic representation of the elongation cycle of translation. Ribosome is displayed in top view with the small subunit represented in transparent yellow and the large subunit represented in transparent blue (i) pre-translocation ribosome with A-site (magenta) and P-site (green) tRNAs. Nascent peptide chain covalently attached to A-site tRNA after spontaneous peptidyl transfer (ii) Elongation Factor G (EF-G)-GTP (blue) binding facilitates tRNA translocation to P-site (green) and E-site (yellow). Translocation is induced by GTP hydrolysis and accompanied by conformational changes in the EF-G complex and the ribosome. (iii) GTP hydrolysis-mediated EF-G release from the ribosome leaves it ready to receive new aminoacyl tRNA along with EF-Tu and GTP (red). (iv) Ribosome with bound ternary complex, aminoacyl tRNA, EF-Tu and GTP. Binding of ternary complex to the ribosome shifts E-site tRNA further away from the P-site to the E2 site (orange). Schematic represents part of the decoding step where selection of cognate aminoacyl tRNA to enter the A-site occurs along with GTP hydrolysis and conformational changes. The EF-Tu with the hydrolysed GTP and E-site tRNA exit the ribosome leaving it in a pre-translocation state [Figure adapted from Frank, 2004]

The encounter of stop codon at the A-site leads to recruitment of release factors (RF1, RF2 and RF3) on the ribosome and the release of the nascent polypeptide chain into the cytosol. The presence of ribosome recycling factor (RRF) along with EF-G helps to disassemble the post termination complex and recycle the ribosomal subunits to allow for their participation in new rounds of translation.

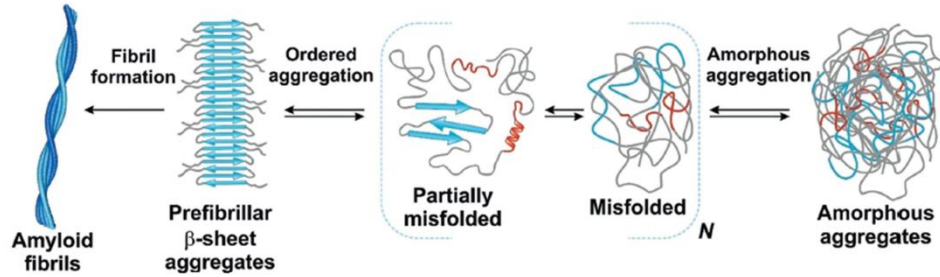
A.2. The fate of the newly synthesized polypeptide inside the cell

In order to achieve the biologically active three-dimensional conformation, folding of the nascent polypeptide chain is crucial. Protein folding involves self-assembly of the unfolded nascent polypeptide chains into their higher ordered structures through intramolecular interactions [Adamcik et al., 2018]. However this folding process can get derailed and the polypeptides can adopt misfolded conformations. Intermolecular interactions among such misfolded polypeptide molecules can lead to the formation of higher ordered aggregates.

Figure 2A includes a schematic representation of the formation of amorphous and amyloid aggregated structures from partially folded or misfolded intermediates. Folding of the polypeptide into its native structure involves a combination of hydrophobic interactions, intramolecular hydrogen bonding, Van der Waal's forces and electrostatic interactions [Adamcik et al., 2018]. The collapse of the hydrophobic portion of the polypeptide chain into the core of the protein is a significant feature of the folding process [Adamcik et al., 2018]. The native structure of the protein to be attained after folding is dictated by the amino acid sequence of the protein [Anfinsen, 1973]. An escape from the folding pathway causes the unfolded polypeptide to acquire misfolded conformation [Chiti et al., 2017] in which the hydrophobic residues and unstructured regions of the polypeptide chain remain exposed to the solvent (**Figure 2A**). In contrast to folded proteins, hydrophobic interactions in misfolded oligomers operate to drive aggregation through intermolecular interactions instead of driving compaction of the protein core [Adamcik et al., 2018]. Aggregation can lead to formation of

undefined and disordered amorphous aggregates or the formation of the highly ordered amyloid fibrils which are thermodynamically stable structures.

A. Slow and irreversible “off-pathway” of protein folding involving intermolecular contacts



B.

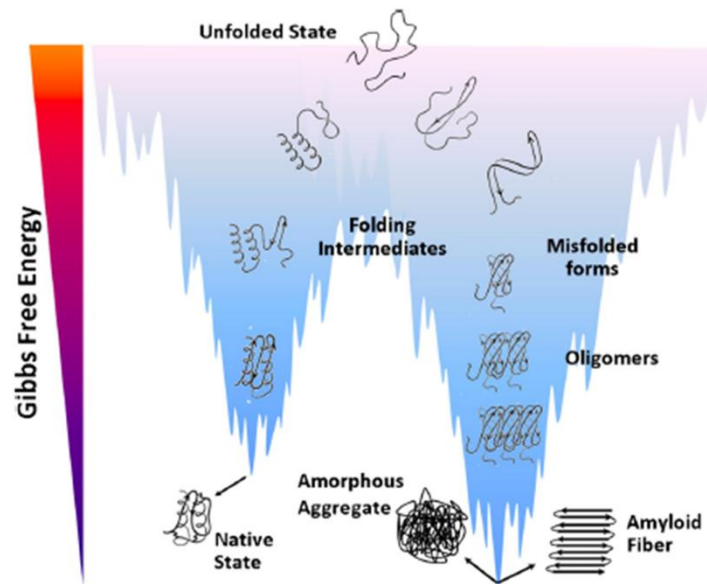


Figure 2: Misfolding of protein folding intermediates leading to aggregation and the protein folding funnel

A. Schematic representation of the folding intermediates assuming incorrect misfolded and partially misfolded conformations. Such conformations favour intermolecular interactions leading to the accumulation of misfolded chains and initiation of the aggregation processes. Aggregation can be “disordered” leading to the formation of undefined amorphous aggregates or “ordered” leading to the formation of ordered amyloid fibrillar aggregates [Figure adapted from Adamcik et al., 2018] **B.** Diagram representing the free energy landscape of the protein folding funnel. Unfolded proteins, being highly flexible structures, occupy the top region of the funnel and have high conformational entropy. As the proteins start to fold into more ordered intermediates, they evolve into the more stable low energy wells of the funnel. These intermediates can follow the native folding pathway to assume their thermodynamically stable native conformations. The intermediates can also escape the native folding pathway and assume metastable conformations (occupying low energy positions of the funnel) that can form stable amorphous aggregates or the most stable amyloid aggregates [Figure adapted from Cordeiro et al., 2014; Silva et al., 2010].

The folding pathway is described by an energy landscape that represents the energy of the protein as a function of its varied conformations which gives this landscape a funnel like appearance [Onuchic et al., 1997]. An unfolded polypeptide sorts through several intermediate conformations in order to arrive at its native conformation. The energy landscape, as shown in **Figure 2B**, is a representation of the relative stabilities of the different states of the proteins as well as the energy barriers separating these states [Balchin et al., 2016]. The unfolded state of a polypeptide occupies the top of the funnel due to its high entropy and free energy. As folding progresses, the possible number of conformational states (i.e. entropy) as well as the free energy decreases, approaching the state of energy minima which provides the folded state its conformational stability. In case of aggregation, the amyloid fibrils represent a stable thermodynamic state in the energy landscape and its energy landscape can be characterized by multiple peaks due to the various morphological conformations of amyloid fibrils [Eichner et al., 2011]. The protein molecules need to overcome significant energy barriers [Dill et al., 1997] to reach its folded form which is reflected in the rugged appearance of the funnel as it approaches the thermodynamically stable native state. The ruggedness of the funnel is more pronounced in the aggregation pathway, primarily due to intermolecular interactions, thereby increasing the possible number of conformations that can be adapted by the aggregates. Hence the correct folding pathway and the aggregation pathway compete with each other and this competition is crucial in deciding the fate of the newly synthesized unfolded polypeptide chain [Adamcik et al., 2018]. This is where the significance of the molecular chaperones comes into play. The chaperones can assist in the folding of polypeptides into their native states as well as prevent aberrant intermolecular interactions between misfolded intermediates, hence preventing aggregation and directing the proteins towards their folded conformations [Adamcik et al., 2018].

A.3. The ribosome associated chaperone network

Molecular chaperones, upon binding to protein folding intermediates, direct them towards acquiring their native structure and suppress aggregation [Bukau et al., 2000]. Although the folding of nascent polypeptides can begin co-translationally, as they exit the polypeptide tunnel of the ribosome, completion of the folding process requires release of the entire sequence from the ribosome [Preissler et al., 2012]. The crowded cytosolic environment enhances the probability of aberrant intermolecular interactions of the nascent polypeptides thereby increasing the probability of protein aggregation [Preissler et al., 2012, Pechmann et al., 2013]. The cellular chaperone system assists in *de novo* protein folding to prevent such fate of the polypeptide. Based on their location, cellular chaperones are classified into two groups. The first group comprises of chaperones that associate with both the ribosome and the synthesizing polypeptide. They act as early protein folding modulators during translation. An example of such a chaperone in the bacterial cells is the Trigger Factor which is an ATP-independent ribosome-bound chaperone, which binds to the ribosome near the exit tunnel and helps in co-translational protein folding in bacteria [Preissler et al., 2012, Pechmann et al., 2013]. Emerging polypeptides are accommodated into the interior cleft of the Trigger Factor where multiple hydrophilic and hydrophobic sites support nascent chain interactions [Pechmann et al., 2013]. The second category of chaperones act post-translationally [Agashe et al., 2004] in an ATP-dependent manner and are also involved in protecting cells from stress [Pechmann et al., 2013]. The two systems that co-operate to facilitate protein folding include the Hsp70 system of chaperones comprised of the DnaK, DnaJ and GrpE as well as the GroEL-GroES chaperonin system. Though most of these chaperones act post-translationally, DnaK can also associate with the polypeptide co-translationally [Pechmann et al., 2013]. The chaperones like DnaK and GroEL and DnaK and Trigger Factor also have overlapping substrates which further add to the robustness of the chaperone network. GroEL

is known to be essential in prokaryotes for the folding of aggregation prone and complex polypeptides [Tartaglia et al., 2010]. A schematic representation of the chaperone network associated with the bacterial 70S ribosome is included in **Figure 3**. In addition to these associated networks, the role of ribosome in influencing the folding of the emerging polypeptide has also been established [Pechmann et al., 2013].

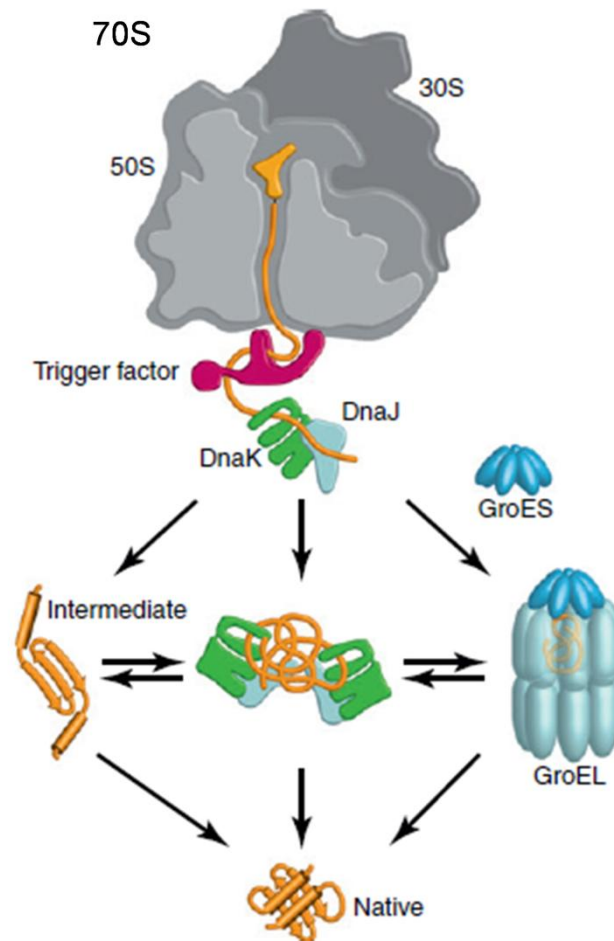


Figure 3: Chaperone networks assisting in de novo protein folding in *E.coli* [Figure adapted from Preissler et al., 2012]

The kinetics of protein folding and the rate of translation are suggested to be co-adjustable [Waudby et al., 2019], in which the relative rates of translation and protein folding are modulated in order to achieve the goal of efficient folding of polypeptides and reducing the

exposure of aggregation prone residues [O'Brien et al., 2014, Waudby et al., 2019]. Co-translational protein folding also involves interaction of the translating polypeptide with the ribosome peptide exit tunnel [Waudby et al., 2019], which is highly charged and is lined by conserved amino acids and rRNA residues. The rate and onset of co-translational protein folding is also affected upon altering the charge distribution of the nascent polypeptides or the residues responsible for maintaining the unique structure of the tunnel [Farias-Rico et al., 2018, Kudva et al., 2018]. The polypeptide tunnel can therefore provide a confined space for protein folding and restrict the protein from diverting to misfolding pathways [Waudby et al., 2019, Liutkute et al., 2020].

A.4. The chaperoning ability of the ribosome

Despite the presence of an elaborate chaperone network, as discussed above, the component chaperones only account for the folding of about 33% of the cellular proteome [Das et al., 2008, Ghosh et al., 2003]. The residual 67% of the proteome hence has to fold without any assistance in the crowded cytosolic environment. Further, the activity of most of the chaperone networks relies on the availability of ATP. The limiting level of ATP under conditions of stress renders the ATP-dependent chaperones incapable of performing their functions [Joyner et al., 2016]. Thus, the folding of the 67% of the proteome presented an intriguing question. The demonstration of the ability of the ribosome to itself act as a protein folding modulator provided a solution to this question [Das et al., 2008]. Ribosomes from diverse origins were shown to possess chaperoning activity which could mediate the folding of a wide range of proteins (**Figure 4**).

A. Proteins folded by ribosomes

- In vitro*
- Bacterial alkaline phosphatase
 - Glucose 6 phosphate dehydrogenase
 - Glucose oxidase
 - Lactate dehydrogenase
 - Malate dehydrogenase
 - Bovine Carbonic Anhydrase
 - Human Carbonic Anhydrase
 - β Lactamase
 - β galactoside
 - DnaK
 - GFP
 - Ricin-A chain
 - T7-RNA Polymerase
 - Rhodanese
 - Horse Radish Peroxidase
 - Restriction Endonuclease EcoRI
 - Restriction Endonuclease BamHI
 - Restriction Endonuclease HindIII
 - HspH from *Bradirhizobium japonicum*

- In vivo*
- β -galactosidase
 - β -lactamase
 - Carbnc anhydrase
 - GFP
 - DnaK
 - HspH
 - Luciferase

B. Source of ribosomes for assessing chaperoning activity

- ❖ Eubacteria
- ❖ Archaeobacteria
- ❖ Eukaryotes (yeast, rat, liver and wheat germ)
- ❖ Rabbit reticulocytes
- ❖ Bovine mitochondria
- ❖ Mitochondria of *Leishmania donovani*

Figure 4: Proteins folded by ribosome from different sources

- A.** List of proteins used to study the chaperoning ability of the ribosome *in vitro* as well as *in vivo*.
B. List of sources from where the ribosomes were isolated for examining their chaperoning ability.

A.4.1. The chaperoning center of the ribosome

The chaperoning ability of the 70S ribosome was demonstrated to reside in the domain V of the 23S rRNA of the 50S large ribosomal subunit. As shown in **Figure 5**, the unfolded protein binds to the RNA1 sub-domain of the domain V and is then transferred to the RNA2 sub-domain from where the protein is released in a folding competent state [Pal et al., 1999]. The chaperoning activity of the ribosome occurs in an ATP-independent manner [Das et al., 2008] making the non-canonical chaperoning function of the ribosome significant, especially under stressful conditions like nutrient deprivation, when ATP is limiting. **Figure 5** includes a schematic representation of the chaperoning mediated by the ribosome along with highlighted domain V RNA at the 50S subunit interface and the involvement of the RNA1

and RNA2 sub-domains of the domain V region of the 23S rRNA in the 50S subunit during the chaperoning process.

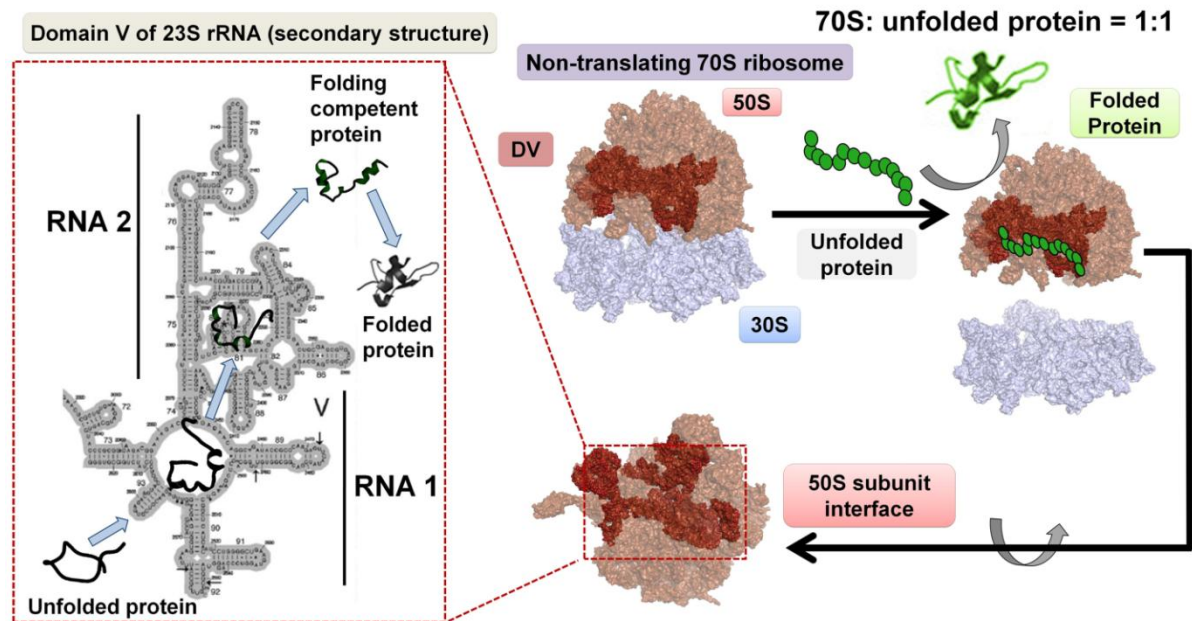


Figure 5: Schematic representation of the mechanism of ribosome mediated protein folding highlighting the centre of chaperoning activity in the ribosome.

Surface representation of the *T.thermophilus* 70S ribosome [PDB ID: IJGQ and IGIY] using PYMOL 2.4 (available at <https://pymol.org/2/>). The domain V region at the 50S subunit interface is highlighted in dark red spheres. The 50S ribosomal subunit is represented in light red and the 30S ribosomal subunit is represented in light blue. Secondary structure of the domain V region is shown with RNA 1 and RNA 2 sub-domains highlighted. RNA 1 sub-domain (nucleotide no.: 2043-2070 and 2441-2625) is discontinuous and is interrupted by RNA 2 sub-domain (nucleotide no.: 2071-2438). The interaction of unfolded protein at the RNA 1 sub-domain and release of protein in a folding competent state from the RNA 2 sub-domain constitutes the chaperoning cycle which is presented schematically [Adapted from Pal et al., 1999].

Previous studies using primer extension analysis have identified five distinct sites on the RNA1 sub-domain which interact with unfolded proteins [Samanta et al., 2008]. The bases constituting these sites are localized in the central loop of the PTC and are highly conserved in nature. Thus, these five nucleotides located in the PTC are implicated in the protein folding activity exhibited by the ribosome [Samanta et al., 2008]. The protein folding activity of the ribosome (PFAR) is inhibited in the presence of an anti-prion drug 6 Aminophenanthridine

(6AP), owing to the fact that 6AP also interacts with the same set of nucleotides on the domain V of the 23S rRNA that are responsible for interaction with the unfolded protein. Thus, 6AP competes with the protein substrate to bind to the domain V of the 23S rRNA and its binding prevents the unfolded protein from accessing the ribosome chaperoning centre which underlies the inhibition of ribosome chaperoning activity in the presence of 6AP [Pang et al., 2013].

Previous studies conducted in our laboratory to assess the chaperoning ability of a P-site tRNA bound ribosome demonstrated that such a ribosome is incapable of performing its protein folding activity [Mondal et al., 2014]. These studies were conducted using the antibiotic Blasticidine S (BLS) which binds to the 23S rRNA mimicking the interaction between PTC and the 3'-CCA end of the P-site tRNA. The study thereby clearly demarcated the two functions of the ribosome between two distinct ribosomal populations. The primary canonical function of the ribosome is translation and it is only a non-translating ribosome (which is not participating in active protein synthesis) which can mediate the non-canonical chaperoning activity. Studies previously conducted in the laboratory also demonstrated the ability of the ribosome as well as the isolated domain V rRNA to act as a “holdase” chaperone and suppress the aggregation of reduced and denatured lysozyme as well as the aggregation prone folding intermediate of BCAII, the molten globule state of BCAII [Pathak et al., 2014].

The ribosome: unfolded protein stoichiometry was demonstrated to be crucial for the chaperoning activity of the ribosome and it was shown that this activity is optimum at stoichiometric concentrations of the ribosome and unfolded protein [Das et al., 2008]. It was also demonstrated that the unfolded protein transiently dissociates the ribosome during the ribosome-unfolded protein interaction process [Basu et al., 2008]. Based on this observation, it was suggested that the dissociation of the ribosomal subunits would enable better access of

the unfolded protein to the domain V region of 23S rRNA. However, subsequent studies with helix 69 binding antibiotic Paromomycin, that was capable of inhibiting unfolded protein mediated ribosome subunit dissociation, revealed that the chaperoning activity of the ribosome did not essentially depend on the transient dissociation of the subunits [Pathak et al., 2017].

A.5. Dissociation of ribosomal subunits

The dissociation of ribosomal subunits is an essential part of the post translation termination ribosome recycling process which releases the bound tRNA and mRNA and the ribosomes are dissociated into their subunits, ready for participation in a new cycle of translation. The ribosome recycling factor (RRF) which acts in concert with GTP mediates this dissociation and recycling process [Kiel et al., 2007]. Several other factors also act to dissociate and recycle ribosomal subunits and the factors that are active under stressful conditions are distinct from those that are active under conditions that are favourable for cell growth. Two of the well-characterized ribosome dissociation factors are ObG and HflX [Feng et al., 2014; Coatham et al., 2016] that belong to the highly conserved P-loop GTPase family [Verstraeten et al., 2011]. ObG acts in concert with GTP and monitors late-stage assembly of the 50S subunit and prevents its early association with 30S subunit during exponential phase of growth [Feng et al., 2014]. Under unfavourable conditions of growth, alarmone molecules like ppGpp are synthesized [Abranches et al., 2009, Diez et al., 2020] which acts with ObG during amino acid starvation and stationary phase to delay 50S maturation. ObG binds to the 50S subunit and acts as an anti-association factor preventing its association with 30S [Feng et al., 2014]. The factor HflX also acts in concert with GTP and is active during heat stress in mediating ribosome subunit dissociation and also possesses 50S subunit based anti-association activity [Dey et al., 2018]. The initiation factor IF3 exhibits 30S subunit based anti-association activity where it binds to the 30S and prevents its reassociation with the 50S

until the 30S pre-initiation complex assembly is completed [Gutu et al., 2013]. The dissociation of the ribosome is also known to make the subunits prone towards degradation by cellular ribonucleases [Zundel et al., 2009]. Degradation of ribosome under nutrient deficient conditions is employed as a cellular survival strategy, since the degraded ribosome can contribute towards the limited nutrient reserve present in the cell during stress, thus providing the cell with better prospect of combating stress [El-Sharoud, 2004, Zundel et al., 2009]. Previous studies have demonstrated that dissociated ribosomal subunits are more susceptible to degradation by cellular nucleases compared to the intact 70S ribosome [Zundel et al., 2009, Sulthana et al., 2016]. Since the biogenesis of ribosome is an energetically expensive process [Liang et al., 2020] and translation is silenced during stress conditions [Starosta et al., 2014], it is crucial for the cells to protect the ribosomal particles during stress in order to resume function upon return of favourable conditions.

The ability of the unfolded proteins to dissociate the ribosome has also been widely studied [Basu et al., 2008, Pathak et al., 2017] and the stoichiometric concentration of the ribosome and the unfolded protein is also crucial here. The unfolded protein can dissociate the ribosome when present at a 5-fold stoichiometric excess compared to the ribosome [Basu et al., 2008, Pathak et al., 2017] (**Figure 6**). Unlike factor-mediated dissociation, the unfolded protein mediated dissociation of ribosomal subunits is not dependent on GTP hydrolysis [Basu et al., 2008].

70S: unfolded protein = 1:5

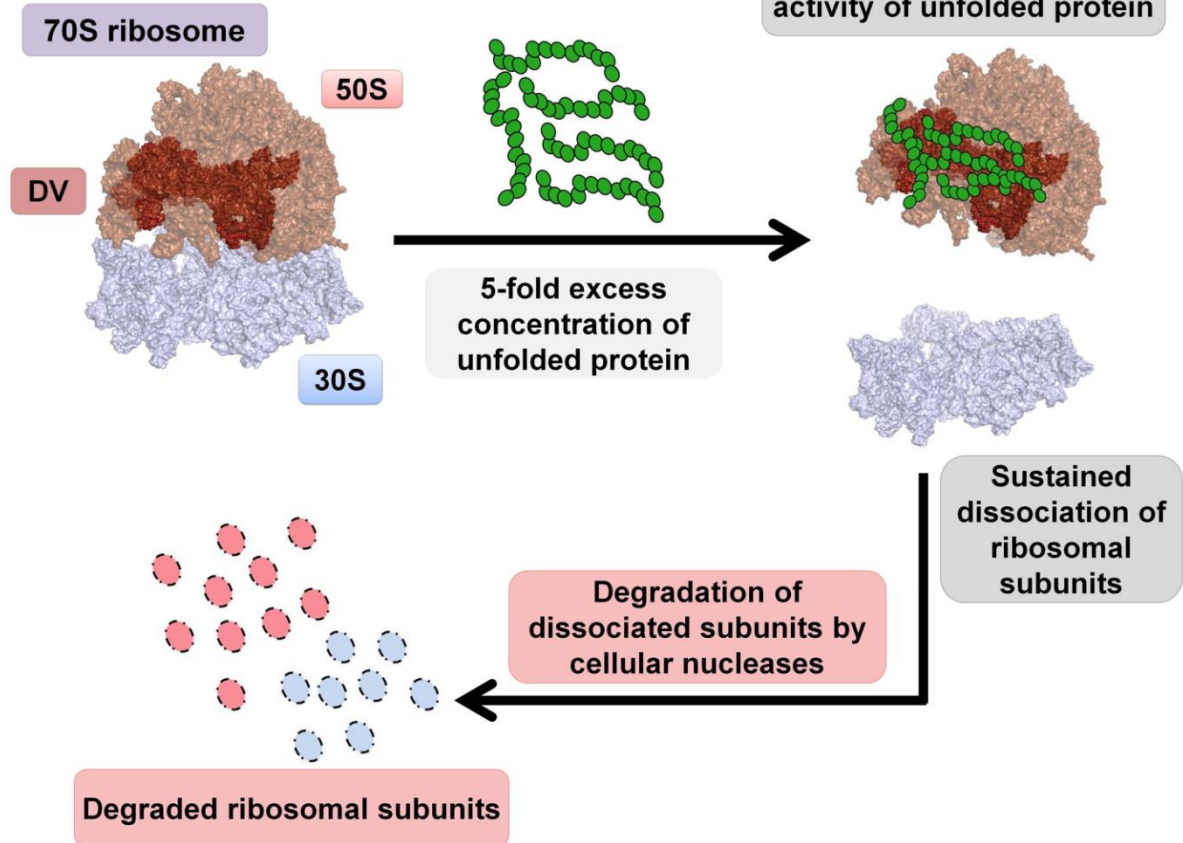


Figure 6: Schematic representation of the dissociation of ribosomal subunits in the presence of 5-fold excess stoichiometric concentration of unfolded protein

The non-translating 70S ribosome is dissociated in the presence of 5-fold excess concentration of unfolded proteins. The unfolded protein acts as the 50S subunit anti-association factor at such concentrations and results in sustained dissociation of the ribosomal subunits, which makes the subunits prone towards degradation by cellular ribonucleases.

Studies by Pathak et al. [2017], also revealed that 5-fold excess concentration of the unfolded protein (with respect to the ribosome) can not only dissociate the ribosomal subunits but also prevent re-association of the subunits, thereby resulting in their stable dissociation. The ability of the unfolded protein to act as a 50S anti-association factor resulted in stable dissociation of the ribosomal subunits (**Figure 6**). The super-stoichiometric concentration of proteins used in these experiments attempted to simulate the conditions faced by the ribosome during stress when the global unfolding of the cellular proteome could cause the

concentration of unfolded proteins within the cells to become unusually high [Guo et al., 2014]. Such a situation could induce the creation of a pool of unfolded protein-mediated dissociated ribosomal subunits, which would be prone to degradation by cellular nucleases [Zundel et al., 2009] (**Figure 6**). Degradation of ribosomal subunits at this extent would bear devastating consequences for the cells. Though a certain extent of ribosomal degradation is favoured for enriching the nutrient reserve during stress, preservation of a portion of the ribosomal population that can resume translation upon removal of stress is also crucial for cell survival. The present study attempts to address this question. In this context it is necessary to discuss the diverse bacterial stress factors that bind to the ribosome and inhibit the translation process under stress conditions.

A.6. Response to cellular stress: Expression of protein factors to modulate translation in bacterial cells

As discussed in the previous section, a global increase in protein unfolding within the cell accompanies the incidence of cellular stress [Guo et al., 2014]. These stressful conditions are marked by nutrient deprivation as well as a drop in the levels of ATP present inside the cells [Tran et al., 1998]. Such ATP-limiting conditions would render the ATP-dependent chaperone networks inside the cells unable to mediate their protein folding activities [Saibil, 2013]. Under conditions of stress, a prominent survival strategy that is employed by the bacterial cells to conserve energy is the silencing of translation. This serves two purposes. Firstly, it prevents the synthesis of new polypeptide chains that helps to reduce the load of unfolded proteins inside the cell. It also helps to maintain the ribosomal particles in a translationally silenced state in order to allow them to resume their translational activity upon return of favourable conditions. Distinct protein factors are expressed under different conditions of stress like nutrient deprivation, antibiotic stress or the conditions prevalent during the stationary phase of growth. They interact with the ribosome upon expression and

help to modulate their translational ability, effectively maintaining them in a silenced state to survive through the stressful conditions. **Figure 7** includes a schematic representation of the variety of stress-response factors that are expressed in the bacterial cells under varied conditions of stress and their mode of action in mediating translational silencing.

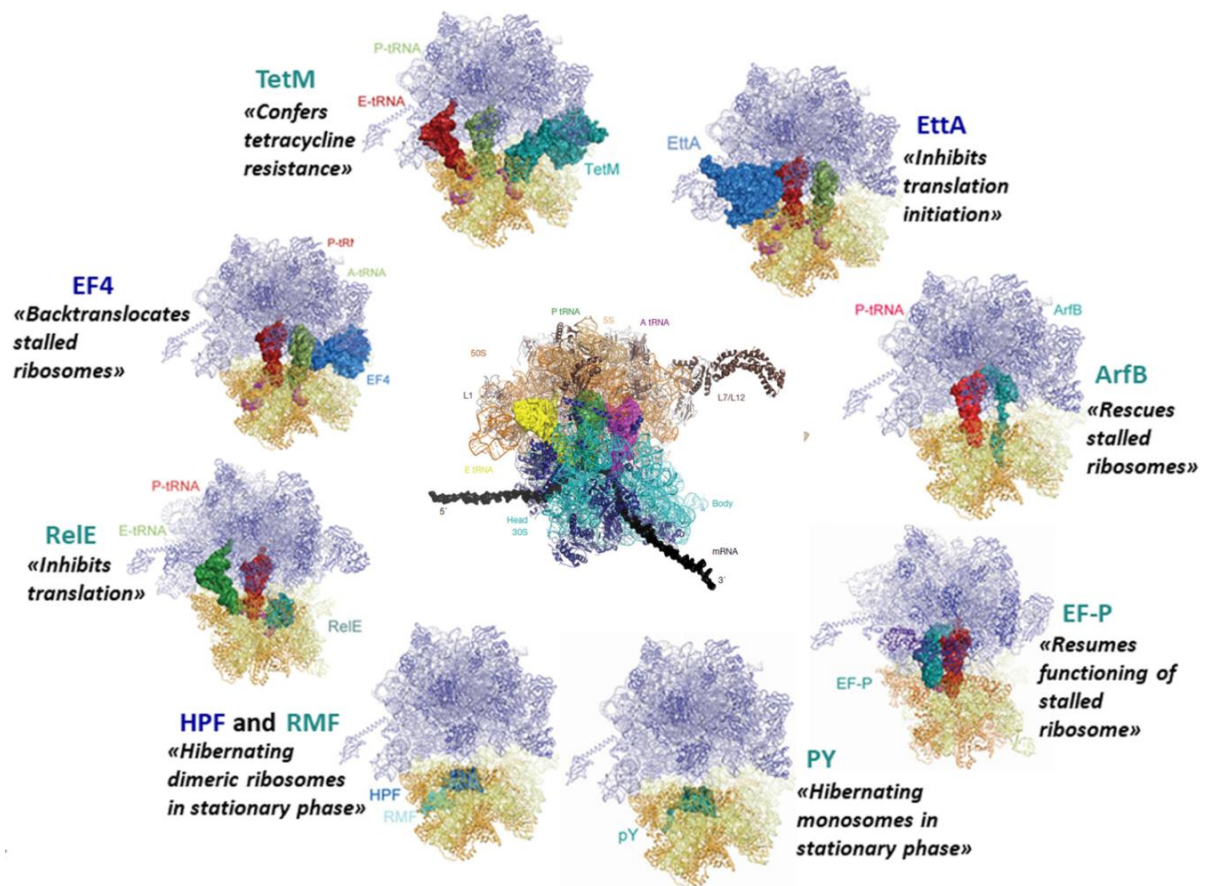


Figure 7: Schematic representation of the diverse ribosome associated stress factors expressed under different conditions of stress [Figure adapted and modified from Starosta et al., 2014, Schmeing et al., 2009].

The stationary phase of bacterial growth presents the cells with a plethora of unfavourable growth conditions like nutrient deprivation and toxin accumulation. The cells respond to such stress conditions by undergoing several morphological and physiological changes that are associated with the expression of stationary phase stress factors. While expression of factors like energy dependent expression throttle A (EttA), helps the cells to resume growth upon

transfer to fresh media [Boel et al., 2014], other factors like ribosome associated inhibitor A (RaiA or YfiA or proteinY or pY), ribosome modulation factor (RMF) and hibernation promoting factor (HPF) bind to the ribosome and maintain them in a translational slumber, a state referred to as “Ribosome Hibernation” [Yoshida et al., 2002].

YfiA is expressed under conditions of starvation as well as cold shock in *E.coli* and its binding to the 30S subunit of the ribosome protects the 70S ribosome against low magnesium induced subunit dissociation [Agafonov et al., 1999, Vila-Sanjurjo et al., 2004] and inhibits the process of translation initiation. Upon restoration of normal growth conditions, YfiA is released from the ribosome with the help of EF-G and RRF which allows the cells to return to its translational activity [Sharma et al., 2010]. RMF is expressed in *E.coli* during the stationary phase and requires ppGpp for its expression [Izutsu et al., 2001]. It acts in concert with HPF during the stationary phase to mediate the formation of the hibernating dimeric 100S ribosome. In *E.coli*, RMF binds to the 30S subunit of the 70S ribosome at a site that is overlapping with the Shine-Dalgarno-anti-Shine-Dalgarno helix. This binding mediates dimerization of the 70S ribosomes into the 90S structures. HPF subsequently binds to 70S within this structure at a position overlapping the tRNA and mRNA binding regions at the A-site and P-site on the 30S subunit and mediates the conversion of the 90S dimers into the 100S dimers. Thus HPF and RMF binding mediates translational silencing by inhibiting the binding of initiator tRNA to the P-site as well as the association of mRNA with the ribosome [Polikanov et al., 2012, Starosta et al., 2014].

The factors HPF and YfiA share about 40% sequence identity and their binding sites on the ribosome are also overlapping indicating at similar mechanism of translational silencing. However, these two proteins have antagonistic actions with respect to the fact that YfiA binding maintains the ribosome in a monomeric hibernating state whereas HPF mediates the formation of the dimeric 100S hibernating ribosome [Polikanov et al., 2012, Ueta et al., 2005,

Maki et al., 2000]. Mention must be made of a different variant of HPF that is expressed in all growth phases of gram-positive bacteria like *S.aureus*. The single long form of HPF (instead of both short HPF and RMF) expressed in the gram-positive bacteria is sufficient to mediate 100S dimerization [Ueta et al., 2013]. It is suggested that the additional C-terminal domain in the long form of HPF might have functions analogous to RMF in mediating 100S dimerization by inducing conformational changes in the head region of the 30S subunit [Starosta et al., 2014].

A.7. Hibernating Ribosomes: Formation and significance

As discussed in the previous section, hibernating ribosomes are formed in the gram-negative bacterial cells like *E.coli* upon their transition from exponential phase of growth to the stationary phase of growth where stressful conditions like nutrient deprivation are prevalent. Ribosome hibernation is a bacterial survival strategy, implemented by the cells to protect the translational machinery from degradation and maintaining them in a silenced form until the return of favourable conditions, when it can resume its translational activity [Yoshida et al., 2002]. The hibernating ribosomes are formed through binding of several protein factors and can be either monomeric or dimeric structures [Starosta et al., 2014, Prossliner et al., 2018]. As discussed before, binding of the factor YfiA maintains the ribosome in a hibernating monomeric 70S form in *E.coli* [Agafonov et al., 1999]. In contrast, binding of the factors RMF and HPF mediates the dimerization of 70S ribosomes to yield the hibernating 100S dimers. HPF can also bind to the ribosome, independent of RMF binding, and mediate its translational silencing [Ueta et al., 2008]. Thus the presence of hibernating ribosomal structures is exclusive to the stationary phase in gram negative bacteria like *E.coli*. **Figure 8** includes a schematic representation of the formation of hibernating ribosomes in gram-negative *E.coli* cells, as they transition from the exponential phase to their stationary phase of growth [Kato et al., 2010].

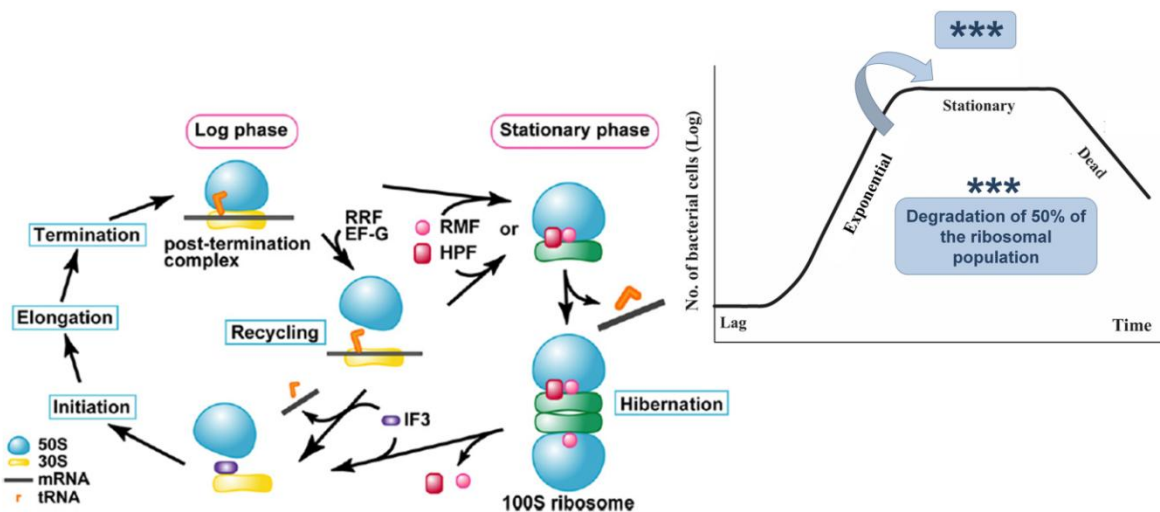


Figure 8: Formation of 100S ribosome in *Escherichia coli* during the stationary phase of bacterial growth

Schematic representing the hibernating 100S ribosome formation as the cells transition from the exponential phase of growth to the stationary phase of growth [Figure adapted from Kato et al., 2010]. Inset includes a graphical representation of the growth of bacterial cells through different phases: initial lag phase, log phase or phase of exponential growth, stationary phase and death phase [Figure adapted from Wang et al., 2015] and degradation of approximately 50% of the ribosomal population occurs as the cells enter stationary phase from the exponential phase of growth [Adapted from Piir et al., 2011]

Figure 8 depicts that in *E.coli*, the ribosomes are in an actively translating state during their exponential phase of growth and the transition to the stationary phase induces the formation of the hibernating ribosomes through the consecutive binding of factors RMF and HPF. The binding of these factors to the ribosome needs to occur before IF3 binding to the ribosome (which initiates a new translational cycle) and thus between the ribosome recycling stage of one translational cycle and the initiation of the next translational cycle [Kato et al., 2010].

The 100S ribosome is also found in gram-positive bacteria like *S.aureus*. However in contrast to the gram negative bacteria like *E.coli*, the 100S dimers are present within gram-positive bacterial cells in all phases of growth, including the exponential phase [Prossliner et al., 2018]. Since the 100S ribosomes are essentially translationally inactive, their maintenance during the active phase of growth presents an intriguing phenomenon. Further studies have

revealed that the continued expression of this long form of HPF and the maintenance of the 100S population is crucial for survival as well as virulence of pathogenic *S.aureus* [Basu et al., 2016, Basu et al., 2018]. Despite being crucial for survival, knowledge about the biological function of these dimeric ribosomes remains elusive [Basu et al., 2016].

A.8. Structure of the 100S ribosome from Escherichia coli and Staphylococcus aureus

As discussed in the previous section, the 100S dimeric ribosome in *E.coli* differ from those present in *S.aureus* and this is reflected in their overall structure as well [Prossliner et al., 2018]. A comparison of the structures of the 100S ribosome from *E.coli* with those from *S.aureus* reveals important points of differences between the two. In *E.coli*, the 100S ribosomes are formed by the concerted action of RMF and HPF during their stationary phase of growth, where the two 70S ribosomes form the dimeric 100S ribosome through interaction between their 30S subunits [Yoshida et al., 2002]. It was also suggested that the 70S ribosomes undergo conformational changes while transitioning into the stationary phase from exponential phase which prevents IF3 binding to the ribosome and favours the binding of RMF and HPF that subsequently leads to the formation of 100S ribosome [Kato et al., 2010]. Studies by Kato et al. [2010] revealed that the 100S formation is mediated between two tRNA free 70S ribosomes through interactions between their 30S subunits, in a 50S-30S-30S-50S alignment. The structure of the 100S ribosome also indicated at the direct involvement of the ribosomal proteins S2, S3 and S5 in mediating the dimerization [Kato et al., 2010]. These proteins have functions related to mRNA binding to the 30S subunit and mRNA movement in the ribosome and they undergo a conformational change upon formation of 100S dimer. This conformational change prevents aberrant interactions of mRNA with the hibernating ribosomes in the stationary phase [Kato et al., 2010]. Recent structural analysis of the *E.coli* 100S ribosomes has also revealed the role of S1 ribosomal protein in mediating dimerization. Inter-subunit bridges are formed between the ribosomal proteins S1, S2, S3 and S4. The C-

terminus of S2 occludes the mRNA entrance channel in the ribosomes constituting the 100S particles. This ensures the participation of only non-translating ribosomes in dimerization [Beckert et al., 2018]. The interactions between the 30S subunits in the 100S ribosomes were also demonstrated to be weak and loose in nature so as to facilitate the rapid 100S to 70S transition upon removal of stress conditions resulting in resumption of protein synthesis. The **Figure 9A** depicts the cryo-EM structure of the *E.coli* 100S ribosome [Beckert et al., 2018].

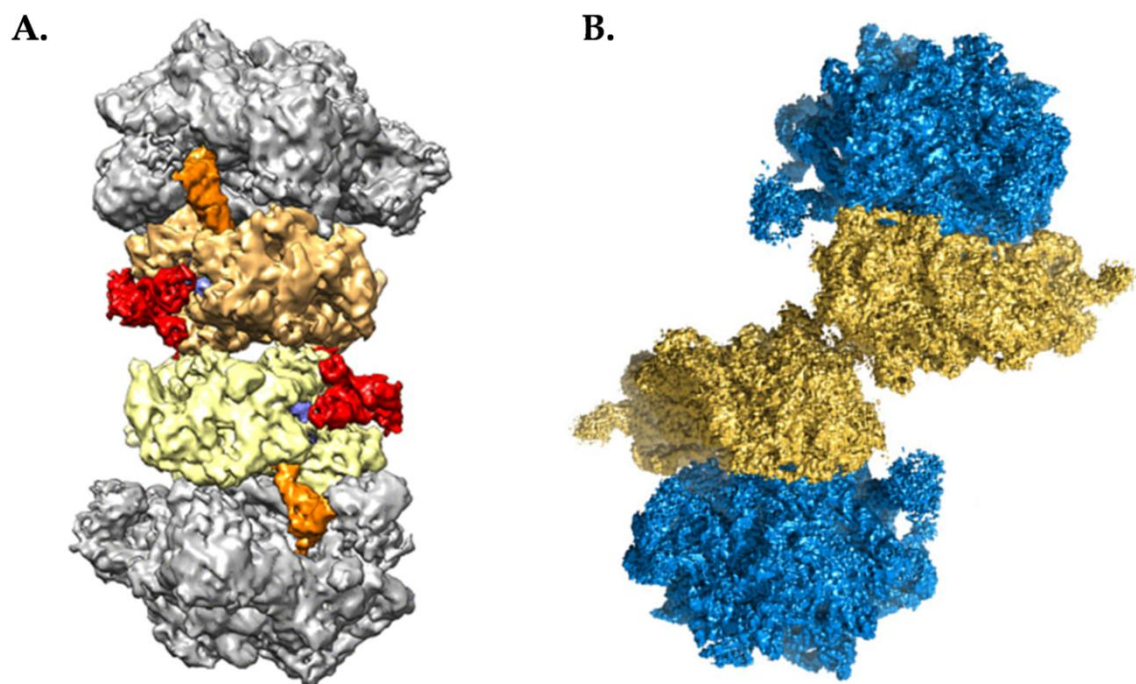


Figure 9: Structure of dimeric 100S ribosome from *Escherichia coli* and *Staphylococcus aureus*

A. Cryo-EM structure of *E.coli* 100S (PDB ID: 6H58, EMD-0139) ribosome constituted by two 70S ribosomes. 50S subunits are depicted in grey, 30S subunit of one 70S is depicted in yellow and that of the other is depicted in tan. The E-site bound deacylated tRNA is depicted in orange and the ribosomal protein S1 is depicted in red [Figure adapted from Beckert et al., 2018]. **B.** *In silico* reconstituted dimeric structures obtained after processing cryo-EM density maps of 100S ribosome from *S.aureus* (PDB ID: 6FXC) [Matzov et al., 2017]. The 30S subunits of the component 70S are depicted in yellow while the 50S subunits are depicted in blue (EMD-3638) [Figure adapted from Khusainov et al., 2017]

Unlike *E.coli*, 100S formation in *S.aureus* involves the binding of a single long form of HPF (HPF_{Sa}) to the 70S ribosomes in order to mediate the dimerization process [Basu et al., 2016]. Structural analysis of the 100S ribosome from *S.aureus* using cryo-electron microscopy have revealed that the N-terminal domain (NTD) of the HPF_{Sa} binds to the 30S subunit whereas its

C-terminal domain (CTD) extends out of each ribosome in order to mediate dimerization of ribosomes. HPF_{Sa}-NTD interacts with both the head and body of the 30S subunit. The HPF_{Sa}-NTD interaction with the body is, however, lost upon subunit rotation indicating that the interactions made with the head are more stable [Khusainov et al., 2017]. Secondary interactions occur between the HPF_{Sa} CTD-dimer and the helix 26 of the 16S rRNA [Khusainov et al., 2017]. The 100S dimers were also shown to be able to accommodate any combination of rotated or unrotated conformations of the component ribosomes constituting the dimers [Khusainov et al., 2017]. It should be noted that the 30S-30S interface of *E.coli* 100S ribosome (**Figure 9A**) is significantly larger compared to *S.aureus* 100S ribosome (**Figure 9B**) [Prossliner et al., 2018]. The distinct features, described above, contribute towards the difference in appearance of the 100S ribosome from *E.coli* and *S.aureus*, which is depicted in **Figure 9** and discussed in further details in the “Introduction” section of Chapter 2.

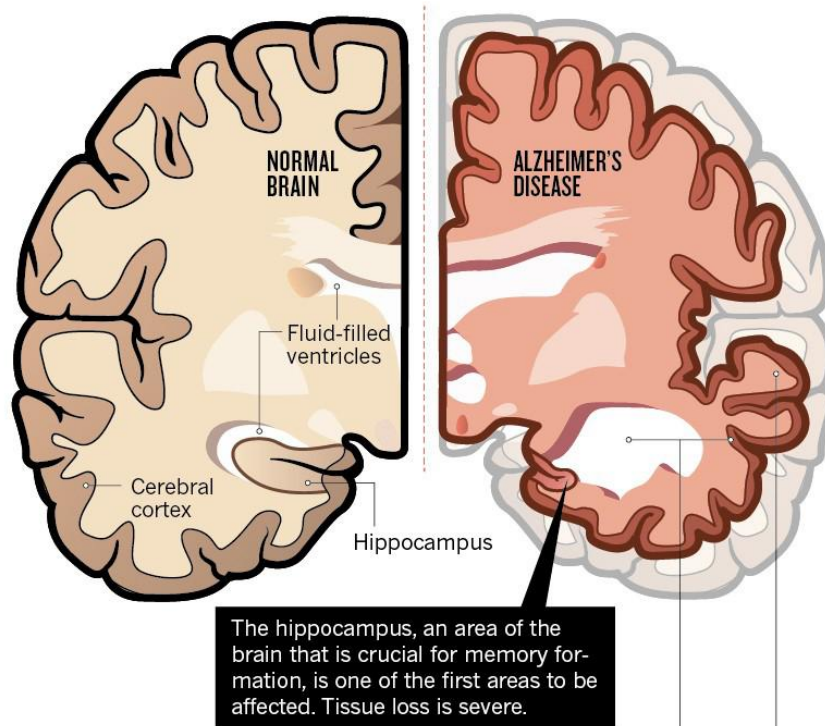
As discussed earlier, previous studies in the laboratory have demonstrated that a P-site tRNA bound ribosome is incapable of mediating its non-canonical chaperoning activity [Mondal et al., 2014], suggesting that an actively translating ribosome would not exhibit chaperoning activity. Since the hibernating ribosome, formed during stress, essentially constitutes a reserve of non-translating ribosome, there is a potential possibility for these ribosomal structures to retain their chaperoning activity. The fact that the chaperoning centre of the ribosome resides in the PTC of the domain V of 23S rRNA in the 50S subunit and formation of the hibernating ribosome involves interactions of the factors with the 30S subunits provides further support to this possibility. The studies performed to assess the effect of unfolded protein on hibernating ribosome and the ability of these translationally silenced ribosome to mediate chaperoning activity are outlined in “Chapter 2” of the thesis.

Section B

Eukaryotic ribosome and aggregating proteins

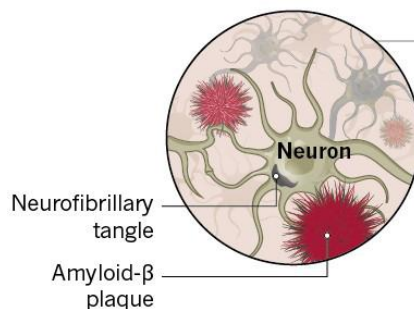
B.1. Protein amyloid aggregation and Alzheimer's disease

Amyloid protein aggregation and accumulation of toxic aggregates is implicated as the major perpetrator of several neurodegenerative disorders. Neurodegeneration is marked by an imbalance in neuronal proteostasis along with a progressive loss in the neuronal structure and function which eventually leads to cell death [Gao et al., 2008; Lim et al., 2015]. Alzheimer's disease (AD) is one of the most prevalent neurodegenerative disorders that is marked by cognitive and behavioral impairment and is a major reason for dementia associated with ageing. The onset of this disease progressively induces loss in synaptic connections in the brain and leads to neuronal atrophy and no curative therapies are currently available to arrest or reverse the progression of the disease [Drew, 2018]. Further, the neuronal cells are terminally differentiated and their incapacity of self-renewal might be a significant factor in the development of the disease [Baas et al., 2016]. A pivotal characteristic of neurodegenerative disorders including AD is that the onset of molecular abnormalities could precede the manifestation of symptoms by a prolonged period [Drew, 2018]. Thus, the early identification of the hallmarks of AD and subsequent therapeutic intervention is crucial for arresting the global threat imposed by the increased occurrence of this disorder.



STRUCTURAL CHANGES

Alzheimer's disease spreads through the brain, causing a progressive loss of the connections between neurons (synapses), and then neurons themselves. In the later stages of the condition, the brain is noticeably shrunken — the cerebral cortex appears shrivelled and the fluid-filled ventricles are expanded.



MICROSCOPIC CHANGES

Two hallmarks of Alzheimer's disease are visible only under the microscope.

Accumulations of the peptide amyloid- β , known as plaques, form between neurons. Microtubule-associated protein tau aggregates into neurofibrillary tangles inside neurons, and these structures persist after neurons have died.

Figure 10: Schematic representation of the structural and microscopic changes that occur in an AD afflicted human brain [Figure adapted from Drew, 2018].

The structural and functional changes occurring in a human brain afflicted with Alzheimer's disease is shown in **Figure 10**. The onset of AD is marked by the appearance of extraneuronal senile plaques constituted by the amyloid β ($A\beta$) peptides as well as the intraneuronal neurofibrillary tangles (NFTs) composed of Tau paired helical filaments [Drew, 2018].

B.2. Formation of A β peptides from the Amyloid Precursor Protein (APP):

The Amyloid Precursor Protein (APP) is a single pass transmembrane protein with large extracellular domains whose precise physiological function is not clearly understood [Chen et al., 2017]. But *in vitro* studies have indicated at the role of APP in development of adult nervous system, including stimulation of neurite outgrowth and synaptogenesis. APP can also modulate synaptic plasticity as well as regulate cell adhesion. It also possesses a protective function against diverse metabolic and oxidative stress [Mattson, 1997]. APP can be processed via the amyloidogenic and the non-amyloidogenic pathways to yield different products (**Figure 11**). The amyloidogenic pathway leads to the formation of the A β peptides through sequential cleavage of APP by β and γ secretase. β secretase first cleaves the APP to yield a soluble sAPP β fragment and a CTF β fragment, the latter of which is further cleaved by γ secretase to yield the A β peptides and the APP intracellular Domain (AICD) [Nunan et al., 2000]. This cleavage is imprecise and can lead to the formation of A β peptides of different lengths [Assarson et al., 2014, Takami et al., 2009] of which the A β 1-40 (A β 40) comprising of 40 amino acid residues is the most abundantly formed (~90%) followed by the A β 1-42 (A β 42), comprising of 42 amino acid residues [Yang et al., 2018, Walsh et al., 2007, Sinha et al., 1999, Van der Kant et al., 2015]. The A β 42 is the more hydrophobic and fibrillogenic form and is the principal species deposited in the amyloid plaques [Walsh et al., 2007, Chen et al., 2017]. The non-amyloidogenic pathway antagonizes the formation of A β peptides as APP is cleaved by α secretase within the A β domain generating the sAPP α fragment and the CTF α fragment. The CTF α is further cleaved by γ secretase to yield the p3 and AICD fragments [Chen et al., 2017, Kahle et al, 2003, Iwatsubo, 2004, Chow et al., 2010]. While the A β peptides have a more neurotoxic role, sAPP α seem to have a more neuroprotective role and modulates neuronal stem cell proliferation and is important for neurodevelopment [Nhan et al., 2015, Furukawa et al., 1996, Habib et al., 2017, Ray et al.,

2011, Chasseigneaux et al., 2012, Zhou et al., 2011]. p3 contains sequences critical for neurotoxicity but can mediate so at a far lower potency than A β making them relatively non-toxic [Lalowski et al., 1996, Higgins et al., 1996, Dulin et al., 2008, Wei et al., 2002, Nhan et al., 2015]

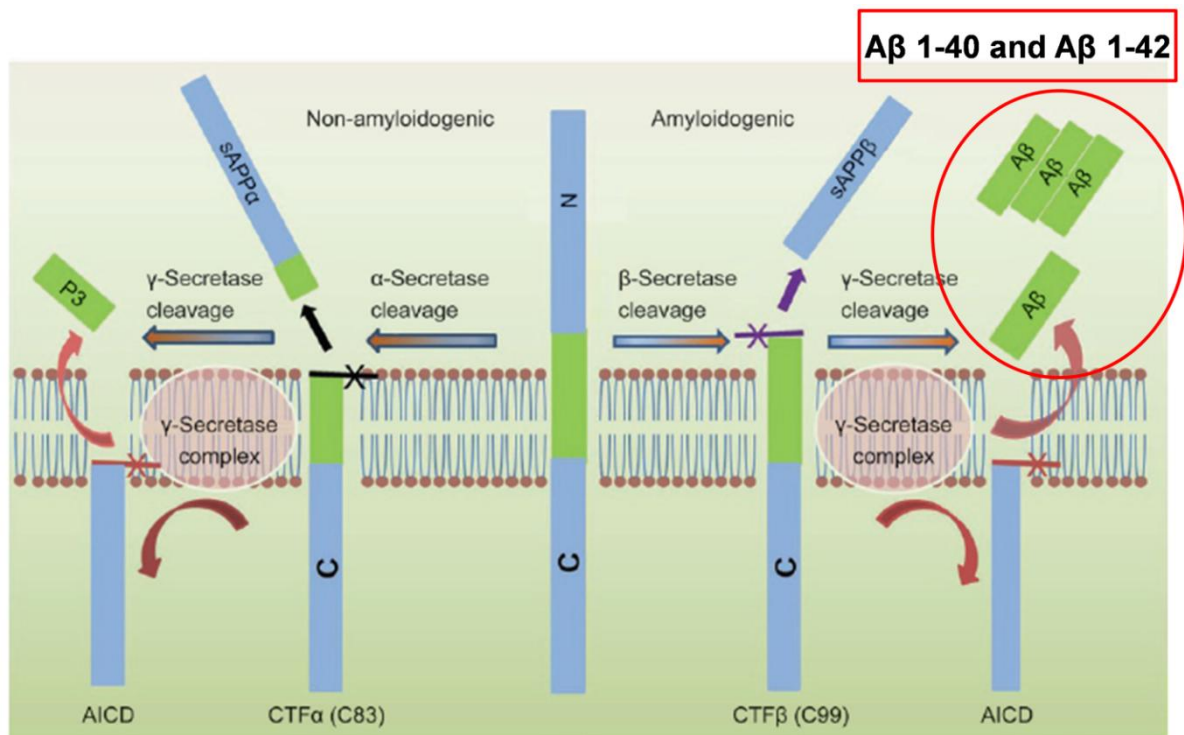


Figure 11: Schematic representation of the Human APP proteolytic pathways via the amyloidogenic and non-amyloidogenic routes.

Non-amyloidogenic pathway involves cleavage of APP within the A β domain by membrane bound α secretase leading to formation of N-terminal sAPP α and CTF α . This is followed by γ secretase mediated cleavage of the membrane attached CTF α fragment to generate the extracellular p3 and APP intracellular Domain (AICD). Amyloidogenic pathway involves sequential cleavage by β secretase and γ secretase to ultimately yield the A β peptides [Figure adapted from Chen et al., 2017]

B.3. Structure of A β 40 and A β 42 fibrils and the mechanism of A β fibrillization

A β monomers can assemble to form oligomeric, protofibrillar and fibrillar amyloid aggregates [Chen et al., 2017]. The fibrillary amyloid aggregates are the large insoluble constituents of the amyloid plaques whereas the soluble oligomeric species may spread throughout the brain [Chen et al., 2017]. Most information about the three-dimensional solution structure of the intrinsically unstructured A β is derived from NMR and molecular

dynamic studies (**Figure 12A-D**) [Chen et al., 2017]. The solution structure of A β 40 (**Figure 12A**) indicates at the presence of a C-terminal α -helix conformation between residues 15-36 with a kink or hinge at 25-27 residues in aqueous SDS micelles. The peptide is unstructured in the first 14 polar residue containing region that is solvated by water. The helix to coil conformational transition, preceding aggregation, is promoted by the deprotonation of two acidic amino acids in the helix [Coles et al., 1998]. Previous NMR studies also revealed distinctly different conformational states of A β 40 (**Figure 12A**) and A β 42 (**Figure 12B**). A β 42 has a more structured C-terminus with a β hairpin formed by residues 31-34 and 38-41 which restricts C-terminal flexibility and is the contributing factor towards its higher propensity for amyloid aggregation making them more neurotoxic in nature compared to A β 40 [Sgourakis et al., 2007]. The hydrophobic C-terminus of A β is crucial for determining the aggregation state of A β in AD and is critical for inducing its transformation from α -helical to β -sheet structure [Mirza et al., 2014]. Although the pathological significance of the minute differences in fibril structure is yet to be clearly deciphered and the correlation among the formation of amyloid plaques, synaptic loss and neuronal cell death in AD brains needs to be further elucidated, the rapid aggregation of A β peptides into fibrils and their deposition in amyloid plaques is indeed a hallmark in AD pathology.

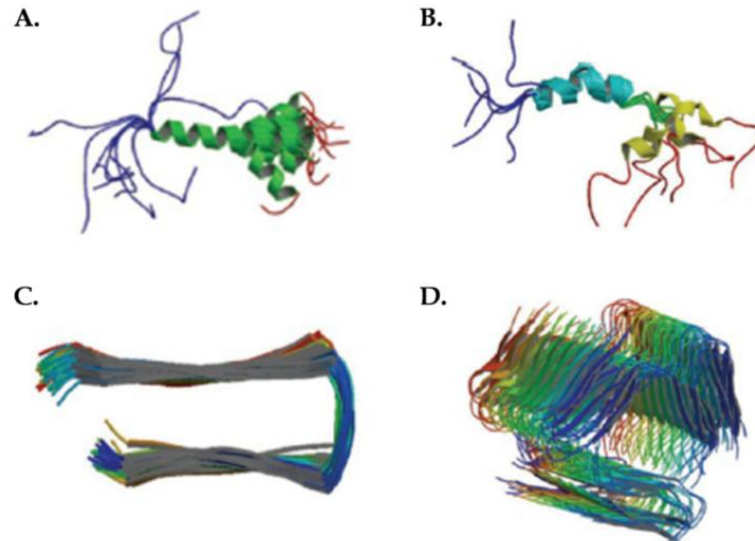


Figure 12: Structures of monomeric and fibrillar $A\beta$ peptides

A. NMR structure of monomeric $A\beta_{40}$ (PDB code: 1BA4) **B.** CD and Solution NMR structure of monomeric $A\beta_{42}$ (PDB code: 1ZOQ) **C.** solution NMR structure of $A\beta_{42}$ fibrils (homopentamer A5) (PDB code: 2BEG) **D.** solid state NMR structure of $A\beta$ fibrils showing the fibril backbone arrangement, stacking registry and steric zipper core interactions (PDB code: 2MPZ) [Figure adapted from Chen et al., 2017]

Amyloid fibril formation involves the conversion of proteins from their soluble monomeric forms to insoluble fibrillary aggregates [Dobson, 2003, Selkoe, 2003, Chiti et al., 2006, Chiti et al., 2017, Chiti et al., 2009]. The “nucleation-dependent polymerization model” is the most widely accepted model explaining amyloid fibril formation. This model suggests that the assembly process follows a sigmoidal curve (as measured by ThT fluorescence or light scattering) which can be segregated into three stages [Adamcik et al., 2018] (**Figure 13A**). The first stage represents the initial long lag phase, which corresponds to the assembly of peptide chains into small nuclei that undergo intermolecular interactions to form oligomeric β sheet structures. The second stage represents the growth phase where nuclei and oligomers interact and assemble to form pre-fibrillar structures that rapidly mature into ordered protofibrils. Amyloid fibrillization is completed by the third “saturation” stage where protofibrils mature into higher ordered amyloid fibrils [Adamcik et al., 2018].

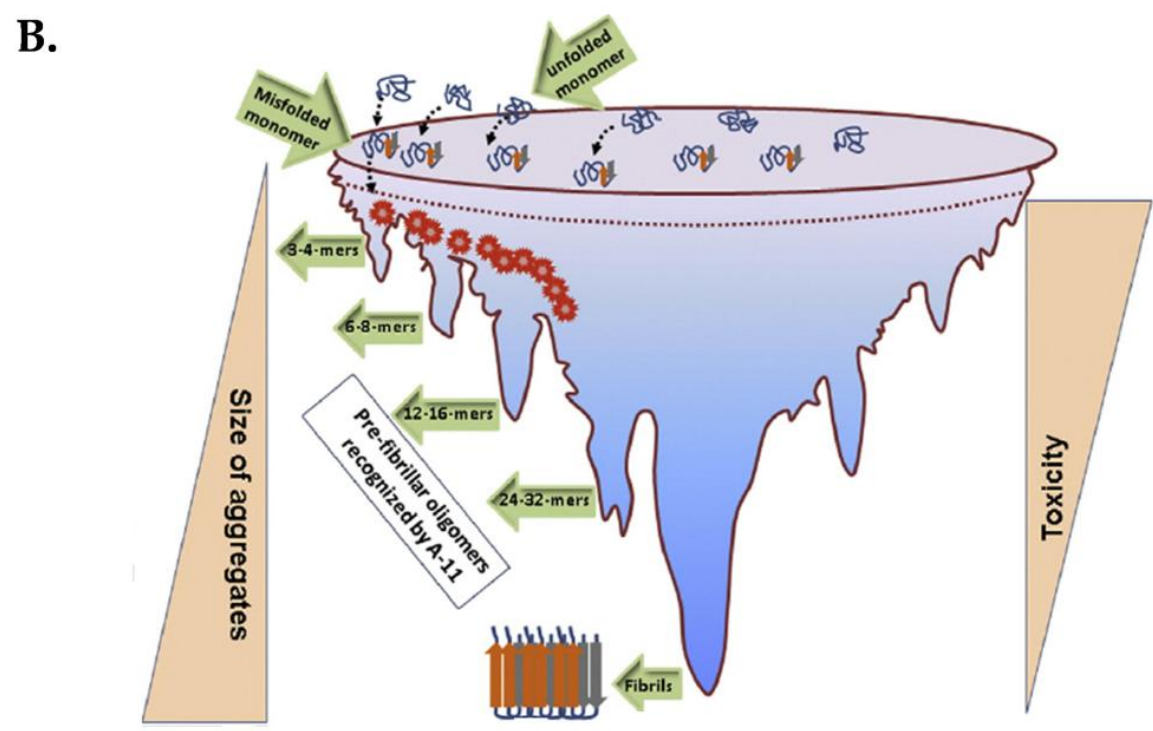
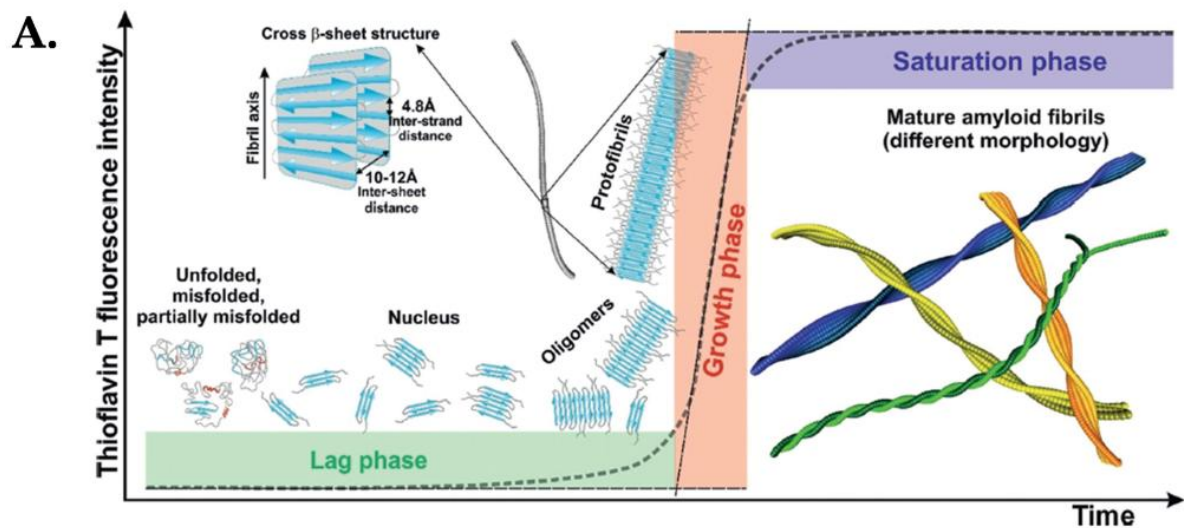


Figure 13: Nucleation-dependent formation of amyloid fibrils and correlation between aggregate size and toxicity

A. Schematic representation of the self-assembly of unfolded and misfolded peptides into mature amyloid fibrils with clear depictions of the three stages of amyloid fibrillization. The lag phase represents the stage of nucleation and oligomerization. The growth phase represents the stage of protofibril assembly while the saturation phase represents the stage of mature amyloid fibril formation. The high expression of A β peptides can lead to its aggregation and accumulation of aggregates of different sizes [Figure adapted from Adamcik et al., 2018]. **B.** Schematic representation of A β assemblies and their toxic effects. An increase in the size of the assemblies correlates with a decrease in their toxicity [Figure adapted from Sengupta et al., 2016].

As discussed previously, the toxic A β oligomers are distinct from their higher ordered fibrillar aggregates [Chen et al., 2017, Lee et al., 2017]. In lieu of the earlier studies which demonstrate that the oligomeric species of A β are the most toxic towards the neuronal cells [Chen et al., 2017], the size of the A β assemblies might be inversely correlated to their exerted toxicity (**Figure 13B**) [Sengupta et al., 2016]. The oligomeric species can mediate their neurotoxicity either directly or by acting as the building blocks of higher ordered aggregates [Sengupta et al., 2016].

B.4. A β oligomer mediated neurotoxicity

As discussed before, unlike the large insoluble amyloid fibrils that constitute plaques, A β oligomers are soluble species that can spread throughout the brain [Chen et al., 2017]. Oligomers are represented as early-stage spherical aggregates which progressively coalesce to form the precursor protofibrils with a bead-like appearance [Chen et al., 2017, Walsh et al., 1997]. Although elucidation of the structure of amyloid oligomers is difficult due to their more transient nature compared to the A β fibrils [Oddo et al., 2003], several studies over the last two decades have indicated that the oligomeric species of A β are the most toxic towards the neuronal cells [Chen et al., 2017]. Oligomers are known to be the kinetic intermediates that are formed during the early stages of fibril development [Harper et al., 1997] and a common mechanism of toxicity is shared by different types of soluble oligomers [Chen et al., 2017, Kaye et al., 2003]. These soluble species can mediate their toxicity by binding to several molecules in the extracellular space including cell surface receptors and the cell membrane [Chen et al., 2017].

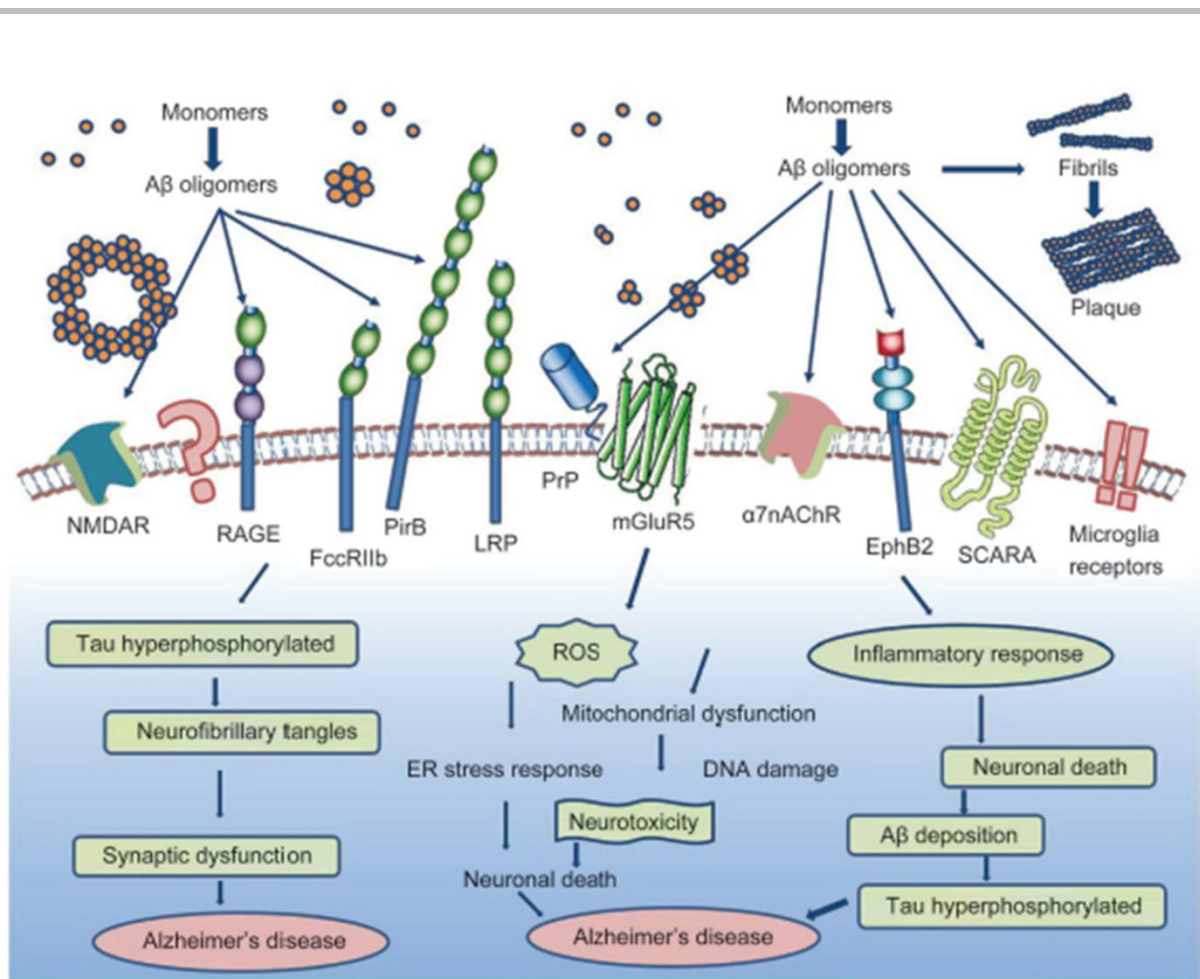


Figure 14: Schematic representation of the modes of toxicity mediated by the soluble A β oligomers.

A β monomers can assemble to form higher ordered structures which range from low molecular weight to high molecular weight: oligomers, protofibrils, fibrils and senile plaques. Interaction of A β oligomers with potential receptors may activate downstream pathways that can cause neurotoxicity and lead to neuronal cell death [Figure adapted from Chen et al., 2017].

The diverse modes of toxicity of soluble A β oligomers and their interaction with a variety of receptors are represented in **Figure 14**. Such interactions with receptors have the potential of generating and transmitting neurotoxic signals that initiates the cellular defects in neurons [Chen et al., 2017].

B.5. Intracellular accumulation of A β oligomers and its implications:

As discussed before, A β peptides are formed by the amyloidogenic cleavage of APP and they are secreted into the extracellular space [Chen et al., 2017, Walsh et al., 2007]. In addition to

interacting with membranes and receptors, these peptides can also be internalized by endocytic vesicles [Lee et al., 2017, LaFerla et al., 2007]. Intracellular accumulation of A β can also occur due to A β production at organelle membranes, where localization of APP can occur [Lee et al., 2017, Umeda et al., 2011, Resende et al., 2008, Cho et al., 2009].

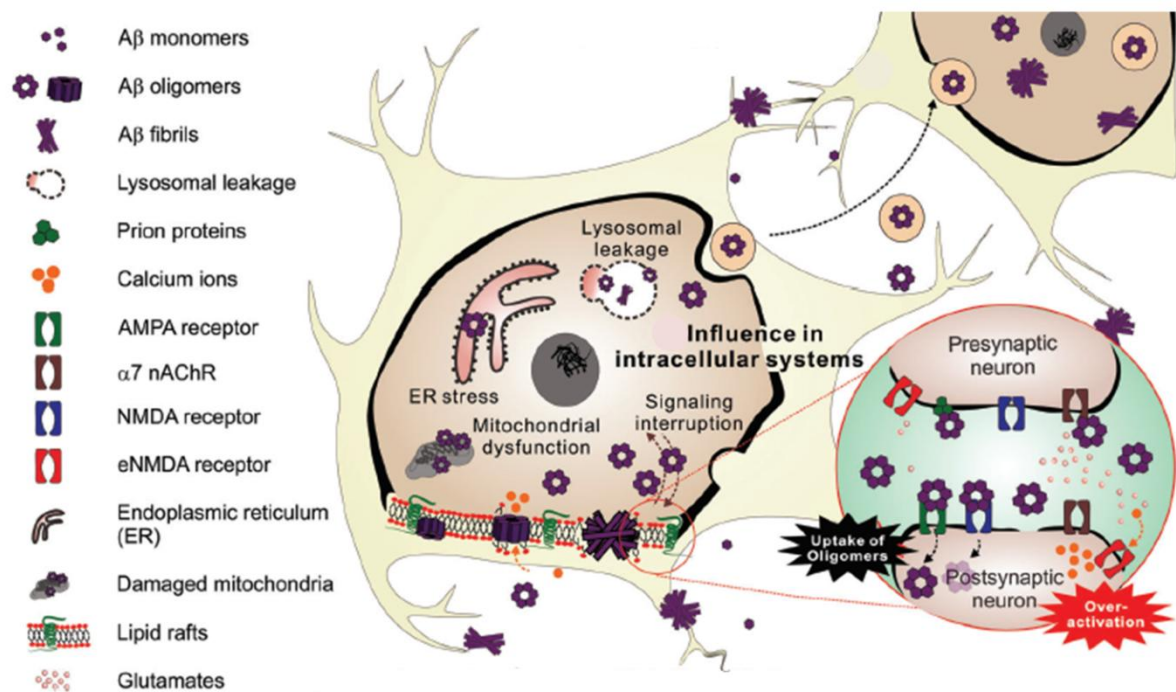


Figure 15: Schematic representation of the intracellular A β oligomer mediated toxicity.

A β oligomers can be re-uptaken by the neuronal cells through association with synaptic receptors. The intracellular accumulation of A β oligomers can damage organelles and disrupt signaling pathways [Figure adapted from Lee et al., 2017].

The **Figure 15**, shown above, outlines the mechanisms of toxicity mediated by the intracellular A β oligomer [Lee et al., 2017]. The mitochondria, ER, trans-Golgi network and lysosomes are some of the implicated organelles that can serve as sites for A β generation due to localization of APP on their membranes [Lee et al., 2017, Umeda et al., 2011, Resende et al., 2008, Cho et al., 2009]. Intracellular presence of A β oligomers can induce a diverse range of cellular damage that can result in neuronal death [Lee et al., 2017]. For example, intracellular A β can trigger mitochondrial dysfunction, by depolarizing the mitochondrial

membrane and can also interfere with proteolysis and intracellular signaling [Lee et al., 2017]. The transmission of A β -associated pathology in human neurons has also been reported to occur in a manner similar to prion disease [Domert et al., 2014, Jaunmuktane et al., 2015]. Studies have also revealed the ability of A β oligomers to travel to distant regions through cell to cell transmission [Domert et al., 2014].

B.6. A β aggregation and loss of ribosomal integrity associated with Alzheimer's disease progression

As discussed above, the accumulation of A β aggregates is a well-established phenomenon associated with the progression of Alzheimer's disease and the onset of molecular abnormalities could precede the manifestation of symptoms by a prolonged period [Drew, 2018]. The aggregation of A β through its three phases of assembly [Adamcik et al., 2018], as discussed before (Section B.3), closely follows the progression of AD through its silent, mild cognitive impairment and advanced stages of progression [Cuello, 2017]. As the disease reaches its advanced stage, the aggregation of A β also reaches saturation [Cuello, 2017]. This is depicted in **Figure 16**.

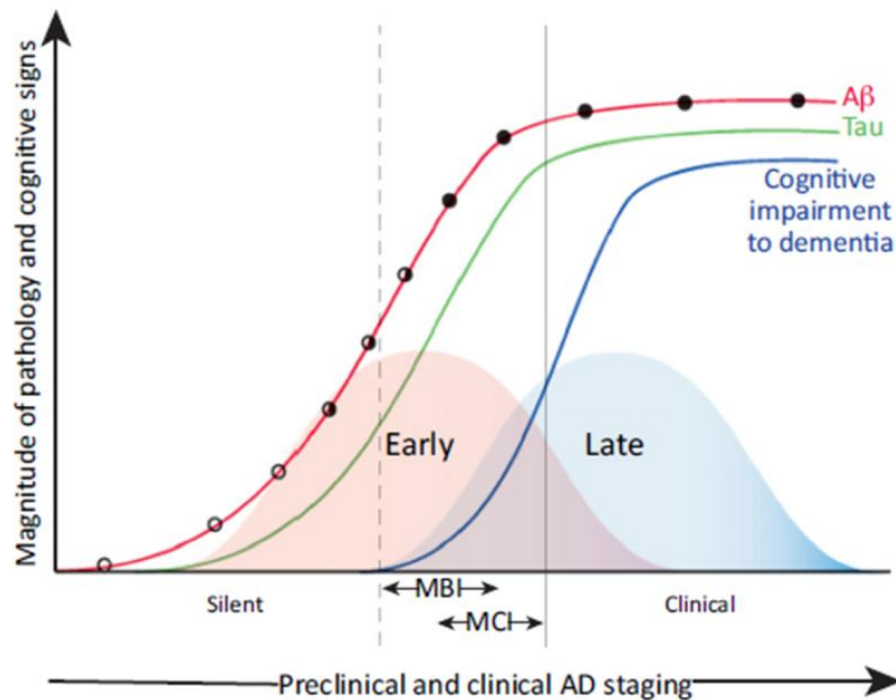


Figure 16: Graphical representation of the progression of Alzheimer's disease along with aggregation of A β and Tau protein.

The progression of Alzheimer's disease through the silent, mild cognitive impairment and advanced clinical stages of dementia has been depicted. Aggregation of A β and Tau follows this progression reaching their saturation as the advanced clinical stages of the disease approaches. [Figure adapted from Cuello, 2017].

Another crucial event occurring parallel to the aggregation of A β during AD progression is the progressive loss of ribosomal population in the neuronal cells [Ding et al., 2006]. Previous studies using sucrose density gradient centrifugation with brain extracts from the inferior parietal lobes of patients suffering from various stages of AD, revealed the disappearance of ribosomal peak with the progression of the disease (**Figure 17**) [Ding et al., 2006]. Such disappearance of ribosomal peak is indicative of the loss in the physical integrity of the ribosome. The reason behind such loss remains to be deciphered.

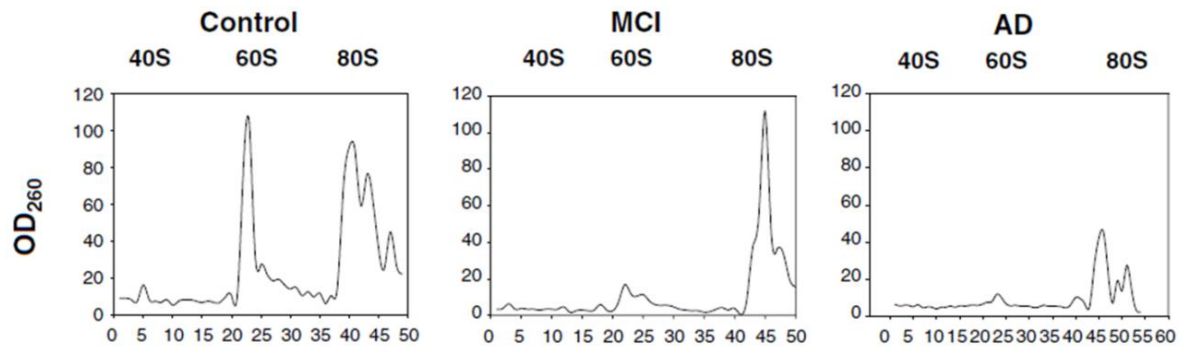


Figure 17: Disappearance of the ribosomal RNA with the progression of Alzheimer's disease to its advanced stages.

$A_{260\text{ nm}}$ profile of ribosomal fractions obtained from the inferior parietal lobule of control, MCI, and AD subjects, indicating the rRNA content [Figure adapted from Ding et al., 2006]

As discussed above (Section B.5), intracellular A β oligomers can mediate the dysfunction of several important cellular organelles [Lee et al., 2017] and resides in the vicinity of the ribosome. Previous studies in the laboratory have demonstrated that the super-stoichiometric presence of aggregating Tau protein (both full length Ht40 and the 4 repeat microtubule binding sub-domain K18) can sequester the eukaryotic ribosome present in its vicinity and hence can be a potential mediator of the ribosome dysfunction observed during AD progression [Banerjee et al., 2020]. The progression of A β aggregation and loss of ribosomal population occurs concomitantly in the neurons during the prognosis of AD, although any direct link between the two events remains to be explored. *In vitro* studies involving the effect of A β peptides on eukaryotic ribosome have been discussed in “Chapter 3” of the thesis. The factors influencing A β -ribosome aggregation in light of nucleic acid acting as a cofactor [Stewart et al., 2017, Cremers et al., 2016, Jiang et al., 2007, Rha et al., 2020] in the aggregation process and the potential for inhibition of such aggregation in the presence of small molecule inhibitors [Freyssin et al., 2018, Zheng et al., 2019, Ono et al., 2012] have also been explored in our study.

References:

1. **Abranches, J.**, Martinez, A. R., Kajfasz, J. K., Chávez, V., Garsin, D. A., &Lemos, J. A. (2009). The molecular alarmone (p) ppGpp mediates stress responses, vancomycin tolerance, and virulence in *Enterococcus faecalis*. *Journal of bacteriology*, *191*(7), 2248-2256.
2. **Adamcik, J.**, &Mezzenga, R. (2018). Amyloid polymorphism in the protein folding and aggregation energy landscape. *Angewandte Chemie International Edition*, *57*(28), 8370-8382.
3. **Agafonov, D. E.**, Kolb, V. A., Nazimov, I. V., &Spirin, A. S. (1999). A protein residing at the subunit interface of the bacterial ribosome. *Proceedings of the National Academy of Sciences*, *96*(22), 12345-12349.
4. **Agashe, V. R.**, Guha, S., Chang, H. C., Genevaux, P., Hayer-Hartl, M., Stemp, M., ... &Barral, J. M. (2004). Function of trigger factor and DnaK in multidomain protein folding: increase in yield at the expense of folding speed. *Cell*, *117*(2), 199-209.
5. **Anfinsen, C. B.** (1973). Principles that govern the folding of protein chains. *Science*, *181*(4096), 223-230.
6. **Assarsson, A.**, Hellstrand, E., Cabaleiro-Lago, C., &Linse, S. (2014). Charge dependent retardation of amyloid β aggregation by hydrophilic proteins. *ACS chemical neuroscience*, *5*(4), 266-274.
7. **Baas, P. W.**, Rao, A. N., Matamoros, A. J., & Leo, L. (2016). Stability properties of neuronal microtubules. *Cytoskeleton*, *73*(9), 442-460.
8. **Balchin, D.**, Hayer-Hartl, M., &Hartl, F. U. (2016). In vivo aspects of protein folding and quality control. *Science*, *353*(6294).
9. **Banerjee, S.**, Ferdosh, S., Ghosh, A. N., & Barat, C. (2020). Tau protein-induced sequestration of the eukaryotic ribosome: Implications in neurodegenerative disease. *Scientific reports*, *10*(1), 1-15.
10. **Basu, A.**, & Yap, M. N. F. (2016). Ribosome hibernation factor promotes *Staphylococcal* survival and differentially represses translation. *Nucleic acids research*, *44*(10), 4881-4893.

11. **Basu, A.**, Samanta, D., Das, D., Chowdhury, S., Bhattacharya, A., Ghosh, J., ... & DasGupta, C. (2008). In vitro protein folding by E. coli ribosome: unfolded protein splitting 70S to interact with 50S subunit. *Biochemical and biophysical research communications*, 366(2), 598-603.
12. **Basu, A.**, Shields, K. E., Eickhoff, C. S., Hoft, D. F., & Yap, M. N. F. (2018). Thermal and nutritional regulation of ribosome hibernation in Staphylococcus aureus. *Journal of bacteriology*, 200(24), e00426-18.
13. **Beckert, B.**, Turk, M., Czech, A., Berninghausen, O., Beckmann, R., Ignatova, Z., ... & Wilson, D. N. (2018). Structure of a hibernating 100S ribosome reveals an inactive conformation of the ribosomal protein S1. *Nature microbiology*, 3(10), 1115-1121.
14. **Boël, G.**, Smith, P. C., Ning, W., Englander, M. T., Chen, B., Hashem, Y., ... & Hunt, J. F. (2014). The ABC-F protein EttA gates ribosome entry into the translation elongation cycle. *Nature structural & molecular biology*, 21(2), 143-151.
15. **Bukau, B.**, Deuerling, E., Pfund, C., & Craig, E. A. (2000). Getting newly synthesized proteins into shape. *Cell*, 101(2), 119-122.
16. **Chasseigneaux, S.**, & Allinquant, B. (2012). Functions of A β , sAPP α and sAPP β : similarities and differences. *Journal of neurochemistry*, 120, 99-108.
17. **Chen, G. F.**, Xu, T. H., Yan, Y., Zhou, Y. R., Jiang, Y., Melcher, K., & Xu, H. E. (2017). Amyloid beta: structure, biology and structure-based therapeutic development. *Acta Pharmacologica Sinica*, 38(9), 1205-1235.
18. **Chiti, F.**, & Dobson, C. M. (2006). Protein misfolding, functional amyloid, and human disease. *Annu. Rev. Biochem.*, 75, 333-366.
19. **Chiti, F.**, & Dobson, C. M. (2009). Amyloid formation by globular proteins under native conditions. *Nature chemical biology*, 5(1), 15-22.
20. **Chiti, F.**, & Dobson, C. M. (2017). Protein misfolding, amyloid formation, and human disease: a summary of progress over the last decade. *Annual review of biochemistry*, 86, 27-68.
21. **Cho, D. H.**, Nakamura, T., Fang, J., Cieplak, P., Godzik, A., Gu, Z., & Lipton, S. A. (2009). S-nitrosylation of Drp1 mediates β -amyloid-related mitochondrial fission and neuronal injury. *Science*, 324(5923), 102-105.

22. **Chow, V. W.**, Mattson, M. P., Wong, P. C., & Gleichmann, M. (2010). An overview of APP processing enzymes and products. *Neuromolecular medicine*, 12(1), 1-12.
23. **Coatham, M. L.**, Brandon, H. E., Fischer, J. J., Schümmer, T., & Wieden, H. J. (2016). The conserved GTPase HflX is a ribosome splitting factor that binds to the E-site of the bacterial ribosome. *Nucleic acids research*, 44(4), 1952-1961.
24. **Coles, M.**, Bicknell, W., Watson, A. A., Fairlie, D. P., & Craik, D. J. (1998). Solution structure of amyloid β -peptide (1– 40) in a water– micelle environment. Is the membrane-spanning domain where we think it is?. *Biochemistry*, 37(31), 11064-11077.
25. **Cordeiro, Y.**, Macedo, B., Silva, J. L., & Gomes, M. P. (2014). Pathological implications of nucleic acid interactions with proteins associated with neurodegenerative diseases. *Biophysical reviews*, 6(1), 97-110.
26. **Cremers, C. M.**, Knoefler, D., Gates, S., Martin, N., Dahl, J. U., Lempart, J., ... & Jakob, U. (2016). Polyphosphate: a conserved modifier of amyloidogenic processes. *Molecular cell*, 63(5), 768-780.
27. **Cuello, A. C.** (2017). Early and late CNS inflammation in Alzheimer's disease: two extremes of a continuum?. *Trends in pharmacological sciences*, 38(11), 956-966.
28. **Das, D.**, Das, A., Samanta, D., Ghosh, J., Dasgupta, S., Bhattacharya, A., ... & Das Gupta, C. (2008). Role of the ribosome in protein folding. *Biotechnology Journal: Healthcare Nutrition Technology*, 3(8), 999-1009.
29. **Dey, S.**, Biswas, C., & Sengupta, J. (2018). The universally conserved GTPase HflX is an RNA helicase that restores heat-damaged Escherichia coli ribosomes. *Journal of Cell Biology*, 217(7), 2519-2529.
30. **Diez, S.**, Ryu, J., Caban, K., Gonzalez, R. L., & Dworkin, J. (2020). The alarmones (p) ppGpp directly regulate translation initiation during entry into quiescence. *Proceedings of the National Academy of Sciences*, 117(27), 15565-15572.
31. **Dill, K. A.**, & Chan, H. S. (1997). From Levinthal to pathways to funnels. *Nature structural biology*, 4(1), 10-19.
32. **Ding, Q.**, Markesbery, W. R., Cekarini, V., & Keller, J. N. (2006). Decreased RNA, and increased RNA oxidation, in ribosomes from early Alzheimer's disease. *Neurochemical research*, 31(5), 705-710.

33. **Dobson, C. M.** (2003). Protein folding and misfolding. *Nature*, 426(6968), 884-890.
34. **Domert, J.,** Rao, S. B., Agholme, L., Brorsson, A. C., Marcusson, J., Hallbeck, M., & Nath, S. (2014). Spreading of amyloid- β peptides via neuritic cell-to-cell transfer is dependent on insufficient cellular clearance. *Neurobiology of disease*, 65, 82-92.
35. **Drew, L.** (2018). An age-old story of dementia. *Nature*, 559(7715), S2-S3.
36. **Dulin, F.,** L veill , F., Ortega, J. B., Mornon, J. P., Buisson, A., Callebaut, I., & Colloc'h, N. (2008). p3 peptide, a truncated form of A β devoid of synaptotoxic effect, does not assemble into soluble oligomers. *FEBS letters*, 582(13), 1865-1870.
37. **Eichner, T.,** & Radford, S. E. (2011). A diversity of assembly mechanisms of a generic amyloid fold. *Molecular cell*, 43(1), 8-18.
38. **El-Sharoud, W. M.** (2004). Ribosome inactivation for preservation: concepts and reservations. *Science progress*, 87(3), 137-152.
39. **Far as-Rico, J. A.,** Selin, F. R., Myronidi, I., Fr uhauf, M., & Von Heijne, G. (2018). Effects of protein size, thermodynamic stability, and net charge on cotranslational folding on the ribosome. *Proceedings of the National Academy of Sciences*, 115(40), E9280-E9287.
40. **Feng, B.,** Mandava, C. S., Guo, Q., Wang, J., Cao, W., Li, N., ... & Gao, N. (2014). Structural and functional insights into the mode of action of a universally conserved Obg GTPase. *PLoS biology*, 12(5), e1001866.
41. **Frank, J.** (2004). Conformational proteomics of macromolecular architectures.
42. **Freyssin, A.,** Page, G., Fauconneau, B., & Bilan, A. R. (2018). Natural polyphenols effects on protein aggregates in Alzheimer's and Parkinson's prion-like diseases. *Neural regeneration research*, 13(6), 955.
43. **Furukawa, K.,** Sopher, B. L., Rydel, R. E., Begley, J. G., Pham, D. G., Martin, G. M., ... & Mattson, M. P. (1996). Increased activity- regulating and neuroprotective efficacy of α - secretase- derived secreted amyloid precursor protein conferred by a C- terminal heparin- binding domain. *Journal of neurochemistry*, 67(5), 1882-1896.
44. **Gao, H. M.,** & Hong, J. S. (2008). Why neurodegenerative diseases are progressive: uncontrolled inflammation drives disease progression. *Trends in immunology*, 29(8), 357-365.

45. **Ghosh, J.**, Basu, A., Pal, S., Chowdhuri, S., Bhattacharya, A., Pal, D., ... & DasGupta, C. (2003). Ribosome–DnaK interactions in relation to protein folding. *Molecular microbiology*, *48*(6), 1679-1692.
46. **Guo, M. S.**, & Gross, C. A. (2014). Stress-induced remodeling of the bacterial proteome. *Current Biology*, *24*(10), R424-R434.
47. **Gutu, A.**, Nesbit, A. D., Alverson, A. J., Palmer, J. D., & Kehoe, D. M. (2013). Unique role for translation initiation factor 3 in the light color regulation of photosynthetic gene expression. *Proceedings of the National Academy of Sciences*, *110*(40), 16253-16258.
48. **Habib, A.**, Sawmiller, D., & Tan, J. (2017). Restoring Soluble Amyloid Precursor Protein α Functions as a Potential Treatment for Alzheimer's Disease. *Journal of neuroscience research*, *95*(4), 973-991.
49. **Harper, J. D.**, Lieber, C. M., & Lansbury Jr, P. T. (1997). Atomic force microscopic imaging of seeded fibril formation and fibril branching by the Alzheimer's disease amyloid- β protein. *Chemistry & biology*, *4*(12), 951-959.
50. **Higgins, L. S.**, Murphy Jr, G. M., Forno, L. S., Catalano, R., & Cordell, B. (1996). P3 beta-amyloid peptide has a unique and potentially pathogenic immunohistochemical profile in Alzheimer's disease brain. *The American journal of pathology*, *149*(2), 585.
51. **Iwatsubo, T.** (2004). The γ -secretase complex: machinery for intramembrane proteolysis. *Current opinion in neurobiology*, *14*(3), 379-383.
52. **Izutsu, K.**, Wada, A., & Wada, C. (2001). Expression of ribosome modulation factor (RMF) in Escherichia coli requires ppGpp. *Genes to Cells*, *6*(8), 665-676.
53. **Jaunmuktane, Z.**, Mead, S., Ellis, M., Wadsworth, J. D., Nicoll, A. J., Kenny, J., ... & Brandner, S. (2015). Evidence for human transmission of amyloid- β pathology and cerebral amyloid angiopathy. *Nature*, *525*(7568), 247-250.
54. **Jiang, W.**, Han, Y., Zhou, R., Zhang, L., & Liu, C. (2007). DNA is a template for accelerating the aggregation of copper, zinc superoxide dismutase. *Biochemistry*, *46*(20), 5911-5923.
55. **Joyner, R. P.**, Tang, J. H., Helenius, J., Dultz, E., Brune, C., Holt, L. J., ... & Weis, K. (2016). A glucose-starvation response regulates the diffusion of macromolecules. *Elife*, *5*, e09376.

56. **Kahle, P. J.**, & De Strooper, B. (2003). Attack on amyloid: International Titisee Conference on Alzheimer's and Parkinson's Disease: From Basic Science to Therapeutic Treatment.
57. **Kato, T.**, Yoshida, H., Miyata, T., Maki, Y., Wada, A., & Namba, K. (2010). Structure of the 100S ribosome in the hibernation stage revealed by electron cryomicroscopy. *Structure*, *18*(6), 719-724.
58. **Kayed, R.**, Head, E., Thompson, J. L., McIntire, T. M., Milton, S. C., Cotman, C. W., & Glabe, C. G. (2003). Common structure of soluble amyloid oligomers implies common mechanism of pathogenesis. *Science*, *300*(5618), 486-489.
59. **Khusainov, I.**, Vicens, Q., Ayupov, R., Usachev, K., Myasnikov, A., Simonetti, A., ... & Hashem, Y. (2017). Structures and dynamics of hibernating ribosomes from *Staphylococcus aureus* mediated by intermolecular interactions of HPF. *The EMBO journal*, *36*(14), 2073-2087.
60. **Kiel, M. C.**, Kaji, H., & Kaji, A. (2007). Ribosome recycling: An essential process of protein synthesis. *Biochemistry and Molecular Biology Education*, *35*(1), 40-44.
61. **Kudva, R.**, Tian, P., Pardo-Avila, F., Carroni, M., Best, R. B., Bernstein, H. D., & Von Heijne, G. (2018). The shape of the bacterial ribosome exit tunnel affects cotranslational protein folding. *Elife*, *7*, e36326.
62. **LaFerla, F. M.**, Green, K. N., & Oddo, S. (2007). Intracellular amyloid- β in Alzheimer's disease. *Nature Reviews Neuroscience*, *8*(7), 499-509.
63. **Lalowski, M.**, Golabek, A., Lemere, C. A., Selkoe, D. J., Wisniewski, H. M., Beavis, R. C., ... & Wisniewski, T. (1996). The "nonamyloidogenic" p3 fragment (Amyloid β 17-42) is a major constituent of Down's syndrome cerebellar preamyloid. *Journal of Biological Chemistry*, *271*(52), 33623-33631.
64. **Lee, S. J. C.**, Nam, E., Lee, H. J., Savelieff, M. G., & Lim, M. H. (2017). Towards an understanding of amyloid- β oligomers: characterization, toxicity mechanisms, and inhibitors. *Chemical Society Reviews*, *46*(2), 310-323.
65. **Liang, X.**, Zuo, M. Q., Zhang, Y., Li, N., Ma, C., Dong, M. Q., & Gao, N. (2020). Structural snapshots of human pre-60S ribosomal particles before and after nuclear export. *Nature communications*, *11*(1), 1-14.

66. **Lim, J., & Yue, Z.** (2015). Neuronal aggregates: formation, clearance, and spreading. *Developmental cell*, 32(4), 491-501.
67. **Liu, Q., & Fredrick, K.** (2016). Intersubunit bridges of the bacterial ribosome. *Journal of molecular biology*, 428(10), 2146-2164.
68. **Liutkute, M., Samatova, E., & Rodnina, M. V.** (2020). Cotranslational folding of proteins on the ribosome. *Biomolecules*, 10(1), 97.
69. **Maki, Y., Yoshida, H., & Wada, A.** (2000). Two proteins, YfiA and YhbH, associated with resting ribosomes in stationary phase Escherichia coli. *Genes to cells*, 5(12), 965-974.
70. **Mattson, M. P.** (1997). Cellular actions of beta-amyloid precursor protein and its soluble and fibrillogenic derivatives. *Physiological reviews*, 77(4), 1081-1132.
71. **Matzov, D., Aibara, S., Basu, A., Zimmerman, E., Bashan, A., Yap, M. N. F., ... & Yonath, A. E.** (2017). The cryo-EM structure of hibernating 100S ribosome dimer from pathogenic Staphylococcus aureus. *Nature communications*, 8(1), 1-7.
72. **Mirza, Z., G Pillai, V., & A Kamal, M.** (2014). Protein Interactions Between the C-Terminus of A β -Peptide and Phospholipase A2-A Structure Biology Based Approach to Identify Novel Alzheimer's Therapeutics. *CNS & Neurological Disorders-Drug Targets (Formerly Current Drug Targets-CNS & Neurological Disorders)*, 13(7), 1224-1231.
73. **Mondal, S., Pathak, B. K., Ray, S., & Barat, C.** (2014). Impact of P-Site tRNA and antibiotics on ribosome mediated protein folding: studies using the Escherichia coli ribosome. *PLoS One*, 9(7), e101293.
74. **Nhan, H. S., Chiang, K., & Koo, E. H.** (2015). The multifaceted nature of amyloid precursor protein and its proteolytic fragments: friends and foes. *Acta neuropathologica*, 129(1), 1-19.
75. **Nunan, J., & Small, D. H.** (2000). Regulation of APP cleavage by α -, β -and γ -secretases. *FEBS letters*, 483(1), 6-10.
76. **O'Brien, E. P., Vendruscolo, M., & Dobson, C. M.** (2014). Kinetic modelling indicates that fast-translating codons can coordinate cotranslational protein folding by avoiding misfolded intermediates. *Nature communications*, 5(1), 1-11.

77. **Oddo, S.**, Caccamo, A., Shepherd, J. D., Murphy, M. P., Golde, T. E., Kaye, R., ... & LaFerla, F. M. (2003). Triple-transgenic model of Alzheimer's disease with plaques and tangles: intracellular A β and synaptic dysfunction. *Neuron*, 39(3), 409-421.
78. **Ono, K.**, Li, L., Takamura, Y., Yoshiike, Y., Zhu, L., Han, F., ... & Yamada, M. (2012). Phenolic compounds prevent amyloid β -protein oligomerization and synaptic dysfunction by site-specific binding. *Journal of Biological Chemistry*, 287(18), 14631-14643.
79. **Onuchic, J. N.**, Luthey-Schulten, Z., & Wolynes, P. G. (1997). Theory of protein folding: the energy landscape perspective. *Annual review of physical chemistry*, 48(1), 545-600.
80. **Pal, S.**, Chandra, S., Chowdhury, S., Sarkar, D., Ghosh, A. N., & Gupta, C. D. (1999). Complementary role of two fragments of domain V of 23 S ribosomal RNA in protein folding. *Journal of Biological Chemistry*, 274(46), 32771-32777.
81. **Pang, Y.**, Kurella, S., Voisset, C., Samanta, D., Banerjee, D., Schabe, A., ... & Sanyal, S. (2013). The antiprion compound 6-aminophenanthridine inhibits the protein folding activity of the ribosome by direct competition. *Journal of Biological Chemistry*, 288(26), 19081-19089.
82. **Pathak, B. K.**, Banerjee, S., Mondal, S., Chakraborty, B., Sengupta, J., & Barat, C. (2017). Unfolded protein exhibits antiassociation activity toward the 50S subunit facilitating 70S ribosome dissociation. *The FEBS journal*, 284(22), 3915-3930.
83. **Pathak, B. K.**, Mondal, S., Ghosh, A. N., & Barat, C. (2014). The ribosome can prevent aggregation of partially folded protein intermediates: studies using the Escherichia coli ribosome. *PloS one*, 9(5), e96425.
84. **Pechmann, S.**, Willmund, F., & Frydman, J. (2013). The ribosome as a hub for protein quality control. *Molecular cell*, 49(3), 411-421.
85. **Piir, K.**, Paier, A., Liiv, A., Tenson, T., & Maiväli, Ü. (2011). Ribosome degradation in growing bacteria. *EMBO reports*, 12(5), 458-462.
86. **Polikanov, Y. S.**, Blaha, G. M., & Steitz, T. A. (2012). How hibernation factors RMF, HPF, and YfiA turn off protein synthesis. *Science*, 336(6083), 915-918.
87. **Preissler, S.**, & Deuerling, E. (2012). Ribosome-associated chaperones as key players in proteostasis. *Trends in biochemical sciences*, 37(7), 274-283.

88. **Prossliner, T.**, SkovboWinther, K., Sørensen, M. A., & Gerdes, K. (2018). Ribosome hibernation. *Annual review of genetics*, 52, 321-348.
89. **Ray, B.**, Long, J. M., Sokol, D. K., & Lahiri, D. K. (2011). Increased secreted amyloid precursor protein- α (sAPP α) in severe autism: proposal of a specific, anabolic pathway and putative biomarker. *PLoS one*, 6(6), e20405.
90. **Resende, R.**, Ferreiro, E., Pereira, C., & De Oliveira, C. R. (2008). Neurotoxic effect of oligomeric and fibrillar species of amyloid-beta peptide 1-42: involvement of endoplasmic reticulum calcium release in oligomer-induced cell death. *Neuroscience*, 155(3), 725-737.
91. **Rha, A. K.**, Das, D., Taran, O., Ke, Y., Mehta, A. K., & Lynn, D. G. (2020). Electrostatic Complementarity Drives Amyloid/Nucleic Acid Co- Assembly. *Angewandte Chemie International Edition*, 59(1), 358-363.
92. **Saibil, H.** (2013). Chaperone machines for protein folding, unfolding and disaggregation. *Nature reviews Molecular cell biology*, 14(10), 630-642.
93. **Samanta, D.**, Mukhopadhyay, D., Chowdhury, S., Ghosh, J., Pal, S., Basu, A., ... & DasGupta, C. (2008). Protein folding by domain V of Escherichia coli 23S rRNA: specificity of RNA-protein interactions. *Journal of bacteriology*, 190(9), 3344-3352.
94. **Schmeing, T. M.**, & Ramakrishnan, V. (2009). What recent ribosome structures have revealed about the mechanism of translation. *Nature*, 461(7268), 1234-1242.
95. **Selkoe, D. J.** (2003). Folding proteins in fatal ways. *Nature*, 426(6968), 900-904.
96. **Sengupta, U.**, Nilson, A. N., & Kaye, R. (2016). The role of amyloid- β oligomers in toxicity, propagation, and immunotherapy. *EBioMedicine*, 6, 42-49.
97. **Sgourakis, N. G.**, Yan, Y., McCallum, S. A., Wang, C., & Garcia, A. E. (2007). The Alzheimer's peptides A β 40 and 42 adopt distinct conformations in water: a combined MD/NMR study. *Journal of molecular biology*, 368(5), 1448-1457.
98. **Sharma, M. R.**, Dönhöfer, A., Barat, C., Marquez, V., Datta, P. P., Fucini, P., ... & Agrawal, R. K. (2010). PSRP1 Is Not a Ribosomal Protein, but a Ribosome-binding Factor That Is Recycled by the Ribosome-recycling Factor (RRF) and Elongation Factor G (EF-G) 2. *Journal of Biological Chemistry*, 285(6), 4006-4014.

99. **Silva, J. L.**, Vieira, T. C., Gomes, M. P., Bom, A. P. A., Lima, L. M. T., Freitas, M. S., ... & Foguel, D. (2010). Ligand binding and hydration in protein misfolding: insights from studies of prion and p53 tumor suppressor proteins. *Accounts of chemical research*, 43(2), 271-279.
100. **Sinha, S.**, & Lieberburg, I. (1999). Cellular mechanisms of β -amyloid production and secretion. *Proceedings of the National Academy of Sciences*, 96(20), 11049-11053.
101. **Starosta, A. L.**, Lassak, J., Jung, K., & Wilson, D. N. (2014). The bacterial translation stress response. *FEMS microbiology reviews*, 38(6), 1172-1201.
102. **Stewart, K. L.**, & Radford, S. E. (2017). Amyloid plaques beyond A β : a survey of the diverse modulators of amyloid aggregation. *Biophysical reviews*, 9(4), 405-419.
103. **Sulthana, S.**, Basturea, G. N., & Deutscher, M. P. (2016). Elucidation of pathways of ribosomal RNA degradation: an essential role for RNase E. *Rna*, 22(8), 1163-1171.
104. **Takami, M.**, Nagashima, Y., Sano, Y., Ishihara, S., Morishima-Kawashima, M., Funamoto, S., & Ihara, Y. (2009). γ -Secretase: successive tripeptide and tetrapeptide release from the transmembrane domain of β -carboxyl terminal fragment. *Journal of Neuroscience*, 29(41), 13042-13052.
105. **Tartaglia, G. G.**, Dobson, C. M., Hartl, F. U., & Vendruscolo, M. (2010). Physicochemical determinants of chaperone requirements. *Journal of molecular biology*, 400(3), 579-588.
106. **Tran, Q. H.**, & Uden, G. (1998). Changes in the proton potential and the cellular energetics of Escherichia coli during growth by aerobic and anaerobic respiration or by fermentation. *European journal of biochemistry*, 251(1- 2), 538-543.
107. **Ueta, M.**, Ohniwa, R. L., Yoshida, H., Maki, Y., Wada, C., & Wada, A. (2008). Role of HPF (hibernation promoting factor) in translational activity in Escherichia coli. *Journal of biochemistry*, 143(3), 425-433.
108. **Ueta, M.**, Wada, C., Daifuku, T., Sako, Y., Bessho, Y., Kitamura, A., ... & Wada, A. (2013). Conservation of two distinct types of 100 S ribosome in bacteria. *Genes to Cells*, 18(7), 554-574.
109. **Ueta, M.**, Yoshida, H., Wada, C., Baba, T., Mori, H., & Wada, A. (2005). Ribosome binding proteins YhbH and YfiA have opposite functions during 100S formation in the stationary phase of Escherichia coli. *Genes to Cells*, 10(12), 1103-1112.

110. **Umeda, T.**, Tomiyama, T., Sakama, N., Tanaka, S., Lambert, M. P., Klein, W. L., & Mori, H. (2011). Intraneuronal amyloid β oligomers cause cell death via endoplasmic reticulum stress, endosomal/lysosomal leakage, and mitochondrial dysfunction in vivo. *Journal of neuroscience research*, 89(7), 1031-1042.
111. **Van Der Kant, R.**, & Goldstein, L. S. (2015). Cellular functions of the amyloid precursor protein from development to dementia. *Developmental cell*, 32(4), 502-515.
112. **Verstraeten, N.**, Fauvart, M., Versées, W., & Michiels, J. (2011). The universally conserved prokaryotic GTPases. *Microbiology and Molecular Biology Reviews*, 75(3), 507-542.
113. **Vila-Sanjurjo, A.**, Schuwirth, B. S., Hau, C. W., & Cate, J. H. (2004). Structural basis for the control of translation initiation during stress. *Nature structural & molecular biology*, 11(11), 1054-1059.
114. **Walsh, D. M.**, & Selkoe, D. J. (2007). A β oligomers—a decade of discovery. *Journal of neurochemistry*, 101(5), 1172-1184.
115. **Walsh, D. M.**, Lomakin, A., Benedek, G. B., Condron, M. M., & Teplow, D. B. (1997). Amyloid β -protein fibrillogenesis: detection of a protofibrillar intermediate. *Journal of Biological Chemistry*, 272(35), 22364-22372.
116. **Wang, L.**, Fan, D., Chen, W., & Terentjev, E. M. (2015). Bacterial growth, detachment and cell size control on polyethylene terephthalate surfaces. *Scientific reports*, 5(1), 1-11.
117. **Waudby, C. A.**, Dobson, C. M., & Christodoulou, J. (2019). Nature and regulation of protein folding on the ribosome. *Trends in biochemical sciences*, 44(11), 914-926.
118. **Wei, W.**, Norton, D. D., Wang, X., & Kusiak, J. W. (2002). A β 17–42 in Alzheimer's disease activates JNK and caspase- 8 leading to neuronal apoptosis. *Brain*, 125(9), 2036-2043.
119. **Yang, X.**, Meisl, G., Frohm, B., Thulin, E., Knowles, T. P., & Linse, S. (2018). On the role of sidechain size and charge in the aggregation of A β 42 with familial mutations. *Proceedings of the National Academy of Sciences*, 115(26), E5849-E5858.
120. **Yoshida, H.**, Maki, Y., Kato, H., Fujisawa, H., Izutsu, K., Wada, C., & Wada, A. (2002). The ribosome modulation factor (RMF) binding site on the 100S ribosome of Escherichia coli. *The Journal of Biochemistry*, 132(6), 983-989.

121. **Zheng, Q.**, Kebede, M. T., Kemeh, M. M., Islam, S., Lee, B., Bleck, S. D., ... &Lazo, N. D. (2019). Inhibition of the self-assembly of A β and of Tau by polyphenols: Mechanistic studies. *Molecules*, 24(12), 2316.
122. **Zhou, Z. D.**, Chan, C. H. S., Ma, Q. H., Xu, X. H., Xiao, Z. C., & Tan, E. K. (2011). The roles of amyloid precursor protein (APP) in neurogenesis: Implications to pathogenesis and therapy of Alzheimer disease. *Cell adhesion & migration*, 5(4), 280-292.
123. **Zundel, M. A.**, Basturea, G. N., &Deutscher, M. P. (2009). Initiation of ribosome degradation during starvation in Escherichia coli. *Rna*, 15(5), 977-983.

Chapter 2

Prokaryotic hibernating ribosome and unfolded proteins

Introduction:

The life of a bacterial cell entails transitioning through different phases of growth. In nutrient-abundant conditions, these cells exhibit exponential growth. A shift from this exponential phase of growth to the stationary phase occurs when the nutrients become limiting and the cells are exposed to harsh and unstable conditions [Starosta et al., 2014]. In order to survive such conditions, these microorganisms employ diverse mechanisms with the primary aim to help in cell survival by reducing energy consumption [Starosta et al., 2014, Prossliner et al., 2018]. The ribosomal response in this aspect is, therefore, of utmost importance. Since translation is one of the most energetically expensive cellular processes, the primary cellular strategy, to combat stress, is the down-regulation of protein synthesis, while maintaining a pool of non-translating ribosome that can resume function upon return of favourable conditions [Starosta et al., 2014, Prossliner et al., 2018, Maki et al., 2000]. Entry into the stationary phase induces several morphological and physiological changes in the bacterial cells which are associated with expression of several stress response factors that can bind to the ribosome and maintain them in a translationally silent state [Starosta et al., 2014, Prossliner et al., 2018, Matzov et al., 2017]. This mechanism of maintaining the ribosomal population in a dormant state is referred to as “Ribosomal Hibernation” which is a prominent molecular strategy to control the pace of protein synthesis under diverse conditions of stress as discussed in Chapter 1, including those prevailing during the stationary phase [Ueta et al., 2008, Starosta et al., 2014]. Such translation-suppressing mechanism involves the formation of either the factor-bound inactive 70S monomers or the dimerization of two ribosomes into the “hibernating” 100S inactive ribosome dimer [Ueta et al., 2008, Basu et al., 2016, Prossliner et al., 2018].

In *Escherichia coli*, a clinically important gram-negative bacterium, ribosome hibernation through 100S (100S_{Ec}) formation in the stationary phase, is mediated by a short form of hibernation promoting factor (HPF) which acts in concert with the ribosome modulation factor (RMF) [Polikanov et al., 2012, Prossliner et al., 2018, Ueta et al., 2008, Maki et al., 2000]. RMF binds to the 70S and converts it to the inactive 90S dimer. Subsequent binding of HPF leads to the formation of the 100S dimeric structure. The 100S complexes are constituted by two 70S ribosomes that dimerize through interaction between the 30S subunits [Polikanov et al., 2012, Starosta et al., 2014]. The *E.coli* HPF (HPF_{Ec}), can alone bind to the 70S ribosome, but cannot dimerize it to form the 100S without the additional help of RMF [Ueta et al., 2008, Polikanov et al., 2012]. HPF binds to the channel lying between the head and body of the 30S subunit where tRNAs and mRNA bind during protein synthesis (**Figure 1**). The HPF binding site overlaps all three tRNA binding sites as well as the binding sites of the initiation factors IF1 and IF3 which are crucial for bacterial translation initiation. It also overlaps with the binding site of the elongation factor G (EF-G) which assists the ribosome recycling factor (RRF) in dissociating post-termination complexes of 70S ribosomes [Polikanov et al., 2012]. Taken together the HPF binding maintains the ribosome in a translationally silent “hibernating” monomeric ribosome state, in which it is unable to participate in the translation process.

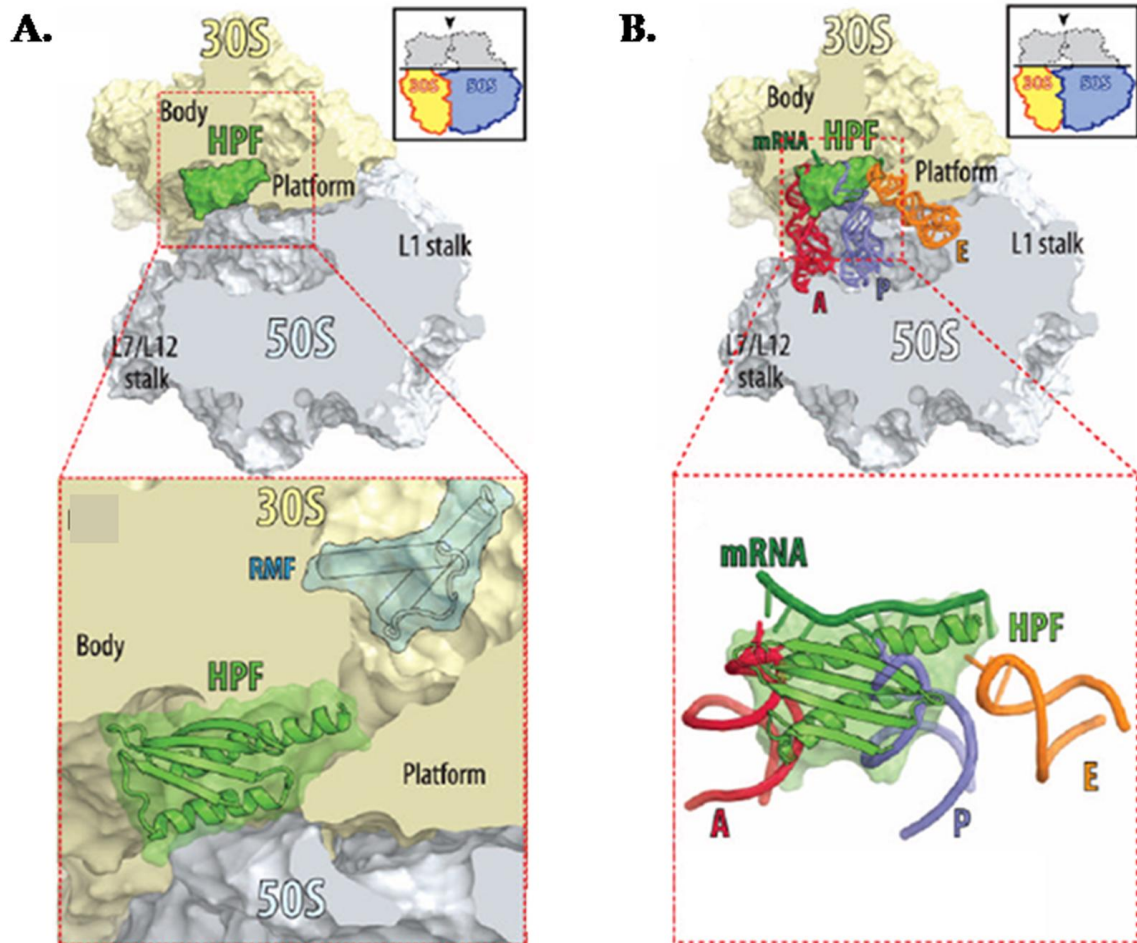


Figure 1: Structural representation of the HPF bound 70S ribosome

A. HPF (depicted in green) bound to the mRNA channel between the head and body of the 30S subunit (depicted in light yellow), as viewed upon removal of the head of the 30S subunit and protuberances of 50S subunit (depicted in light blue) (indicated in inset). HPF bound portion is highlighted with superimposed RMF protein (depicted in blue). **B.** Steric clash between binding of HPF and that of mRNA and tRNA. Figure includes the structure and highlighted view of the HPF (green) bound to the ribosome with superimposed mRNA (dark green) and tRNAs in A-site (red), P-site (blue) and E-site (orange). Highlighted view has the ribosome omitted for clarity of view. [Figure adapted from Polikanov et al., 2012]

Though HPF_{Ec} mediates its role in hibernation by dimerization of 70S ribosome into 100S, essentially with the help of RMF, it can also bind to the 70S ribosome independently without the simultaneous binding of RMF [Ueta et al., 2008]. Previous studies have demonstrated the presence of such HPF-bound 70S ribosome in *E.coli* cells, when the stationary phase cells are transferred into fresh medium and the 100S ribosomal structures are monomerized. These

HPF-bound ribosomal particles are also found in the stationary phase itself, albeit at a lower level compared to the presence of 100S ribosome in *E.coli* (**Figure 1A** and **1B**) [Maki et al., 2000].

In *E.coli*, the concerted action of RMF (**Figure 2Ai**) and HPF (**Figure 2Aii**) under nutrient deprivation conditions, leads to the formation of 100S ribosome (100S_{Ec}) (**Figure 2Aiii**) and these dimers are only encountered during the late stationary phase. It not only maintains the ribosome in a translationally inactive form, but is also believed to prevent rapid ribosomal turnover under unfavourable conditions. Such a pool of dimeric ribosomes can act as a reservoir of ribosome which can be disassembled and recycled for translation when the conditions return to favourable and are conducive to bacterial growth [Gohara et al., 2018]. The precise role of ribosome dimerization is however unclear and whether the maintenance of the ribosome in its translationally inactivated state can provide further assistance to the bacteria in combating stress conditions is yet to be deciphered [Gohara et al., 2018].

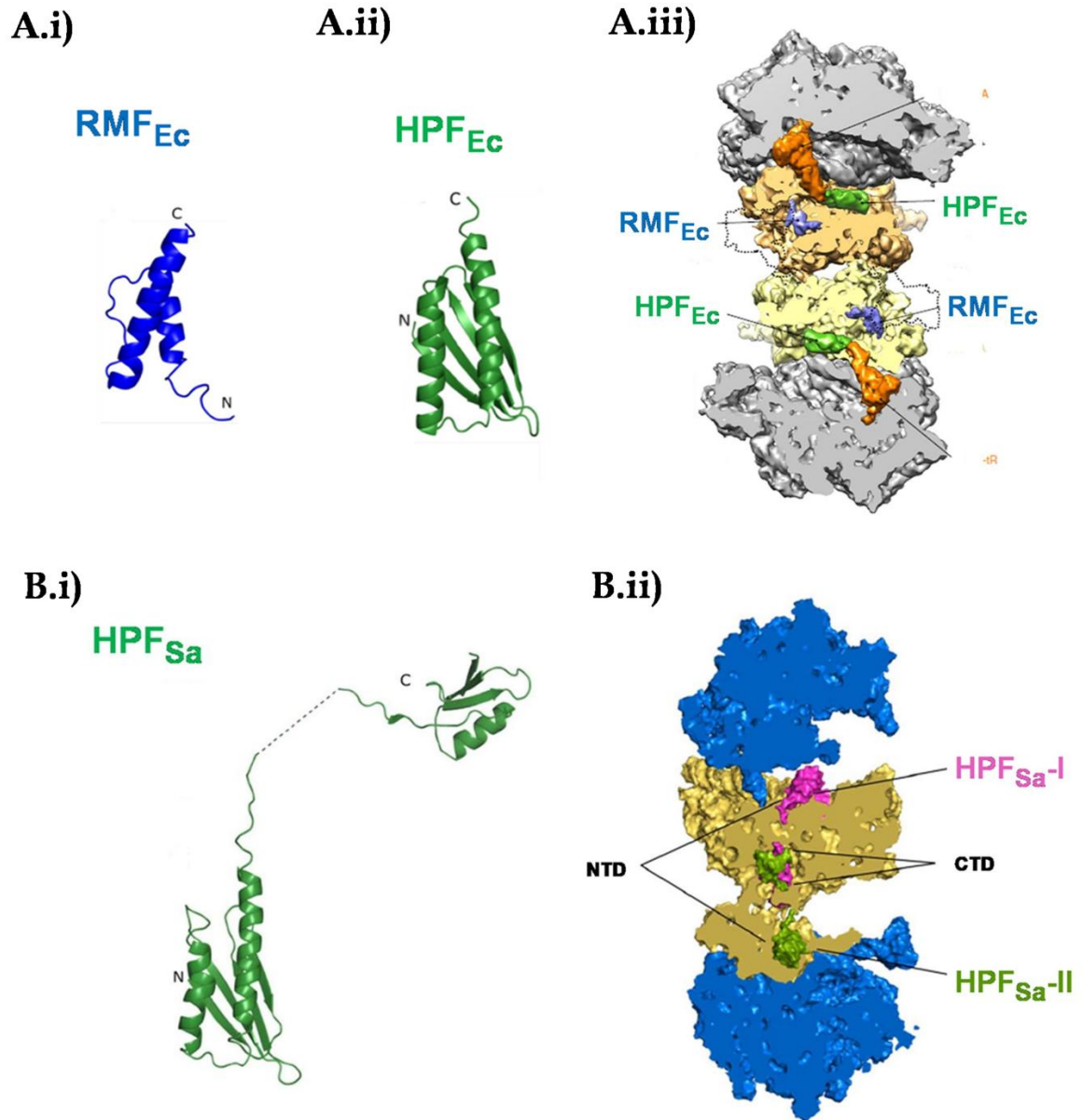


Figure 2: Structural representations of stationary phase factors or hibernation promoting factors and the dimeric 100S ribosome

A. (i) Structure of Ribosome Modulation Factor (RMF_{Ec}) from *Escherichia coli* [Figure adapted from Usachev et al., 2020] (ii) Structure of Hibernation Promoting Factor (HPF_{Ec}) from *Escherichia coli* [Figure adapted from Usachev et al., 2020] (iii) Cryo-EM structure (Transverse section) of *E.coli* 100S ribosome (PDB ID: 6H58; EMD-0139) with highlighted binding positions of HPF_{Ec} (green), RMF_{Ec} (blue), E-site tRNA (orange). 50S subunits of both ribosomes are depicted in grey while the 30S subunit of one ribosome is depicted in tan and that of the other ribosome is depicted in yellow [Figure adapted from Beckert et al., 2018]. **B.** (i) Structure of long form of Hibernation promoting Factor (HPF_{Sa}) from *Staphylococcus aureus* [Figure adapted from Usachev et al., 2020]. (ii) Sliced view of the *S.aureus* 100S ribosome (PDB ID: 6FXC; EMD 3638) indicating the position and interaction of two HPF_{Sa} molecules, each of which is composed of an N-terminal domain (NTD) with residues 1-95 and a C-terminal domain (CTD) with residues 130-190. These are connected by a flexible linker of 30-35 residues. HPF_{Sa} interact via their CTDs at the 30S/30S interface [Figure adapted from Gohara et al., 2018]

In contrast to *E. coli*, the 100S ribosome formation in the clinically important gram-positive bacterium *Staphylococcus aureus* (100S_{Sa}) is mediated by the long form of HPF (HPF_{Sa}) (**Figure 2Bi**) and such dimeric 100S_{Sa} ribosomes (**Figure 2Bii**) are present in all growth phases even when the nutrients are abundant [Prossliner et al., 2018, Basu et al., 2016, Ueta et al., 2010, Ueta et al., 2013]. HPF_{Sa} has two structured domains. The N-terminal domain (NTD), composed of residues 1-95 [Gohara et al., 2018], binds near the A- site and P-site of the 70S ribosome. The C-terminal domain (CTD), composed of residues 130-190 [Gohara et al., 2018], extends out of the ribosome and is responsible for mediating dimerization [Usachev et al., 2020]. The NTD and CTD are connected by a flexible and unstructured linker region of 30-35 residues [Gohara et al., 2018, Usachev et al., 2020] (**Figure 2Bi**). The NTD of HPF_{Sa} has functions analogous to short form of HPF (found in *E.coli*, HPF_{Ec}) and this domain anchors the factor to the ribosome. The protruded CTD recruits another 70S ribosome and mediates the dimerization [Usachev et al., 2020] (**Figure 2Bi** and **2Bii**). Thus, unlike HPF_{Ec}, HPF_{Sa} contains a C-terminal extension and can mediate the dimerization into 100S on its own. A model based on recent studies proposed that HPF_{Sa} in its free form exists as a dimer and this dimer binds to the 70S ribosome suppressing protein synthesis. This complex recruits another 70S to form the 100S dimer, which can exist even during their exponential phase of growth (**Figure 3**). This HPF_{Sa} bound 70S ribosome constitutes a distinct group of hibernating 70S ribosomes that can exist alongside the 100S_{Sa} dimers [Prossliner et al., 2018]. The presence of such translationally silent ribosome in the exponential phase of growth is a curious phenomenon. However, the HPF_{Sa} knock-out in *Staphylococcus aureus* leads to attenuated virulence of the microorganisms and causes ribosome breakdown upon entering the stationary phase that correlates with the onset of cell death [Basu et al., 2018].

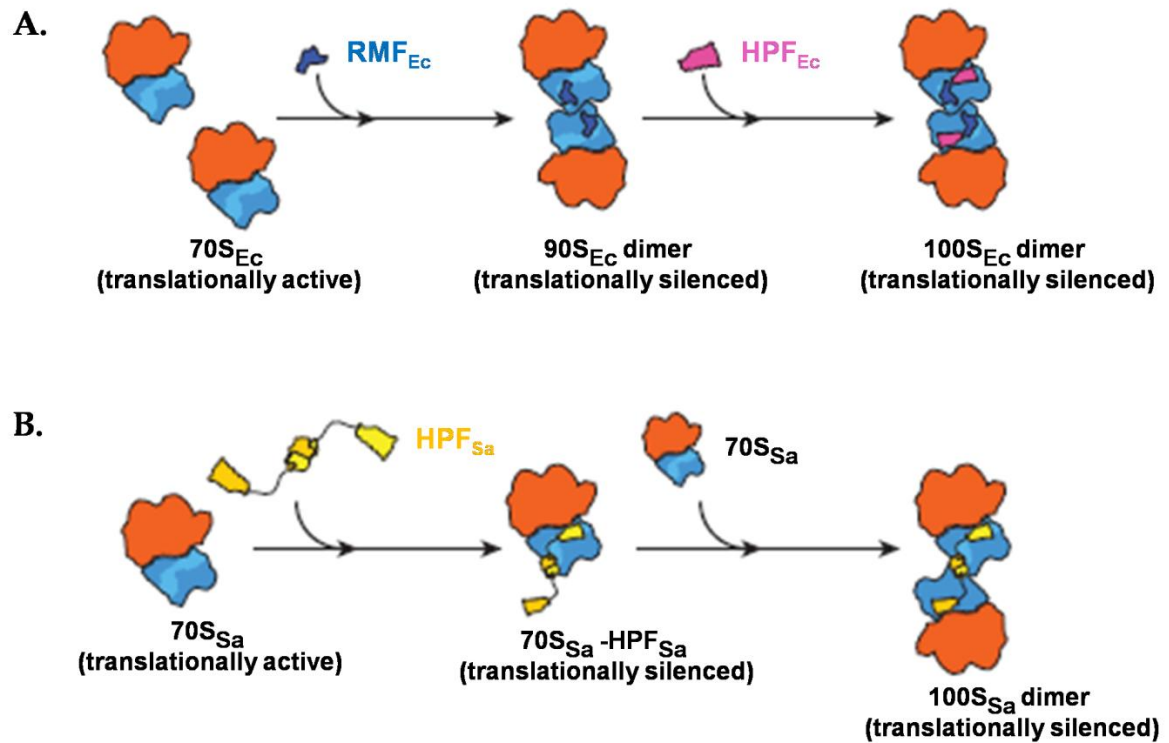


Figure 3: Formation of 100S ribosome in *Escherichia coli* and *Staphylococcus aureus*

A. In *E.coli*, 100S dimerization involves initial binding of Ribosome Modulation Factor (RMF_{Ec}) to 70S ribosomes in order to transiently dimerize them into the translationally silent 90S dimers. Subsequent binding of HPF_{Ec} results in maturation of 90S into 100S dimers. **B.** In *S.aureus*, a single long form of Hibernation Promoting Factor (HPF_{Sa}) dimerizes the ribosomes. HPF_{Sa} exists as a dimer which binds to 70S ribosome and inhibits translation. Another 70S ribosome is recruited by this complex to complete the formation of the 100S dimer [Figure adapted from Prossliner et al., 2018]

Recent studies have confirmed that in both *E.coli* and *S. aureus*, the formation of the 100S ribosome is essential for long-term cell viability and stress tolerance [Gohara et al., 2018, Yamagishi et al., 1993, Basu et al., 2016]. The actively translating ribosomes in *E. coli* are stable under normal growth conditions. However, under adverse conditions like starvation, the cellular ribosomes become prone towards degradation and such ribosomal metabolism might be expensive for growing cells [Deutscher, 2003, Deutscher, 2006, Deutscher, 2009, Piir et al., 2011]. It has been suggested that (as stated above), the resistance of the translationally silent ribosomes towards degradation or a possible biological role of the hibernating ribosomes, could contribute to the increased viability associated with their formation [Gohara et al., 2018].

In the cellular context, the dissociation of the ribosomal subunits is enabled by translation factors like Ribosome Recycling Factor (RRF) as discussed in Chapter 1. Ribosome subunit dissociation activity is relevant in three cellular contexts: (i) to conduct the recycling of ribosomal subunits, which is necessary in protein synthesis and is enabled by RRF-EFG-GTP [Kiel et al., 2007] (ii) to recycle stalled ribosomal complexes and hibernating ribosomes that have been formed under stress conditions and is mediated by the factor HflX in concert with GTP hydrolysis [Zhang et al., 2015] (iii) to lead to the accumulation of the pool of dissociated subunits in the cytosol under stress conditions, which increases the vulnerability of ribosomes towards degradation [Piir et al., 2011]. Previous studies in our laboratory have shown that chemically denatured proteins (uBCAII) and intrinsically unfolded proteins (HYPK) are capable of inducing ribosome dissociation [Pathak et al., 2017]. These studies imply that the unfolded protein present in the cell, irrespective of its identity, has the ability to dissociate the ribosome, thereby creating a pool of isolated subunits. The sustained pool of dissociated ribosomal subunits formed due to interaction between unfolded protein and the ribosome can make the subunits prone to degradation by cellular nucleases and such a phenomenon could influence the ribosomal metabolism [Piir et al., 2011, Zundel et al., 2009]. Earlier studies also demonstrated that the unfolded protein possesses 50S subunit based anti-association activity and the sustained physical association of uBCAII with the 50S subunit formed the basis of this anti-association activity [Pathak et al., 2017]. Under nutrient-deprivation conditions of the stationary phase, ATP levels are low [Tran et al., 1998] and there is a rise in the global unfolding of the proteome [Walter et al., 2002]. Hence, it is probable that under such circumstances, the ATP-independent mode of sustained ribosomal dissociation, mediated by the high concentration of accumulating unfolded protein population, can be detrimental for cellular ribosome due to the consequences discussed above. Viewed from the perspective that ribosome biosynthesis is an energetically expensive cellular process, inhibiting such ribosome degradation and preservation of the ribosome under stress conditions would be crucial for cell survival.

Further as discussed in Chapter 1, a network of chaperones inside the cell is involved in the maintenance of an active cellular proteome, a majority of which rely on ATP-hydrolysis for their activity [Pechmann et al., 2013]. However, under stress conditions, especially nutrient starvation during stationary phase, a significant depletion of ATP would render all ATP-dependent chaperoning activity ineffective. Extensive studies have indicated that even though the process of translation is the primary function of the ribosome, it also possesses a non-canonical chaperoning activity [Das et al., 2008]. Earlier studies in the laboratory have demonstrated that a P-site tRNA bound ribosome is inactive as a chaperone [Mondal et al., 2014]. This study implied that a clear demarcation might exist between the active translating ribosomal population and the empty or translationally hibernating ribosomal population, which might still be available for chaperoning function. The chaperoning activity of the prokaryotic ribosome resides in the domain V of the 23S rRNA in the 50S ribosomal subunit [Das et al., 2008]. Since the binding site of HPF and RMF on the *E.coli* ribosome lies in the 30S subunit [Polikanov et al., 2012], it is possible that such translationally inactive ribosome would retain its chaperoning function. Under stress conditions, considering the large population of the ribosome present in the cells (approximately 10^4 ribosomal particles inside an *E.coli* cell; obtained from <https://bionumbers.hms.harvard.edu/search.aspx>), the cell might benefit from such ATP-independent chaperoning ability of the hibernating ribosomes. Hence our studies discussed below are aimed at understanding (i) whether unfolded proteins have the ability to dissociate HPF-bound 70S ribosomes and the 100S ribosomes isolated from *E.coli* as well as *S.aureus* into their component subunits and thereby influence the subsequent degradation of the ribosome and (ii) whether the hibernating ribosomes (HPF bound *E.coli* 70S, *E.coli* 100S and *S.aureus* 100S) retain their chaperoning function.

Materials and Methods:

Reagents

The DreamTaq DNA polymerase and dNTPs were purchased from ThermoScientific™, Thermo Fisher Scientific. The primers, antibiotics kanamycin and blasticidine S(BLS), anti-prion drug 6-Aminophenanthridine (6AP), protein bovine carbonic anhydrase II (BCAII), Guanidine Hydrochloride (GuHCl), GTP as well as the chemicals used for preparing buffers were purchased from Sigma-Aldrich (St. Louis, MO, USA). Genomic DNA isolation from *E.coli* MG1655 (for use as template in PCR) and 70S_{Ec} ribosome purification from *E.coli* MRE600 cells were performed as reported earlier [Das et al., 1996, Mondal et al., 2014, Pathak et al., 2014]. Ni²⁺-NTA agarose was purchased from QIAGEN. 100S_{Ec} ribosomes were prepared from the *E. coli* BW25113Δ*yfiA* cells which were purchased from the Keio Knockout Collection of the Coli Genetic Stock Centre (CGSC), Yale University, USA [Baba et al., 2006]. 70S_{Sa} and 100S_{Sa} ribosomes were isolated from *S. aureus* MTCC 3160 cells obtained from Microbial Type Culture Collection and Gene Bank, MTCC, CSIR Institute of Microbial Technology, Chandigarh, India. The Luria Broth (LB), Tryptic Soy Broth (TSB) and skimmed milk powder were purchased from Himedia Laboratories Pvt. Limited, India. DNase I (RNase-free) enzyme was purchased from Fermentas, Thermo Fisher Scientific. Amicon Ultra centrifugal filters, Polyvinylidene difluoride (PVDF) membrane and Immobilon western chemiluminescence horse radish peroxidase (HRP) substrate were purchased from Millipore (Billerica, MA, USA). Zeba™ Spin desalting columns were purchased from ThermoScientific™, Thermo Fisher Scientific. CAII rabbit polyclonal IgG, His-probe rabbit polyclonal IgG and goat anti-rabbit IgG-HRP secondary antibodies were purchased from Santa Cruz Biotechnology (Dallas, TX, USA). All other chemicals were local products of analytical grade. Experimental data analysis was performed using OriginPro 8

(OriginLab Corp., Northampton, MA, USA) and SIGMAPLOT 13 (Systat Software Inc., San Jose, CA, USA) software. Structural illustrations have been made using PYMOL 2008 (De Lano Scientific, Palo Alto, CA, USA).

Cloning and Purification of HPF:

The DNA corresponding to the stationary phase factor HPF was PCR amplified using *E. coli* genomic DNA, extracted from *E. coli* (MG1655) cells, as template, DreamTaq DNA Polymerase and appropriate primers. The PCR amplified products were cloned into the pET-28a (+) (NOVAGEN, Merck-Millipore) expression vector. The gene now contained a T7 promoter upstream of a ribosome binding site with the “epsilon sequence” originating from bacteriophage T7 promoter, followed by a Shine–Dalgarno sequence. The *E. coli* BL21 (DE3) cells, transformed with the recombinant plasmids, were grown in the presence of kanamycin (50 µg/ml) for 7 hours without induction. The induction step was avoided as it resulted in significant loss in cell mass. The cells were harvested by centrifugation at 11,400 g for 6 minutes at 4 °C. Cell pellet was washed using wash buffer containing 20 mM Tris-HCl (pH 7.5), 10 mM Mg(OAc)₂, 100 mM NH₄Cl and 5 mM β-mercaptoethanol and disrupted by sonication. Cell debris was pelleted by centrifugation for 45 minutes at 17,100 g. The supernatant was loaded on a Ni⁺²-NTA affinity flow column and eluted with a linear gradient of imidazole (50–200 mM) in wash buffer (50 mM Phosphate buffer pH 8, 300 mM NaCl with different amounts of imidazole) [Pathak et al., 2014 with minor modifications]. Eluted fractions (corresponding to different imidazole washes) were subjected to SDS-PAGE with appropriate protein ladder. Selected fractions corresponding to HPF were pooled separately, subjected to centrifugal ultrafiltration using Amicon Ultra 3 KDa molecular weight cut-off filters and protein concentration was estimated by measuring the absorbance at 280 nm. The residual imidazole from the protein was removed using 7 KDa desalting

column. The purification of HflX protein was performed as reported earlier [Dey et al., 2018].

Purification and enrichment of 70S and 100S ribosomes:

Ribosomes used in this study were purified from both *E. coli* (gram-negative bacteria) and *S. aureus* (gram-positive bacteria). The *E. coli* 70S_{Ec} ribosome was purified from MRE600 cells [Das et al., 1996] and the purification was performed as reported earlier (described in detail in Chapter 4 “General Materials and Methods”). The *E. coli* 100S_{Ec} ribosome was purified from the BW25113 Δ *yfiA* cells and the purification was performed as reported earlier with minor modifications [Beckert et al., 2018]. *E. coli* BW25113 Δ *yfiA* cells were grown in M9 minimal media (33.7 mM Na₂HPO₄, 22 mM KH₂PO₄, 8.55 mM NaCl, 9.35 mM NH₄Cl, 1 mM MgSO₄, 0.3 mM CaCl₂ complemented with 0.4% D-glucose) for 33 hours [Beckert et al., 2018] and then allowed to cool to 4 °C to produce run-off ribosomes. The cells were then harvested in B100S buffer [25 mM HEPES-KOH pH 7.5, 100 mM KOAc, 15 mM Mg(OAc)₂, 1 mM DTT] through centrifugation at 5000 g for 15 minutes at 4 °C. The frozen cells were resuspended in B100S buffer containing 2 µg/ml DNase I and lysed using the French Pressure cell. The cell lysate was cleared of debris by centrifuging the suspension twice at 12000 g for 30 minutes in a Sigma 12158-H rotor. The crude ribosome was pelleted through a 25% w/v sucrose cushion (in B100S buffer supplemented with 0.01% Triton-X-100) by centrifugation at 2,88,350 g for 4 hours (using Beckman Ti70 rotor). The pellet was resuspended in B100S buffer [Beckert et al., 2018]. The 100S_{Ec} ribosomes were next enriched by loading on a 10-60% sucrose gradient in Buffer G (10 mM Tris-HCl pH 7.5, 50 mM KCl, 10 mM NH₄Cl, 25 mM MgCl₂) and centrifugation at 1,55,000 g for 3 hours in a MLS 50 rotor (Beckmann Coulter Life sciences, Indianapolis, IN, USA) [Beckert et al., 2017, Khusainov et al., 2017 with minor modifications]. The gradient was monitored at 260 nm and appropriate fractions containing the 100S_{Ec} particles were pooled. Sucrose was removed from

the pooled fractions using Amicon Ultra 10 KDa filters and the fractions were concentrated using the same Buffer G with 25 mM MgCl₂ (10 mM Tris-HCl pH 7.5, 50 mM KCl, 10 mM NH₄Cl and 25 mM MgCl₂) [Beckert et al., 2017, Khusainov et al., 2017 with minor modifications] at 4 °C. These concentrated fractions were subjected to repeated rounds of such centrifugation until substantially purified and enriched fractions of 100S_{Ec} ribosome were obtained. These were stored at -80 °C until further use.

In case of *S. aureus*, both 70S_{Sa} and 100S_{Sa} ribosomes were purified and enriched using similar method as that for 100S_{Ec}. *S. aureus* MTCC 3160 cells were grown in TSB media for 4 hours [Ueta et al., 2010, with minor modifications] and the cells were harvested in the same manner as described earlier. The subsequent steps used were identical to those used for 100S_{Ec} purification. In this case, during enrichment, appropriate fractions for both 70S_{Sa} and 100S_{Sa} particles were pooled and processed in a similar manner to obtain enriched and purified 70S_{Sa} and 100S_{Sa} particles, which were stored at -80 °C until further use.

Ribosome-HPF complex preparation

Ribosome-bound HPF complexes were prepared by incubating 0.1 or 0.3 μM ribosome (70S_{Ec}-free) with different stoichiometric concentrations of HPF (1x, 3x and 10x, x = 0.1 μM or 0.3 μM, as indicated in the figure legends) in HPF binding buffer (5 mM Tris-HCl pH 7.5, 50 mM KCl, 10 mM NH₄Cl, 7.5 or 10 mM MgCl₂ as indicated in figure legends) at 37 °C for 30 minutes with a final binding volume of 50 μl or 80 μl [Basu et al., 2016]. After incubation, 150 μl (for light scattering studies) or 220 μl (for refolding assay) of BCAII refolding buffer or Buffer G was added to the reaction mixture and then these HPF bound ribosome complexes were used for BCAII reactivation as well as ribosomal subunit dissociation studies. For dissociation studies, the MgCl₂ concentration was 7.5 mM in HPF binding buffer, refolding buffer and Buffer G. However, for dissociation of HPF bound 70S_{Ec} in 1 mM

MgCl₂, the binding of the factors with 70S_{Ec} was performed in HPF binding buffer with 7.5 mM MgCl₂ (binding volume: 50 µl) as described above, and then added to refolding buffer with 1 mM MgCl₂ (150 µl). The reaction mixture was analyzed both by Sucrose density gradient centrifugation (SDGC) and light scattering analysis. For SDGC, the reaction mixture was incubated for 300 seconds and layered on a 17-25% sucrose density gradient prepared in refolding buffer with 1 mM MgCl₂. For light scattering studies, the change in light scattering intensity at 350 nm of the reaction mixture was immediately measured for a period of 300 seconds. The complexes were also used for refolding studies where recovery of enzymatic activity was assayed by adding 500 mM para-nitro-phenyl acetate (PNPA) to the refolding mixture and measuring the increase in absorbance of PNP (para-nitro-phenol) at 420 nm over a period of 120 seconds [Mondal et al., 2014].

Ribosome–antibiotic complex preparation

Ribosome-bound antibiotic complexes were prepared by incubating 0.3 µM ribosome (either 70S_{Ec}-free or A_{260 nm} units equivalent concentration of 100S_{Ec} or 70S_{Ec}-HPF) with different stoichiometric concentrations of BLS (0-10 µM, as indicated in the figure legends) in BLS binding buffer (100 mM Tris-HCl pH 7.2, 10 mM MgCl₂, 100 mM NH₄Cl pH 7.2, 6 mM β-mercaptoethanol), at 37 °C for 20 min, then at 20 °C for 15 min and finally kept on ice for 5 min [Mondal et al., 2014]. The final volume for binding was maintained at 50-100 µl (50 µl for empty ribosomes and 100 µl for factor-bound ribosomes). After incubation, 250-200 µl of BCaII refolding buffer (50 mM Tris-HCl pH 7.5, 100 mM NaCl and specified concentrations of MgCl₂) [Mondal et al., 2014, Pathak et al., 2014] or Buffer G (10 mM Tris-HCl pH 7.5, 50 mM KCl, 10 mM NH₄Cl and specified concentrations of MgCl₂) (as indicated in the figure legends) [Khusainov et al., 2017 with minor modifications] was added to the mix, and then, these ribosome-bound antibiotic complexes were used for BCaII reactivation studies.

Ribosome-6AP complex preparation

Ribosome-bound 6AP complexes were prepared by incubating 0.1 or 0.3 μM ribosome (either 70S_{Ec}-free or A_{260 nm} units equivalent concentration of 100S_{Ec} or 70S_{Ec}-HPF) with different stoichiometric concentrations of 6AP (100-500 μM , as indicated in the figure legends) in refolding buffer (50 mM Tris-HCl pH 7.5, 100 mM NaCl, 7.5 mM MgCl₂; for 70S_{Ec} or HPF bound 70S_{Ec}) [Mondal et al., 2014, Pathak et al., 2014] or in Buffer G (10 mM Tris-HCl pH 7.5, 50 mM KCl, 10 mM NH₄Cl, 7.5 mM MgCl₂, 1 mM DTT; for 100S_{Ec}) [Khusainov et al., 2017 with minor modifications] at 29°C for 10 minutes [Dos Reis et al., 2011]. The final volume of binding was maintained at 50 μl . After incubation, 250 μL of BCAII refolding buffer or Buffer G (as indicated in the figure legends) was added to the reaction mixture and then these ribosome complexes were used for BCAII reactivation studies.

Unfolding and refolding studies of BCAII

BCAII was unfolded with 6 M GuHCl in the presence of 3.5 mM EDTA for 3 hours, refolded in BCAII refolding buffer or Buffer G (as indicated in the figure legends), and recovery of enzymatic activity was assayed as described earlier [Basu et al., 2008, Pathak et al., 2017]. BCAII (Sigma Aldrich) (30 μM) was denatured to equilibrium with 6 M GuHCl and 3.5 mM EDTA at 29 °C for 3 hours and refolding was initiated by 100-fold dilution in refolding buffer in presence of equimolar concentration of chaperone. The volume of the refolding mix was 300 μl . BCAII and the ribosome (or its complexes) were each present at concentration of 0.3 μM (or A_{260 nm} units equivalent to 0.3 μM). The refolding mix was incubated at 29 °C for a period of 30 minutes as reported earlier [Pal et al., 1999, Mondal et al., 2014, Pathak et al., 2014]. Recovery of enzymatic activity was assayed by adding 500 mM PNPA to the refolding mixture and measuring the increase in absorbance of PNP at 420 nm with time

(over a period of 120 seconds) [Pal et al., 1999, Mondal et al., 2014, Pathak et al., 2014]. Control experiments were performed in which BCAII was allowed to refold, in absence of any chaperone under the various buffer conditions stated in figure legends. The results obtained are referred to as 'uBCAII self' in this study. The refolding of BCAII was unaffected under the conditions used in our studies. The refolding of 0.3 μM uBCAII was performed in the presence and absence of 0.3 μM 70S_{Ec}-free, 70S_{Ec} bound to the antibiotic BLS (present in different concentrations of 0-10 μM , as indicated in figure legends) [Mondal et al. 2014]. Similar refolding studies were also performed in the presence and absence of 70S_{Ec} bound to stationary phase factor HPF, 70S_{Ec} bound to both, the factor and BLS, 70S_{Ec} bound to 6-AP (present in different concentrations of 0-500 μM) [Dos Reis et al., 2011] and 70S_{Ec} bound to both the factor and 6AP. Refolding studies with 0.3 μM uBCAII were also performed with A_{260 nm} units equivalent of 0.3 μM of 100S_{Ec} as well as 70S_{Sa} and 100S_{Sa}. Care was taken to ensure that in each case control experiment of unassisted (self) folding and the 70S_{Ec}-free or 70S_{Sa}-free ribosome-assisted folding was performed under the same salt and buffer conditions. Control experiments were also performed to ensure that the factors or antibiotics themselves do not affect self-folding of BCAII under the conditions used in our study. Aggregation of mBCAII (0.9 μM) was monitored by turbidity measurements in Hitachi Spectrophotometer (U-1900). The effect of 70S_{Ec}-free (0.9 μM), HPF (9 μM) bound 70S_{Ec} (HPF in 10-fold excess concentration of that used for ribosome), 100S_{Ec} (0.9 μM equivalent A_{260 nm} units), 70S_{Sa}-free (0.9 μM equivalent A_{260 nm} units) and 100S_{Sa} (0.9 μM equivalent A_{260 nm} units) on mBCAII (molten globule form of BCAII) aggregation was monitored at 450 nm over a period of 1200 seconds [Pathak et al., 2014].

Aggregation of reduced-denatured lysozyme

Lysozyme (2 μM) was reduced and denatured (R/D Lyso) for 3 hours at room temperature using 6 M GuHCl and 100 mM DTT [Pathak et al., 2014]. Aggregation of R/D Lyso (2 μM)

was monitored by turbidity measurements in Hitachi Spectrophotometer (U-1900). The effect of 70S_{Ec}-free (2 μM), HPF (20 μM) bound 70S_{Ec} (HPF in 10-fold excess concentration of that used for ribosome) and 100S_{Ec} (A_{260 nm} units equivalent of 2 μM) on R/D Lyso was monitored at 450 nm over a period of 720 seconds [Pathak et al., 2014].

Dissociation of ribosomal subunits: Light scattering studies

Dissociation of 70S_{Ec}-free or 70S_{Ec} ribosome bound to stationary phase factor HPF or 100S_{Ec} ribosomes in the presence of unfolded proteins or HflX was measured by following ribosomal light scattering (Hitachi F-2700 fluorescence spectrophotometer, Tokyo, Japan; excitation: 5 mm slit; emission: 5 mm slit; wavelength at 350 nm at 90° angle) at a temperature of 16 °C. Buffers used for 70S_{Ec} and 100S_{Ec} dissociation were Refolding Buffer (50 mM Tris-HCl pH 7.5, 100 mM NaCl, MgCl₂ concentration was 7.5 mM or as stated in the figure legends) and Buffer G (10 mM Tris-HCl pH 7.5, 50 mM KCl, 10 mM NH₄Cl, 7.5 mM MgCl₂, 1 mM DTT) respectively; unfolded BCAII or HflX was mixed in stoichiometric amounts as specified in the figure legends. For studies with HflX, 1 μM HflX was incubated with 100 μM GTP for 30 seconds in Buffer G with 7.5 mM MgCl₂ at room temperature [Coatham et al., 2016 with minor modifications]. 0.1 μM 70S_{Ec}-free, or the 70S_{Ec} ribosome (0.1 μM) pre-bound to factors (1 μM) or equivalent A_{260 nm} units of 100S_{Ec} was rapidly added to the mixture and the change in light scattering intensity was measured at 350 nm for 300 seconds. For studies with uBCAII, 0.1 μM 70S_{Ec}-free or the 70S_{Ec} ribosome (0.1 μM) pre-bound to factors (1 μM) or the 100S_{Ec} (A_{260 nm} units equivalent to 0.1 μM) ribosome was added first to the reaction mixture followed by rapid addition of uBCAII and the change in light scattering intensity was measured at 350 nm for 300 seconds. Conditions used for light scattering studies were followed as reported previously [Pathak et al., 2017]. Similar studies were also performed with 70S_{Sa}-free and 100S_{Sa} ribosomes where dissociation of the subunits

in the presence of uBCAII was measured under similar experimental conditions as stated above.

Sucrose density gradient centrifugation

0.5 μM uBCAII was incubated with 0.1 μM of 70S_{Ec}-free or 100S_{Ec} ribosome (0.1 μM equivalent $A_{260\text{ nm}}$ units) or similar concentrations of 70S_{Ec} bound to HPF (1 μM) in Refolding buffer or Buffer G (with 7.5 mM MgCl₂) for 5 min. After incubation, 100 μl of reaction mixtures was applied on 5 ml of a 17–25% sucrose gradient (for 70S_{Ec}-free or HPF bound 70S_{Ec}) prepared in the Refolding buffer and 5 ml of 10-60% sucrose gradient (for 100S_{Ec}) prepared in Buffer G containing MgCl₂ concentrations as mentioned in the figure legends. Samples were centrifuged at 1,98,000 g for 2.5 hours at 4 °C for 70S_{Ec}-free and HPF bound 70S_{Ec}. Samples were centrifuged at 1,55,000 g for 3 hours at 4°C for 100S_{Ec} [Beckert et al., 2017 with minor modifications]. The rotor used for ultracentrifugation of both gradients was MLS 50 (Beckman Coulter). Fractions were collected (200 μl or 100 μl as indicated in figure legends) from the top to the bottom of the tube and absorbance at 260 nm was measured using a UV-visible spectrophotometer. For studies with HflX, 1 μM HflX was incubated with 100 μM GTP for 30 seconds in Buffer G with 7.5 mM MgCl₂ at room temperature [Coatham et al., 2016 with minor modifications]. 0.1 μM 70S_{Ec}-free or equivalent $A_{260\text{ nm}}$ units of 100S_{Ec} was rapidly added to the mixture and layered on a 10-60% sucrose density gradient and the subsequent steps followed were similar to as described above.

Ultrafiltration and dot blot analysis

100 μl of reaction mix containing 0.1 μM 70S_{Ec}-free or HPF bound 70S_{Ec} was incubated with uBCAII (0.5 μM) at 29°C for 10 min and then loaded on an Amicon Ultra 100 K filter. The column was washed thrice with one part of refolding buffer and three parts of HPF binding

buffer. The retained fraction was eluted by centrifuging the inverted column at 13,860 g for 2 minutes and used for dot blot. In the dot blot analysis, the PVDF membrane was soaked in methanol for 15 seconds followed by 1x PBST for 15 minutes before dotting the samples. Each sample was divided into two 20 μ l aliquots which were dotted on two separate PVDF membranes, and the membranes were allowed to dry for 1 hour at room temperature. The membranes were then blocked with 5% skimmed milk prepared in 1x PBST for 1 hour. One membrane was then incubated with primary antibody CAII rabbit polyclonal IgG; 1:5000 dilution for detecting bound BCAII. The other membrane was probed with His-probe rabbit polyclonal IgG; 1:1000 dilution for detecting bound HPF. Both membranes were incubated with the respective primary antibodies at 4 °C overnight. The membranes were then washed five to six times (15-min intervals) with 1x PBST and then incubated with secondary antibody (goat anti-rabbit IgG horseradish peroxidase-conjugated; 1:10,000 dilution) for 1.5 hours at room temperature. Then, the membranes were washed with 1x PBST five times and incubated with chemiluminescent horseradish peroxidase substrate and the signal was recorded using photographic plates [Pathak et al., 2017].

Preparation of cell-free extract

Escherichia coli MG1655 cells were grown, pelleted, and lysed using a French press as reported earlier [Zundel et al., 2009, with minor modifications]. The lysate was centrifuged at 8630 g for 20 minutes to remove the cell debris. The resulting supernatant was centrifuged at 1,40,992 g for 2 hours at 4 °C. The pellet was discarded, and the supernatant was again centrifuged for 3 hours at 4 °C, and the ribosome-deficient supernatant was stored at –80 °C [Pathak et al., 2017].

Ribosome degradation experiment

The binding of HPF to 70S_{Ec} was performed as described above, but with a 5-fold excess concentration of the factors and the ribosome. The bound complexes were then added to refolding buffer such that a 5-fold dilution occurs. Thus, the final concentrations of the factors and the ribosome were maintained at 1 μ M and 0.1 μ M respectively to which 0.5 μ M uBCAII was added such that the final reaction volume was 10 μ l. The reaction mixtures were incubated with 90 μ l of cell-free extract (prepared as stated above) for 90 min at 37 °C [Pathak et al., 2017, Zundel et al., 2009]. Following this, the reaction mixtures were loaded on to a 17–25% sucrose gradient (for the 70S_{Ec}-free and HPF bound 70S_{Ec} samples) in refolding buffer and on to a 10-60% sucrose gradient (for 100S_{Ec} samples) in Buffer G containing 7.5 mM MgCl₂. The fractions (200 μ l for the 17-25% gradient and 100 μ l for the 10-60% gradient) were collected from the top to the bottom, and absorbance values were measured at 260 nm using a UV-visible spectrophotometer.

Results and Discussion:

Section A

Effect of HPF on unfolded protein-ribosome interaction

As discussed in the “Introduction” section above, the unfolded protein, when present at a higher stoichiometric concentration with respect to the ribosome, acts as a 50S subunit anti-association factor [Pathak et al., 2017]. The stable ribosome subunit dissociation thus engendered can increase the susceptibility of the subunits towards degradation by cellular nucleases [Pirr et al., 2011, Zundel et al., 2009]. The imminent reduction in the ribosomal population would have a direct effect on cell viability. The question of preservation of ribosomal population in the face of elevating concentration of unfolded proteins under stressful circumstances therefore needs to be answered. As discussed in “Chapter 1”, the cell, under stress conditions synthesizes multiple protein factors, a few amongst which are ribosome hibernation factors [Starosta et al., 2014]. The *E.coli* Hibernation Promoting Factor (HPF_{Ec}) is one such factor which is expressed under the nutrient deficient conditions of the stationary phase and enables switching off of the translational function of the ribosome [Polikanov et al., 2012].

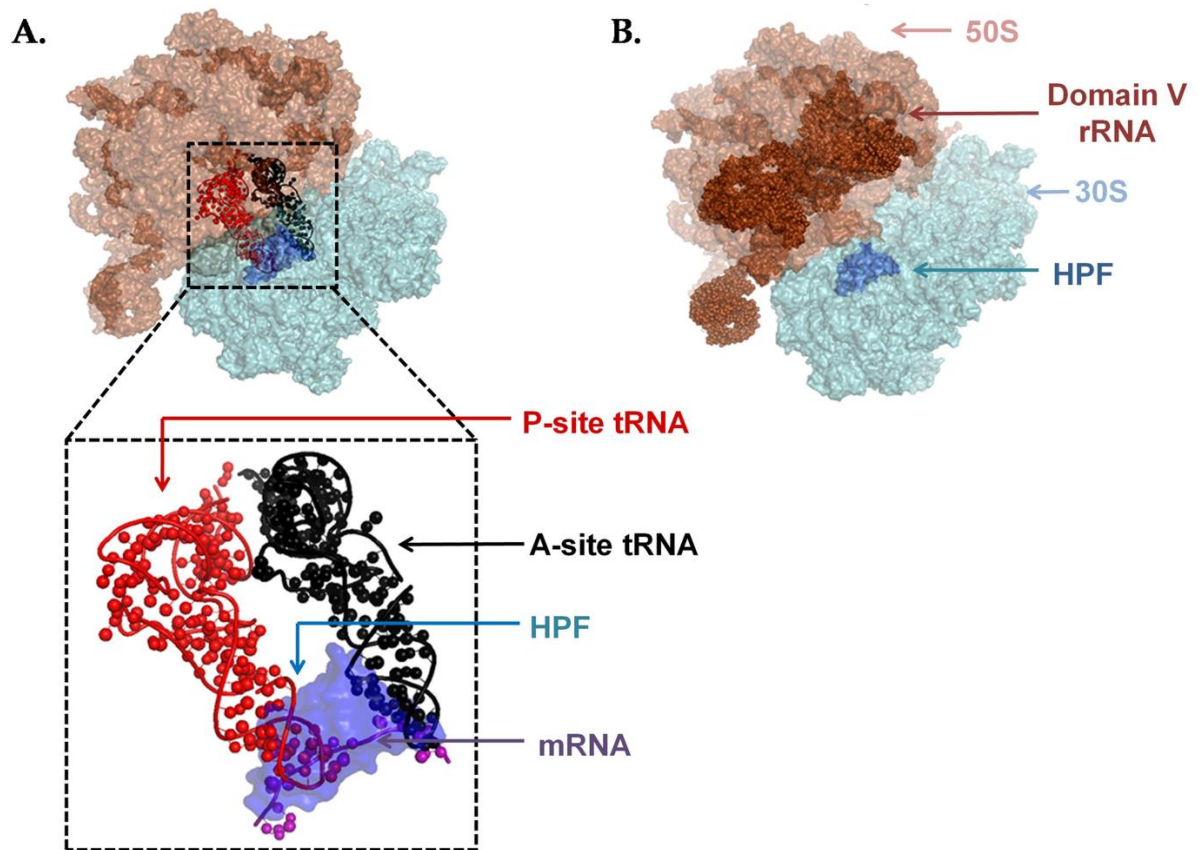


Figure 4: Structural representation of HPF binding to the 70S ribosome

Surface representation of HPF bound *T.thermophilus* ribosome (using PyMOL 2.4, PDB ID: 4V8H) highlighting **A**) the overlapping binding site of HPF with the P-site tRNA (Red), A-site tRNA (Black) and mRNA binding channel (Purple) and **B**) the domain V region (Dark red spheres) which remains unoccupied in HPF (Blue) bound ribosome. The 50S subunit is represented in light red and the 30S subunit is represented in light blue.

The **Figure 4A**, illustrates the mechanism of translation inhibition upon binding of HPF to the ribosome. The HPF binds to the 30S ribosomal subunit such that it inhibits the binding of A-site and P-site tRNA, as well as occludes the mRNA binding channel. The HPF bound ribosome, which is also observed in stationary phase *E.coli* cells (“Introduction” section of this chapter), thus constitutes a ribosomal population of translationally inactive 70S monosomes [Starosta et al., 2014].

It is to be noted that the chaperoning activity of the 70S ribosome resides in the domain V of 23S rRNA of the 50S ribosomal subunit [Das et al., 2008]. The **Figure 4B**, based on the structure of 70S ribosome bound to HPF protein [Polikanov et al., 2012], clearly shows that the HPF performs its role of translation inhibition through exclusive binding to the 30S subunit, thereby raising the possibility that the HPF bound 70S monosome would still be able to perform its non-canonical chaperoning function. Hence, studies were performed to investigate whether: a) the unfolded protein can bind to and dissociate the HPF bound ribosome and b) whether the HPF bound ribosome can retain chaperoning activity towards the unfolded proteins.

A1. Cloning, expression and purification of HPF

A.1.a. Cloning strategy of HPF

The objective of the initial studies was the cloning, expression and purification of recombinant *E.coli* HPF protein. Towards this objective, the *E.coli* genomic DNA was isolated from MG1655 cells according to the procedure described in the “Materials and Methods” section in this chapter and in chapter 4. The *hpf* gene was PCR amplified from the genomic DNA by using appropriate primers, designed according to the known gene sequence of the *hpf* gene present in *E. coli* genome, as shown in **Figure 5A**. The forward primer contained the recognition site for the restriction endonuclease enzyme BamHI and the reverse primer contained the recognition site for the enzyme HindIII, both of which were present in the multiple cloning site (MCS) of the vector in the required orientation. The PCR product obtained was analyzed on 1% agarose gel with EtBr (ethidium bromide) staining and a 1Kb DNA ladder was also run simultaneously on the same gel in order to verify the molecular weight of the obtained product (**Figure 5B**). The PCR product was thereafter purified and digested with BamHI and HindIII enzymes. The expression vector chosen for cloning the

E.coli hpf gene was pET28a (+) (**Figure 5C**), since it offers the advantage of inducible expression of the cloned insert gene, a kanamycin marker for screening of transformant bacterial colonies and inserts a 6X poly-histidine tag at the N-terminus of the recombinant protein that facilitates the affinity purification of the protein.

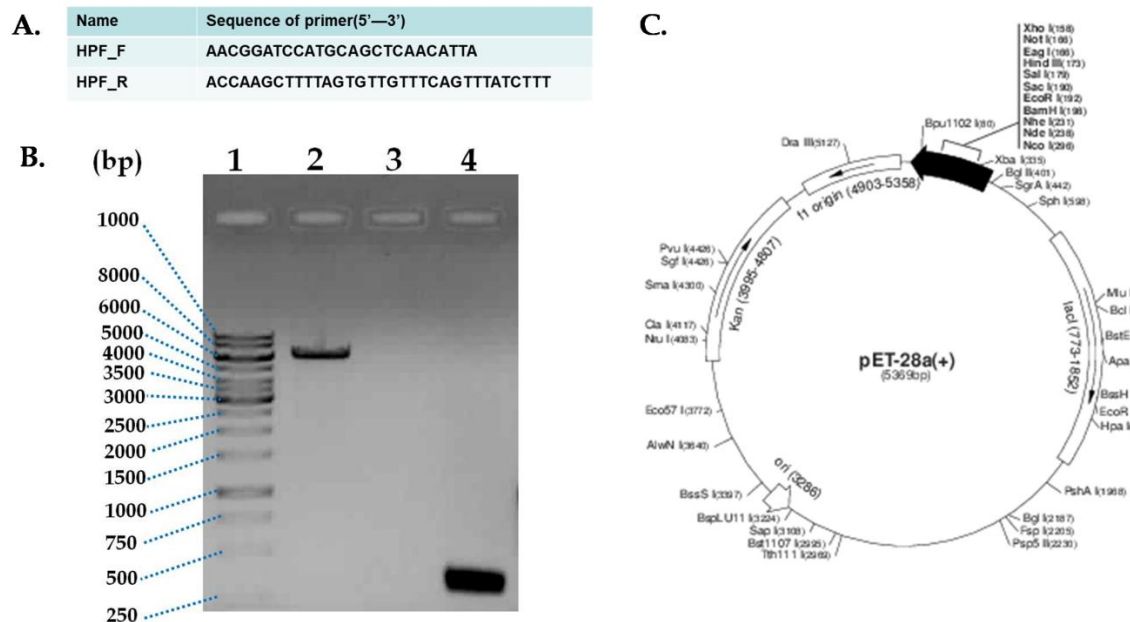


Figure 5: PCR amplification and cloning of *hpf* gene

A. Sequences of the forward (HPF_F) and reverse (HPF_R) primers used for the PCR amplification of *E.coli hpf* gene from the genomic DNA of *E.coli* MG1655 cells. **B.** Agarose gel electrophoretic analysis of the PCR product obtained. Lanes from left to right contain: 1- Molecular weight marker, 2-pET28a (+) vector, 3-Blank, 4- PCR product (*hpf*). **C.** Schematic representation of the vector map of pET28a (+) vector used for cloning the *hpf* gene.

The BamHI and HindIII enzymes were used to digest the pET28a (+) vector. The vector and inserts were ligated and the ligation mix was used to transform *E.coli* XL1-Blue competent cells and the transformants were selected on a kanamycin LB agar plate. The clones containing the insert in the appropriate site were identified after DNA isolation and digestion with the appropriate restriction enzymes. The recombinant vector containing the *hpf* gene

inserted in the BamHI-HindIII site of the pET28a (+) vector was purified as described in the section below.

A.1.b. Expression and purification of recombinant *E.coli* HPF

The recombinant plasmids [pET28a (+) with inserted *hpf* gene] were transformed into *E.coli* BL21(DE3) cells to check the expression of the protein upon induction by Isopropyl β -D-1-thiogalactopyranoside (IPTG) (1mM). The transformed cells were grown in small culture volumes as two separate sets and upon reaching mid log phase ($O.D_{600\text{ nm}}=0.6$), one of the cultures was induced using 1mM IPTG while the other was left uninduced. After induction for 4 hours, the cells were centrifuged at 11,400 g and 4 °C for 6 minutes. During the course of the incubation, the optical density (O.D) values at 600 nm (reflective of cellular growth and replication) were recorded at hourly intervals post IPTG induction for both induced and uninduced populations and plotted against time. As shown in **Figure 6Ai**, IPTG induced population showed no significant increase in the $O.D_{600\text{ nm}}$ with time, as compared to the uninduced population of cells. Upon comparing, the total cell pellet mass of the induced (I) and uninduced (U) population, after 4 hours of induction, also showed that mass of the induced (I) cell pellet was significantly lesser than that of the uninduced (U) cell pellet (**Figure 6Aii**). It was then realized that the overexpression of the translation inhibition factor HPF in the *E.coli* cells, could have resulted in the bacteriostatic effect observed above [Ueta et al., 2008, Prossliner et al., 2018, Basu et al., 2016].

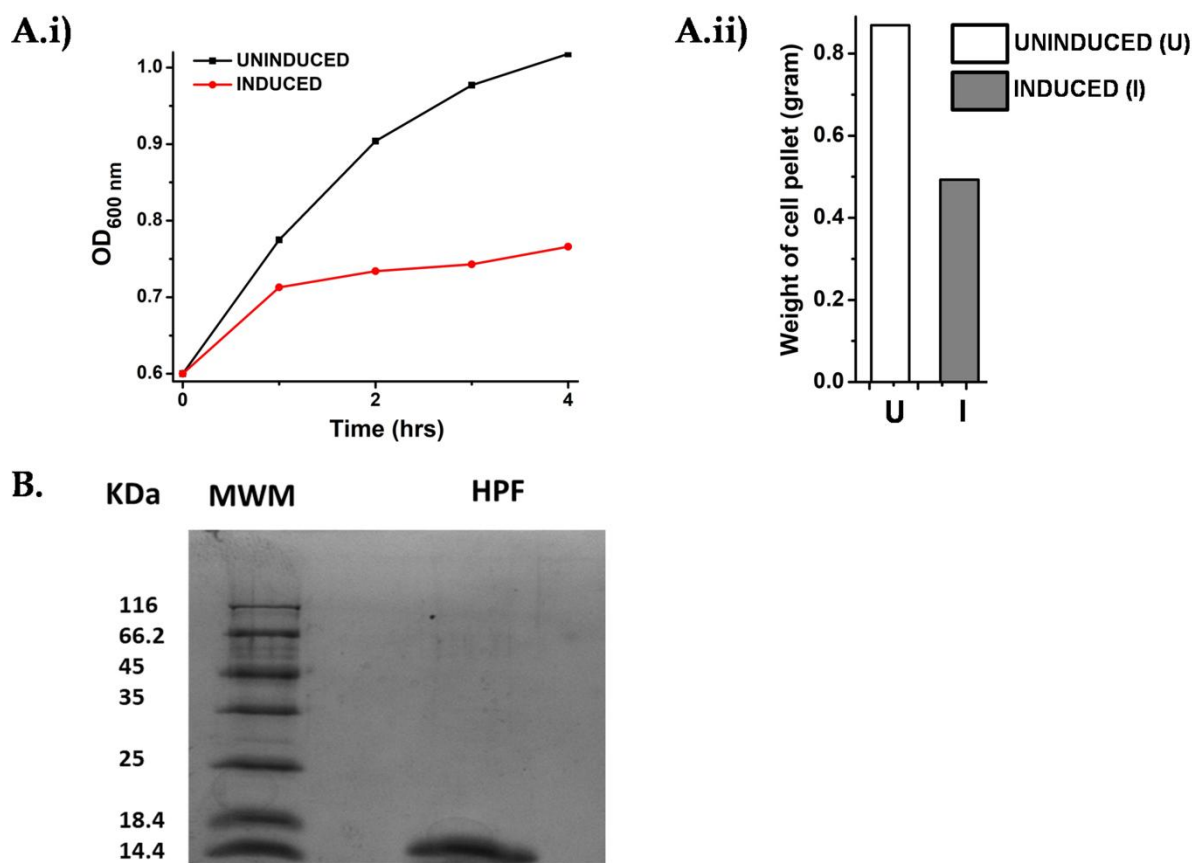


Figure 6: Comparison of cell growth between IPTG induced and uninduced cellular population:

A.i) Comparison of growth curve of the uninduced and induced cell cultures. The uninduced set shows a greater growth in cells over 4 hours, as compared to the induced set indicating at the toxic nature of the expressed protein. **ii)** Bar graph showing the difference in cell mass of the uninduced and induced cell cultures. The cell mass of the induced set (I) is significantly lesser than that of the cell mass of the uninduced set (U) indicating that the protein being expressed in the induced set is toxic and leading to cell death. **B.** A 12% SDS-PAGE analysis showing the band of a purified sample of HPF protein after final buffer exchange and concentration.

Subsequent studies however showed that low levels of leaky expression of the HPF protein is observed even without IPTG induction and hence we proceeded with the expression in the absence of any inducer. The transformed BL21(DE3) cells were thus grown in large cultures (3 litres) without induction for obtaining sufficient yield (68 μ M; 731 μ g/ml) and the HPF protein was purified using His-tag chromatography (“Materials and Methods” section of this chapter). An SDS-PAGE analysis of the final purified HPF protein that was used for performing further experiments has been included in **Figure 6B**.

A.2. Effect of hibernation promoting factor (HPF) on unfolded protein mediated ribosome subunit dissociation

Our next objective was to determine the effect of unfolded protein on the dissociation of the HPF bound 70S ribosome. The *E.coli* 70S ribosome ($70S_{Ec}$) ($x=0.1 \mu\text{M}$) was incubated with increasing concentrations of recombinant HPF protein (1x, 3x, 10x), under conditions mentioned in the “Materials and Methods” section. The ability of the guanidine hydrochloride denatured unfolded bovine carbonic anhydrase II (uBCAII) protein, when present at five-fold excess concentration [5x uBCAII ($x=0.1\mu\text{M}$)] with respect to the ribosome [1x ribosome ($x=0.1 \mu\text{M}$)], to dissociate the HPF associated 70S *E.coli* ribosome was followed by monitoring the time course of change in light scattering intensity at 350 nm. Monitoring the change in Rayleigh light scattering over time is a well-established technique used to study the association or dissociation of ribosomal subunits [Antoun et al., 2004]. An intact ribosome, being essentially larger in size compared to its component subunits, exhibits a higher intensity of light scattering at 350 nm [Basu et al., 2003]. Thus a time course change in light scattering can be measured as an indicator of ribosomal subunit dissociation. This method has been extensively used in literature [Goerisch et al., 1976 and Feng et al., 2014] as well as in the previous studies conducted in our laboratory [Pathak et al., 2017] to study ribosomal subunit dissociation.

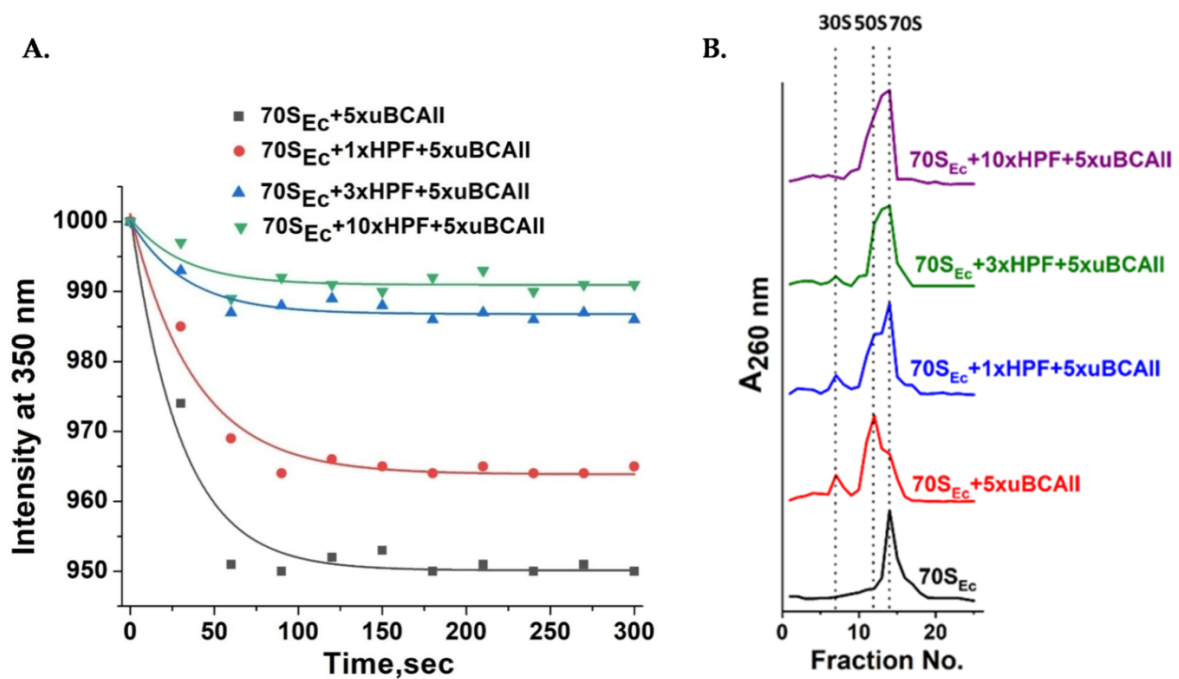


Figure 7: HPF-mediated inhibition of unfolded protein-mediated dissociation of 70S ribosome

A. Light scattering analysis of uBCAII-mediated 70S_{Ec} dissociation in presence of HPF: Time course change in light scattering intensity at 350 nm upon interaction of 70S_{Ec} ribosome (1x = 0.1 μM) with uBCAII (5x), in the presence of different stoichiometric concentrations of HPF. 70S_{Ec}+5x uBCAII (■), 70S_{Ec}+1x HPF+5x uBCAII (●), 70S_{Ec}+3x HPF+5x uBCAII (▲), 70S_{Ec}+10x HPF+5x uBCAII (▼). **B.** Sedimentation analysis of dissociation of 70S_{Ec} ribosome (1x = 0.1 μM); (1) alone, (2) upon interaction with uBCAII (5x), (3) upon interaction with uBCAII (5x) in the presence of HPF (1x), (4) upon interaction with uBCAII (5x) in the presence of HPF (3x), (5) upon interaction with uBCAII (5x) in the presence of HPF (10x). The dotted lines represent the positions of the 70S_{Ec} ribosome peak as well as the positions of the 50S and 30S subunits.

Our studies show that with increasing concentrations of HPF, there is an increased inhibition of uBCAII-mediated dissociation of the 70S_{Ec} ribosome (**Figure 7A**). When HPF was present at 10-fold stoichiometric excess (10x) with respect to the ribosome, complete inhibition of uBCAII-mediated ribosomal dissociation was observed. Our observations were further confirmed by the equilibrium sucrose density gradient centrifugation (SDGC) analysis as shown in **Figure 7B**.

A.3. HPF and uBCAII can simultaneously bind to the 70S ribosome

The next question that arises is whether the HPF binding had directly inhibited the interaction of uBCAII to the ribosome. In order to verify this possibility, the 70S_{Ec} (1x, x=0.1 μM) ribosome priorly bound to the HPF (10x) protein, was incubated with 5x uBCAII and the reaction mixture was subjected to ultrafiltration using a 100 KDa filter. Since the molecular weight of BCAII is 29 KDa, and HPF is 10.75 KDa, BCAII and the recombinant HPF can only be expected to be retained on the filter if they are bound to the 70S ribosome. The retained fractions (bound fractions: BP) were divided into two equal aliquots and analyzed for the presence of BCAII and HPF by dot-blot analysis using anti-BCAII and anti-His tag antibody respectively (Materials and Methods).

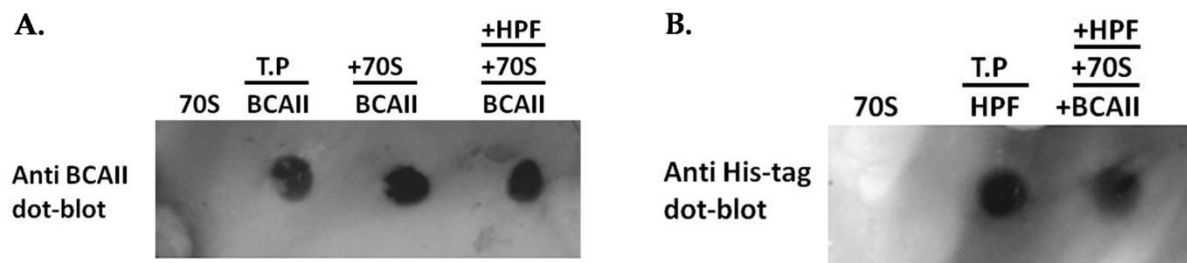


Figure 8: Simultaneous binding of HPF and uBCAII to the 70S ribosome

0.1 μM of *E.coli* 70S ribosome, empty or bound to 1 μM HPF was incubated with 0.5 μM uBCAII for 5 minutes at room temperature. The reaction mix was loaded on a 100 KDa Amicon Ultra filter, centrifuged, washed and dot blot analysis was performed with the 70S_{Ec} bound fraction retained on the filter using (A) Carbonic anhydrase II polyclonal antibody to detect the presence of uBCAII and (B) anti-His tag antibody to detect the presence of HPF. The total amount of unfolded protein and HPF used in the experiment has been included as controls.

A. Dots from left to right contain: (1) total 70S_{Ec} (0.1 μM), (2) total protein uBCAII (0.5 μM) (TP), uBCAII retained for; (3) 70S_{Ec} (0.1 μM) + uBCAII (0.5 μM), (4) 70S_{Ec} (0.1 μM) +HPF (1μM) + uBCAII (0.5 μM)

B. Dots from left to right contain: (1) total 70S_{Ec} (0.1μM), (2) total protein HPF (1 μM) (T.P.), (3) HPF retained for 70S_{Ec} (0.1 μM) +HPF (1μM) + uBCAII (0.5 μM).

As shown in **Figure 8**, the dot-blot shows that the binding of HPF to the 70S ribosome did not affect the interaction of the ribosome with the unfolded protein and uBCAII is able to bind simultaneously to the HPF bound 70S ribosome. Hence the HPF mediated inhibition of 70S dissociation observed above (**Figure 7A and 7B**) is not due to the inhibition of binding of uBCAII to the ribosome.

A.4. Basis of HPF mediated inhibition of 70S dissociation

The subsequent experiments were conducted to further investigate the mechanism of resistance of HPF bound 70S ribosome towards uBCAII mediated subunit dissociation. As suggested by Polikanov et al. [2012], HPF binding can stabilize the ribosome against dissociation. Hence, experiments were performed to study whether the inability of uBCAII to dissociate the 70S ribosome arises due to increased association between the ribosomal subunits in presence of the factor HPF, under the conditions used in our experiments. It is well established that the destabilization of the inter-subunit bridges at low magnesium ion concentrations leads to dissociation of the 70S ribosome into its subunits [Nierhaus, 2014].

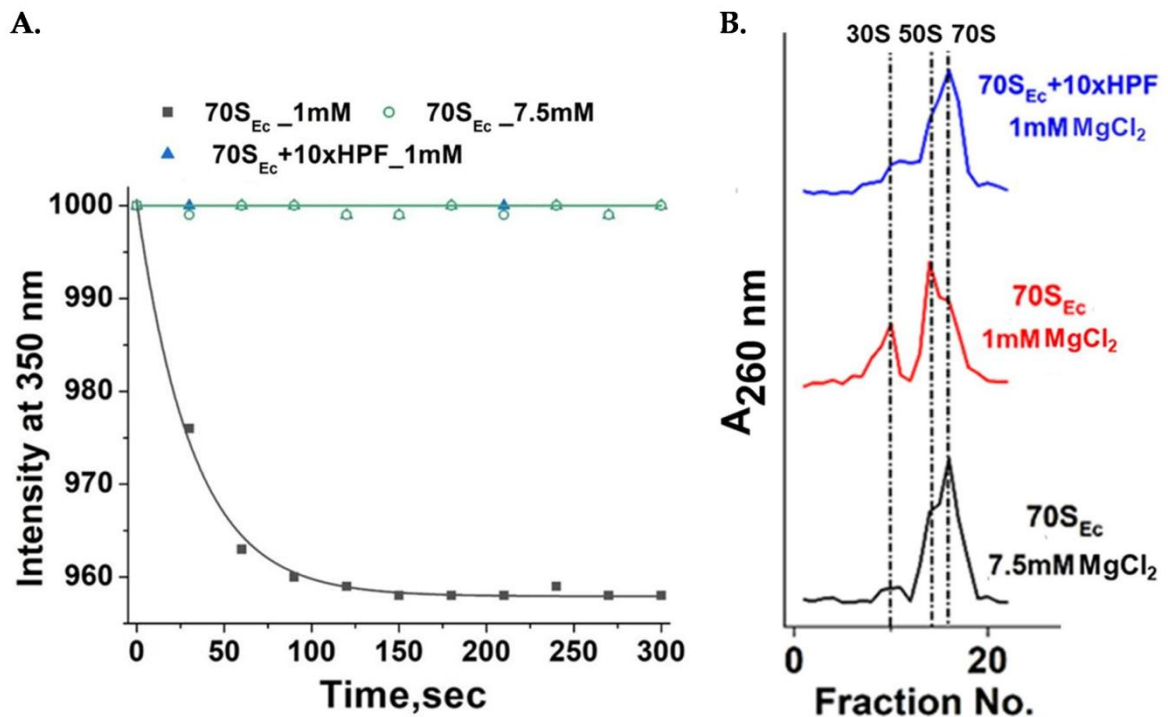


Figure 9: HPF prevents low magnesium induced dissociation of 70S ribosome

A. Light scattering analysis of 70S_{Ec} dissociation at 1 mM MgCl₂ in the presence of HPF: Time course change in light scattering intensity at 350 nm of 0.1 μM (x) 70S_{Ec} ribosome bound to 10x HPF (binding was performed at 7.5 mM MgCl₂: “Materials and Methods”) at MgCl₂ concentration of 1 mM. 70S_{Ec} ribosome in 1 mM MgCl₂ (■), 70S_{Ec} ribosome in 7.5 mM MgCl₂ (○) and 70S_{Ec} ribosome + 10x HPF in 1 mM MgCl₂ (▲).

B. Sedimentation analysis of 70S_{Ec} ribosome profile in the presence of HPF at 1 mM MgCl₂: Sedimentation profile of (1) 70S_{Ec} in 7.5 mM MgCl₂, (2) 70S_{Ec} in 1 mM MgCl₂ and (3) 70S_{Ec}+10xHPF in 1 mM MgCl₂. The dotted lines represent the positions of the 70S_{Ec} ribosome peak as well as the positions of the 50S and 30S subunits.

A comparison of the dissociation of empty 70S_{Ec} ribosome and HPF bound 70S_{Ec} ribosome at low magnesium ion (Mg²⁺) concentration (1 mM) was performed using light scattering measurements and sucrose density gradient centrifugation studies. The light scattering experiments as shown in **Figure 9A** demonstrated that, while the empty 70S_{Ec} ribosome (0.1 μM) is dissociated into its subunits at low concentrations of magnesium (1 mM), the 70S_{Ec} ribosome in the presence of 10-fold excess concentrations of HPF (1 μM), can resist such spontaneous dissociation. The negligible amount of dissociated ribosomal subunits present even at Mg²⁺ ion concentration as low as 1 mM, observed in the SDGC profile (**Figure 9B**)

also confirmed that in presence of the factor (HPF), the dissociation of the 70S_{Ec} ribosome is prevented.

Hence, the increased association between ribosomal subunits in the HPF bound ribosome could explain why HPF can resist the unfolded protein mediated dissociation. Previous studies by Pathak et al. [2017] had shown that 5x uBCAII mediated 70S dissociation does not occur at higher magnesium concentration (10 mM). Hence, the unfolded protein mediated ribosome subunit dissociation thereby also relies on a population of pre-dissociated subunits, which is present at a lower Mg²⁺ concentration (7.5 mM). The increased association between the 50S and 30S subunits in HPF bound ribosome could reduce the population of dissociated ribosomal subunits which is proposed to contribute to the ribosome dissociation ability of the unfolded protein [Pathak et al., 2017]. The next question was whether HPF could also prevent 70S dissociation mediated by a bona fide stress associated ribosome recycling factor HflX and GTP [Zhang et al., 2015, Coatham et al., 2016, Basu et al., 2017].

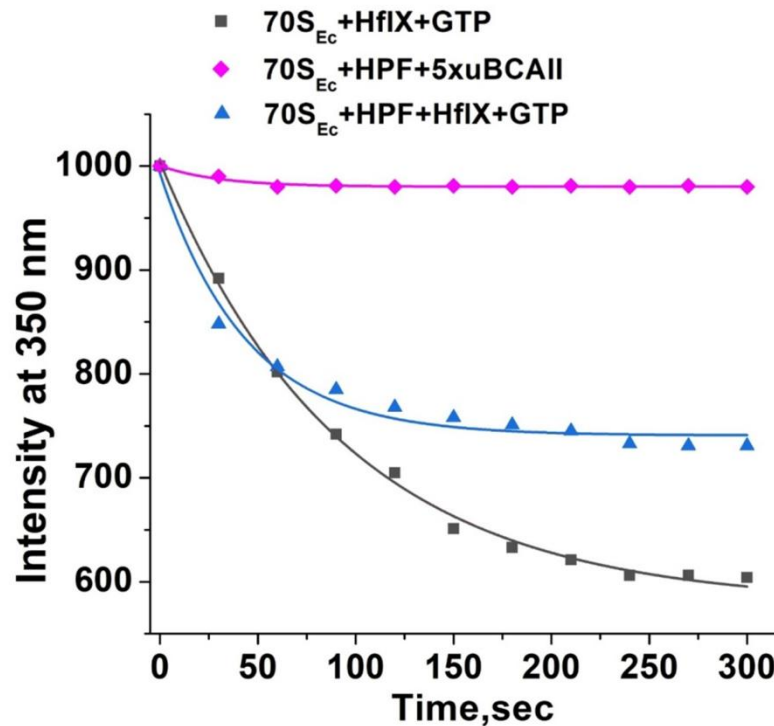


Figure 10: HPF bound 70S ribosome is dissociated by HflX-GTP

Light Scattering analysis of 70S_{Ec} dissociation by HflX-GTP in presence of HPF: 0.1 μM (x) 70S_{Ec} ribosome in the presence and absence of 10x (1 μM) HPF, was rapidly mixed with 1 μM HflX and 100 μM GTP in 7.5 mM MgCl₂ (Materials and Methods). Time course change in the intensity of light scattering at 350 nm of the reaction mixtures was measured. 70S_{Ec}+HflX+GTP (■), 70S_{Ec}+HPF+HflX+GTP (▲) and 70S_{Ec}+HPF+5x uBCAII (◆)

Although HPF binding could not prevent the dissociation of 70S ribosome mediated by HflX-GTP (**Figure 10**), it could prevent the dissociation mediated by uBCAII. This may be expected since the mechanisms of uBCAII and HflX-GTP mediated ribosome dissociation are distinct, although this phenomenon requires further investigations.

A.5. Effect of HPF on ribosome degradation

Earlier studies in the laboratory had demonstrated that uBCAII-mediated ribosome dissociation makes the ribosome more prone to degradation by cellular ribonucleases [Pathak et al., 2017]. In our current studies, similar ribosome degradation assays were performed to assess whether the ability of HPF bound ribosome to resist unfolded protein-mediated 70S

dissociation could also protect the ribosome from degradation by cellular nucleases. The 70S ribosome bound to 10x HPF ($x = 0.1 \mu\text{M}$) protein was incubated with mS30 cellular extract containing nucleases in the presence and absence of 5x uBCAII and the outcome was analyzed using equilibrium sucrose density gradient centrifugation (SDGC) (Materials and Methods).

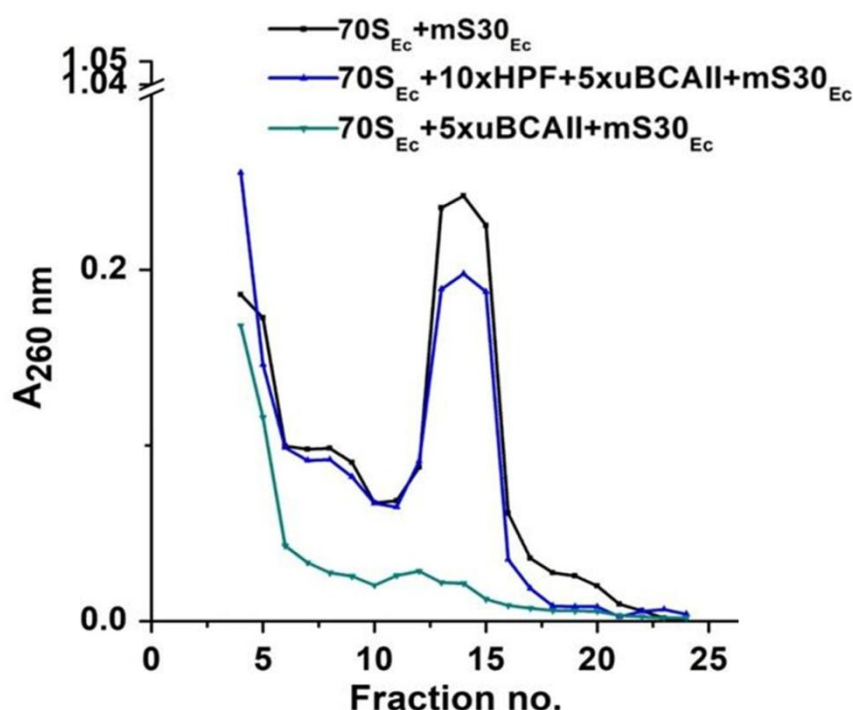


Figure 11: HPF can protect the ribosome from degradation mediated by nucleases present in cellular extract

Sedimentation analysis of degradation of E. coli 70S ribosome (1x = 0.1 μM) in the presence of HPF (10x) upon incubation with mS30_{Ec} extract for 90 minutes in the presence of 5x uBCAII. As control sets, 70S_{Ec} ribosome alone was incubated with mS30_{Ec} extract and 70S_{Ec} ribosome was incubated with mS30_{Ec} extract in the presence of 5x uBCAII in the absence of HPF. Gradient profile when 70S_{Ec} alone was incubated with mS30_{Ec} extract (■), 70S_{Ec} was incubated in the presence of 10x HPF and 5x uBCAII with mS30_{Ec} extract (▲) and 70S_{Ec} was incubated in the presence of 5x uBCAII with mS30_{Ec} extract (▼).

As observed from the equilibrium SDGC A_{260 nm} profile in **Figure 11**, the binding of HPF to the ribosome could significantly protect the ribosomal population from getting degraded by cellular nucleases, in the presence of super-stoichiometric concentration of unfolded BCAII.

This significance and functional implication of this observation should be assessed in light of the earlier discussion (Chapter 1, Section A.5). The binding of HPF to the ribosome in the stationary phase does not only translationally silence the ribosome but also protects the ribosome from the harmful effects of the elevated levels of unfolded protein that might trigger ribosome dissociation and degradation.

A.6. HPF bound ribosome can act as a chaperone

In order to determine whether the HPF bound ribosome was capable of acting as a chaperone, the following experiments were performed. The ability of the *E.coli* 70S ($70S_{Ec}$) ribosome ($0.3 \mu\text{M}$) to assist in the refolding of uBCAII ($0.3 \mu\text{M}$) in the presence of 10-fold excess concentration ($3 \mu\text{M}$) of HPF was analyzed as discussed in the “Materials and Methods” section. Since BCAII is an enzyme, examining its enzymatic activity after refolding of its completely denatured form has been used in literature [Pal et al., 1999] as a test of its successful reactivation. An active BCAII enzyme can successfully catalyze the transformation of paranitrophenyl acetate into paranitrophenol and this conversion is tracked by measuring the increase in absorbance at 420 nm with time. The reactivation of uBCAII in presence of the empty *E.coli* 70S ribosome ($70S_{Ec}$ -free) and the 70S ribosome bound to 10-fold excess concentration of HPF ($70S_{Ec}$ -HPF) was compared to the self-reactivation of BCAII in absence of the ribosome (“Materials and Methods” section).

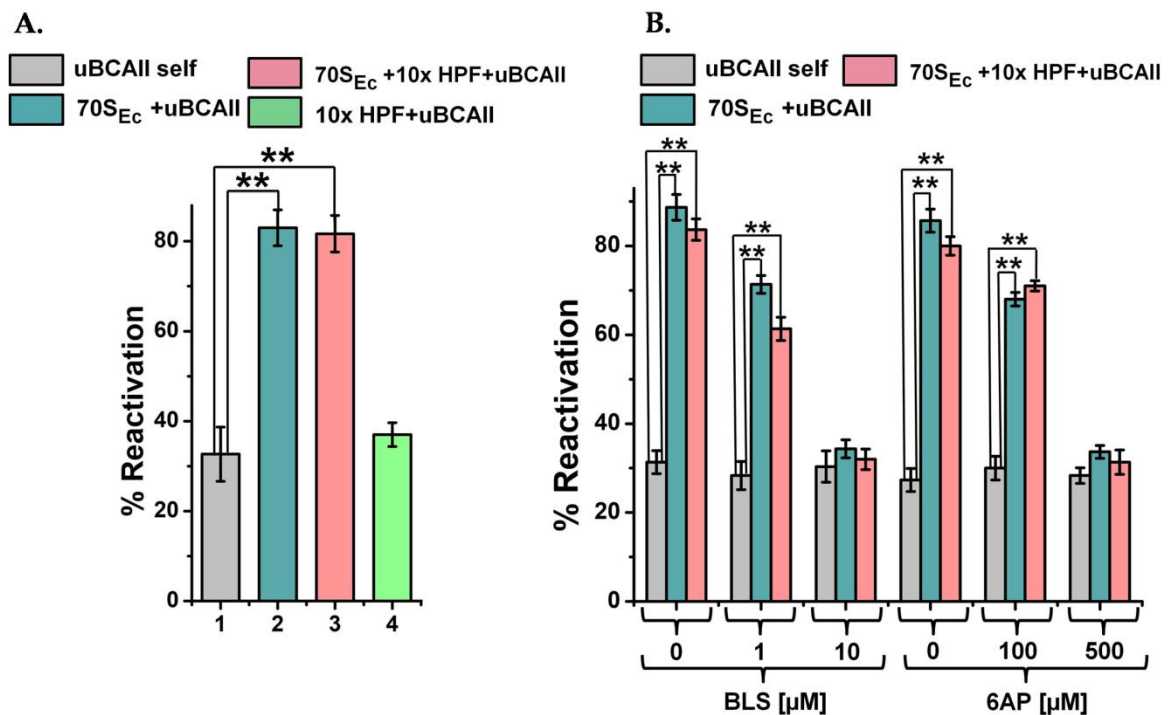


Figure 12: HPF bound 70S ribosome can exhibit chaperoning activity and increase the reactivation yield of BCAII

A. Refolding assay of uBCAII in the presence of 70S_{Ec} with 10x ($x = 0.3 \mu\text{M}$) concentrations of HPF:

0.3 μM of uBCAII was refolded in the presence and absence of 1x 70S_{Ec} alone ($x = 0.3 \mu\text{M}$), 70S_{Ec} in the presence 10x concentration of HPF. Bar graph showing percentage of reactivation of (1) uBCAII self, (2) 70S_{Ec} + uBCAII, (3) 70S_{Ec}+10x HPF+ uBCAII and (4) 10x HPF+ uBCAII. The experiments were repeated thrice and the data are presented as means \pm SEM; *P< 0.05 or **P< 0.001 in one –way ANOVA (N= 3). **B.** Refolding assay of uBCAII in the presence of 70S_{Ec} and 10x ($x = 0.3 \mu\text{M}$) concentration of HPF with Blastidicine S (BLS) and 6-Aminophenanthridine (6AP): 0.3 μM of uBCAII was refolded in the presence and absence of 1x 70S_{Ec} alone ($x=0.3 \mu\text{M}$), 70S_{Ec} in the presence of 10x concentrations of HPF, along with the presence of 0 μM , 1 μM and 10 μM BLS (Materials and Methods). 0.3 μM of uBCAII was also refolded in the presence and absence of 70S_{Ec} alone ($x=0.3 \mu\text{M}$), 70S_{Ec} in the presence of 10x concentrations of HPF, along with the presence of 0 μM , 100 μM and 500 μM 6AP (Materials and Methods). Bar graph showing percentage of reactivation of uBCAII self, 70S_{Ec}+uBCAII and 70S_{Ec}+10x HPF+ uBCAII in the presence of (1) 0 μM BLS, (2) 1 μM BLS, (3) 10 μM BLS, (4) 0 μM 6AP, (5) 100 μM 6AP and (6) 500 μM 6AP. The experiments were repeated thrice and the data are presented as means \pm SEM; *P< 0.05 or **P< 0.001 in one –way ANOVA (N= 3).

As shown in **Figure 12A**, comparable increase in reactivation of uBCAII, in presence of the 70S_{Ec}-free and 70S_{Ec}-HPF, was observed which implies that the ability of the ribosome to act as a protein folding modulator remains unaffected upon binding of the HPF protein to the ribosome.

The next question which arises is whether the chaperoning activity of the HPF bound ribosome is also PTC mediated. Earlier studies have demonstrated that Blastidine S (BLS), a PTC substrate analog that mimics the binding of the 3'-CCA end of the P-site tRNA [Mondal et al., 2014], inhibits the ribosome assisted reactivation of unfolded BCAII. BLS acts by binding to the G2252 and G2253 residues of the PTC loop. Previous studies in the laboratory were conducted with BLS to confirm that an interaction between the domain V and the 3'-CCA end of the tRNA effectively inhibited the chaperoning activity of the ribosome [Mondal et al., 2014]. Thus binding of BLS to the ribosome inhibits its PTC-mediated chaperoning ability. The anti-prion drug 6-Aminophenanthridine (6AP) has also been demonstrated to inhibit ribosomal protein folding activity [Banerjee et al., 2014]. It functions by inhibiting the specific interactions between the five sites on the peptidyl transferase center (PTC) and the unfolded protein that is necessary for initial interaction of the unfolded protein with the PTC of the ribosome. 6AP competes with the unfolded protein substrate for binding to the domain V of 23S rRNA due to their overlapping binding sites [Pang et al., 2013]. Thus, in order to answer the question of whether HPF bound 70S also follows a PTC mediated mechanism, we examined the inhibition of BCAII reactivation yield in presence of these substrates. As shown in **Figure 12B**, the 70S_{Ec}-HPF shows a dose-dependent inhibition of chaperoning activity, similar to that of the empty 70S ribosome, in presence of increasing concentrations of BLS and 6AP, thus confirming that the mechanism of chaperoning action in HPF bound 70S ribosome, similar to the empty 70S ribosome, is also PTC-mediated.

It is to be noted that during stressful situations, the cell is in more dire need of controlling protein aggregation caused due to the accumulation of unfolded or misfolded proteins. Earlier studies have demonstrated that the ribosome has the ability to suppress protein aggregation [Pathak et al., 2014]. Hence, further studies were performed to analyze the effect of 70S_{Ec}-HPF on the aggregation of reduced denatured lysozyme (R/D Lyso) and molten globule form

of BCAII protein (mBCAII). Since the formation of protein aggregates involves an increase in association between protein molecules, progressively larger sized complexes are formed which leads to increase in scattering of incident light of appropriate wavelength and a lower transmittance of incident light wave. The resultant reduction in transmittance leads to an increase in turbidity signifying the formation of large sized aggregates with time and this method has been widely used to study protein aggregation in literature [Hall et al., 2016, Raman et al., 1996] and in the laboratory [Pathak et al., 2014].

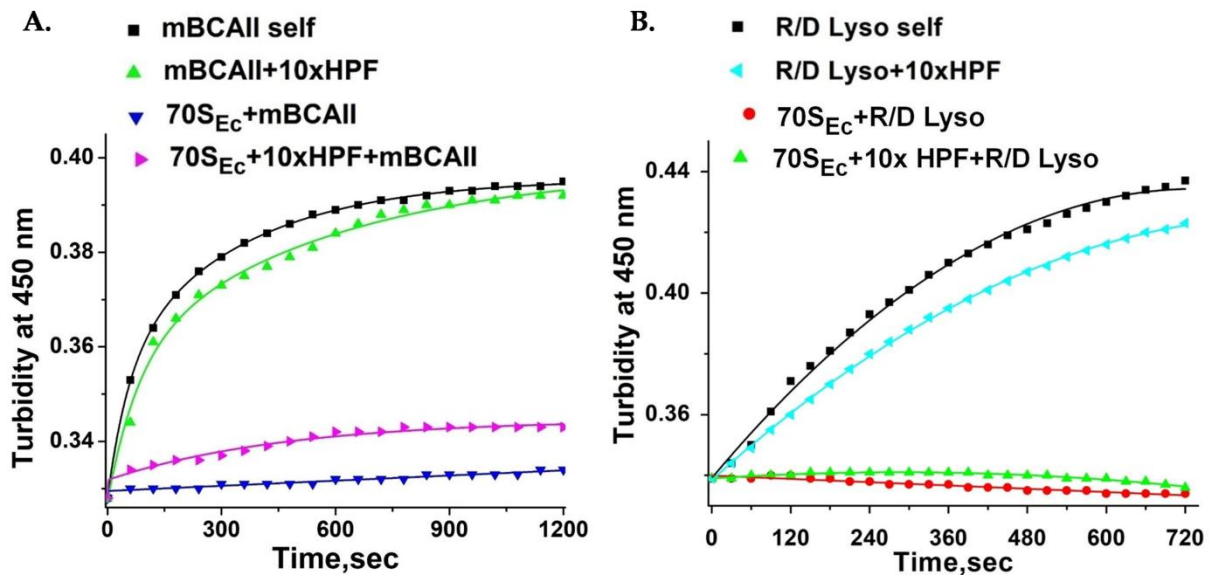


Figure 13: HPF bound 70S ribosome can suppress aggregation

A. Time course change in the aggregation of mBCAII in presence of 70S_{Ec} with 10x ($x = 0.9 \mu\text{M}$) HPF: The time course change in turbidity at 450 nm was measured for $0.9 \mu\text{M}$ mBCAII (Materials and Methods) for 1200 seconds in the presence and absence of 1x 70S_{Ec} alone ($x=0.9 \mu\text{M}$), 70S_{Ec}+10xHPF: mBCAII self (■), mBCAII+10xHPF (▲), 70S_{Ec}+ mBCAII (▼) and 70S_{Ec}+10x HPF+ mBCAII (◆).

B. Time course change in the aggregation of reduced-denatured lysozyme in presence of 70S_{Ec} with 10x ($x = 2 \mu\text{M}$) HPF: The time course change in turbidity at 450 nm was measured for $2 \mu\text{M}$ of reduced-denatured lysozyme (R/D Lyso) (Materials and Methods) for 720 seconds in the presence and absence of 1x 70S_{Ec} alone ($x=2 \mu\text{M}$), 70S_{Ec}+10xHPF: R/D Lyso self (■), R/D Lyso+10xHPF (◀), 70S_{Ec}+R/D Lyso (●), 70S_{Ec}+10x HPF+R/D Lyso (▲).

As shown in **Figure 13**, both 70S_{Ec}-free as well as 70S_{Ec}-HPF could effectively suppress the increase in turbidity and hence aggregation of mBCAII (**Figure 13A**) and R/D Lyso (**Figure 13B**), respectively. This study implies that the HPF bound 70S ribosome retains the holdase chaperoning activity of the ribosome [Pathak et al., 2014] and is capable of suppressing protein aggregation. In the context of cellular stress encountered by the *E.coli* cells in the stationary phase, such an ability of the HPF-bound monomeric ribosome to assist in protein folding and suppress protein aggregation in an ATP-independent manner might contribute significantly towards cell viability and maintenance of the active cellular proteome.

A.7. Molecular interpretation of the resistance of folded protein-mediated disassembly of the hibernation promoting factor-bound 70S ribosome

It has been shown that ribosomal RNA-catalyzed folding of denatured protein followed by disassembly of ribosome into subunits is a universally conserved function of ribosome across the species [Das et al., 2008, Das et al.,1996 , Pal et al., 1999, Chattopadhyay et al.,1996]. The domain V of large subunit rRNA, that acts as the chaperone in this process [Pal et al., 1999], occupies the intersubunit side of the large subunit when it is associated with the small subunit to form 70S ribosome [Ben-shem, 2011].

Our biochemical assays demonstrated that hibernating ribosome (as well as 100S ribosome, discussed later in Section B of this chapter) can successfully fold the denatured uBCAII protein. However, the associated next step, in which the protein induces splitting of the 70S ribosome, is resisted by the factor-bound ribosome. To understand the mechanism underpinning the inability of uBCAII to induce dissociation of HPF-bound 70S ribosome into subunits, we have closely inspected the available HPF-bound ribosome structures [PDB ID: 4V8H].

Earlier studies have demonstrated that, during the universal process of ribosome-assisted protein folding [Das et al., 2008], the unfolded protein binds first at the RNA1 subdomain of domain V of 23S rRNA (residues involved in the folding process cluster mostly on helices 89 and 92 of RNA1) which remain mostly exposed in the 70S ribosome (**Figure 14**). The subsequent release of the folded protein (and disassembly of the 70S ribosome) occurs by the assistance of RNA2 subdomain of domain V which remains buried in the intersubunit space [Das et al., 2008]. It has been proposed that RNA1 assists the denatured protein to become folding competent, which then moves onto RNA2 thus clashing with helix 69 of 23S rRNA [Chakraborty et al., 2016] and destabilizing the central inter-subunit bridge B2a (formed

between helix 69 of the 23S rRNA and helix 44 of the 16S rRNA) [Liu et al., 2016] thereby leading to the dissociation of ribosomal subunits. BCAII protein structure was docked on domain V (RNA2 region) of the 50S ribosomal subunit of HPF-bound *T.thermophilus* ribosome [Polikanov et al., 2012, (Protein Data Bank: 4V8H)] in a similar way as done previously [Pathak et al., 2017, Chakraborty et al., 2016] to mimic the state of uBCAII when it is released from the ribosome following ribosome-assisted folding. Folded BCAII protein on RNA2 does create steric clash with the helix 69 of 23S rRNA of the HPF-bound ribosome (**Figure 14**) as also seen in previous study [Chakraborty et al., 2016].

However, despite the steric hindrance, it is unable to dissociate the hibernating ribosome indicating that there must be additional factors associated with the steric clash playing crucial role in ribosome disassembly. The small ribosomal subunit by nature is intrinsically flexible and free movement of its head and body is allowed. Interestingly, HPF locks the small subunit conformation by binding at the mRNA channel (head and body junction of the inter-subunit interface) and restricts the free movement of small subunit, which apparently is necessary for disruption of the bridge B2a, thereby arresting denatured or unfolded protein-mediated ribosome recycling. Based on this observation, we extend the previously proposed mechanism [Chakraborty et al., 2016] that steric clash due to the presence of RNA2-bound folding competent protein induces a conformational change in the small subunit of empty ‘unlocked’ ribosome [Valle, 2003] which helps to disrupt 16S rRNA helix 44 interaction with 23S rRNA helix 69 (bridge B2a) and subsequently disassemble the ribosome.

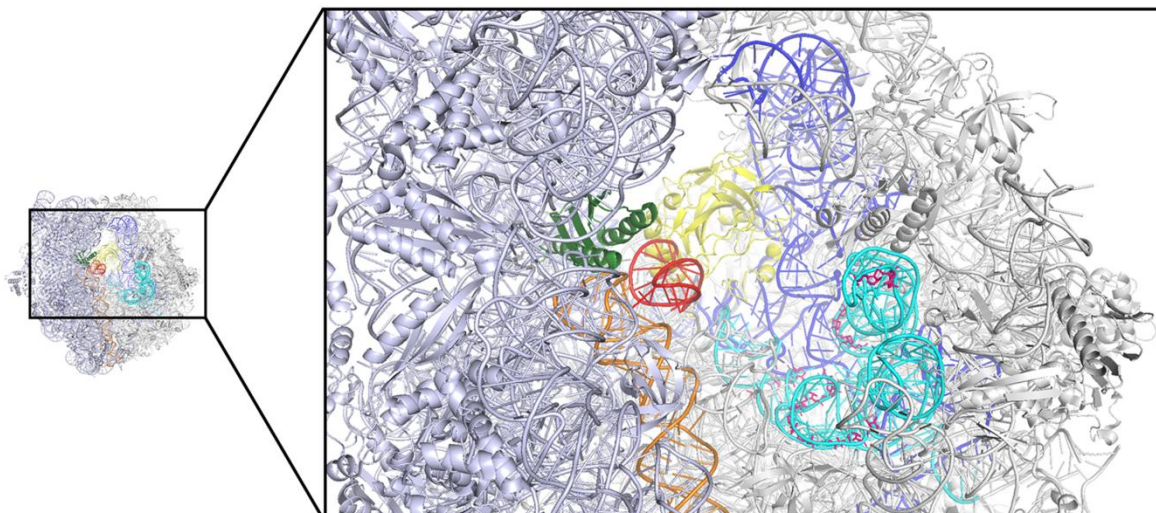


Figure 14: Structural analysis of interaction of the 70S-HPF complex with BCAII protein:

Crystal structure of HPF bound to *Thermus thermophilus* 70S ribosome (PDB ID: 4V8H) where BCAII protein (Protein Data Bank: 1V9E; yellow) placed onto RNA2 region (dark blue), buried in the intersubunit space, is shown. The docked position of BCAII is presented following a previous study [Chakraborty et al., 2016]. The right panel shows close-up view of the selected area of the image. The HPF (green) protein occupies the mRNA channel at the junction of head and body of the 30S ribosomal subunit and stays in contact with helix 44 (orange) of the 16S rRNA. It is seen that BCAII makes a physical contact with helix 69 (red). The sites of five nucleotides of RNA1 (cyan) that interact with the unfolded protein [Samanta et al., 2008], represented in stick model (pink), are clearly accessible to the unfolded protein.

On the other hand, RNA1 region is exposed and therefore remains accessible to the unfolded protein in case of factor-bound ribosome also. The accessibility of the five nucleotides on domain V (RNA1) [Das et al., 2012] that are responsible for ribosome-mediated protein folding explains observed folding activity of the factor-bound ribosome (**Figure 14**). Thus, the structural analyses provide a plausible explanation for why HPF binding to the ribosome leads to resistance of unfolded protein-mediated subunit dissociation without interrupting chaperoning activity of the ribosome.

A schematic summarizing the above observations and representing the outcomes of ribosome-unfolded protein interaction depending on their mutual stoichiometric ratios and in the presence of HPF has been shown in **Figure 15**.

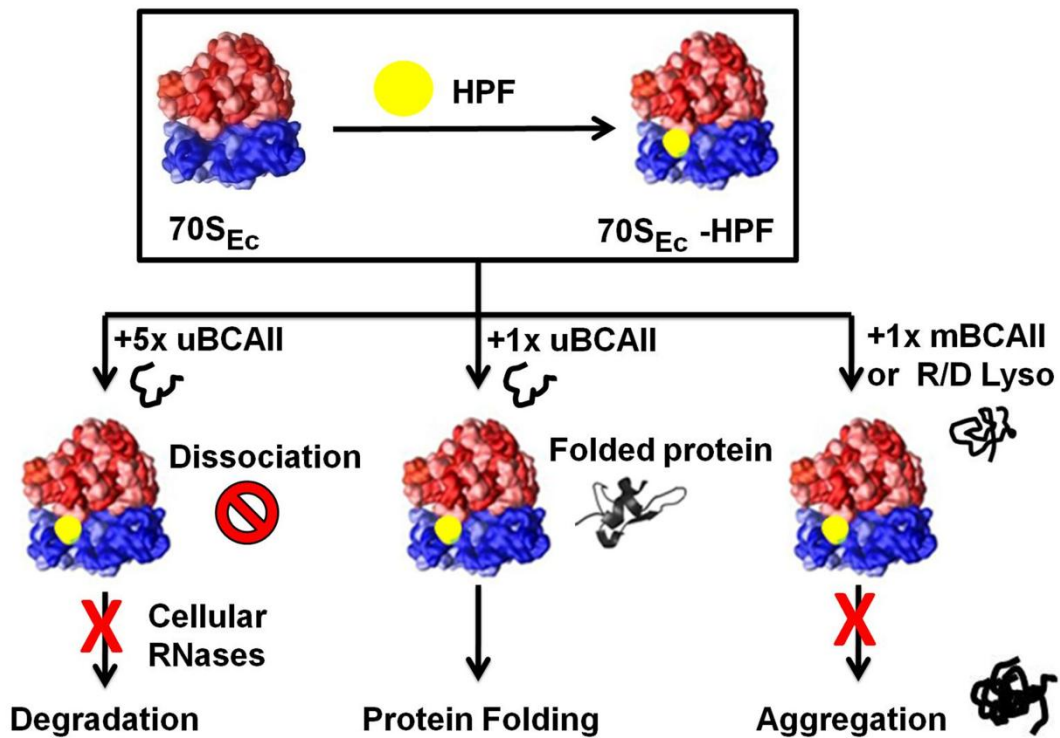


Figure 15: Schematic depicting the outcomes of interaction of unfolded protein and *E. coli* 70S ribosome in the presence of HPF

Empty non-translating $70S_{Ec}$ ribosome undergoes sustained dissociation in presence of a five-fold stoichiometric excess of unfolded protein which makes the dissociated ribosomal subunits vulnerable to degradation in presence of cellular nucleases. Binding of HPF to the ribosome protects it from unfolded protein mediated dissociation and subsequent degradation by cellular ribonucleases.

At stoichiometric concentrations, the $70S_{Ec}$ ribosome, in free as well as the HPF-bound state, can act as an energy-independent foldase chaperone towards the unfolded protein and release it in a folding competent state. It can also act as an energy-independent holdase chaperone and mediate the suppression of protein aggregation under similar conditions.

Section B

Effect of unfolded protein on hibernating 100S dimers

As discussed previously, a predominant molecular strategy employed by the bacterial cells to combat stress, like nutrient deprivation and harsh environmental conditions, is “Ribosome Hibernation”, where ribosomal particles are maintained in a translationally silent state [Starosta et al., 2014, Ueta et al., 2008, Maki et al., 2000, Prossliner et al., 2018]. This translational silencing is mediated by either the binding of stress factors that keep the 70S ribosome in a dormant monomeric state or by dimerizing them into the 100S form. This dimerization of the ribosome is also distinctly different in gram-negative and gram-positive bacteria. In gram-negative bacteria like *Escherichia coli*, these 100S dimeric ribosomal structures characterize the stationary phase and are formed by the concerted action of the factors hibernation promoting factor (HPF) and ribosome modulation factor (RMF). In gram-positive bacteria like *Staphylococcus aureus*, these dimers are present in all growth phases, including the exponential phase, and dimerization is mediated by the singular action of the long form of hibernation promoting factor, HPF_{Sa} [Prossliner et al., 2018, Ueta et al., 2010]. The 100S ribosomal particles from *E.coli* and *S.aureus* also have subtle differences in the mode of association of the 70S monomers into the 100S dimeric structure, in addition to differences in their pattern of formation and stability. In case of 100S dimeric ribosome from *E.coli* (100S_{Ec}), one of the constituent 70S ribosome is rotated by an angle of approximately 110° with respect to that in 100S ribosome from *S.aureus* (100S_{Sa}). This results in a significantly larger interface between the two 30S ribosomal subunits in 100S_{Ec} (**Figure 16A**). Interactions between helices h26 and h40 of the 16S rRNA and the uS2 ribosomal protein are involved in forming the 100S_{Sa} dimerization interface in *S.aureus* [Khusainov et al., 2017]. In contrast, interactions between helix 39 and ribosomal proteins uS9, uS10 or uS2, uS3 and uS5 are involved in forming the expanded interface of 100S_{Ec} in *E.coli* [Kato et

al., 2010]. Thus, the participating structural elements and the nature of interactions that constitute the 100S dimeric ribosome in *E.coli* and *S.aureus* are distinct and species specific [Matzov et al., 2017]. The singular involvement of HPF_{Sa} and direct contact between two of these molecules during dimerization ensures a more stable association of 70S in the 100S dimers of *S.aureus* (**Figure 16B**) compared to *E.coli* [Prossliner et al., 2018].

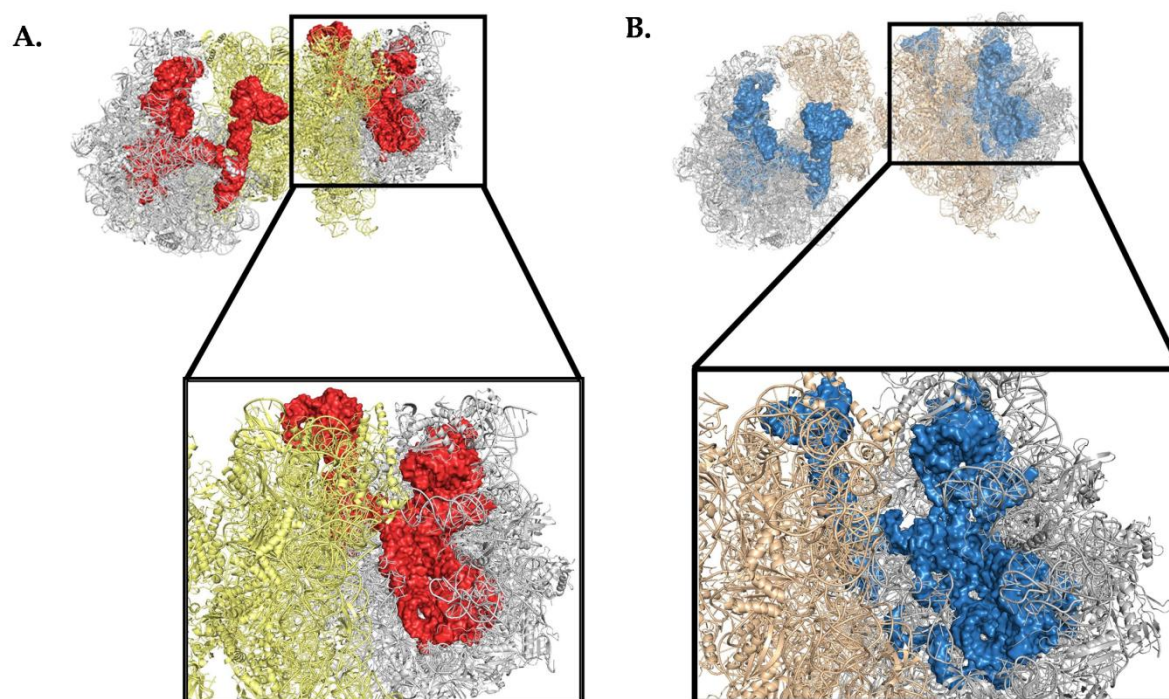


Figure 16: Structural representations of the availability of the domain V region of the 100S ribosome from *Escherichia coli* and *Staphylococcus aureus*

A. Crystal structure of the *E.coli* 100S ribosome (100S_{Ec}) (Protein Data Bank: 6H58) is shown with the close-up view of one 70S_{Ec} counterpart in the bottom panel. Light yellow represents the 30S subunit, grey represents the 50S subunit, red represents the domain V region of the 23S rRNA.

B. Crystal structure of the *S.aureus* 100S ribosome (100S_{Sa}) (Protein Data Bank: 6FXC), and the close-up view of one 70S_{Sa} counterpart in the bottom panel. Light orange represents the 30S subunit, grey represents the 50S subunit and the domain V region of the 23S rRNA is presented in blue.

Clearly, RNA1 part of the domain V rRNA is quite accessible to the unfolded protein encountered by the 100S ribosome in both the structures (A and B).

Structural illustrations have been made using PYMOL 2008 (De Lano Scientific, Palo Alto, CA, USA, available at: www.pymol.org).

As discussed above in Section A, our studies with the unfolded protein and HPF bound *E. coli* 70S ribosome have demonstrated that the monomeric 70S factor bound hibernating ribosomal structures can mediate their protective effect on the ribosomal population during stress by resisting unfolded protein mediated subunit dissociation. Our studies also showed that 70S_{Ec}-HPF complexes are able to assist in protein folding and suppress protein aggregation. The dimerization of 70S into 100S involves binding of factors (HPF and RMF in *E. coli* and HPF_{Sa} in *S. aureus*) to the 30S subunit of the individual 70S ribosomes that constitute the dimer [Prossliner et al., 2018]. As discussed earlier, the 50S subunit of the 70S ribosome houses the chaperoning center of the ribosome that resides in the domain V of 23S rRNA co-localizing with Peptidyl Transferase Centre (PTC) [Das et al., 2008]. Structural display of the 100S_{Ec} ribosome (PDB: 6H58) (**Figure 16A**) and the 100S_{Sa} ribosome (PDB: 6FXC) (**Figure 16B**) shows that domain V of 23S rRNA is accessible for binding to the unfolded protein in the 70S_{Ec} or 70S_{Sa} monomers that constitute the 100S dimeric ribosome.

Hence, studies were performed to investigate whether: a) the unfolded protein can bind to and dissociate the 100S ribosome isolated from both gram-negative (*E. coli*) and gram-positive (*S. aureus*) bacteria and b) whether these 100S ribosomes can retain their chaperoning activity towards the unfolded proteins.

B.1. Purification and enrichment of E. coli 100S (100S_{Ec}) ribosome

The 100S_{Ec} ribosome was isolated from BW25113 Δ yfiA strain of *E. coli*, enriched and purified as reported earlier [Beckert et al., 2018] and stated in the “Materials and Methods” section. The reason behind selection of this particular strain requires the mention of another stress factor YfiA (Ribosome associated inhibitor A or RaiA) that is expressed in *E. coli* under conditions of both cold shock and starvation [Vila-Sanjurjo et al., 2004, Agafonov et al., 1999]. It binds to the 70S ribosome and maintains it in a monomeric hibernating state and essentially antagonizes the HPF mediated 100S dimerization [Maki et al., 2000, Ueta et al.,

2005]. The BW25113 $\Delta yfiA$ strain of *E. coli* is a deletion mutant which lacks the expression of YfiA protein [Beckert et al., 2018]. Thus, in the absence of YfiA, HPF and RMF together can drive the formation of dimeric 100S to a greater extent, thereby facilitating a greater yield of 100S population, when isolated from this strain. These bacterial cells were grown in minimal media for 33 hours to allow the cells to reach stationary phase for isolation of the 100S dimers. The ribosomal profile of the crude cell lysate obtained after cell lysis and removal of cell debris, using sucrose density gradient centrifugation, demonstrated the presence of a significant population of 100S ribosome (**Figure 17A**). The relevant fractions corresponding to the 100S ribosomal peak were pooled and subjected to repeated rounds of concentration and sucrose density gradient centrifugation to obtain an enriched and purified population of *E. coli* 100S (100_{Ec}) ribosome (**Figure 17A**). Studies have revealed that under laboratory conditions, the stability of the *E. coli* 100S ribosome is reduced in the presence of low magnesium concentrations [Gohara et al., 2018]. To navigate this issue, a high concentration of magnesium (25 mM) [Khusainov et al., 2017] was maintained in all buffers and gradients involved in the purification process to maintain the stability of 100S ribosome. As shown in **Figure 17A**, after sequential rounds of concentration and SDGC, a pure and enriched population of 100S_{Ec} ribosome was obtained that was used in our subsequent experiments.

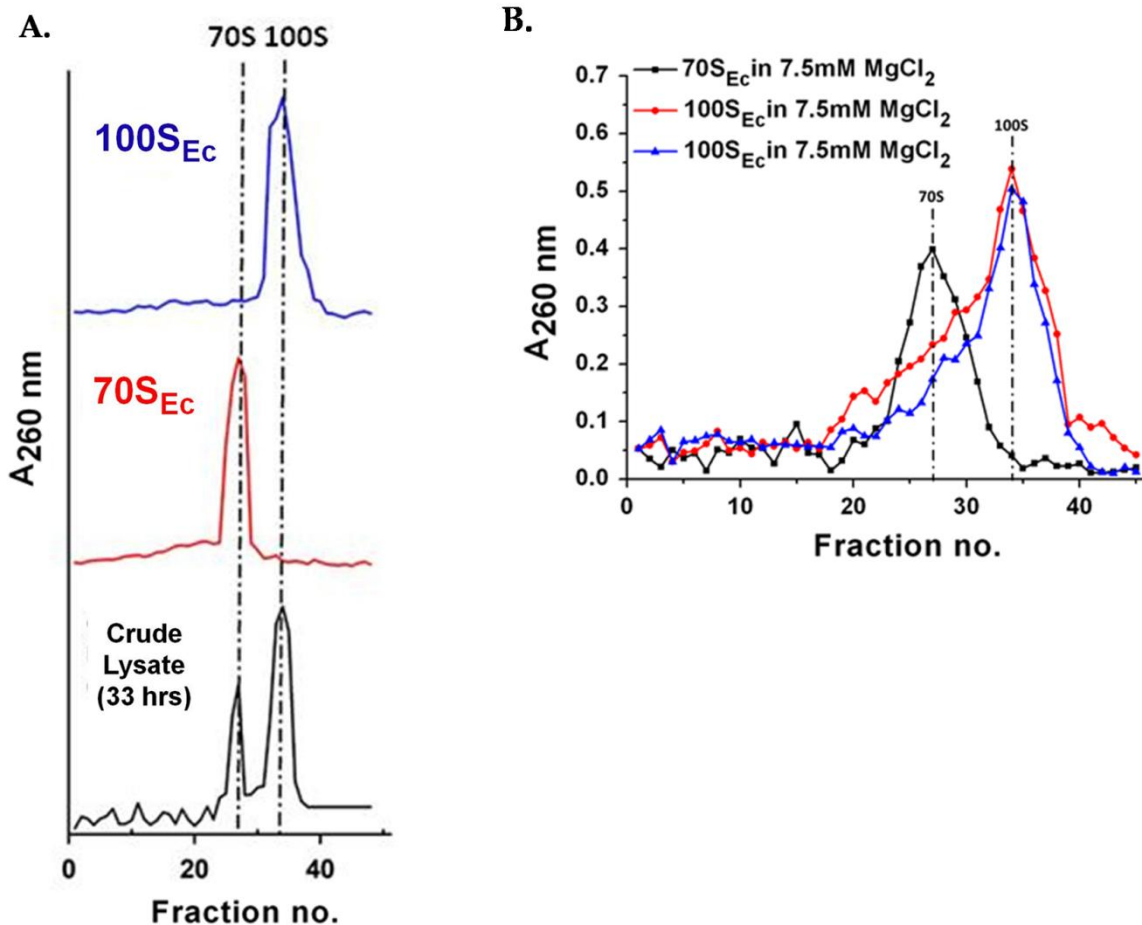


Figure 17: Purification and enrichment of 100S ribosome from BW25113 Δ yfa strain of *E. coli* (100S_{Ec})

Purification and enrichment of 100S_{Ec} ribosome from BW25113 Δ yfa strain of *E. coli* was performed as described in “Materials and Methods”.

A. Sucrose density gradient centrifugation profile (in 10%-60% gradient in Buffer G containing 25 mM MgCl₂) of (1) crude cell lysate of BW25113 Δ yfa strain of *E. coli* after 33 hours of incubation in minimal media at 37 °C, containing a major proportion of 100S_{Ec}, (2) 70S_{Ec} isolated from MRE600 strain of *E. coli* run on gradient and plotted to mark the position of the 70S_{Ec} ribosome and (3) 100S_{Ec} ribosome obtained after enrichment through sequential sucrose density gradient centrifugation. The dotted lines represent the positions of the 70S_{Ec} and 100S_{Ec} ribosome peaks.

B. Sucrose density gradient profile depicting the varying levels of overlap that is obtained between the 70S_{Ec} and 100S_{Ec} peaks when the respective ribosomes are exposed to 7.5 mM MgCl₂ concentration and run on the 10%-60% sucrose density gradient in different ultracentrifugation runs under the same conditions as stated in “Materials and Methods”.

However, as discussed above, previous studies have demonstrated that unfolded protein-mediated ribosome subunit dissociation occurs optimally at 7.5 mM magnesium ion concentration [Pathak et al., 2017]. Hence for our studies with 100S ribosome and unfolded

protein, the required magnesium ion concentration that was needed to be maintained was 7.5 mM. Therefore, a comparison of the stability of the 100S ribosome at this lower concentration of magnesium (7.5 mM) to that used for purification (25 mM) was essential before proceeding with any further experiments with unfolded protein. The sucrose density gradient profile of 100S_{Ec} ribosome was compared in presence of 7.5 mM and 25 mM Mg⁺² ion concentrations. A comparative analysis of the areas under the 70S_{Ec} and 100S_{Ec} ribosomal peaks reveals a variable overlap between the ribosomal peaks in different experiments, possibly due to the reduced stability of the dimeric ribosome at low Mg⁺² concentration [Gohara et al., 2018]. This is indicative of contribution (approximately 30%- 40%) of the 70S_{Ec} ribosome in the 100S_{Ec} preparation (**Figure 17B**). Keeping a note of this observation subsequent experiments were carried out to study the outcomes of unfolded protein-100S interactions.

B.2. Unfolded protein mediated dissociation of 100S ribosome isolated from Escherichia coli (100S_{Ec})

The first objective of our studies with unfolded protein (uBCAII) and 100S_{Ec} was to explore the ability of the unfolded protein to dissociate the 100S_{Ec} ribosome using light scattering analysis and SDGC, as detailed in Section A. For this purpose A_{260 nm} units equivalent of 0.1 μM 100S_{Ec} ribosome was incubated with 5-fold and 10-fold excess concentrations of chemically denatured BCAII (uBCAII) and the change in light scattering intensity was monitored at 350 nm over a period of 300 seconds to assess the ability of uBCAII to dissociate the 100S_{Ec}. As discussed in Section A, a change in Rayleigh light scattering over time is a technique used extensively to study ribosomal subunit dissociation [Antoun et al., 2004, Pathak et al., 2017].

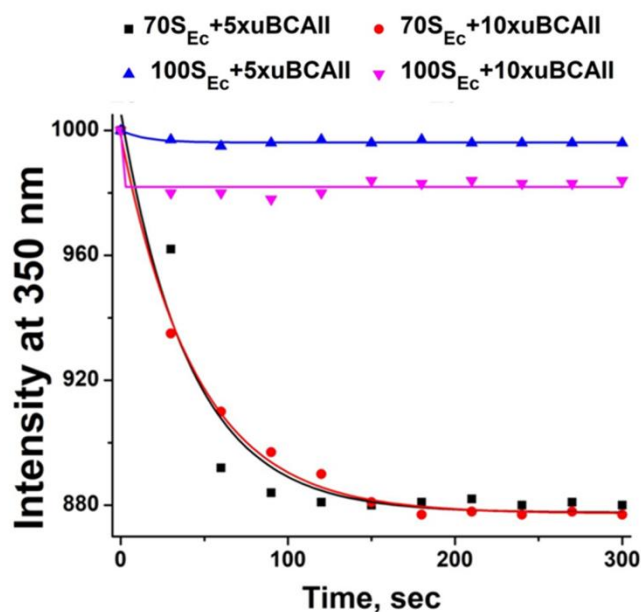
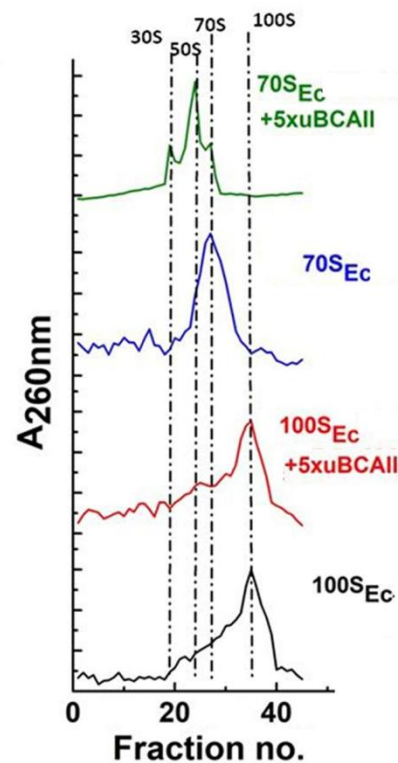
A.**B.**

Figure 18: *100S* ribosome from *E. coli* (*100S_{Ec}*) can resist unfolded protein mediated subunit dissociation

A. Light scattering analysis of uBCAII mediated *70S_{Ec}* and *100S_{Ec}* ribosome subunit dissociation: Time course change in light scattering intensity at 350 nm upon interaction of *70S_{Ec}* (0.1 μ M) and *100S_{Ec}* ($A_{260\text{ nm}}$ units equivalent of 0.1 μ M) ribosome (1x = 0.1 μ M or $A_{260\text{ nm}}$ units equivalent of 0.1 μ M) with uBCAII (5x) and uBCAII (10x) concentrations (Materials and Methods). *70S_{Ec}*+5x uBCAII (■), *100S_{Ec}*+5x uBCAII (▲), *70S_{Ec}*+10x uBCAII (●) and *100S_{Ec}*+10x uBCAII (▼) in Buffer G containing 7.5 mM Mg^{2+} ion concentration.

B. Sedimentation analysis of uBCAII mediated *70S_{Ec}* and *100S_{Ec}* ribosome (x = 0.1 μ M or $A_{260\text{ nm}}$ units equivalent of 0.1 μ M) subunit dissociation: Sucrose gradient profile of (1) *100S_{Ec}* in Buffer G containing 7.5mM $MgCl_2$, (2) *100S_{Ec}* +5x uBCAII in Buffer G containing 7.5mM $MgCl_2$, (3) *70S_{Ec}* in Buffer G containing 7.5mM $MgCl_2$ and (4) *70S_{Ec}*+5x uBCAII in Buffer G containing 7.5mM $MgCl_2$. The dotted lines represent the positions of the *100S_{Ec}* and *70S_{Ec}* ribosome peak as well as the positions of the respective 50S and 30S subunits.

As shown in **Figure 18A**, a reduction in light scattering intensity was observed when the empty *70S_{Ec}* ribosome was treated with 5-fold excess concentration of unfolded BCAII (uBCAII). However, no similar reduction was observed upon treatment of *100S_{Ec}* ribosome with 5-fold or even 10-fold excess concentration of the unfolded protein. This experiment suggests that, unlike the *70S_{Ec}* ribosome, the unfolded protein is incapable of dissociating the

dimeric 100S_{Ec} ribosome under the conditions used in our experiments. Sucrose density gradient centrifugation studies also confirmed that the peak corresponding to the 100S_{Ec} ribosomal population remains intact in presence of unfolded BCAII (**Figure 18B**). As stated above, the 100S_{Ec} ribosome preparation also contains a population of 70S_{Ec} ribosome (**Figure 17B**). The inability of the unfolded protein to dissociate even the 70S_{Ec} ribosome present in the 100S_{Ec} preparation therefore implies that, the 70S_{Ec} monomers which originate from the 100S_{Ec} ribosome might still remain bound to the hibernation factor HPF. As shown in **Figure 7A** and **7B**, HPF itself can inhibit the uBCAII-mediated subunit dissociation of 70S_{Ec}. Earlier studies performed *in vivo* have indeed demonstrated that when the stationary phase cells are transferred into fresh medium, although 100S_{Ec} ribosomal dimers are dissociated into 70S_{Ec} ribosomes, HPF still remains associated with these monomeric ribosomes [Maki et al., 2000]. Our studies therefore imply that unfolded protein is unable to dissociate the 100S_{Ec} ribosome into its constituent ribosomal subunits.

It has been shown in earlier studies that HflX in concert with GTP is capable of dissociating the 100S_{Ec} ribosome [Basu et al., 2017] and 70S_{Ec} ribosome bound to the ribosomal stress factors [Zhang et al., 2015]. Hence, further experiments were performed to study the ability of HflX-GTP to dissociate the 100S_{Ec} ribosome. Light scattering experiments demonstrated that HflX-GTP is capable of dissociating the empty 70S_{Ec} and the 100S_{Ec} ribosome under the conditions used in our experiment (**Figure 19A**). Sucrose density gradient centrifugation experiments also showed that the treatment of the ribosome with HflX-GTP leads to dissociation of the 70S_{Ec} ribosome. The ability of HflX-GTP to dissociate the 100S_{Ec} ribosome into its constituent subunits was also confirmed by sucrose density gradient centrifugation studies as shown in **Figure 19B**.

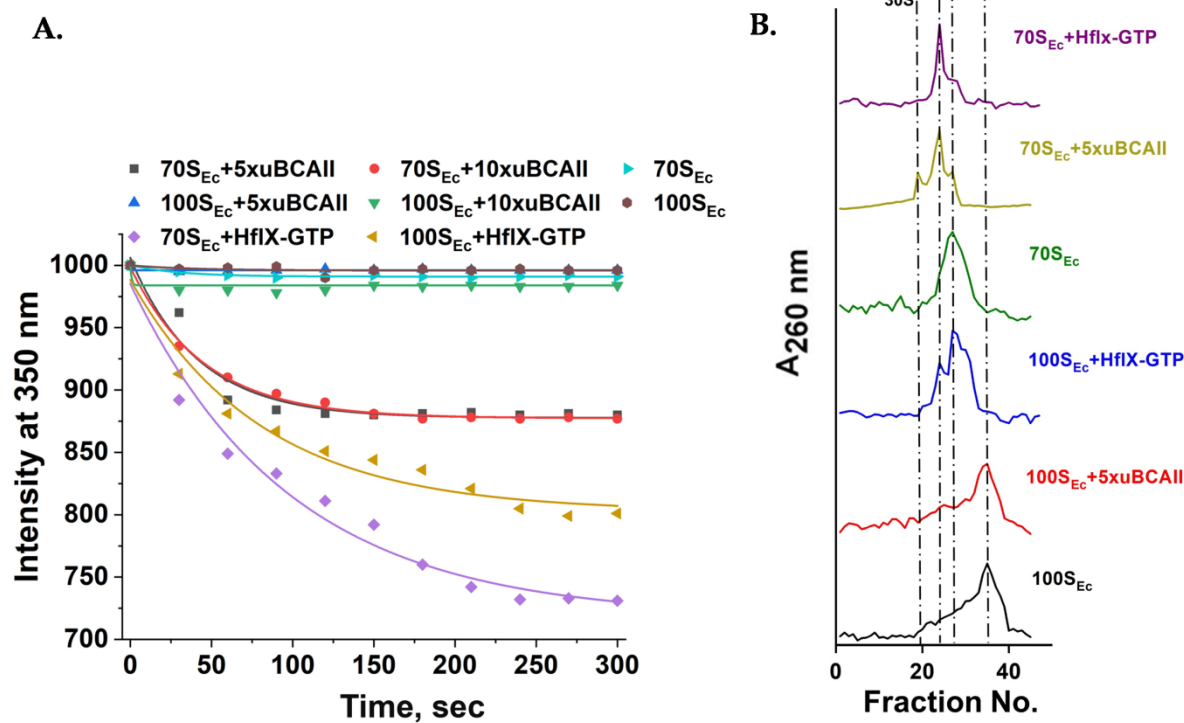


Figure 19: Comparison of uBCAII and HflX-GTP mediated dissociation of 70S (70S_{Ec}) and 100S (100S_{Ec}) ribosome from *E. coli*

A. Light scattering analysis of uBCAII and HflX-GTP mediated 70S_{Ec} and 100S_{Ec} ribosome subunit dissociation: Time course change in light scattering intensity at 350 nm upon interaction of 70S_{Ec} (0.1 μM) and 100S_{Ec} (A_{260 nm} units equivalent of 0.1 μM) ribosome (1x = 0.1 μM or A_{260 nm} units equivalent of 0.1 μM) with uBCAII (5x) and uBCAII (10x) concentrations or with 10x HflX (1 μM) in presence of 100 μM GTP (Materials and Methods). 70S_{Ec}+5x uBCAII (■), 100S_{Ec}+5x uBCAII (▲), 70S_{Ec}+ HflX + GTP (◆), 70S_{Ec}+10x uBCAII (●), 100S_{Ec}+10x uBCAII (▼), 100S_{Ec}+HflX+ GTP (◄), 70S_{Ec} (▶) and 100S_{Ec} (●) in Buffer G containing 7.5 mM Mg²⁺ ion concentration.

B. Sedimentation analysis of uBCAII and HflX-GTP mediated 70S_{Ec} and 100S_{Ec} ribosome (1x = 0.1 μM or A_{260 nm} units equivalent of 0.1 μM) subunit dissociation: Sucrose gradient profile of (1) 100S_{Ec} in Buffer G containing 7.5mM MgCl₂, (2) 100S_{Ec} +5x uBCAII in Buffer G containing 7.5mM MgCl₂, (3) 100S_{Ec}+10x HflX+1000x GTP in Buffer G containing 7.5mM MgCl₂, (4) 70S_{Ec} in Buffer G containing 7.5mM MgCl₂, (5) 70S_{Ec}+5x uBCAII in Buffer G containing 7.5mM MgCl₂ and (6) 70S_{Ec} +10x HflX+1000x GTP in Buffer G containing 7.5mM MgCl₂. The dotted lines represent the positions of the 100S_{Ec} and 70S_{Ec} ribosome peak as well as the positions of the respective 50S and 30S subunits.

Taken together, these studies suggest that while the dissociation of the 100S_{Ec} ribosome is necessarily factor-mediated, these dimeric ribosomal structures remain protected from unfolded protein-mediated subunit dissociation.

B.3. Degradation of 100S ribosome isolated from *E.coli* ($100S_{Ec}$) in the presence of cellular nucleases

As discussed above in Section A, the unfolded protein (uBCAII)-mediated ribosome dissociation renders the ribosome prone to degradation by cellular ribonucleases [Pathak et al., 2017]. Our previous experiments revealed that the binding of HPF can protect the ribosomal population from being degraded in the presence of 5-fold excess concentration of uBCAII and the cellular nucleases present in the mS30 extract (**Figure 11**). The next question was whether the $100S_{Ec}$ ribosome dimers that are resistant towards unfolded protein mediated subunit dissociation are also protected from subsequent degradation by cellular nucleases. In this experiment, the $100S_{Ec}$ ribosome was incubated with mS30 cellular extract containing nucleases in the presence and absence of 5x uBCAII and the outcome was analyzed using equilibrium sucrose density gradient centrifugation (SDGC) (“Materials and Methods”).

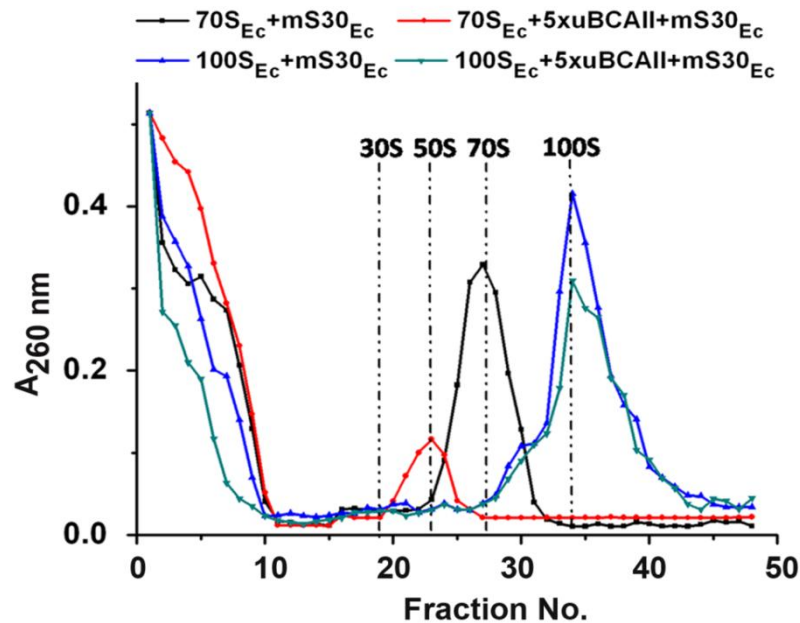


Figure 20: $100S$ ($100S_{Ec}$) ribosome from *E.coli* is protected from degradation mediated by nucleases present in cellular extract

*Sedimentation analysis of the degradation of $70S_{Ec}$ and $100S_{Ec}$ ribosome (1x = 0.1 μM or $A_{260\text{ nm}}$ units equivalent of 0.1 μM) upon incubation with *E. coli* mS30 extract ($mS30_{Ec}$) for 90 minutes in the presence of 5x uBCAII (Materials and Methods). As control sets, $70S_{Ec}$ ribosome and $100S_{Ec}$ ribosome alone were incubated with $mS30_{Ec}$ extract for the same period of time. Gradient profiles shown are $70S_{Ec} + mS30_{Ec}$ extract (\blacksquare), $100S_{Ec} + mS30_{Ec}$ extract (\blacktriangle), $70S_{Ec} + 5x\text{uBCAII} + mS30_{Ec}$ extract (\bullet) and $100S_{Ec} + 5x\text{uBCAII} + mS30_{Ec}$ extract (\blacktriangledown). The dotted lines represent the positions of the $100S_{Ec}$ and $70S_{Ec}$ ribosome peaks as well as the positions of the respective 50S and 30S subunits.*

As observed from the equilibrium SDGC $A_{260\text{ nm}}$ profile in **Figure 20**, when the empty 70S_{Ec} and the 100S_{Ec} ribosomes were treated with unfolded protein and incubated with the mS30 extract (prepared from MG1655 *E. coli* cells), the nucleases present in the extract were capable of degrading subunits formed from the 70S_{Ec} ribosome, while the undissociated 100S_{Ec} ribosome was resistant to similar degradation in presence of the unfolded protein.

B.4. 100S ribosome isolated from E.coli (100S_{Ec}) can assist in protein folding

Our next objective was to assess whether the 100S_{Ec} ribosome could act as a chaperone and assist in the folding of unfolded protein. Subsequent experiments were performed, along the lines of our previously discussed experiments with HPF bound 70S ribosome, to compare the chaperoning activity of the dimeric 100S_{Ec} ribosome and the 70S_{Ec} ribosome. The empty 70S_{Ec} ribosome and the 100S_{Ec} ribosome preparation (0.3 μM based on $A_{260\text{ nm}}$), were incubated at stoichiometric concentrations with uBCAII and the chaperoning activity was measured as stated in “Materials and Methods” and as discussed in Section A. As shown in **Figure 21**, the empty 70S_{Ec} and the 100S_{Ec} ribosome showed comparable chaperoning ability. To test whether the chaperoning activity observed could originate from the residual population of the 70S_{Ec} ribosome present in the 100S_{Ec} preparation, refolding of 0.3 μM uBCAII was performed with sub-stoichiometric (uBCAII: ribosome ratios of 1:0.5, 1:0.25) concentrations of the 70S_{Ec} and 100S_{Ec} ribosomes with respect to the unfolded protein. The outcome of the ribosome assisted BCAII refolding was, as with *E. coli* 70S ribosome, influenced by the different stoichiometry of unfolded protein and ribosome (the relative unfolded protein: ribosome ratio) present during the experiment (**Figure 21**). This experiment also implies that the contribution of the residual 70S_{Ec} ribosome, present in the 100S_{Ec} preparation, towards the chaperoning activity of the latter, though present, is negligible.

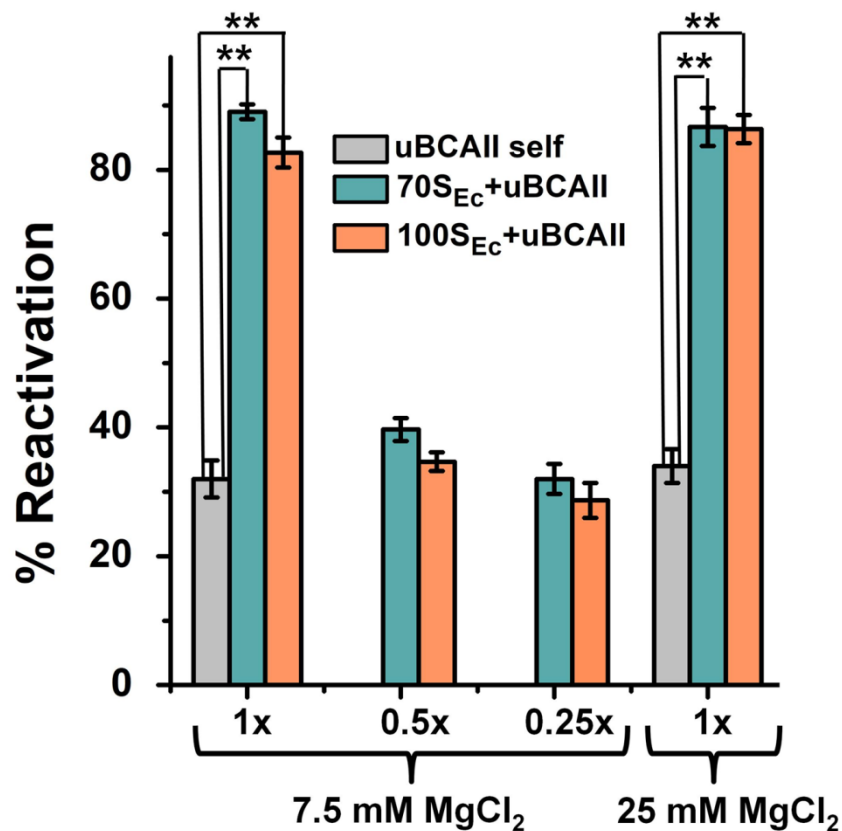


Figure 21: Chaperoning activity of 100S (100S_{Ec}) ribosome from *E.coli*

Refolding assay of uBCAII (0.3 μ M) in the presence and absence of different stoichiometric concentrations of 70S_{Ec} and 100S_{Ec} (Materials and Methods). Bar graph showing percentage reactivation of uBCAII self, 70S_{Ec}+uBCAII and 100S_{Ec}+uBCAII when 70S_{Ec} (0.3 μ M, 0.15 μ M and 0.075 μ M) and 100S_{Ec} (equivalent A_{260 nm} units corresponding to 0.3 μ M, 0.15 μ M and 0.075 μ M) are present in concentrations (1) 1x (0.3 μ M or equivalent A_{260 nm} units corresponding to 0.3 μ M in Buffer G containing 7.5 mM MgCl₂), (2) 0.5x (0.15 μ M or equivalent A_{260 nm} units corresponding to 0.15 μ M in Buffer G containing 7.5 mM MgCl₂), (3) 0.25x (0.075 μ M or equivalent A_{260 nm} units corresponding to 0.075 μ M in Buffer G containing 7.5 mM MgCl₂) and (4) 1x (0.3 μ M or equivalent A_{260 nm} units corresponding to 0.3 μ M in Buffer G containing 25 mM MgCl₂). The experiments were repeated thrice and the data are presented as means \pm SEM; *P< 0.05 or **P< 0.001 in one-way ANOVA (N= 3).

Further studies also showed that the 100S_{Ec} and 70S_{Ec} ribosome have comparable chaperoning activity at higher Mg⁺² concentration (25 mM) (**Figure 21**) at which there is negligible contribution of 70S_{Ec} in the 100S_{Ec} preparation (**Figure 17A**). These studies imply that the 100S_{Ec} dimeric ribosome exhibits chaperoning activity that is comparable to that of the 70S_{Ec} ribosome. Subsequent refolding experiments were performed with the 70S_{Ec} and the

100S_{Ec} ribosomes in the presence of increasing concentrations of the PTC binding substrates like Blasticidine S (BLS) and 6-aminophenanthridine (6AP) that are, as discussed previously, known inhibitors of PTC mediated ribosome chaperoning activity (Section A). Hence refolding studies were conducted in the presence of BLS and 6AP, to observe whether chaperoning ability exhibited by the 100S_{Ec} ribosome was mediated by the PTC of the individual 70S ribosomal particles constituting the dimer.

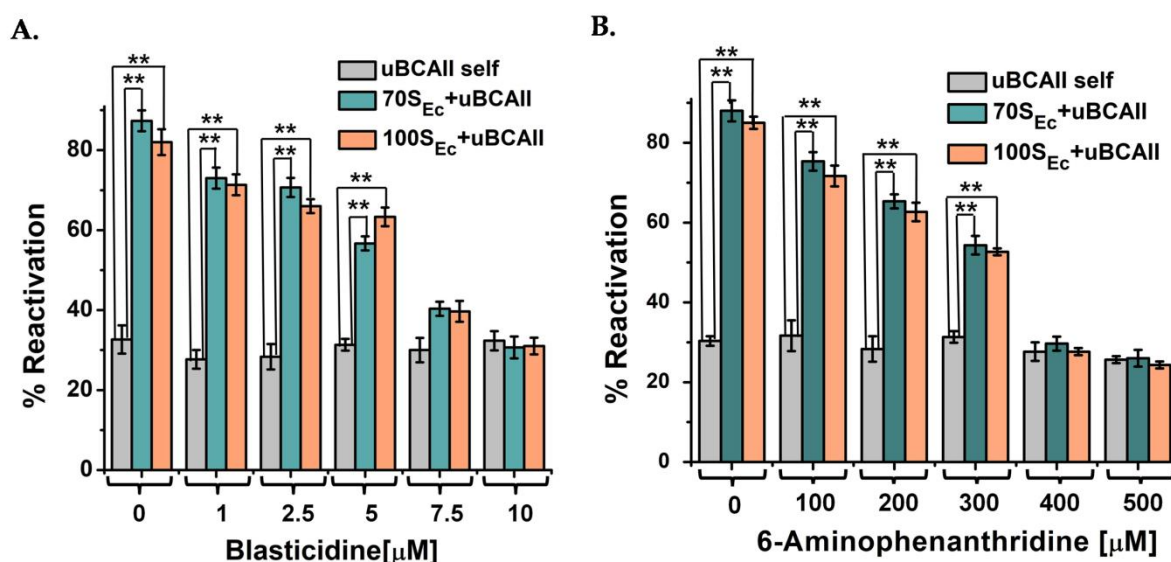


Figure 22: Chaperoning activity of 100S (100S_{Ec}) ribosome from *E.coli* in the presence of Blasticidine S (BLS) and 6-Aminophenanthridine (6AP)

A. Refolding assay of uBCAII in the presence of 70S_{Ec} and 100S_{Ec} with Blasticidine S (BLS): Bar graph showing percentage reactivation of uBCAII self (0.3 μM), uBCAII assisted by 70S_{Ec} (0.3 μM) or 100S_{Ec} (A_{260 nm} units equivalent of 0.3 μM) in the presence of (1) 0 μM BLS (2) 1 μM BLS, (3) 2.5 μM BLS, (4) 5 μM BLS, (5) 7.5 μM BLS and (6) 10 μM BLS.

B. Refolding assay of uBCAII in the presence of 70S_{Ec} and 100S_{Ec} with 6-Aminophenanthridine (6AP): Bar graph showing percentage reactivation of uBCAII self (0.3 μM), uBCAII assisted by 70S_{Ec} (0.3 μM) or 100S_{Ec} (A_{260 nm} units equivalent of 0.3 μM) in the presence of (1) 0 μM 6AP, (2) 100 μM 6AP, (3) 200 μM 6AP, (4) 300 μM 6AP, (5) 400 μM 6AP and (6) 500 μM 6AP. The experiments were repeated thrice and the data are presented as means ± SEM; *P < 0.05 or **P < 0.001 in one-way ANOVA (N = 3).

Lowering of BCAII reactivation yield in the presence of increasing concentrations of BLS and 6AP would be an indicator that the chaperoning is PTC-mediated. A dose-dependent suppression of chaperoning activity in presence of increasing concentrations BLS (Figure

22A) and 6AP (Figure 22B) was observed. Hence, it could be concluded that the ability of both 70S_{Ec} and the 100S_{Ec} ribosome to act as protein folding modulators originated from the PTC of the respective ribosomes and the chaperoning action of the 70S_{Ec} and the 100S_{Ec} ribosomes could occur following a similar mechanism [Das et al., 2008].

B.5. 100S ribosome isolated from *E.coli* (100S_{Ec}) can suppress protein aggregation

As discussed previously, during stressful situations, the more urgent requirement for cell viability is the control of protein aggregation due to accumulation of misfolded and unfolded proteins (Section A). Hence, we conducted further studies, along the lines of the experiments performed with HPF bound 70S ribosome, on the effect of 100S_{Ec} on aggregating protein systems like the reduced-denatured lysozyme (R/D Lyso) or molten globule form of BCAII protein (mBCAII).

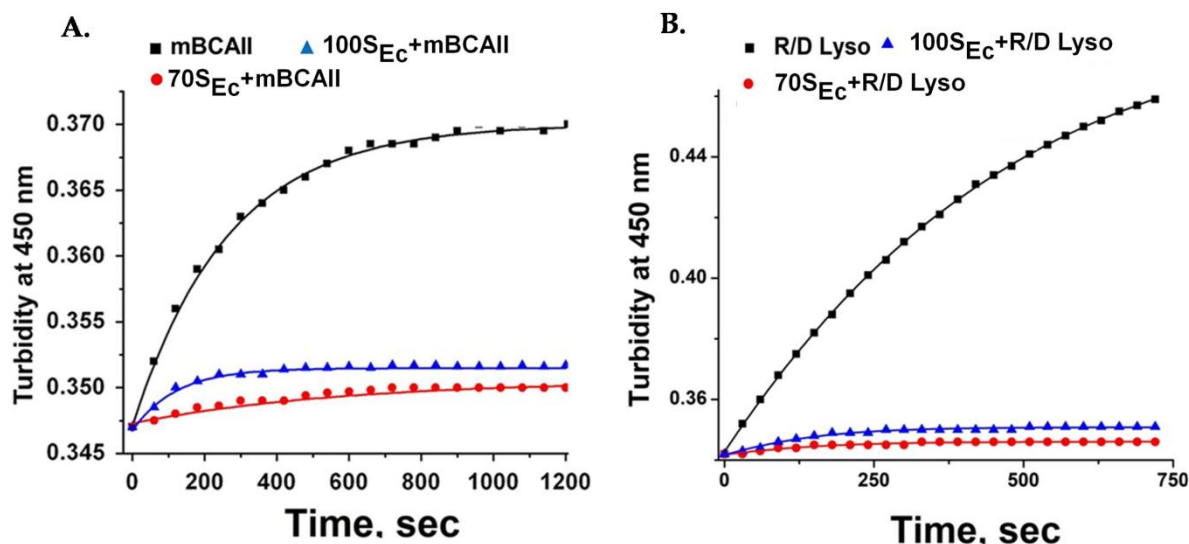


Figure 23: 100S (100S_{Ec}) ribosomes from *E.coli* can suppress aggregation of proteins

A. Time course of aggregation of mBCAII in the presence of 70S_{Ec} and 100S_{Ec} ribosome: The time course of change in turbidity at 450 nm was measured for 0.9 μM of mBCAII (Materials and Methods) for 1200 seconds in the presence and absence of 0.9 μM of 70S_{Ec} ribosome and A_{260 nm} units equivalent of 0.9 μM of 100S_{Ec} ribosome. mBCAII self (■), 70S_{Ec}+ mBCAII (●), 100S_{Ec}+mBCAII (▲).

B. Time course of aggregation of R/D Lyso in the presence of 70S_{Ec} and 100S_{Ec} ribosome: The time course of change in turbidity at 450 nm was measured for 2 μM of R/D Lyso (Materials and Methods) for 720 seconds in the presence and absence of 2 μM of 70S_{Ec} ribosome and A_{260 nm} units equivalent of 2 μM of 100S_{Ec} ribosome. R/D Lyso self (■), 70S_{Ec}+R/D Lyso (●), 100S_{Ec} +R/D Lyso (▲).

As shown in **Figure 23A** (for mBCAII) and **Figure 23B** (for R/D Lyso), 100S_{Ec} ribosome was indeed capable of suppressing protein aggregation. Considering the large number of ribosomes present in the cell, our present studies suggest that the chaperoning activity of the translationally suppressed ribosome might be capable of assisting in protein folding and mitigating protein aggregation under stress conditions.

B.6. Purification and enrichment of *S.aureus* 100S (100S_{Sa}) ribosome

The 100S_{Sa} ribosomal particles were isolated from MTCC 3160 strain of *S.aureus*, enriched and purified as reported earlier [Beckert et al. 2018, Ueta et al. 2010] and stated in the “Materials and Methods” section. As stated earlier (in the “Introduction” section of this chapter) , the 100S_{Sa} ribosome is present in the cells even during the exponential phase of their growth under nutrient abundant conditions [Basu et al., 2016, Prossliner et al., 2018, Ueta et al., 2010]. Hence, with the aim of isolating the 100S_{Sa} ribosome from the exponential phase, these bacterial cells were grown in TSB (Tryptic soy broth) for 4 hours. The ribosomal profile of the crude cell lysate obtained after cell lysis and removal of cell debris, using sucrose density gradient centrifugation, demonstrated the presence of a significant population of 70S_{Sa} as well as 100S_{Sa} ribosomes. The relevant fractions corresponding to the 70S_{Sa} and 100S_{Sa} ribosomal peak were pooled and subjected to repeated rounds of concentration and sucrose density gradient centrifugation to obtain an enriched and purified population of *S.aureus* 70S_{Sa} and 100S_{Sa} ribosomes. As mentioned before, the stability of the 100S ribosome is reduced in the presence of low magnesium concentrations [Gohara et al., 2018]. Hence, similar to the 100S_{Ec} purification, a high concentration of magnesium (25 mM) [Khusainov et al., 2017] was maintained in all buffers and gradients involved in the purification process to maintain the stability of the 100S_{Sa} ribosome.

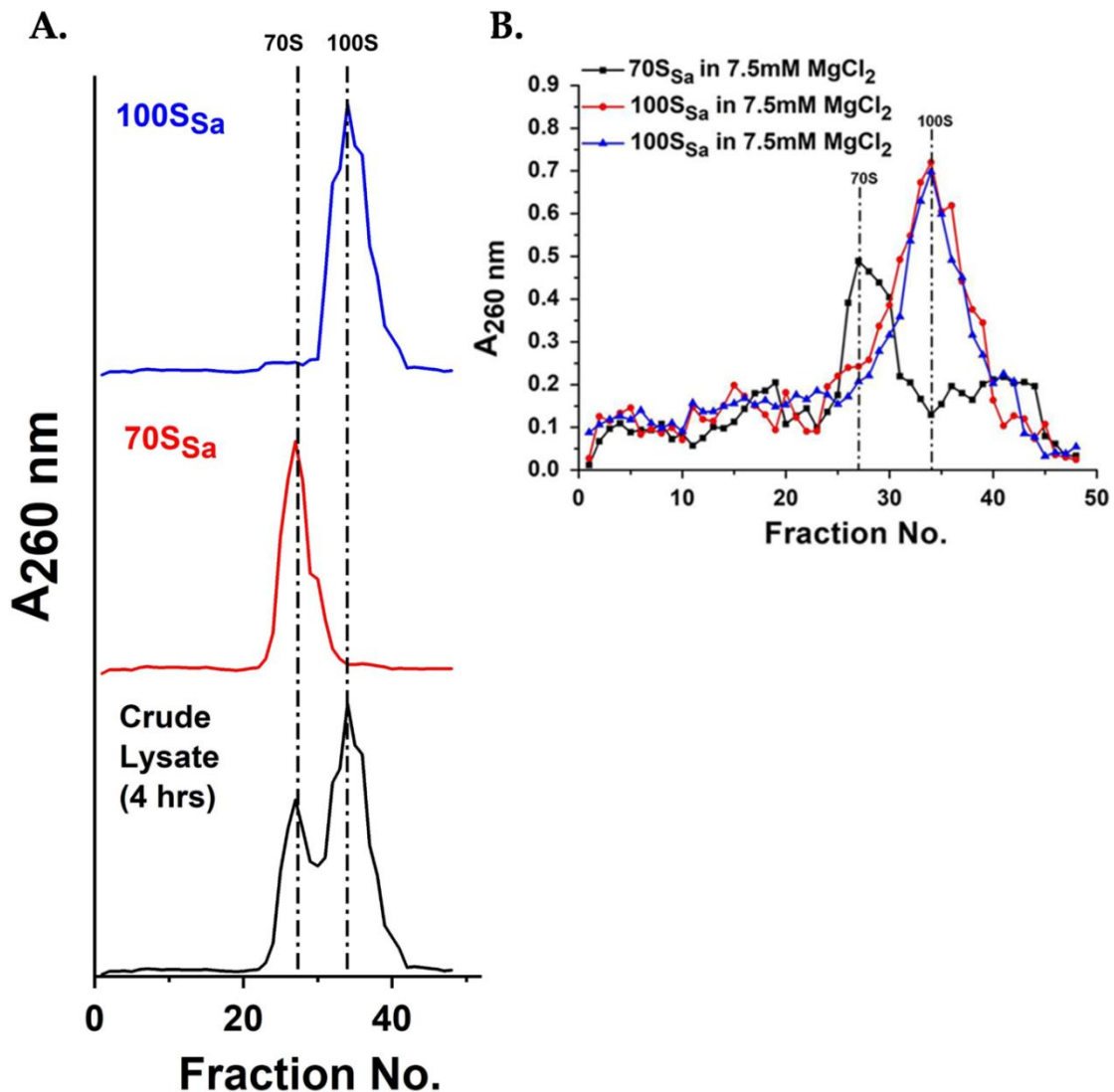


Figure 24: Purification and enrichment of 70S (70S_{Sa}) and 100S (100S_{Sa}) ribosome from MTCC 3160 strain of *Staphylococcus aureus*

A. Purification and enrichment of 70S_{Sa} and 100S_{Sa} ribosome from *Staphylococcus aureus* (*S.aureus*) was performed using the MTCC 3160 strain of *S.aureus* cells that were harvested after 4 hours of incubation at 37 °C in TSB media. The crude lysate from the cells was prepared and subjected to sucrose cushion, the pellet obtained dissolved in B100S buffer (Materials and Methods) and purification and enrichment of 70S_{Sa} and 100S_{Sa} was performed on a sucrose density gradient (Materials and Methods). Sucrose density gradient centrifugation profile of (in 10%-60% gradient in Buffer G containing 25 mM MgCl₂) (1) Crude lysate pellet of MTCC 3160 strain of *S.aureus*, prepared after 4 hours of incubation at 37 °C in TSB media, (2) 70S_{Sa} ribosome isolated, purified and enriched from crude lysate pellet via sequential sucrose density gradient centrifugation, (3) 100S_{Sa} ribosome isolated, purified and enriched from the crude lysate pellet via sequential sucrose density gradient centrifugation. The dotted lines represent the positions of the 70S_{Sa} and 100S_{Sa} ribosome peaks.

B. Sucrose density gradient profile depicting the varying levels of overlap that is obtained between the 70S_{Sa} and 100S_{Sa} peaks when the respective ribosomes are exposed to 7.5 mM MgCl₂ concentration and run on the 10%-60% sucrose density gradient in different ultracentrifugation runs under the same conditions as stated in the “Materials and Methods” section.

As shown in **Figure 24A**, after sequential rounds of concentration and SDGC, a pure and enriched population of 100S_{Sa} as well as 70S_{Sa} ribosome was obtained that was used in our subsequent experiments. It should be noted that as in the studies with the *E. coli* ribosomes (stated above), light scattering and refolding experiments with the *S. aureus* ribosomes were also performed at Mg²⁺ concentration of 7.5 mM. The variable overlap between the 100S and 70S ribosomal peaks that is observed in sucrose density gradient profiles at 7.5 mM Mg²⁺ concentration (**Figure 24B**), indicates that at the lower Mg²⁺ ion concentration there is a contribution of 70S_{Sa} ribosomes (30-40%) in the 100S_{Sa} preparation. Bearing this in mind, subsequent experiments were carried out to study the outcomes of unfolded protein-100S interactions.

B.7. Unfolded protein-mediated subunit dissociation of 100S ribosome isolated from Staphylococcus aureus (100S_{Sa})

Preliminary studies performed with unfolded protein (uBCAII) and 70S_{Sa} and 100S_{Sa} explored the ability of the unfolded protein to dissociate the respective ribosomes and a comparison was drawn. For this purpose, A_{260 nm} units equivalent of 0.1 μM 70S_{Sa} and 100S_{Sa} ribosomes were incubated with 5-fold and 10-fold excess concentrations of chemically denatured BCAII (uBCAII) and the change in light scattering intensity was monitored at 350 nm over a period of 300 seconds to assess the ability of uBCAII to dissociate the 100S_{Sa}.

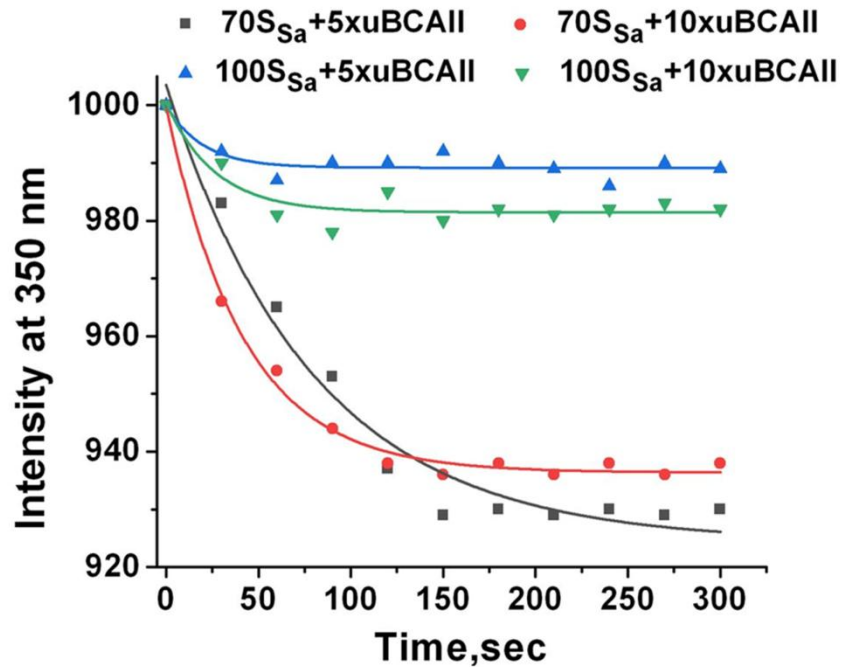


Figure 25: *100S* ribosome from *S.aureus* (*100S_{Sa}*) can resist unfolded protein-mediated subunit dissociation

Light scattering analysis of uBCAII-mediated 70S_{Sa} and 100S_{Sa} ribosome subunit dissociation: Time course change in light scattering intensity at 350 nm upon interaction of 70S_{Sa} (1x = A_{260 nm} units equivalent 0.1 μM) and 100S_{Sa} (A_{260 nm} units equivalent of 0.1 μM) ribosome with 5x and 10x concentrations of unfolded BCAII (uBCAII), denatured with 6 M Guanidine hydrochloride. 70S_{Sa}+5x uBCAII (■), 100S_{Sa}+5x uBCAII (▲), 70S_{Sa}+10x uBCAII (●) and 100S_{Sa}+10x uBCAII (▼).

As shown in **Figure 25**, a reduction in light scattering is observed when the empty 70S_{Sa} ribosome is treated with 5-fold excess concentration of unfolded BCAII (uBCAII). However no similar reduction is observed upon treatment of 100S_{Sa} ribosome with 5-fold or even 10-fold excess concentration of the unfolded protein. These studies therefore indicate that, similar to that observed with the 100S_{Ec} ribosome (isolated from gram-negative *E.coli* cells), the dimeric ribosome isolated from gram-positive *S. aureus* bacteria is also resistant towards dissociation by unfolded proteins.

B.8. 100S ribosome isolated from *Staphylococcus aureus* (100S_{Sa}) can assist in protein folding

Subsequent experiments were performed to assess the chaperoning activity of ribosomes isolated from *S. aureus*. In these experiments 0.3 μM of uBCAII was incubated with or without the 70S_{Sa} and the 100S_{Sa} ribosomes (A_{260 nm} units equivalent of 0.3 μM) and the reactivation of the uBCAII was assayed in Buffer G (containing 7.5 mM Mg²⁺). As shown in **Figure 26A**, both the 100S_{Sa} and the 70S_{Sa} ribosome could assist in the refolding and reactivation of the BCAII protein. The outcome of the ribosome assisted BCAII refolding was, as with *E. coli* ribosomes, influenced by the different stoichiometry of unfolded protein and ribosome (the relative unfolded protein: ribosome ratio) present during the experiment (**Figure 26B**).

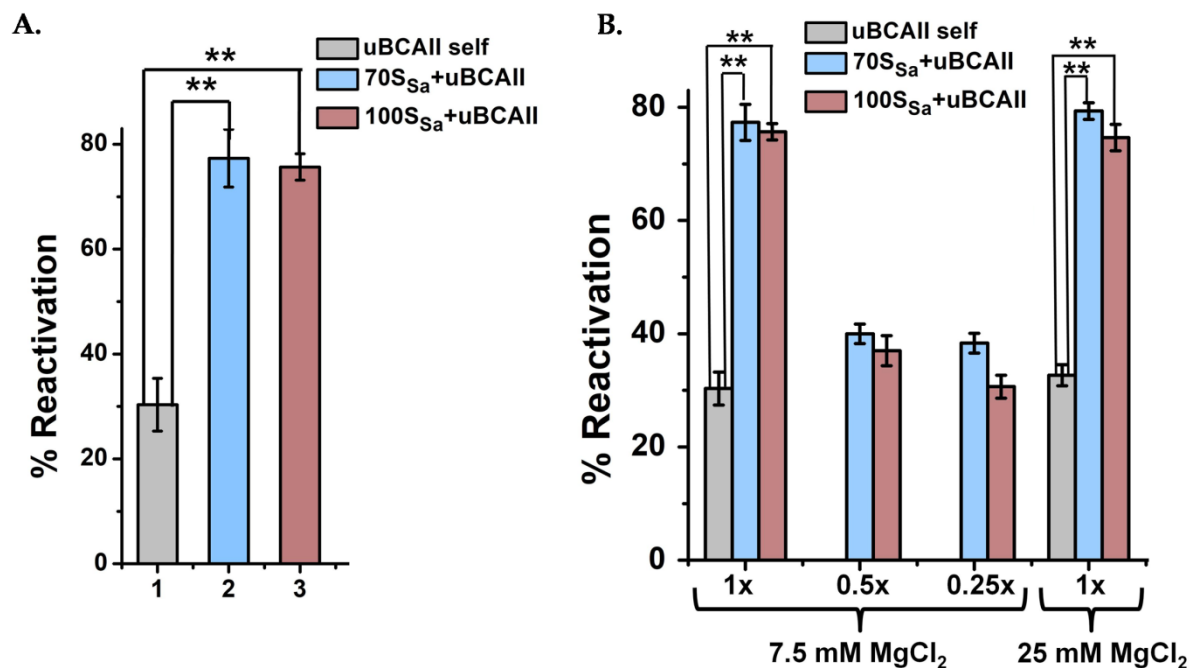


Figure 26: Chaperoning activity of 70S (70S_{Sa}) and 100S (100S_{Sa}) ribosomes from *S. aureus*

A. Refolding assay of uBCAII in the presence of 70S_{Sa} and 100S_{Sa} ribosomes: 0.3 μM of uBCAII was refolded in the presence and absence of 70S_{Sa} and 100S_{Sa} ribosomes (0.3 μM equivalent A_{260 nm} units in Buffer G containing 7.5 mM MgCl₂). The chaperoning activity of the ribosomes was measured by monitoring the recovery of BCAII enzyme activity (Materials and Methods). Bar graph showing percentage reactivation of (i) uBCAII self, (ii) 70S_{Sa}+uBCAII and (iii) 100S_{Sa}+uBCAII. The experiments were repeated thrice and the data are presented as means± SEM; *P< 0.05 or **P< 0.001 in one –way ANOVA (N= 3).

B. Refolding assay of uBCAII in the presence of 70S_{Sa} and 100S_{Sa} ribosomes: 0.3 μM of uBCAII was refolded in the presence and absence of different stoichiometric concentrations of 70S_{Sa} and 100S_{Sa} ribosomes. The chaperoning activity of the ribosomes was measured by monitoring the recovery of BCAII enzyme activity (Materials and Methods). Bar graph showing percentage reactivation of uBCAII self, 70S_{Sa}+uBCAII and 100S_{Sa}+uBCAII when 70S_{Sa} (equivalent A_{260 nm} units corresponding to 0.3 μM, 0.15 μM and 0.075 μM) and 100S_{Sa} (equivalent A_{260 nm} units corresponding to 0.3 μM, 0.15 μM and 0.075 μM) are present in concentrations (1) 1x (0.3 μM equivalent A_{260 nm} units in Buffer G containing 7.5 mM MgCl₂), (2) 0.5x (0.15 μM equivalent A_{260 nm} units in Buffer G containing 7.5 mM MgCl₂), (3) 0.25x (0.075 μM equivalent A_{260 nm} units in Buffer G containing 7.5 mM MgCl₂) and (4) 1x (0.3 μM equivalent A_{260 nm} units in Buffer G containing 25 mM MgCl₂). The experiments were repeated thrice and the data are presented as means± SEM; *P< 0.05 or **P< 0.001 in one –way ANOVA (N= 3).

This experiment also implies that the contribution to chaperoning activity of residual 70S_{Sa} ribosomes present in the 100S_{Sa} preparation is negligible. The chaperoning activity of 70S_{Sa} and 100S_{Sa} were also comparable in Buffer G containing 25 mM Mg²⁺ concentration (**Figure 26B**), at which there is negligible contribution of 70S_{Sa} in the 100S_{Sa} preparation (**Figure 24A**). These studies therefore demonstrated the ability of both 70S_{Sa} and 100S_{Sa} to act as a protein folding modulator.

B.9. 100S ribosome isolated from *Staphylococcus aureus* (100S_{Sa}) can suppress protein aggregation

As discussed previously, during stressful situations, a major challenge faced by the cell is protein aggregation that occurs due to the accumulation of misfolded and unfolded proteins. Hence, we conducted further studies on the effect of 100S_{Sa} as well as 70S_{Sa} on aggregating protein systems like molten globule form of BCAII protein (mBCAII).

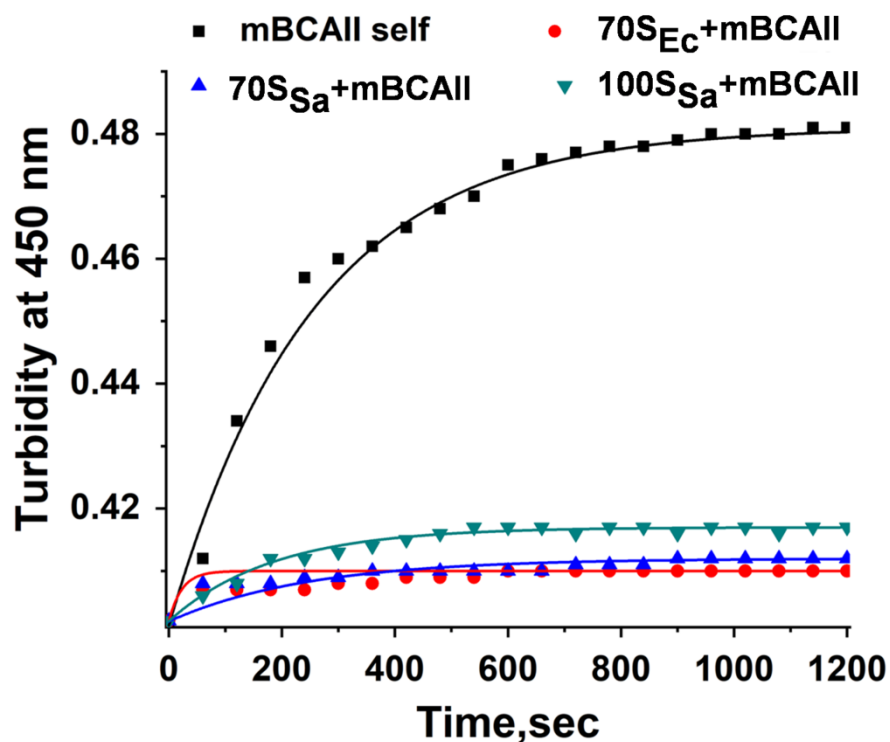


Figure 27: 70S (70S_{Sa}) and 100S (100S_{Sa}) ribosomes from *S.aureus* can suppress aggregation of proteins

Time course of aggregation of mBCAII in presence of 70S_{Sa} and 100S_{Sa} ribosome: The time course change in turbidity at 450 nm of 0.9 μM of mBCAII was measured for 1200 seconds in the absence and presence of stoichiometric concentrations (1x= 0.9 μM equivalent A_{260 nm} units) of 70S_{Sa} ribosome and 100S_{Sa} ribosome: mBCAII self (■), 70S_{Sa} + mBCAII (▲), 70S_{Ec}+ mBCAII (●), 100S_{Sa}+ mBCAII (▼).

Turbidity measurement studies, as shown in **Figure 27**, showed that both 70S_{Sa} and 100S_{Sa} ribosomes were indeed capable of suppressing aggregation of the mBCAII protein.

Conclusion

Earlier studies had demonstrated that, the outcomes of the ribosome-unfolded protein interaction are distinct and depend upon the unfolded protein concentration as follows: (a) At stoichiometric ribosome: protein ratio of 1:1, the empty ribosome acts as a protein folding modulator and the binding of the unfolded protein and its subsequent release leads to high BCAII reactivation yields [Das et al., 2008], (b) when a 5-fold excess amount of uBCAII is present with respect to the empty ribosome, the stable association between 50S and unfolded protein leads to lowered reactivation yields and the manifestation of 50S anti-association activity of unfolded proteins [Pathak et al., 2017]. The stable dissociation of empty ribosome into its subunits leads to their vulnerability towards degradation by cellular nucleases [Pathak et al., 2017]. Our studies suggest that in the presence of stationary phase associated factor HPF, the *E. coli* 70S ribosome retains the peptidyl transferase center-mediated protein folding activity and the ability to suppress protein aggregation. Further, the presence of these factors renders the 70S ribosome resistant to unfolded protein-mediated subunit dissociation. Based on the model shown in **Figure 14**, it has been proposed that the suppression of ribosome subunit dissociation might be due to the restriction in the movement of subunits of the factor-bound ribosome or might be correlated to the increase in association between the subunits of the stationary phase factor-bound ribosome. Such resistance of the factor-bound ribosome towards dissociation prevents its subsequent degradation by cellular nucleases. The 100S ribosome isolated from *E. coli* also displays chaperoning activity and can assist in refolding of unfolded protein and suppress aggregation of the aggregation prone molten globule form of BCAII (mBCAII) and reduced-denatured form of lysozyme (R/D Lyso). The dimeric ribosome also exhibits resistance towards uBCAII-mediated dissociation and subsequent degradation by cellular RNases. Preliminary studies performed with 70S and 100S ribosomes isolated from gram-positive *S. aureus* also revealed that (i) the 100S ribosome is relatively

resistant towards unfolded protein-mediated subunit dissociation and (ii) both the 70S and 100S ribosomes exhibit chaperoning activity. These observations are summarized in the model shown in **Figure 28**.

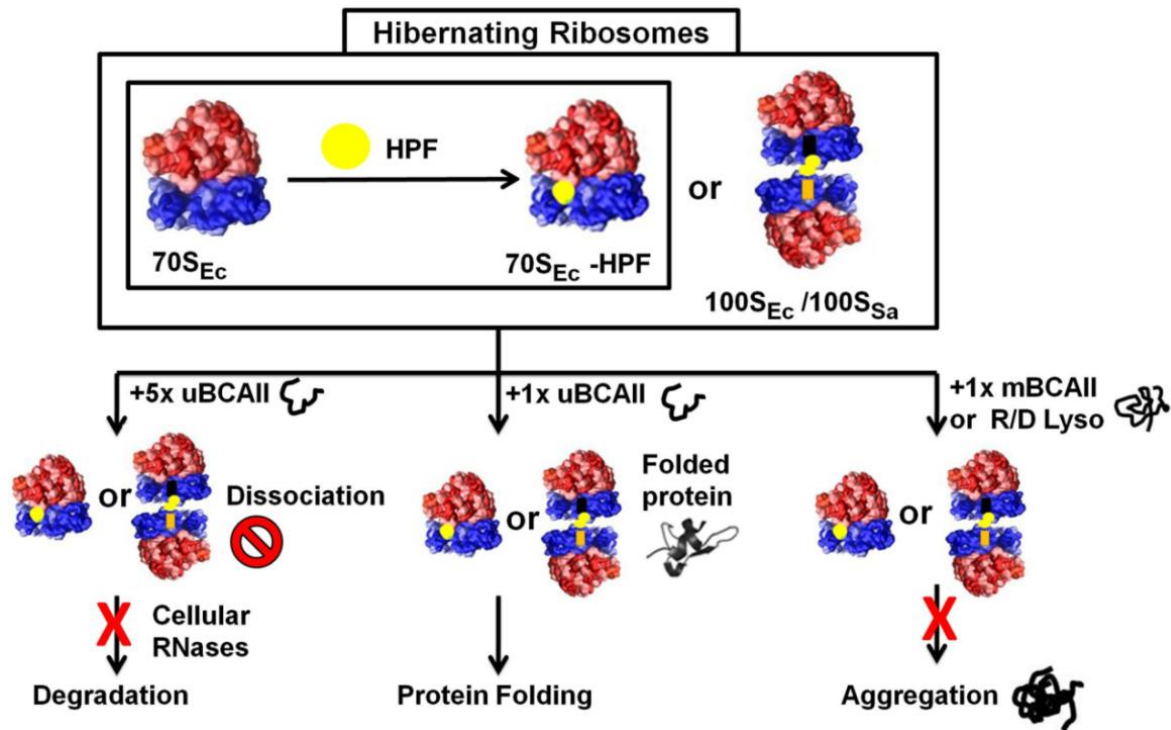


Figure 28: Model depicting the outcomes of unfolded protein-hibernating ribosome interaction:

In the presence of 5-fold excess concentration of uBCAII, stable dissociation of 70S_{Ec} ribosome into its subunits takes place which leaves them prone to degradation by the cellular ribonucleases. Hibernating ribosomes, 70S_{Ec}-HPF, 100S_{Ec} and 100S_{Sa}, are resistant to such unfolded protein-mediated subunit dissociation and subsequent degradation.

In the presence of stoichiometric concentrations of unfolded protein, 70S_{Ec} and 70S_{Sa} can assist in protein folding and act as an energy independent foldase chaperone. Hibernating ribosomes, 70S_{Ec}-HPF, 100S_{Ec} and 100S_{Sa}, can also exhibit such chaperoning activity in the presence of stoichiometric concentrations of unfolded protein. 70S ribosomes can also act as holdase chaperone and suppress aggregation of proteins. The hibernating ribosomes can also exhibit this activity and suppress protein aggregation

Previous studies on unfolded protein-ribosome interaction [Pathak et al., 2014, Pathak et al., 2017] provide ample evidence in support of a direct link that might exist between the accumulation of unfolded proteins during cellular stress and the increased probability of ribosome subunit dissociation and subsequent degradation. The hibernating ribosomal

complexes constitute a pool of non-translating ribosomes in the cell that are immune to dissociation and degradation. Our studies with hibernating ribosomes and HflX-GTP (**Figure 10** and **Figure 19**) demonstrate that the dissociation of these translationally silenced ribosomes is essentially factor-mediated and the presence of unfolded proteins is insufficient to induce such ribosomal subunit dissociation. The resistance of the hibernating ribosome (70S-HPF complex or the 100S ribosome) towards such dissociation might explain their stabilizing effect on the ribosomal population during the stationary phase. Ribosomal hibernation is not only significant for survival through the stationary phase, but is also implicated in the maintenance of virulence as well as the tolerance towards antibiotics displayed by the persister cell states of many pathogenic bacteria [Mckay et al., 2015, Prossliner et al., 2018, Basu et al., 2018]. The reason behind such observations is yet to be understood. It should be noted that, the molecular chaperoning activities were conventionally considered to be performed uniquely by the proteins themselves. However, several recent studies have recognized that RNA possesses protein folding ability which can indeed be more effective than the known chaperone proteins in facilitating protein folding and preventing protein aggregation [Docter et al., 2016]. The ribosome and its component 23S rRNA have been reported to behave like molecular chaperones *in vitro* in a *trans* acting mode, although their relevance to *de novo* protein folding *in vivo* still remains to be further characterized [Das et al., 2008]. The inability of P-site tRNA bound ribosome to act as a chaperone essentially segregates the population of ribosome involved in active translation from those involved in chaperoning activity [Mondal et al., 2014]. The hibernating translational machinery which is formed from the necessity of translation suppression under stress conditions would therefore be available for performing the non-canonical chaperoning activity. The biological significance of the formation of the hibernating ribosomes and their correlation to bacterial resilience under stress conditions is not completely understood [Basu et al., 2016]. The chaperoning activity of these ribosomes is the first evidence of a potential biological activity of the hibernating ribosome that might be crucial for cell survival under stress conditions.

The persister cells are subpopulations of dormant cells that are stress tolerant and present a significant clinical problem. However, the mechanism by which the microbial cells attain such resilience is poorly understood [Mckay et al., 2015]. This study provides further insights into how the hibernating ribosome might contribute towards cellular survival in a broad spectrum of stress conditions like stationary phase and the clinically relevant dormant persister cell states.

References

1. **Agafonov, D. E.**, Kolb, V. A., Nazimov, I. V., & Spirin, A. S. (1999). A protein residing at the subunit interface of the bacterial ribosome. *Proceedings of the National Academy of Sciences*, 96(22), 12345-12349.
2. **Antoun, A.**, Pavlov, M. Y., Tenson, T., & Ehrenberg, M. (2004). Ribosome formation from subunits studied by stopped-flow and Rayleigh light scattering. *Biological Procedures Online*, 6(1), 35-54.
3. **Baba, T.**, Ara, T., Hasegawa, M., Takai, Y., Okumura, Y., Baba, M., ... & Mori, H. (2006). Construction of Escherichia coli K-12 in-frame, single-gene knockout mutants: the Keio collection. *Molecular systems biology*, 2(1), 2006-0008.
4. **Banerjee, D.**, & Sanyal, S. (2014). Protein Folding Activity of the Ribosome (PFAR)—A Target for Antiprion Compounds. *Viruses*, 6(10), 3907-3924.
5. **Basu, A.**, Ghosh, J., Bhattacharya, A., Pal, S., Chowdhury, S., & DasGupta, C. (2003). Splitting of ribosome into its subunits by unfolded polypeptide chains. *Current Science*, 1123-1125.
6. **Basu, A.**, Samanta, D., Das, D., Chowdhury, S., Bhattacharya, A., Ghosh, J., ... & DasGupta, C. (2008). In vitro protein folding by E. coli ribosome: unfolded protein splitting 70S to interact with 50S subunit. *Biochemical and biophysical research communications*, 366(2), 598-603.
7. **Basu, A.**, Shields, K. E., Eickhoff, C. S., Hoft, D. F., & Yap, M. N. F. (2018). Thermal and nutritional regulation of ribosome hibernation in Staphylococcus aureus. *Journal of bacteriology*, 200(24), e00426-18.
8. **Basu, A.**, & Yap, M. N. F. (2016). Ribosome hibernation factor promotes Staphylococcal survival and differentially represses translation. *Nucleic acids research*, 44(10), 4881-4893.
9. **Basu, A.**, & Yap, M. N. F. (2017). Disassembly of the Staphylococcus aureus hibernating 100S ribosome by an evolutionarily conserved GTPase. *Proceedings of the National Academy of Sciences*, 114(39), E8165-E8173.

10. **Beckert, B.**, Abdelshahid, M., Schäfer, H., Steinchen, W., Arenz, S., Berninghausen, O., ... & Wilson, D. N. (2017). Structure of the *Bacillus subtilis* hibernating 100S ribosome reveals the basis for 70S dimerization. *The EMBO journal*, 36(14), 2061-2072.
11. **Beckert, B.**, Turk, M., Czech, A., Berninghausen, O., Beckmann, R., Ignatova, Z., ... & Wilson, D. N. (2018). Structure of a hibernating 100S ribosome reveals an inactive conformation of the ribosomal protein S1. *Nature microbiology*, 3(10), 1115-1121.
12. **Ben-Shem, A.**, de Loubresse, N. G., Melnikov, S., Jenner, L., Yusupova, G., & Yusupov, M. (2011). The structure of the eukaryotic ribosome at 3.0 Å resolution. *Science*, 334(6062), 1524-1529.
13. **Chakraborty, B.**, Bhakta, S., & Sengupta, J. (2016). Disassembly of yeast 80S ribosomes into subunits is a concerted action of ribosome-assisted folding of denatured protein. *Biochemical and biophysical research communications*, 469(4), 923-929.
14. **Chattopadhyay, S.**, Das, B., & Dasgupta, C. (1996). Reactivation of denatured proteins by 23S ribosomal RNA: role of domain V. *Proceedings of the National Academy of Sciences*, 93(16), 8284-8287.
15. **Chattopadhyay, S.**, Pal, S., Pal, D., Sarkar, D., Chandra, S., & Gupta, C. D. (1999). Protein folding in *Escherichia coli*: role of 23S ribosomal RNA. *Biochimica et Biophysica Acta (BBA)-Protein Structure and Molecular Enzymology*, 1429(2), 293-298.
16. **Coatham, M. L.**, Brandon, H. E., Fischer, J. J., Schümmer, T., & Wieden, H. J. (2016). The conserved GTPase HflX is a ribosome splitting factor that binds to the E-site of the bacterial ribosome. *Nucleic acids research*, 44(4), 1952-1961.
17. **Das, B.**, Chattopadhyay, S., Bera, A. K., & DasGupta, C. (1996). In vitro protein folding by ribosomes from *Escherichia coli*, wheat germ and rat liver: the role of the 50S particle and its 23S rRNA. *European journal of biochemistry*, 235(3), 613-621.
18. **Das, D.**, Das, A., Samanta, D., Ghosh, J., Dasgupta, S., Bhattacharya, A., ... & Das Gupta, C. (2008). Role of the ribosome in protein folding. *Biotechnology Journal: Healthcare Nutrition Technology*, 3(8), 999-1009.

19. **Das, D.**, Samanta, D., Hasan, S., Das, A., Bhattacharya, A., Dasgupta, S., ... & Gupta, C. D. (2012). Identical RNA-protein interactions in vivo and in vitro and a scheme of folding the newly synthesized proteins by ribosomes. *Journal of Biological Chemistry*, 287(44), 37508-37521.
20. **Deutscher, M. P.** (2003). Degradation of stable RNA in bacteria. *Journal of Biological Chemistry*, 278(46), 45041-45044.
21. **Deutscher, M. P.** (2006). Degradation of RNA in bacteria: comparison of mRNA and stable RNA. *Nucleic acids research*, 34(2), 659-666.
22. **Deutscher, M. P.** (2009). Maturation and degradation of ribosomal RNA in bacteria. *Progress in molecular biology and translational science*, 85, 369-391.
23. **Dey, S.**, Biswas, C., & Sengupta, J. (2018). The universally conserved GTPase HflX is an RNA helicase that restores heat-damaged Escherichia coli ribosomes. *Journal of Cell Biology*, 217(7), 2519-2529.
24. **Docter, B. E.**, Horowitz, S., Gray, M. J., Jakob, U., & Bardwell, J. C. (2016). Do nucleic acids moonlight as molecular chaperones?. *Nucleic acids research*, 44(10), 4835-4845.
25. **Dos Reis, S.**, Pang, Y., Vishnu, N., Voisset, C., Galons, H., Blondel, M., & Sanyal, S. (2011). Mode of action of the antiprion drugs 6AP and GA on ribosome assisted protein folding. *Biochimie*, 93(6), 1047-1054.
26. **Feng, B.**, Mandava, C. S., Guo, Q., Wang, J., Cao, W., Li, N., ... & Gao, N. (2014). Structural and functional insights into the mode of action of a universally conserved Obg GTPase. *PLoS biology*, 12(5), e1001866.
27. **Goerisch, H.**, Goss, D. J., & Parkhurst, L. J. (1976). Kinetics of ribosome dissociation and subunit association studied in a light-scattering stopped-flow apparatus. *Biochemistry*, 15(26), 5743-5753.
28. **Gohara, D. W.**, & Yap, M. N. F. (2018). Survival of the drowsiest: the hibernating 100S ribosome in bacterial stress management. *Current genetics*, 64(4), 753-760.

29. **Hall, D.**, Zhao, R., Dehlsen, I., Bloomfield, N., Williams, S. R., Arisaka, F., ... & Carver, J. A. (2016). Protein aggregate turbidity: Simulation of turbidity profiles for mixed-aggregation reactions. *Analytical biochemistry*, 498, 78-94.
30. **Kato, T.**, Yoshida, H., Miyata, T., Maki, Y., Wada, A., & Namba, K. (2010). Structure of the 100S ribosome in the hibernation stage revealed by electron cryomicroscopy. *Structure*, 18(6), 719-724.
31. **Khusainov, I.**, Vicens, Q., Ayupov, R., Usachev, K., Myasnikov, A., Simonetti, A., ... & Hashem, Y. (2017). Structures and dynamics of hibernating ribosomes from *Staphylococcus aureus* mediated by intermolecular interactions of HPF. *The EMBO journal*, 36(14), 2073-2087.
32. **Kiel, M. C.**, Kaji, H., & Kaji, A. (2007). Ribosome recycling: An essential process of protein synthesis. *Biochemistry and Molecular Biology Education*, 35(1), 40-44.
33. **Liu, Q.**, & Fredrick, K. (2016). Intersubunit bridges of the bacterial ribosome. *Journal of molecular biology*, 428(10), 2146-2164.
34. **Maki, Y.**, Yoshida, H., & Wada, A. (2000). Two proteins, YfiA and YhbH, associated with resting ribosomes in stationary phase *Escherichia coli*. *Genes to cells*, 5(12), 965-974.
35. **Matzov, D.**, Aibara, S., Basu, A., Zimmerman, E., Bashan, A., Yap, M. N. F., ... & Yonath, A. E. (2017). The cryo-EM structure of hibernating 100S ribosome dimer from pathogenic *Staphylococcus aureus*. *Nature communications*, 8(1), 1-7.
36. **McKay, S. L.**, & Portnoy, D. A. (2015). Ribosome hibernation facilitates tolerance of stationary-phase bacteria to aminoglycosides. *Antimicrobial agents and chemotherapy*, 59(11), 6992-6999.
37. **Mondal, S.**, Pathak, B. K., Ray, S., & Barat, C. (2014). Impact of P-Site tRNA and antibiotics on ribosome mediated protein folding: studies using the *Escherichia coli* ribosome. *PLoS One*, 9(7), e101293.
38. **Nierhaus, K. H.** (2014). Mg²⁺, K⁺, and the ribosome. *Journal of bacteriology*, 196(22), 3817-3819.

39. **Pal, S.**, Chandra, S., Chowdhury, S., Sarkar, D., Ghosh, A. N., & Gupta, C. D. (1999). Complementary role of two fragments of domain V of 23 S ribosomal RNA in protein folding. *Journal of Biological Chemistry*, 274(46), 32771-32777.
40. **Pang, Y.**, Kurella, S., Voisset, C., Samanta, D., Banerjee, D., Schabe, A., ... & Sanyal, S. (2013). The antiprion compound 6-aminophenanthridine inhibits the protein folding activity of the ribosome by direct competition. *Journal of Biological Chemistry*, 288(26), 19081-19089.
41. **Pathak, B. K.**, Banerjee, S., Mondal, S., Chakraborty, B., Sengupta, J., & Barat, C. (2017). Unfolded protein exhibits antiassociation activity toward the 50S subunit facilitating 70S ribosome dissociation. *The FEBS journal*, 284(22), 3915-3930.
42. **Pathak, B. K.**, Mondal, S., Ghosh, A. N., & Barat, C. (2014). The ribosome can prevent aggregation of partially folded protein intermediates: studies using the Escherichia coli ribosome. *PloS one*, 9(5), e96425.
43. **Pechmann, S.**, Willmund, F., & Frydman, J. (2013). The ribosome as a hub for protein quality control. *Molecular cell*, 49(3), 411-421.
44. **Piir, K.**, Paier, A., Liiv, A., Tenson, T., & Maiväli, Ü. (2011). Ribosome degradation in growing bacteria. *EMBO reports*, 12(5), 458-462.
45. **Polikanov, Y. S.**, Blaha, G. M., & Steitz, T. A. (2012). How hibernation factors RMF, HPF, and YfiA turn off protein synthesis. *Science*, 336(6083), 915-918.
46. **Prossliner, T.**, SkovboWinther, K., Sørensen, M. A., & Gerdes, K. (2018). Ribosome hibernation. *Annual review of genetics*, 52, 321-348.
47. **Raman, B.**, Ramakrishna, T., & Rao, C. M. (1996). Refolding of denatured and denatured/reduced lysozyme at high concentrations. *Journal of Biological Chemistry*, 271(29), 17067-17072.
48. **Samanta, D.**, Mukhopadhyay, D., Chowdhury, S., Ghosh, J., Pal, S., Basu, A., ... & DasGupta, C. (2008). Protein folding by domain V of Escherichia coli 23S rRNA: specificity of RNA-protein interactions. *Journal of bacteriology*, 190(9), 3344-3352.

49. **Starosta, A. L.**, Lassak, J., Jung, K., & Wilson, D. N. (2014). The bacterial translation stress response. *FEMS microbiology reviews*, *38*(6), 1172-1201.
50. **Tran, Q. H.**, & Uden, G. (1998). Changes in the proton potential and the cellular energetics of *Escherichia coli* during growth by aerobic and anaerobic respiration or by fermentation. *European journal of biochemistry*, *251*(1- 2), 538-543.
51. **Ueta, M.**, Ohniwa, R. L., Yoshida, H., Maki, Y., Wada, C., & Wada, A. (2008). Role of HPF (hibernation promoting factor) in translational activity in *Escherichia coli*. *Journal of biochemistry*, *143*(3), 425-433.
52. **Ueta, M.**, Wada, C., & Wada, A. (2010). Formation of 100S ribosomes in *Staphylococcus aureus* by the hibernation promoting factor homolog SaHPF. *Genes to Cells*, *15*(1), 43-58.
53. **Ueta, M.**, Wada, C., Daifuku, T., Sako, Y., Bessho, Y., Kitamura, A., ... & Wada, A. (2013). Conservation of two distinct types of 100 S ribosome in bacteria. *Genes to Cells*, *18*(7), 554-574.
54. **Ueta, M.**, Yoshida, H., Wada, C., Baba, T., Mori, H., & Wada, A. (2005). Ribosome binding proteins YhbH and YfiA have opposite functions during 100S formation in the stationary phase of *Escherichia coli*. *Genes to Cells*, *10*(12), 1103-1112.
55. **Usachev, K. S.**, Yusupov, M. M., & Validov, S. Z. (2020). Hibernation as a Stage of Ribosome Functioning. *Biochemistry (Moscow)*, *85*(11), 1434-1442.
56. **Valle, M.**, Zavialov, A., Sengupta, J., Rawat, U., Ehrenberg, M., & Frank, J. (2003). Locking and unlocking of ribosomal motions. In *Single-Particle Cryo-Electron Microscopy: The Path Toward Atomic Resolution: Selected Papers of Joachim Frank with Commentaries* (pp. 347-358).
57. **Vila-Sanjurjo, A.**, Schuwirth, B. S., Hau, C. W., & Cate, J. H. (2004). Structural basis for the control of translation initiation during stress. *Nature structural & molecular biology*, *11*(11), 1054-1059.
58. **Walter, S.**, & Buchner, J. (2002). Molecular chaperones—cellular machines for protein folding. *Angewandte Chemie International Edition*, *41*(7), 1098-1113.

59. **Yamagishi, M.**, Matsushima, H., Wada, A., Sakagami, M., Fujita, N., & Ishihama, A. (1993). Regulation of the Escherichia coli rmf gene encoding the ribosome modulation factor: growth phase- and growth rate- dependent control. *The EMBO Journal*, *12*(2), 625-630.
60. **Zhang, Y.**, Mandava, C. S., Cao, W., Li, X., Zhang, D., Li, N., ... & Gao, N. (2015). HflX is a ribosome-splitting factor rescuing stalled ribosomes under stress conditions. *Nature structural & molecular biology*, *22*(11), 906-913.
61. **Zundel, M. A.**, Basturea, G. N., & Deutscher, M. P. (2009). Initiation of ribosome degradation during starvation in Escherichia coli. *Rna*, *15*(5), 977-983.

Chapter 3

Eukaryotic ribosome and aggregating proteins

Introduction:

The increased incidence of amyloid pathologies, like the neurodegenerative disorder Alzheimer's disease (AD), has made it critical to delineate the molecular basis of amyloidosis. As discussed earlier (in Chapter 1, Section B.1), onset of AD is marked by the appearance of senile plaques composed of A β peptides. The most well characterized forms of A β are the abundantly present 40 residue, A β 1-40 (A β 40) and the aggregation prone 42 residue, A β 1-42 (A β 42), which mostly constitute the amyloid plaques. Previous studies have revealed that the ratio of A β 42:A β 40 in the cerebrospinal fluid is a significant biomarker that can distinguish AD from other forms of dementia [Wiltfang et al., 2007]. The A β peptide comprises of a polar N-terminal region (residues 1-22) and a hydrophobic C-terminal region (residues 23 to 40/42). The highly hydrophobic central region, comprising of residues 16-21(KLVFFA), constitutes the most aggregation prone part of the sequence which can mediate fibril formation on its own [Preston et al., 2012]. As discussed earlier (Chapter 1, Section B.3), aggregation of A β proceeds in a nucleation-dependent manner where several peptide molecules interact amongst each other through hydrophobic [Kim et al., 2006] or electrostatic interactions [Buell et al., 2013]. These interactions lead to the formation of oligomers and oligomeric nuclei, following which aggregation proceeds rapidly to form proto-fibrillar and fibrillar structures that are ultimately deposited in the amyloid plaques.

Amyloid aggregation and its modulators:

Extensive *in vitro* and *in vivo* studies characterizing A β amyloid fibrils have revealed that they are heterogeneous structures [Eichner et al., 2011] and differences in fibril morphology can culminate in differences in disease progression among individuals. In addition to being composed of A β 40 and A β 42 peptides, the plaques also host several non-proteinaceous macromolecular components which might be of physiological importance (**Figure 1**).

Interaction of the amyloid fibrils with such macromolecules can also alter their aggregation properties [Stewart et al., 2017].

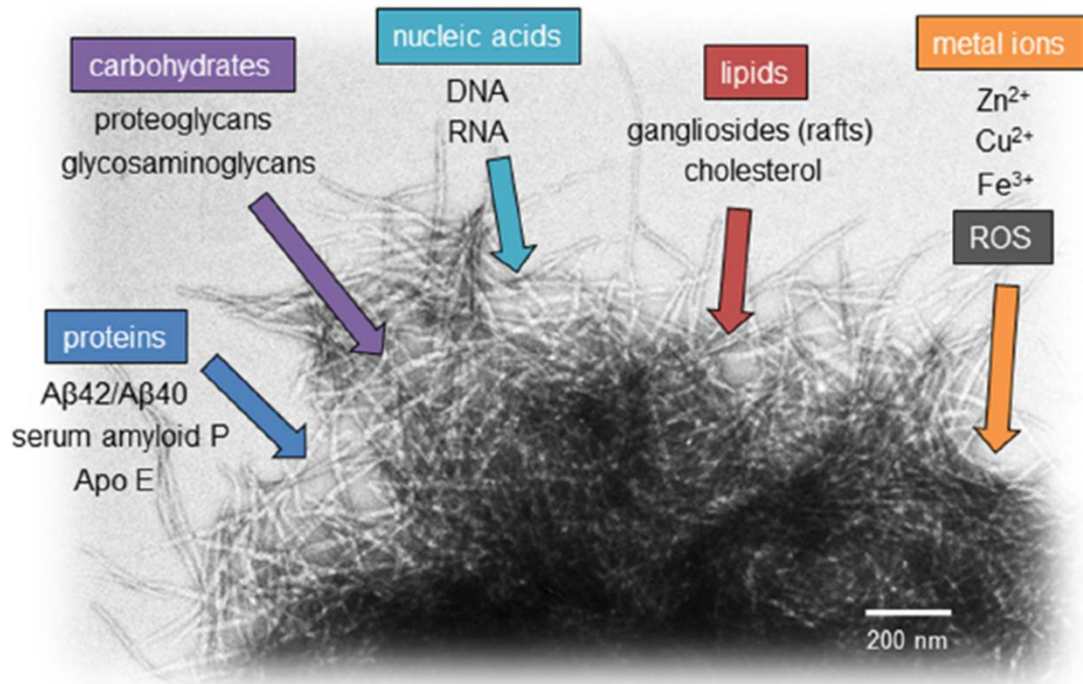


Figure 1: *The diverse contents of Amyloid β plaques*

Amyloid β ($A\beta$) plaques can have non-proteinaceous macromolecular components as shown in the TEM image of aggregated $A\beta$ fibrils [Figure adapted from Stewart et al., 2017].

Carbohydrates are often found in amyloid plaques in the form of sulphated proteoglycans and glycosaminoglycans (GAGs). Studies with heparan sulphate and heparin have revealed that negatively charged sulphate moieties of the GAGs are critical to the interaction with amyloid fibrils implying the role of electrostatics in such interactions [Castillo et al., 1999]. It should be noted that although the $A\beta$ peptides are not predominantly positively charged entities, they possess clusters of positively and negatively charged residues distributed along their length. Studies also revealed that binding of heparin to amyloids is also dependent on specific topological requirements for both the interacting partners and the complete removal of the negatively charged sulphate moieties from heparin inhibited its ability to stimulate

aggregation thereby implying that the ions individually do not stimulate aggregation and a linear chain of repeating negatively charged units on a sugar backbone chain might be crucial for fibril stabilization [Castillo et al., 1999]. This study therefore highlighted the importance of electrostatics as well as topology in interactions between A β peptides and its aggregation modulators. Amyloid fibrils also associate strongly with polyanions and the structure of fibrillar aggregates are stabilized by non-covalent interactions. The strength of such interactions depend on the charge density of the polyanionic molecules and is facilitated by the clusters of positive charges distributed throughout the A β amino acid sequence [Calamai et al., 2006].

Cellular modulators of amyloid aggregation also include lipids, metal ions and polyphosphates. The detection of lipids in the amyloid plaques also brought forth the possibility of their modulatory effect on A β aggregation. These molecules influence amyloidogenic protein aggregation by increasing their local concentration [Kiskis et al., 2015]. Lipid rafts composed of laterally associated gangliosides and cholesterol can affect the oligomerization of A β 42, while those enriched with gangliosides can enhance A β 40 fibrillization and modify the fibril structure thereby increasing their neurotoxic effects [Kim et al., 2006, Stewart et al., 2017]. Lipid membranes can also affect A β aggregation by inducing the formation of amyloid pore structures [Arispe et al., 1993] that are composed of protofibrils [Inoue, 2008]. Pore formation can induce cellular toxicity by enabling passive transport of small molecules or induce reactive oxygen species generation, which have damaging consequences towards the cells, as well as dysregulation of metal ions [Butterfield et al., 2010]. Hence the modulatory role of lipids towards A β aggregation can have important cellular implications [Stewart et al., 2017]. Metal ions constitute another group of non-proteinaceous components of the amyloid plaques. Previous studies have revealed that A β 40 can act as deviant Zn²⁺ and Cu²⁺ ion chelator, thus causing an imbalance of metal ions in the

brain by assisting in the formation of amyloid pores. A β -ion interaction depends on the surrounding pH, relative concentration of the interacting partners as well as oxidative states of the ions. Other metal ions like Fe³⁺, Ca²⁺, Mg²⁺, Mn²⁺ and Al³⁺ can also have indirect modulatory effect on amyloid aggregation [Hare et al., 2016, Li et al., 2013]. It has been demonstrated that polyphosphates are another group of amyloid aggregation modulators that can serve as amyloid binding scaffold which stabilizes the peptides in fibril competent β sheet conformation [Cremers et al., 2016]. Physiological concentration of polyphosphates was shown to be capable of accelerating the transition of amyloid monomers into cross β sheet amyloid fibrils and can effectively prevent shedding off of pre-formed fibrils. The presence of polyphosphates can thus reduce the lag phase and increase the rate of nucleation of A β and thus modulates the amyloidogenic process in a more general way [Cremers et al., 2016].

Nucleic Acids as modulators of amyloid β aggregation

The aggregation of A β peptides proceeds in an inducer-independent manner which is in contrast to the aggregation of Tau-protein variants that require the presence of a polyanionic inducer for the initiation of aggregation [Ramachandran et al., 2011]. Nucleic acids form a group of abundantly available cellular polyanions. Extensive studies with prion proteins and prion-like proteins have shown that RNA can act as a modulator of prion aggregation [Kovachev et al., 2019, Cordeiro et al., 2019, Kovachev et al., 2017] and the stimulatory or inhibitory nature of such modulation depends on the relative concentrations of the protein and RNA [Kovachev et al., 2017, Kovachev et al., 2019]. Prion protein interaction with RNA has also been implied to form the basis of their liquid-liquid phase separation and crystalline aggregate formation [Louka et al., 2020]. It has been suggested in previous studies that association between amyloid proteins and nucleic acids is electrostatically driven through interactions between basic regions of the A β peptide chains and nucleic acid phosphate groups and that nucleic acids can induce and accelerate the aggregation of amyloid proteins

through a template effect. The template effect entails the restriction of amyloid protein orientation along the nucleic acid chain, effectively increasing their local concentrations and intermolecular hydrophobic interactions that facilitate aggregation [Jiang et al., 2007]. Molecular dynamic studies have also revealed that RNA-amyloid recognition might be peptide sequence dependent with certain sequences on the amyloid peptides displaying affinity towards RNA which might engage with the cellular RNA and hence disturb the designated biochemical pathway for that RNA molecule [Meli et al., 2018].

Nucleic acids are also found within the amyloid plaques as one of the non-proteinaceous components. Several studies have identified RNA within the A β plaques thereby establishing intraneuronal participation of RNA in A β aggregation within diseased neurons [Ginsberg et al., 1997, Ginsberg et al., 1998]. Previous studies have demonstrated that cytoplasmic RNA molecules, besides acting as inducer of Tau aggregation in the formation of PHFs, may also act as “pathological chaperones” and interact with intracellular A β to form toxic fibrillary aggregates that are deposited in plaques [Ginsberg et al., 1998].

Based on the studies stated above, it can be concluded that the role of nucleic acids as amyloid aggregation modulators is well-established and the active participation of RNA is implicated in neurodegenerative diseases [Louka et al., 2020]. However, the consequences of A β -RNA interaction remain to be deciphered. Our study aims to gain further insights into this interaction with respect to the factors that might influence their outcome and whether such an interaction could underlie the destabilization of ribosomal population observed during AD.

Inhibitors of amyloid aggregation:

Polyphenols are widely known to have beneficial effects on prion-like diseases and extensive studies have demonstrated that high levels of polyphenol consumption can reduce the risk of dementia by 50% [Commenges et al., 2000]. These compounds have an inhibitory effect on

the deposition of neurodegenerative disease related proteins, like the AD associated A β and Tau proteins. This effect is mediated by either impeding their fibril formation or by inducing their disaggregation. Polyphenolic inhibitors mediate their function by directly interacting with the proteins or by interacting with the metal ions that promote aggregation. They are able to bind to and chelate many bivalent cations that are implicated in amyloid aggregation. These compounds have also been shown to exert their inhibitory effect through interactions with A β oligomers and preventing the maturation of these structures into A β fibrils that are deposited in the plaques [Freyssin et al., 2018].

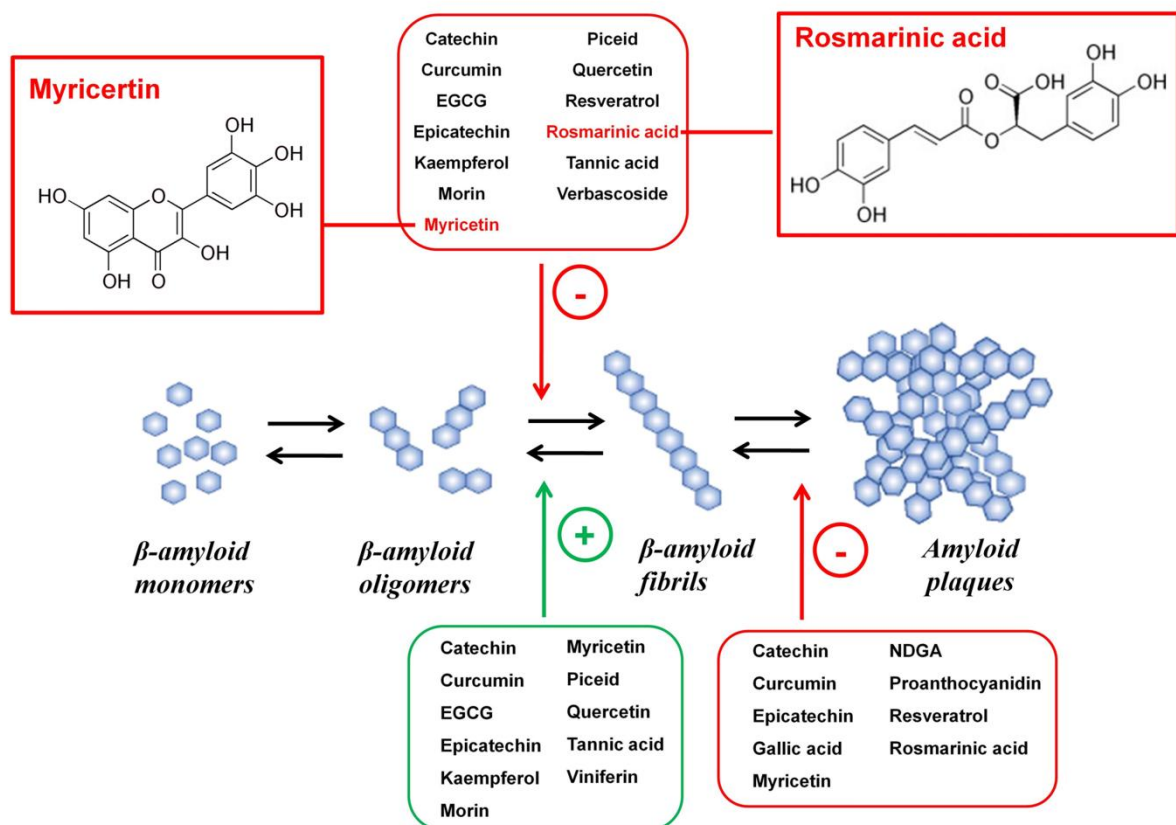


Figure 2: Polyphenolic compounds as inhibitors of amyloid aggregation

Schematic representation of polyphenols modulating the aggregation of Amyloid β in Alzheimer's disease. [Figure adapted from Freyssin et al., 2018].

Studies by Ono et al., [2012] have demonstrated that the polyphenolic compound myricetin (Myr) can dose dependently inhibit formation of A β 40 and A β 42 fibrils as well as inhibit the further extension of these fibrillary aggregates. It could also destabilize fibrillar A β in a dose dependent manner. Rosmarinic acid (RA) is another such polyphenolic inhibitor which mediates its effect by directly interacting and interfering with the β -sheet structures in A β peptides [Ono et al., 2012, Taguchi et al., 2017]. A schematic depicting the mode of inhibitory action of these polyphenols towards β amyloid aggregation is included in **Figure 2**. Since previous works in our laboratory have demonstrated that aggregating proteins in the vicinity of the ribosome can induce its co-aggregation [Pathak et al., 2017, Banerjee et al., 2020], this study aimed to investigate if inhibition of protein aggregation, in the presence of such polyphenolic inhibitors, could mitigate the ribosomal co-aggregation as well.

Materials and Methods:

Materials

Bovine Carbonic Anhydrase II (BCAII), NaCl, MgCl₂, DTT, GuHCl, Sucrose, DEPC, Tris-base, DEAE-Cellulose, ampicillin were purchased from Sigma Aldrich (St. Louis, MO, USA). Polyadenylic acid [Poly(A)], Polyuridylic acid [Poly(U)], rosmarinic acid and myricetin were also purchased from Sigma Aldrich. The expression plasmids encoding A β 1-40 [pET-Sac-A β (M-1-40) plasmid #71876] and A β 1-42 [pET-Sac-A β (M-1-42) plasmid #71875] were purchased from Addgene. Polyallomer ultracentrifuge tubes were purchased from Beckman Coulter (Indianapolis, IN, USA). Molecular weight cut-off centrifugal filters were purchased from Amicon Ultra [Millipore (Billerica, MA, USA)]. Nitrocellulose filter was purchased from Millipore. All other chemicals were local products of analytical grade. Experimental data analysis was performed using OriginPro8 (Origin Corp., Northampton, MA, USA), QuantityOne Bio-Rad (Hercules, CA, USA) and SIGMA-PLOT 14 (Systat Software, Inc., San Jose, CA, USA) software. PyMOL 2.4 (PyMOL by Schrödinger, available at: <https://pymol.org/2/>) was used to display the Protein Data Bank (PDB) files. Charge distribution of the A β peptides as well as the colour coded amino acid sequence of A β peptides according to their physicochemical properties was obtained using the software CIDER (available at: <http://pappulab.wustl.edu/CIDER/analysis/>). The 3-D models for the peptides A β 40 and A β 42 were generated using the I-TASSER software (available at: <https://zhanglab.ccmb.med.umich.edu/I-TASSER/>).

Methods

Studies on A β -80S ribosome co-aggregation: Buffers: Buffer A for cell lysis and protein purification: 10 mM Tris-HCl pH 8, 1 mM EDTA pH 8 (with added 5 mM DTT and 1 mM PMSF during lysis) [Walsh et al., 2009 with minor modifications]; Buffer B for final buffer exchange and protein storage: 25 mM Tris-HCl pH 8; Buffer C for aggregation reactions: 25 mM Tris-HCl pH 7.5, 50 mM NaCl, 5 mM MgCl₂ [Banerjee et al., 2020].

Purification of yeast 80S ribosome, A β 40 and A β 42:

The 80S ribosome was isolated from yeast *Saccharomyces cerevisiae* according to purification protocol outlined by Chakraborty et al. [2016]. The total ribosomal RNA was extracted from yeast 80S ribosome as mentioned in Piir et al. [2014]. The purification of both A β 1-40 (A β 40) and A β 1-42 (A β 42) was done according to the method outlined by Walsh et al. [2009]. A β 40 and A β 42 coding sequences together with added ATG codons cloned directly into a pET vector are available from Addgene [pET-Sac-A β (M-1-40) plasmid #71876 and pET-Sac-A β (M-1-42) plasmid #71875]. These plasmids (containing ampicillin selection marker) were transformed into *E.coli* BL21(DE3) cells in the presence of 100 μ g/ml ampicillin and grown in enriched media, Terrific Broth (2.4% Yeast Extract, 1.2% Tryptone, 0.231% KH₂PO₄, 1.254% K₂HPO₄ w/v along with 0.4% glycerol v/v) for 4 hours after induction with IPTG (42 μ M). The respective cells for A β 40 and A β 42 were harvested from their mid-log phase for large scale purification by centrifugation and subjected to three cycles of sonication as mentioned in Walsh et al. [2009]. The harvested cell pellets were individually resuspended in Buffer A (10 mM Tris-HCl pH 8, 1mM EDTA) and sonicated for 2 minutes on ice (Amplitude: 65; Duty cycle: 0.5) followed by centrifugation at 13, 000 g for 20 minutes. This process was repeated twice where the supernatant was removed and the pellet was resuspended in Buffer A, sonicated for 2 minutes on ice and centrifuged. The third

supernatant was removed and the pellet was resuspended in Buffer A containing 8 M Urea. Induced expression of recombinant A β peptides form inclusion bodies and thus after every cycle of sonication, the pellet was collected for further processing. The final pellet obtained after the third round of sonication was solubilized in Buffer A containing 8M Urea and subjected to anion-exchange chromatography using DEAE-cellulose. The protein was equilibrated with the resin at pH 8 and eluted using increasing concentrations of NaCl. The purification was performed using the “Batch method”. In brief, the urea-solubilized pellets were diluted with Buffer A and added to pH equilibrated DEAE-cellulose for anion-exchange chromatography (since the A β peptides are expected to have a net charge between -3 and -4 at neutral pH) [Yang et al., 2018] and gently agitated for an hour. The slurry was then added to a Buchner’s funnel with nitrocellulose filter on a vacuum glass bottle. The resin was washed with 50 ml Buffer A and then twice with 50 ml Buffer A with added 25 mM NaCl. This was followed by four 50 ml washes with Buffer A containing 125 mM NaCl. Eluted fractions were analyzed using SDS-PAGE, on a 12% SDS-Polyacrylamide gel, to detect the presence of impurities. Since the peptides were too small (~ 4.5 KDa) to be just analyzed by SDS-PAGE , pure fractions of A β 40 and A β 42 were pooled together and concentrated using 10 KDa and 3 KDa molecular mass cut-off filters consecutively. The purified protein fractions were then analyzed using mass spectrometry (performed in IICB, Kolkata) which revealed two sharp peaks corresponding to the m/z (mass-to-charge) ratios of A β 40 and A β 42 respectively thus confirming with the molecular weights of our purified peptides (molecular weight of A β 40: 4.458 KDa; molecular weight of A β 42: 4.642 KDa). For concentration determination, the peptides were denatured with 1 M GuHCl and passed through 10 KDa centricon filters and centrifuged for 2 minutes at 12000 g. The filtrate was collected and the concentration of the peptides was determined by BCA assay as well as measurement of absorbance at 275 nm (Molar Extinction co-efficient = 1400 M⁻¹cm⁻¹) [Walsh et al., 2009].

The peptides were stored in Buffer B (25 mM Tris-HCl, pH 8) and frozen at -80°C until further use.

Aβ-ribosome/ribosomal RNA aggregation:

25 μM Aβ40 or Aβ42 was incubated with 0.1 μM 80S ribosome or 1 μM 80S rRNA for 6 hours at 37 °C in Buffer C (25 mM Tris-HCl pH 7.5, 50 mM NaCl, 5 mM MgCl₂). In control experiments, 25 μM of K18 (4 repeat microtubule binding subdomain of Tau protein) was incubated with 0.1 μM 80S ribosome or 1 μM 80S rRNA for 6 hours at 37 °C. K18 was reduced in the presence of 1 mM DTT for 2 hours at 37 °C in Buffer C, following which 80S ribosome or 80S rRNA was added to it. For aggregation reactions with increasing concentrations of the Aβ peptides, 0.01 μM, 0.1 μM, 1 μM, 10 μM and 25 μM of Aβ40 and Aβ42 were used and the reactions were continued for 3 hours. Control aggregation reactions with increasing concentrations of K18 were also set with 1 μM, 10 μM and 25 μM of the reduced protein and the reactions were continued for 3 hours.

Aggregation reactions of the Aβ peptides and 80S ribosome were also set in the presence of the polyphenolic inhibitor compounds, rosmarinic acid (RA) and myricetin (Myr). 25 μM of Aβ40 and Aβ42 were incubated in Buffer C with 0.1 μM of the 80S ribosome in the presence and absence of 100 μM RA and Myr. 25 μM of K18 (after reduction with 1 mM DTT for 2 hours at 37 °C) was also incubated with 0.1 μM 80S in the presence and absence of 100 μM RA and Myr.

80S (0.1 μM) ribosome and 80S rRNA (1 μM) were also incubated alone for 6 hours in Buffer C at 37 °C. Aggregation reaction mixtures were centrifuged at 21,380 g for 45 minutes at 4 °C and the pellet and supernatant fractions were separated. Earlier studies on Poly(A) RNA induced Tau aggregation recommend centrifugation at 1,00,000 g for separation of monomeric Tau and Tau-RNA aggregate [Dinkel et al., 2015]. However, at this speed the

ribosome and rRNA themselves are incorporated in the pellet regardless of the presence of the protein. Hence, the centrifugal speed of 21,380 g was used, at which the larger aggregates constituted the pellet while the supernatant comprised of residual ribosome or smaller aggregates [Pathak et al., 2017, Banerjee et al., 2020]. The constituents of the pellet fractions were analyzed using 12% SDS-PAGE or 0.8% agarose gel electrophoretic analysis. The supernatant fractions were analyzed using sucrose density gradient centrifugation (SDGC).

Gel electrophoretic analysis of insoluble aggregates

Aggregation samples were centrifuged at 21,380 g for 45 minutes at 4 °C. The pellets were analyzed for their total rRNA content in a non-denaturing 0.8% agarose gel, using a procedure used earlier to study interaction of Tau with cellular RNA (with minor modifications) [Wang et al., 2006]. Briefly, the pellets were treated with 4 M Urea and incubated for 20 minutes at room temperature, 10 minutes at 65 °C and finally 5 minutes on ice. Such treatment before loading on the 0.8% agarose gel for electrophoresis was necessary to allow the RNA in the large aggregates to enter the gel. The electrophoresis was performed in 1X TAE at 65 V for 10 minutes before visualizing under ultraviolet light using the GelDoc imaging system (MEGA BIO-PRINT 1100/20M). The total RNA runs as a single band in this experiment. Previous studies in the laboratory used this procedure to study the lysozyme-ribosome co-aggregation process [Pathak et al., 2017]. The intensities of the rRNA bands were compared by densitometric analysis (QuantityOne Bio-Rad). The total ribosome or rRNA used in the experiment was also treated similarly and analyzed. For analysis of the protein constituents in the pellets, the pellets were resuspended in Laemmli buffer containing 4M urea and boiled before loading on to a 12% SDS-PAGE. The SDS-PAGE was stained with Coomassie Brilliant Blue (CBB) at 37 °C and the agarose gels were stained with ethidium bromide (EtBr).

Sucrose Density Gradient Centrifugation

Aggregation reaction mixtures were centrifuged at 21,380 g for 45 minutes at 4 °C and the supernatant fractions were layered on to a 5 ml or 30 ml 17-25% sucrose gradient. The 5 ml gradient was centrifuged at 1,98,000 g for 2.5 hours at 4 °C with MLS 50 rotor (Beckman Coulter) and 200 µl fraction volumes were collected from top to bottom. The SW40.1 rotor (Beckman Coulter) was used for the 30 ml gradients which were centrifuged at 1,50,000 g for 2.5 hours at 4 °C and 500 µl fraction volumes were collected from top to bottom. The absorbance of the collected fractions at 260 nm was measured for analyzing the 80S ribosomal profile. These values reflect the difference between the sedimentation pattern of an intact 80S ribosome population and that of an 80S population whose physical integrity has been compromised. Formation of large insoluble aggregates results in the reduction of area under the ribosomal peak, in the supernatant fractions, and simultaneous appearance of high $A_{260\text{ nm}}$ readings at regions corresponding to lower sedimentation co-efficient.

The destruction of the physical integrity of the ribosome and the sequestration of ribosomal components in the large aggregates is marked by the disappearance of the ribosomal peak in the supernatant and the simultaneous appearance of rRNA in the pellet.

Electron Microscopy:

25 µM Aβ40 and Aβ42 were incubated with 0.1 µM 80S ribosome for 24 hours at 37 °C. As positive control, 50 µM K18 was reduced with 1 mM DTT for 2 hours at 37 °C and then incubated with 0.1 µM 80S ribosome for 24 hours at 37 °C. K18 was used as control, since our previous electron microscopic studies under similar conditions have demonstrated the formation of K18-ribosome co-aggregated structures [Banerjee et al., 2020]. Imaging of aggregation in the samples was done by using a transmission electron microscope (FEI Tecnai12 BioTwin) with an acceleration voltage of 120 kV. Aliquots (5 µl) containing the

aggregation mix were placed on the copper grid coated with carbon film (300 meshes) and a drop of 2% uranyl acetate was placed on the grid. The excess water was removed carefully with filter paper and the grid was left to dry in air.

Human in vitro transcription-translation assay

The *in vitro* translation assay was done using the 1-step Human Coupled IVT-Kit-DNA; 88881, Thermo Fisher Scientific. A β 40, A β 42, K18 (reduced with 1 mM DTT) and native BCAII were added to the prescribed reaction mix to attain final concentrations of 25 μ M and 50 μ M. The positive control set contained no proteins and the negative control set did not contain the GFP (reporter gene) plasmid. All the reaction sets were incubated till 6 hours at 30^oC (as prescribed) and the reporter GFP fluorescence was monitored at excitation/emission: 482/512 nm. The experiment was repeated three times.

Seeding assay for A β induced 80S aggregation

25 μ M A β 40 and A β 42 were individually incubated in Buffer C with 0.1 μ M of 80S ribosome for 3 hours at 37^oC. As positive control, 25 μ M of K18 was also incubated with 0.1 μ M of 80S ribosome for 3 hours at 37^oC. The K18 was reduced with 1 mM DTT for 2 hours before incubation with 80S. As negative control, the 80S ribosome was incubated alone under similar conditions and for similar period of time. At the end of incubation period, 1 μ l aliquots were drawn from each of the reaction mixtures and added to 999 μ l of fresh 0.1 μ M 80S ribosome in Buffer C. This was further incubated for 24 hours at 37^oC and the resultant reaction mixtures were centrifuged at 21,380 g for 45 minutes at 4^oC. The large insoluble aggregate containing pellets were resuspended in 4 M Urea containing Buffer C (and incubated at room temperature for 20 minutes, followed by incubation at 65^oC for 10 minutes and finally kept on ice for 5 minutes before loading on the gel) and analyzed using 0.8% agarose gel electrophoresis.

Delayed rosmarinic acid (RA)/myricetin (Myr) addition assay for A β induced 80S aggregation

0.1 μ M 80S ribosome was added to 25 μ M A β 40, A β 42 and K18. K18 was reduced in Buffer C for 2 hours at 37 $^{\circ}$ C in the presence of 1 mM DTT, before ribosome was added to it. 100 μ M of RA and Myr were added to the reaction mixtures after 45 minutes of addition of the ribosome to each of the proteins. The incubation of the reaction mixtures was continued till 3 hours at 37 $^{\circ}$ C. The resultant reaction mixtures were centrifuged at 21,380 g for 45 minutes at 4 $^{\circ}$ C. The insoluble pellet fractions were resuspended in 4 M Urea containing Buffer C (and incubated at room temperature for 20 minutes, followed by incubation at 65 $^{\circ}$ C for 10 minutes and finally kept on ice for 5 minutes before loading on the gel) and analyzed using 0.8% agarose gel electrophoresis.

Light Scattering Study

Light scattering studies were performed with A β 40, A β 42 and K18 in the presence of Poly(A) RNA, Poly(U) RNA and LiCl extracted 80S rRNA, with the added presence or absence of the inhibitor molecules, rosmarinic acid (RA) and myricetin (Myr). The ratio of protein: RNA was maintained at 50:1 for these studies and the inhibitors were used at a 4-fold excess concentration with respect to the protein concentration used in the experiment [Ono et al., 2012]. K18 was reduced in the presence of 1 mM DTT in Buffer C for 2 hours at 37 $^{\circ}$ C prior to addition of RNA. 0.2 μ M of Poly(A), Poly(U) and LiCl extracted 80S rRNA were added to 10 μ M of A β 40, A β 42 and reduced K18 (t=0 hr) and further incubated for 3, 6, 15, 24 and 48 hours (hrs) at 37 $^{\circ}$ C. The change in light scattering intensity of the solutions was monitored at t=0 hr, t=3 hrs, t=6 hrs, t= 15 hrs, t= 24 hrs and t= 48 hrs. The increase in light scattering intensity with time was plotted in the form of line graphs and the net increase after 48 hrs was plotted in the form of bar diagrams. Similar experiments were performed with the additional presence of 40 μ M RA and Myr which were added at t=0 hr. As control, Poly(A)

alone, Poly(U) alone, 80S rRNA alone, K18 alone, A β 40 alone and A β 42 alone reaction sets were similarly incubated and the increase in their light scattering intensity was measured at t=0 hr, t=3 hrs, t=6 hrs, t=15 hrs, t=24 hrs and t=48 hrs. Light scattering studies were also performed to study the effect of stoichiometry of protein and RNA on the RNA-mediated stimulation of aggregation of A β 40/A β 42/Tau-K18. For these studies, the two RNA: protein ratios that were selected were 1:50 and 1:8 [according to Kovachev et al., 2017]. 10 μ M of A β 40, A β 42 and K18 (reduced with 1mM DTT) were incubated with 0.2 μ M (50-fold less) and 1.25 μ M (8-fold less) of Poly(A), Poly(U) and 80S rRNA for 48 hrs at 37 $^{\circ}$ C. The change light scattering intensity of the solutions was measured at t=0 hrs and t= 48 hrs and the net increase was plotted in the form of bar diagrams. As control, both concentrations of Poly(A), Poly(U) and 80S rRNA as well as the proteins alone were incubated for 48 hrs at 37 $^{\circ}$ C and their increase in light scattering intensity was measured. Before measuring light scattering intensity, all the solutions were pipetted multiple times. The intensity was measured at excitation: 450 nm and emission: 450 nm in Hitachi F-2700 spectrofluorometer.

Poly(A) and Poly(U) were purchased from Sigma Aldrich. The lyophilized RNA was dissolved in DEPC-treated water and the concentration of the resulting solution was determined by measuring absorbance at 260 nm for Poly(U) [Extinction co-efficient: 9600 M $^{-1}$ cm $^{-1}$] and absorbance at 257 nm for Poly(A) [Extinction co-efficient: 10,100 M $^{-1}$ cm $^{-1}$] [Zhigalova et al., 2020]

Results and Discussion

Section A

Effect of A β aggregation on eukaryotic ribosome

As discussed in the “Introduction” section, our study next attempts to demonstrate the effect of Amyloid β (A β) peptides on the eukaryotic ribosome. The aggregation of A β peptides marks the onset of Alzheimer’s disease (AD) and is considered to be the causal event of this neurodegenerative disorder [Chen et al., 2017]. A β peptides are derived through the amyloidogenic cleavage of the Amyloid Precursor Protein (APP) which is a single pass transmembrane glycoprotein with a long N-terminal domain and a cytoplasmic C-terminal domain. APP can localize on the membranes of different types of cells as well as the membranes of cellular organelles [Lee et al., 2017, Chen et al., 2017]. APP is involved in different neuronal events like synaptogenesis, synapse remodeling and neurite outgrowth [Zheng et al., 2006]. It can also affect neural stem cell maturation [Trazzi et al., 2013, Coronel et al., 2019].

The Section B.2 in Chapter 1, discusses the non-amyloidogenic and amyloidogenic processing of APP that yields different products. The non-amyloidogenic processing of APP yields the soluble ectodomain of APP (sAPP $_{\alpha}$) through α -secretase cleavage and the p3 peptide and APP Intracellular Domain (AICD) through the subsequent γ -secretase cleavage. The amyloidogenic pathway leads to the production of the A β peptides through sequential cleavage by β -secretase and γ -secretase. **Figure 3A** shows a schematic depiction of the full-length APP with its A β domain highlighted and the cleavage sites for β -secretase and γ -secretase marked. Sequential cleavage by these two enzymes yields the A β peptides of different lengths [Assarson et al., 2014]. The most abundantly formed variants are the A β 1-40 or A β 40 (comprising of 40 residues) followed by A β 1-42 or A β 42 (comprising of 42

residues) (discussed in Chapter 1, Section B.2). The amino acid sequences of these two peptides are depicted in **Figure 3A**, with physicochemical colour coding that was obtained using the software CIDER (available at: <http://pappulab.wustl.edu/CIDER/analysis/>). This software allows the high-throughput analysis of the sequences of intrinsically unstructured proteins and generates an output that shows the linear hydrophobicity, charge distribution as well as the colour coded amino acid sequence based on their physicochemical properties [Holehouse et al., 2017]. Analysis of the A β peptide sequences using CIDER also shows the clustered distribution of positively and negatively charged residues along their lengths (**Figure 3A**).

Previous reports about the software I-TASSER (available at: <https://zhanglab.ccmb.med.umich.edu/I-TASSER/>) suggest that model structures of intrinsically unstructured proteins like A β can be obtained using this computational tool [Mylonas et al., 2008]. For this purpose, the amino acid sequences of our peptides of interest, A β 40 and A β 42, were submitted to the I-TASSER server which runs iterative structural assembly simulations and generates a predicted 3-D model for the peptides [Zhang et al., 2008, Roy et al., 2010, Yang et al., 2015]. I-TASSER generated 5 models with individual confidence scores for each of the peptides. Among these the ones with the highest confidence scores were selected and displayed using the PyMOL DeLano scientific software. The vacuum protein contact potential display of the A β 40 (**Figure 3Bi**) and A β 42 (**Figure 3Bii**) revealed the surface electrostatic potential of the two peptides which demonstrated the uneven distribution of positive and negative charges. **Figure 3C** includes the eukaryotic *Saccharomyces cerevisiae* 80S structure (PDB ID: 3Z22 and 3O58). The presence of ribosomal RNA in the solvent exposed surface of the ribosome is represented in red.

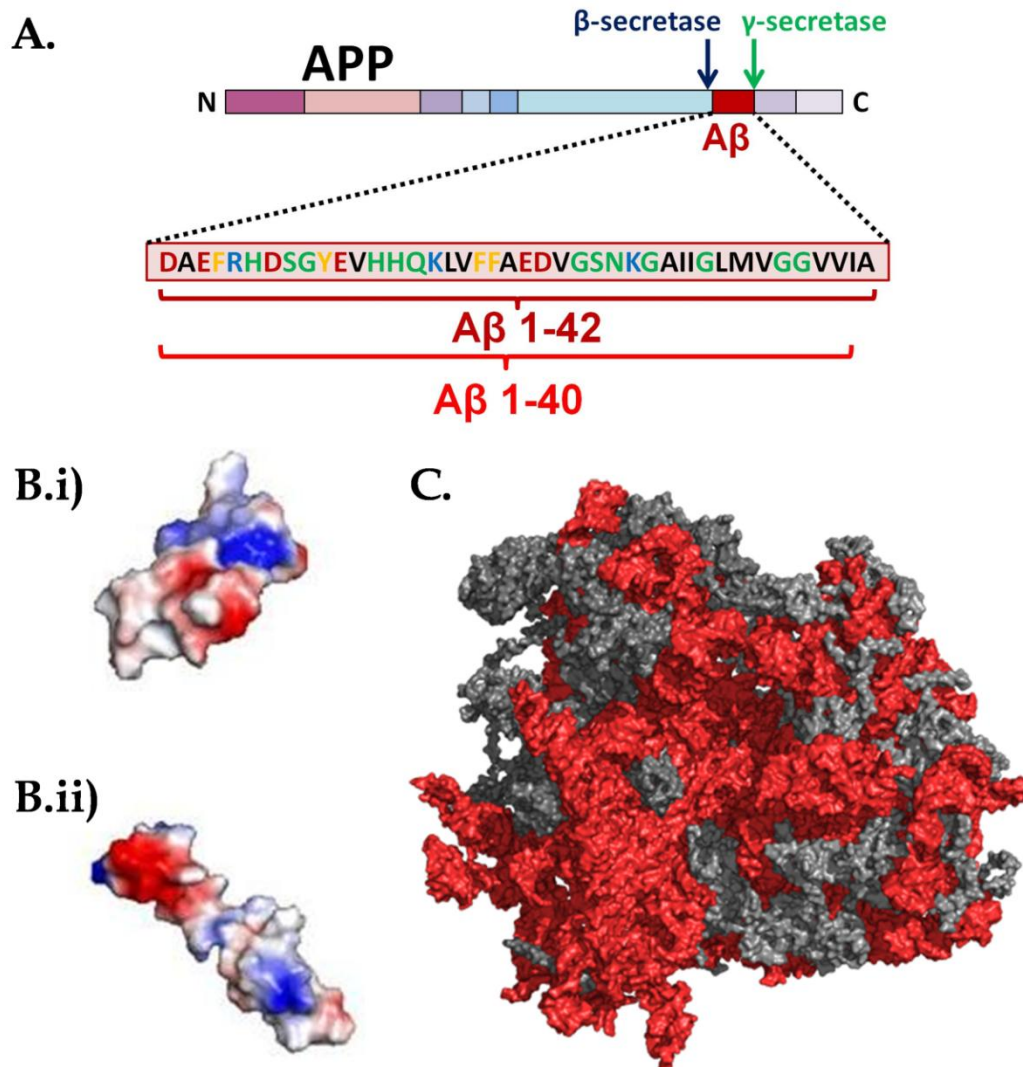


Figure 3: Structure of the Amyloid β peptides and the yeast 80S ribosome

A. A schematic representation of the Amyloid Precursor Protein (APP) highlighting its Amyloid β domain and the Amyloid β peptides $A\beta$ 1-40 ($A\beta$ 40) and $A\beta$ 1-42 ($A\beta$ 42) that are formed through amyloidogenic cleavage of the protein. The physicochemically colour coded amino acid sequences of the $A\beta$ 40 and $A\beta$ 42 peptides are displayed here: Black denotes hydrophobic residues, green denotes polar residues and blue and red denotes positively and negatively charged residues [Colour coding of amino acid sequences and charge distribution obtained using CIDER (available at: <http://pappulab.wustl.edu/CIDER/analysis/>)]. **B.i)** Surface Representation of $A\beta$ 40 model structure obtained using I-TASSER. The colour blue represents positive electrostatic potential and the colour red represents negative electrostatic potential. The model displayed was chosen based on the C-score. Images are not to scale. **B.ii)** Surface Representation of $A\beta$ 42 model structure obtained using I-TASSER. The colour blue represents positive electrostatic potential and the colour red represents negative electrostatic potential. The model displayed was chosen based on the C-score. Images are not to scale. **C.** Surface Representation of *Saccharomyces cerevisiae* 80S ribosome (PDB ID: 3Z22 and 3O58) [using Pymol version 2.4 available at: <https://pymol.org/2/>]. Solvent exposed surface of the yeast 80S ribosome. The rRNA is represented in red and the ribosomal proteins are represented in grey.

Previous studies have indicated that cellular RNAs, owing to their negative charge, can interact with positively charged intrinsically unstructured Tau protein (which is implicated in AD as well) and serve as the polyanionic inducer that is crucial for their aggregation [Zhang et al., 2017, Fichou et al., 2018, Ramachandran et al., 2011]. Studies in the laboratory also revealed the interaction between Tau (both the full length Ht40 and the 4 repeat microtubule binding subdomain K18) and the ribosome, which has a highly negative surface electrostatic potential due to the presence of rRNA and that such an interaction could lead to co-aggregation of ribosomal components [Banerjee et al., 2020].

A β peptides are however, not predominantly positively charged, but the presence of RNA has been detected in the plaques constituted by them [Stewart et al., 2017]. The role of RNA as a “pathological chaperone” that can modulate A β fibril formation [Ginsberg et al., 1998] has also been discussed before in the “Introduction” section. Equipped with this information, further experiments were conducted to determine the effect of aggregating A β peptides, A β 40 and A β 42, on the eukaryotic 80S ribosome.

A.1. Purification of A β variants: A β 40 and A β 42

The purification of both A β 1-40 (A β 40) and A β 1-42 (A β 42) was done according to the method outlined by Walsh et al. [2009]. A β 40 and A β 42 coding sequences together with added ATG codons cloned directly into a pET vector are available from Addgene [pET-Sac-A β (M-1-40) plasmid #71876 and pET-Sac-A β (M-1-42) plasmid #71875]. These plasmids (containing ampicillin selection marker) were transformed into *E.coli* BL21(DE3) cells in the presence of 100 μ g/ml ampicillin and grown in enriched media, Terrific Broth, for 4 hours after induction with IPTG (42 μ M). The respective cells for A β 40 and A β 42 were harvested from their mid-log phase for large scale purification by centrifugation and subjected to three cycles of sonication as mentioned in Walsh et al. [2009]. The harvested cell pellets were

individually resuspended in Buffer A and sonicated for 2 minutes on ice (Amplitude: 65; Duty cycle: 0.5), followed by centrifugation at 13, 000 g for 20 minutes. This process was repeated twice, where the supernatant was removed and the pellet was resuspended in Buffer A, sonicated for 2 minutes on ice and centrifuged. The third supernatant was removed and the pellet was resuspended in Buffer A containing 8 M urea. Induced expression of A β peptides results in their aggregation (due to their strong aggregation propensity) and formation of inclusion bodies. The incorporation of the A β peptides into inclusion bodies ensures that they are protected from degradation in the bacterial cytosol and can be purified more efficiently with minimal contamination due to bacterial proteins. Formation of inclusion bodies also allows for high expression of the peptides as they are clearly segregated from the bacterial cytosol and do not impact any essential functions [Walsh et al., 2009]. Thus after every cycle of sonication, the pellet comprising of the inclusion bodies was collected for further processing. The final pellet obtained after the third round of sonication was solubilized in 8 M Urea containing Buffer A and subjected to anion-exchange chromatography using DEAE-cellulose. The protein was equilibrated with the resin at pH 8 and eluted using increasing concentrations of NaCl. The purification was performed using the “Batch method”. In brief, the urea-solubilized pellets were diluted with Buffer A and added to pH equilibrated DEAE-cellulose for anion-exchange chromatography (since the A β peptides are expected to have a net charge between -3 and -4 at neutral pH) [Yang et al., 2018] and gently agitated for an hour. The slurry was then added to a Buchner’s funnel with nitrocellulose filter on a vacuum glass bottle. The resin was washed with 50 ml Buffer A and then twice with 50 ml Buffer A with 25 mM NaCl. This was followed by four 50 ml washes with Buffer A containing 125 mM NaCl. Eluted fractions were analyzed using SDS-PAGE on a 12% SDS-Polyacrylamide gel to detect the presence of impurities. A flowchart outlining the purification procedure is

included as **Figure 4A**. **Figure 4Bi-ii** shows the purified A β peptide bands for both A β 40 and A β 42 on a 12% SDS-PAGE respectively.

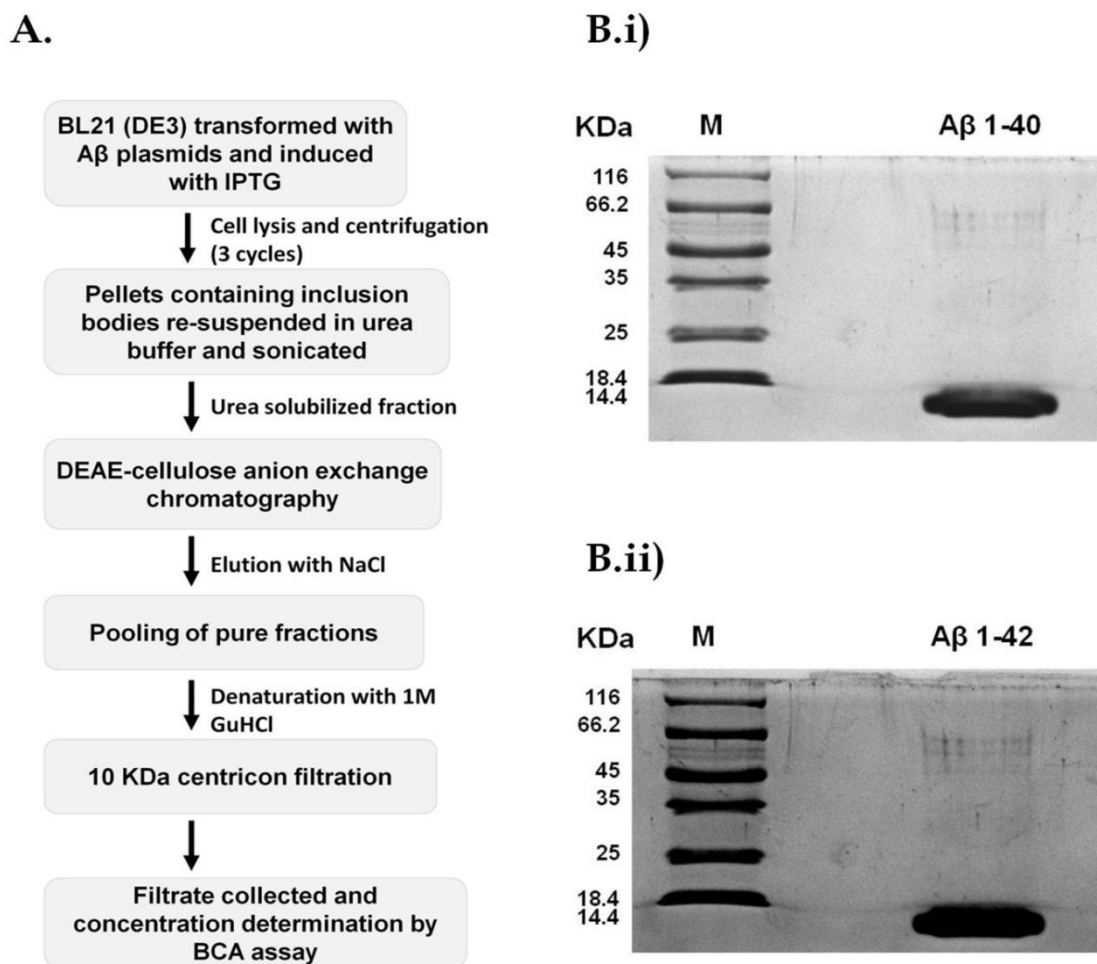


Figure 4: Purified recombinant A β 1-40 (A β 40) and A β 1-42 (A β 42)

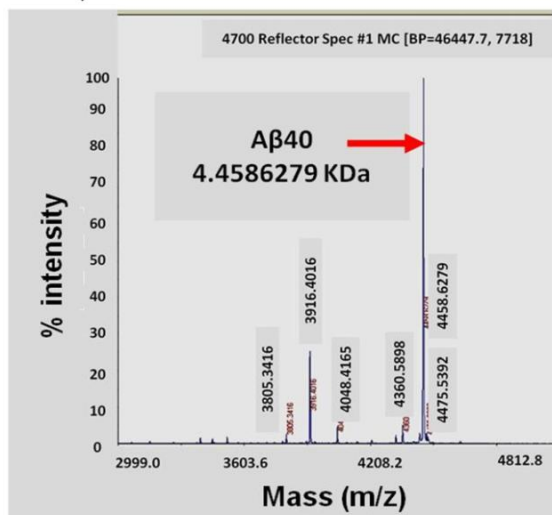
A. An outline of the procedure followed for purification of A β 40 and A β 42 depicted in the form of a flowchart. **B.** 12% SDS-PAGE analysis showing (i) Purified A β 40: lanes from left to right contain molecular weight marker and A β 1-40 (A β 40). (ii) Purified A β 42: lanes from left to right contain molecular weight marker and A β 1-42 (A β 42).

Since the peptides were too small (~ 4.5 KDa) to be just analyzed by SDS-PAGE, pure fractions of A β 40 and A β 42 were pooled together and concentrated using 10 KDa and 3 KDa molecular mass cut-off filters consecutively. For concentration determination, the peptides were denatured with 1 M GuHCl and passed through 10 KDa centricon filters and centrifuged for 2 minutes at 12000 g. The filtrate was collected and the concentration of the peptides was

determined by BCA assay as well as measurement of absorbance at 275 nm (Molar Extinction co-efficient = $1400 \text{ M}^{-1}\text{cm}^{-1}$) [Walsh et al., 2009]. The peptides were frozen at -80°C until further use.

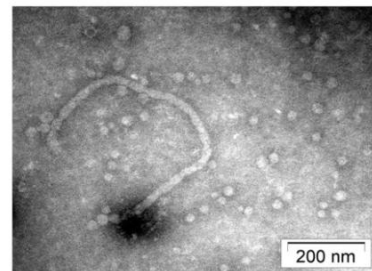
The purified protein fractions were then analyzed using mass spectrometry (performed in IICB, Kolkata) which revealed two sharp peaks corresponding to the m/z (mass-to-charge) ratios of A β 40 and A β 42 respectively thus confirming with the molecular weights of our purified peptides.

A. i)

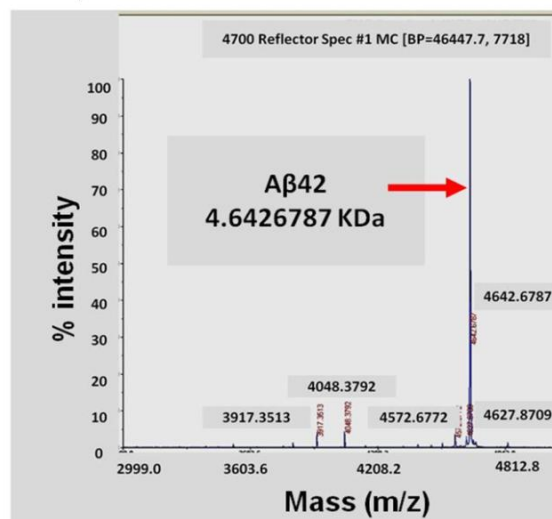


A. ii)

A β 40_72 hrs



B. i)



B. ii)

A β 42_72 hrs

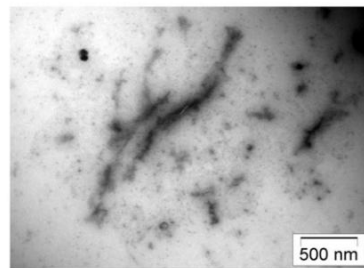


Figure 5: Analysis of the purified A β peptides using mass spectrometry and transmission electron microscopy.

A.i) Mass spectrometric analysis of the purified protein sample showing the presence of the peptide with molecular weight corresponding to A β 1-40 (A β 40). **ii)** Transmission electron microscopic analysis of A β 40 self-aggregation. Micrographs prepared from samples withdrawn at 72 hours after incubation of the reaction mix containing A β 40 in Buffer C at 37 °C. Imaging of aggregation in the sample was done by using a transmission electron microscope (FEI Tecnai12 BioTwin). **B.i)** Mass spectrometric analysis of the purified protein sample showing the presence of the peptide with molecular weight corresponding to A β 1-42 (A β 42). **ii)** Transmission electron microscopic analysis of A β 42 self-aggregation. Micrographs prepared from samples withdrawn at 72 hours after incubation of the reaction mix containing A β 42 in Buffer C at 37 °C. Imaging of aggregation in the sample was done by using a transmission electron microscope (FEI Tecnai12 BioTwin)

The amyloid forming ability of the purified A β variants was also analyzed using transmission electron microscopy (TEM). The individual peptides were incubated alone at 37 °C for a period of 72 hours and the resultant reaction mixtures were subjected to TEM (described in Materials and Methods). **Figure 5Ai** shows the peak corresponding to the molecular weight of A β 40 obtained using mass spectrometric analysis and **Figure 5Aii** shows the TEM images obtained for A β 40 which demonstrates its ability to form fibrillary aggregates. Similarly, **Figure 5Bi** shows the peak corresponding to the molecular weight of A β 42 obtained using mass spectrometric analysis and **Figure 5Bii** shows the TEM images obtained for A β 42 revealing its ability to form fibrillary aggregates, characteristic of A β , as well. This confirmed the amyloid forming ability of our purified peptides.

A.2. Methodologies used for the assessment of the effect of A β variants on yeast 80S ribosome

A flowchart outlining the basic experimental procedures performed while studying the effects of the A β variants (A β 40 and A β 42) on the yeast 80S ribosome has been included as **Figure 6**. In these experiments, the concentration of A β peptides was maintained at a 250-fold excess compared to that used for the yeast 80S ribosome. Since previous studies in our laboratory demonstrated that similar concentrations of Tau-K18 (reduced with 1 mM DTT and used in 250-fold as well as 500-fold excess) (Tau-K18 is the 4-repeat microtubule binding subdomain

of Tau protein) can induce the co-aggregation of yeast 80S ribosome [Banerjee et al., 2020], reaction sets with K18 instead of A β were kept as positive control in our experiments with A β peptides and yeast 80S ribosome. Thus, in our experimental reaction sets 25 μ M of each of the A β peptides was incubated with 0.1 μ M of purified yeast 80S ribosome under physiological conditions (37 $^{\circ}$ C, pH 7.5; Materials and Methods) for different time periods. The conditions and concentrations of A β chosen for our reactions favour the aggregation of A β peptides [Ge et al., 2012, Bourhim et al., 2007]. After incubation for the designated time periods, the reaction mixtures were subjected to centrifugation for separation of the supernatant from the pellet.

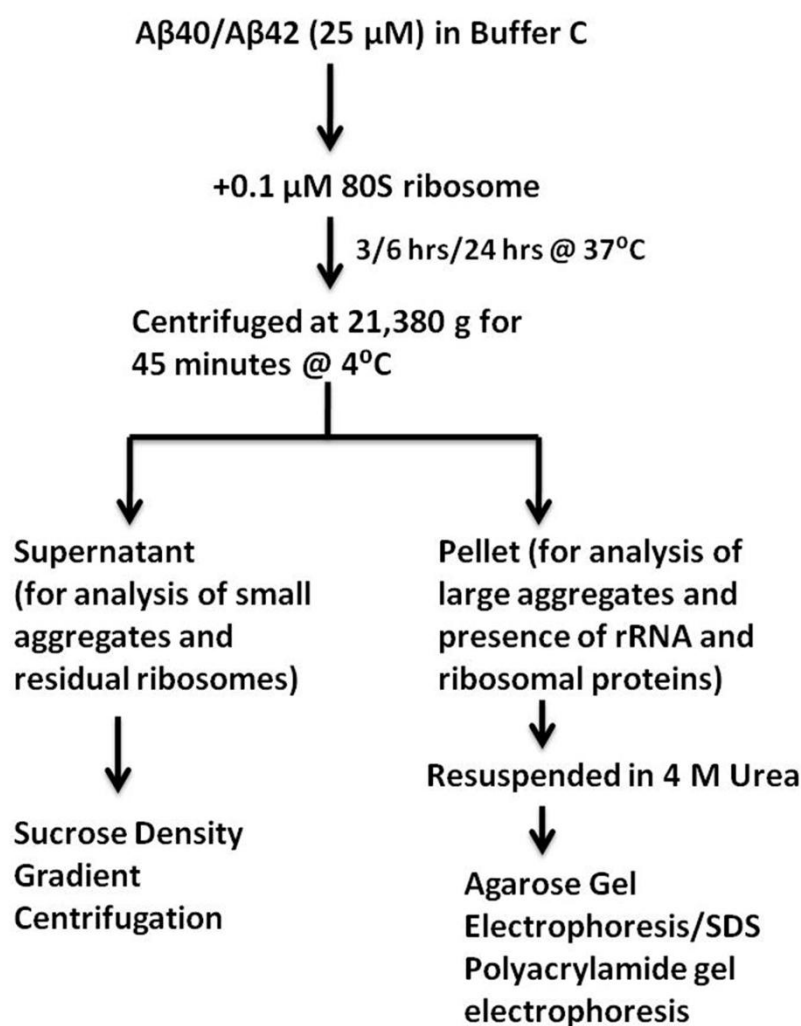


Figure 6: A flowchart outlining the basic experimental procedures followed in this study

The centrifugal speed of choice for our experiments is 21,380 g, which is significantly lower than that recommended for separation of monomeric protein from fibrillar protein aggregates [Dinkel et al., 2015]. The recommended speed is avoided as it can induce the precipitation of the ribosome or rRNA themselves. Hence, at the centrifugal speed used in our study, pellets would contain the large insoluble aggregates while the supernatant would comprise of the residual ribosomal particles and possibly smaller aggregates.

- (i) *Analysis of the supernatant:* Analysis of the supernatant fractions after centrifugation of the reaction mixtures was conducted using equilibrium Sucrose density gradient centrifugation (SDGC). The obtained $A_{260\text{ nm}}$ profile provides an indication of the effect of the A β peptides on the physical integrity of the 80S ribosomal population.
- (ii) *Analysis of the pellets:* The contents of the pellet fractions were analyzed using agarose gel electrophoresis as well as SDS-PAGE analysis. Agarose gel electrophoresis was performed to detect the presence of rRNA among the constituents of the large aggregated structures forming the pellet. The presence of ribosomal proteins among these structures was investigated using SDS-PAGE analysis.

These experimental procedures have been described in detail in the “Materials and Methods” section of this chapter.

A.3. Effect of A β variants on yeast 80S ribosome

In order to assess the effect of A β variants on the yeast 80S ribosome, 25 μM of both A β 40 and A β 42, were incubated with 0.1 μM of 80S ribosome for 6 hours at 37 $^{\circ}\text{C}$ in our initial experiments. The reaction mixtures were subjected to centrifugation after incubation and the obtained supernatants were subjected to SDGC in order to obtain the $A_{260\text{ nm}}$ profile. The

obtained profiles for 80S incubated with A β variants and that for equivalent amounts of untreated 80S ribosome were compared to ascertain the effect of A β on the ribosomal integrity. As shown in **Figure 7Ai**, incubation with both the A β variants resulted in a significant reduction of the 80S ribosomal peak and appearance of ribonucleoprotein particle peaks of lower sedimentation co-efficient. This reduction in the ribosomal peak is indicative of the loss of physical integrity of the 80S ribosome.

Agarose gel electrophoretic analysis was used to investigate the constituents of the pellets obtained after centrifugation of the reaction mixtures (incubated for 6 hours at 37⁰ C). It demonstrated the presence of a significant proportion of the total ribosomal RNA in the pellets, obtained after incubation of 80S ribosome with the A β peptides as well as with K18 (to a comparatively lower extent). The incubation of the 80S ribosome alone, under similar conditions, showed insignificant presence of rRNA in the pellet. These observations implied that the formation of the RNA containing aggregates might be induced by the presence of the A β peptides (**Figure 7Aii**).

We next wanted to investigate if prolonging the incubation time of the A β peptides with the 80S ribosome further affected the ribosomal profile. Similar reduction of the ribosomal peak, as that obtained after 6 hours of incubation, was observed even when the incubation period was extended to 24 hours. This is demonstrated in **Figure 7B**. In this case also the appearance of ribonucleoprotein particle peaks with lower sedimentation co-efficient was observed, the characterization of which would require further analysis. Since similar changes to the ribosomal profile was obtained with both, longer and shorter, periods of incubation, the A β peptides were incubated with the 80S ribosome for shorter time periods in our subsequent experiments.

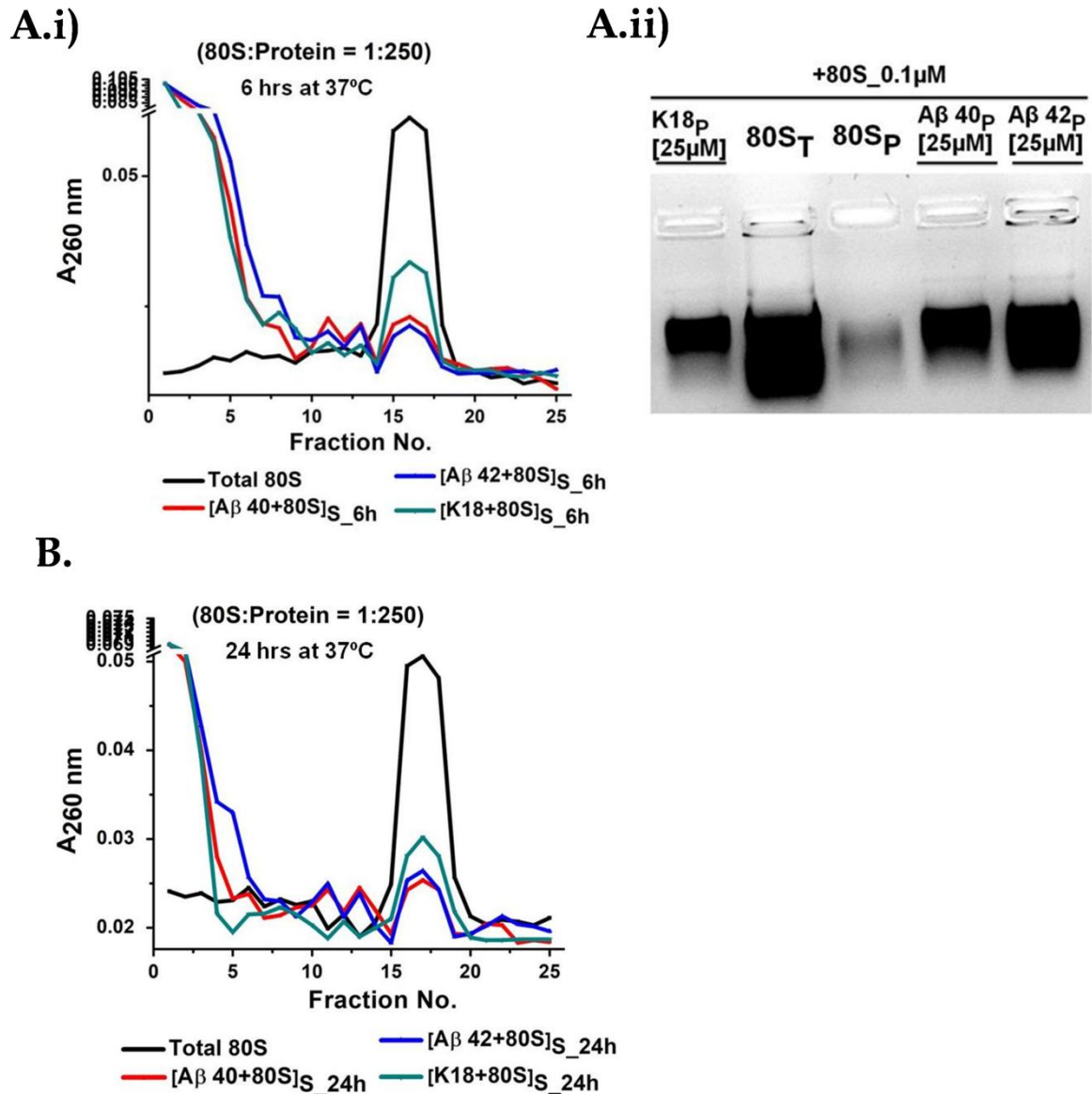


Figure 7: Effect of Aβ peptides on purified yeast 80S ribosome

A.i) Sedimentation profile of the supernatant after incubating 80S with 250x ($x = 0.1 \mu\text{M}$) Aβ40 and Aβ42 peptides (and Tau-K18 as positive control) for 6 hours at 37 °C. (1) Total 80S ribosome (■) (2) (Aβ40+80S)_{S_6h} (●) (3) (Aβ42+80S)_{S_6h} (▲) (4) (K18+80S)_{S_6h} (▼). **ii)** Agarose gel electrophoretic analysis of the pellet after incubating 80S with 250x ($x = 0.1 \mu\text{M}$) Aβ40 and Aβ42 peptides (and Tau-K18 as positive control) for 6 hours at 37 °C for the presence of ribosomal RNA: lanes from left to right contain (1) (K18+80S)_{P_6h} (2) Total 80S (80S)_T (3) (80S)_{P_6h} (4) (Aβ40+80S)_{P_6h} (5) (Aβ42+80S)_{P_6h}. **B.** Sedimentation profile of the supernatant after incubating 80S with 250x ($x = 0.1 \mu\text{M}$) Aβ40 and Aβ42 peptides (and Tau-K18 as positive control) for 24 hours at 37 °C. (1) Total 80S ribosome (■) (2) (Aβ40+80S)_{S_24h} (●) (3) (Aβ42+80S)_{S_24h} (▲) (4) (K18+80S)_{S_24h} (▼).

An interesting observation from both these profiles was made. A comparison of the $A_{260\text{ nm}}$ profile obtained upon incubation of the 80S ribosome with the A β variants to that obtained upon incubation of 80S with K18 (positive control), revealed the higher efficiency of the A β peptides in disrupting the physical integrity of the 80S ribosome (**Figure 7Ai**, **Figure 7B**). An understanding of the underlying reasons for it, requires further characterization.

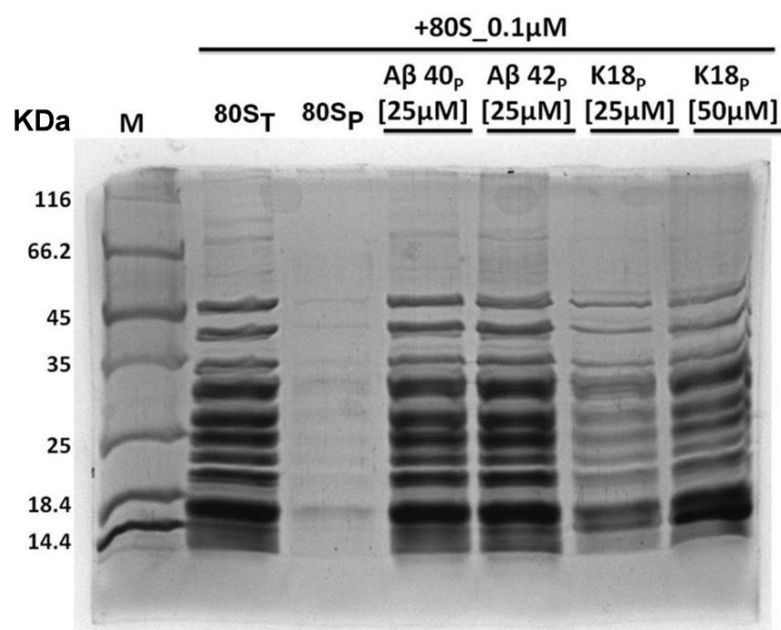


Figure 8: *Effect of A β peptides on purified yeast 80S ribosome: SDS-PAGE analysis of the pellets*

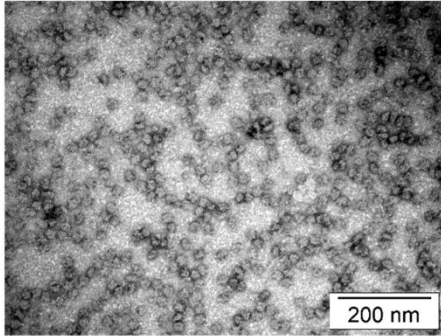
SDS-PAGE analysis of the pellet after incubating 80S with 250x ($x= 0.1\ \mu\text{M}$) A β 40 and A β 42 peptides (and Tau-K18 as positive control) for 6 hours at 37 °C for the presence of ribosomal proteins; lanes from left to right contain (1) Molecular weight marker (2) Total 80S ($(80\text{S})_{\text{T}}$) (3) $(80\text{S})_{\text{P}_{6\text{h}}}$ (4) $(\text{A}\beta 40+80\text{S})_{\text{P}_{6\text{h}}}$ (5) $(\text{A}\beta 42+80\text{S})_{\text{P}_{6\text{h}}}$. (6) $(25\ \mu\text{M}\ \text{K18}+80\text{S})_{\text{P}_{6\text{h}}}$ (7) $(50\ \mu\text{M}\ \text{K18}+80\text{S})_{\text{P}_{6\text{h}}}$. 250x as well as 500x K18 was incubated with 80S in accordance with our previously conducted studies [Banerjee et al., 2020]

The presence of ribosomal proteins in the pellets was also demonstrated by denaturing SDS-PAGE analysis. Incubation of A β 40 and A β 42 for 6 hours with 80S ribosome led to the partitioning of a significant proportion of ribosomal proteins into the large aggregated structures forming the pellets (**Figure 8**).

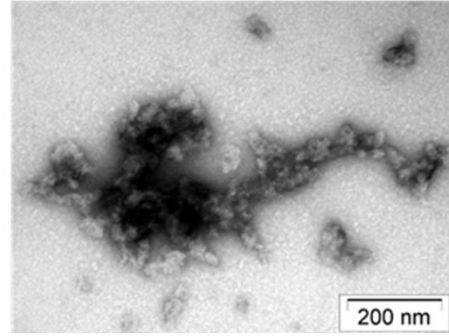
A.4. Electron microscopy of A β -ribosome aggregation

A well-established method for characterizing protein aggregate morphology is transmission electron microscopy (TEM) [Sung et al., 2015]. Extensive studies have provided visual details of the A β aggregation process using electron microscopic techniques [Vandersteen et al., 2012]. This technique provides structural information about the protein aggregates at a resolution of nanometer to picometer [Li et al., 2009]. Low resolution electron microscopy has also been used to explore the molecular structure of amyloids [Fitzpatrick et al., 2017], besides studying the aggregate morphology. In order to attain a visual evidence of the A β -ribosome co-aggregation process, 25 μ M of each of A β 40 and A β 42 was incubated in the presence and absence of 0.1 μ M of yeast 80S ribosome for 24 hours at 37 °C (pH was maintained at 7.5). Since our previous studies have already demonstrated the co-aggregation of Tau-K18 and 80S [Banerjee et al., 2020], a reaction set with K18 (reduced with 1 mM DTT) instead of A β peptides was kept as positive control. The 80S ribosome was also incubated alone under similar conditions as a negative control. A detailed description of the procedure is included in “Materials and Methods”.

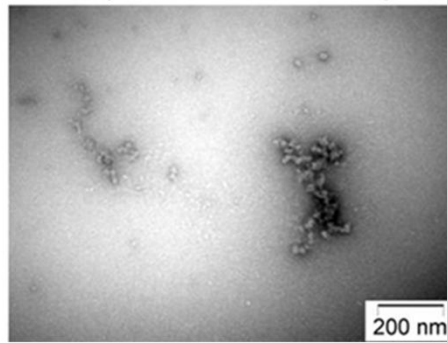
A.i)



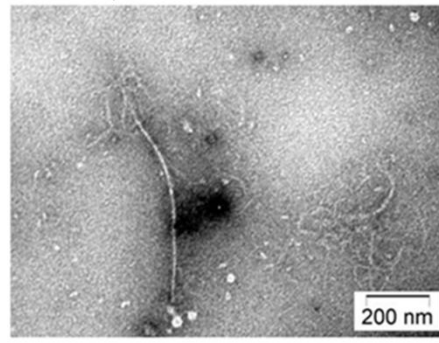
A.ii)



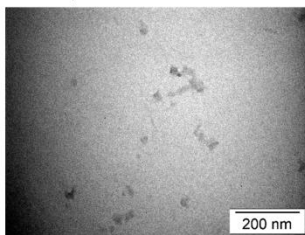
A.iii)



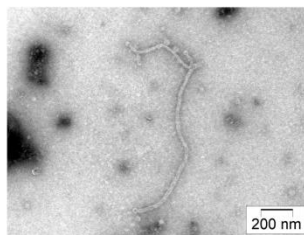
A.iv)



B.i)



B.ii)



B.iii)

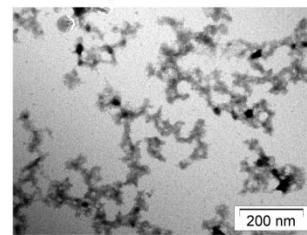


Figure 9: Visualization of the effect of A β 40 and A β 42 on yeast 80S ribosome

Transmission electron microscopic analysis of aggregates. **A.** Micrographs of (i) Total 80S ribosome (ii) K18 incubated with 80S for 24 hours (iii) A β 40 incubated with 80S for 24 hours (iv) A β 42 incubated with 80S for 24 hours. **B.** Control micrographs of (i) K18 (ii) A β 40 and (iii) A β 42 incubated for 24 hours in absence of the ribosome under conditions used in our experiments. All incubations were performed at 37 °C. Ratio of 80S: A β peptides is maintained at 1:250 and ratio of 80S:K18 is maintained at 1:500.

Figure 9Ai includes the TEM image of the intact 80S ribosome with a distinct bead-like appearance, which is completely disrupted upon incubation with K18 (as positive control) (**Figure 9Aii**) as well as with both the A β peptides, A β 40 (**Figure 9Aiii**) and A β 42 (**Figure 9Aiv**) for 24 hours. Interestingly, the nature of the aggregates formed in the presence of K18 and those formed in the presence of A β peptides are distinctly different. The aggregates formed with Tau have a clumped fibrillar appearance while those formed with the A β peptides appear to be cleaner and thinner amyloid fibrils. Although both the A β peptides and K18 seem to be able to affect the physical integrity of the 80S ribosome, the distinction in the appearance of their respective aggregates is possibly due to the innate properties of the individual proteins. Unlike the control micrograph of K18 (**Figure 9Bi**), which shows no fibril formation in the absence of the ribosome, the micrographs for both A β peptides, A β 40 (**Figure 9Bii**) and A β 42 (**Figure 9Biii**) show formation of fibrillary aggregates on their own. This is in agreement with the well-established fact that unlike Tau, A β peptides can aggregate in an inducer-independent manner [Lee et al., 2017]. Thus, a visual evidence of the A β -ribosome co aggregation process is obtained from these electron microscopic images.

A.5. Effect of A β variants on the human ribosome

The studies conducted so far explored the effects of the A β peptides on the 80S ribosome isolated from *Saccharomyces cerevisiae*. In order to investigate whether these peptides could also affect the human ribosome and induce loss of their function, *in vitro* transcription-translation assay was performed using Human coupled IVT kit (Thermo scientific; Materials and Methods). The HeLa cell lysate provided with the kit is a heterogeneous system comprising of the translational machinery. The retention of the translational ability of this ribosomal population, present in the cellular extract, was assessed post incubation of the extract with A β 40 and A β 42 (Materials and Methods). Since earlier studies in the laboratory demonstrated that presence of K18 can induce loss of function of these ribosomes [Banerjee

et al., 2020], K18 was incubated with the reaction mix and kept as a positive control in these experiments along with other suitable controls.

The fluorescence activity exhibited by the reporter GFP protein (GFP is used as the reporter gene; Materials and Methods), is indicative of the translational efficiency exhibited by the ribosomes present in the cell extract. This efficiency was measured 6 hours after the initiation of translation which was continued at 30 °C.

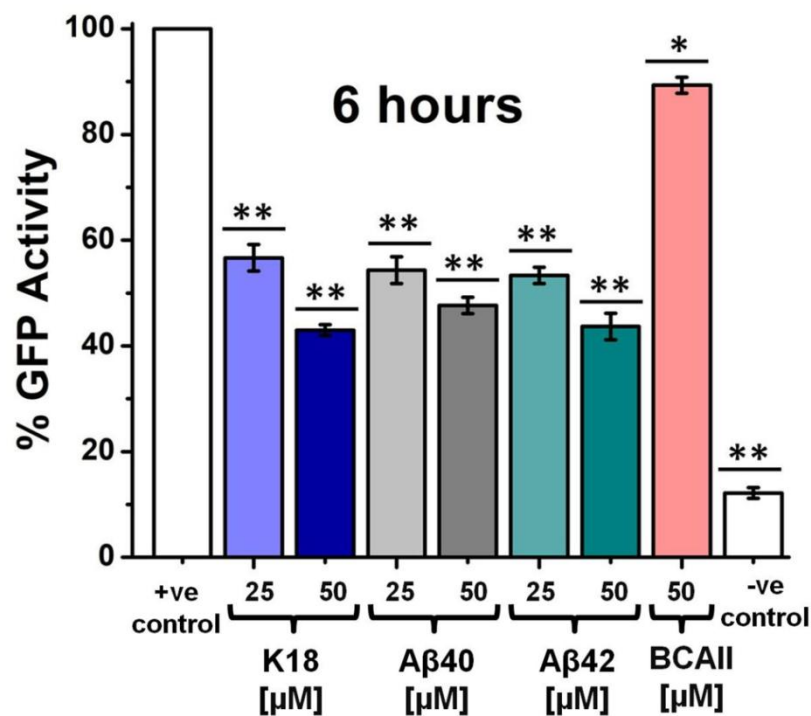


Figure 10: *Aβ* peptides can affect and induce loss in function of human ribosome.

In vitro transcription-translation assay using Human coupled IVT-kit and Aβ peptides. Bar graphs show the percentage GFP activity in the presence and absence of Aβ peptides after 6 hours of translation. The GFP fluorescence activity observed in the reaction mix containing the plasmid and no peptides is considered as 100%. (1) +GFP plasmid (2) 25 μM K18 +GFP plasmid (3) 50 μM K18 +GFP plasmid (4) 25 μM Aβ40+GFP plasmid (5) 50 μM Aβ40+GFP plasmid (6) 25 μM Aβ42+GFP plasmid (7) 50 μM Aβ42+GFP plasmid (8) 50 μM nBCaII+GFP plasmid and (9) – GFP plasmid. The experiments were repeated thrice and the data are presented as means+_{SEM}; *P<0.05 or **P<0.001 in one-way ANOVA (N=3).

A significant reduction in the reporter GFP activity was observed upon incubation with increasing concentrations of both the Aβ peptides, Aβ40 and Aβ42, as well as with K18 (as

expected from earlier studies) [Banerjee et al., 2020]. Incubation with native BCAII (nBCAII) protein induced no significant reduction in the GFP activity. These observations implied that the presence of A β peptides could affect the translational ability of the ribosomes present in the HeLa cell extract. This indicates that the presence of A β peptides could affect the physical integrity and induce loss of function of the human ribosome as well (**Figure 10**). Though further studies with purified human 80S ribosome is necessary to obtain a better understanding of the phenomenon, our studies provide a preliminary evidence that A β -ribosome interaction could affect the ribosomal profile in diseased neuronal cells. The similar observations obtained, in terms of the effect of A β peptides on the yeast and human ribosomes, along with the established role of yeast as a model for studies of neurodegenerative diseases [Tenreiro et al., 2010, Tenreiro et al., 2013], are the reasons for the selection of yeast 80S ribosome for our studies with A β peptides.

A.6. Seeding ability of the A β -ribosome co-aggregates

Our studies on the effect of A β peptides on yeast 80S ribosome have demonstrated that A β peptides can induce the co-aggregation of ribosomal components. In order to investigate whether this aggregation process was co-operative in nature, seeding experiments were performed. In these experiments 250-fold excess of the A β peptides was incubated with the 80S ribosome (0.1 μ M) for 3 hours at 37 $^{\circ}$ C. Aliquots were withdrawn at the end of the incubation period from each experimental set and added to 1000-fold excess of fresh untreated ribosome (0.1 μ M). These mixtures were incubated for another 24 hours at 37 $^{\circ}$ C, following which they were centrifuged at 21,380 g for 45 minutes to separate the pellets containing the large insoluble aggregates from the supernatant. These pellet fractions were analyzed using 0.8% agarose gel electrophoresis. As done in all our previously conducted experiments, reaction sets with K18 instead of A β were kept as positive control for the experiment. A schematic representation of this procedure is included in **Figure 11**.

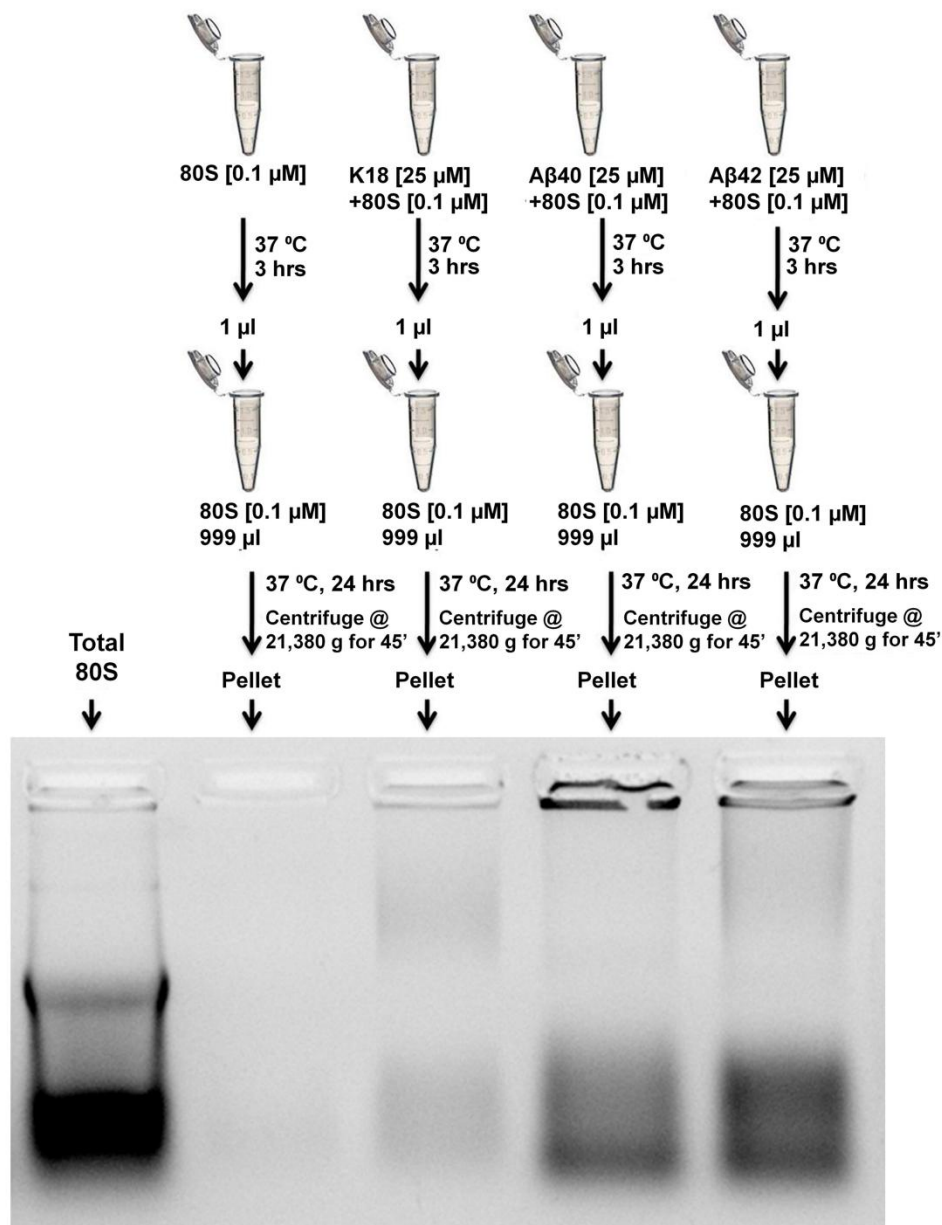


Figure 11: Ability of A β -ribosome co-aggregates to induce aggregation of untreated ribosomes

Seeding experiments with A β -ribosome co-aggregates were performed as discussed in “Materials and Methods”. 0.1 μ M of 80S ribosome was incubated with 25 μ M A β 40 or A β 42 and K18 (as positive control) and as negative control the ribosome was incubated alone at 37 $^{\circ}$ C for 3 hours. After incubation, 1 μ l aliquot was withdrawn from each reaction mixture and added to 999 μ l of fresh 0.1 μ M 80S ribosome. This was further incubated for 24 hours, centrifuged and the pellets were analyzed using 0.8% agarose gel electrophoresis.

A schematic outline of the seeding experiment is included in the figure. Agarose gel electrophoretic analysis for presence of rRNA in the pellet when 0.1 μ M 80S was incubated with aliquots of protein-ribosome aggregation mix, withdrawn after 3 hours of incubation. Lanes from left to right contain (i) Total 80S ribosome (ii) 80S ribosome incubated with aliquot of untreated ribosome (iii) 80S ribosome incubated with aliquot of (K18+80S)_{3h} (iv) 80S ribosome incubated with aliquot of (A β 40+80S)_{3h} and (v) 80S ribosome incubated with aliquot of (A β 42+80S)_{3h}.

This experiment aimed to investigate the ability of A β -ribosome co-aggregates to seed the aggregation of untreated ribosome. As shown in **Figure 11**, aliquots withdrawn at the end of 3 hours of A β -80S incubation could induce the formation of rRNA containing aggregates when added to fresh ribosome at a 1000-fold dilution. Aliquots withdrawn from the control experimental set, where 0.1 μ M 80S was incubated alone for 3 hours, were unable to induce the aggregation of fresh ribosome (when added at a 1000-fold dilution and the fresh ribosomal particles are incubated for an additional 24 hours with the added aliquot). These observations indicate at the self-perpetuating nature of the A β -ribosome co-aggregation phenomenon after the process is induced due to A β ribosome interaction. However, it remains to be determined whether the aggregation of the fresh ribosome is mediated by the aggregated ribosomal components or by a fragmented element of the A β -ribosome co-aggregated complex. Further studies may help to answer these questions.

“Seeding” refers to the self-propagating tendency of prion and amyloid forming proteins. Seeds are represented by small oligomeric species that can induce conformational changes in the monomers present in its vicinity, leading them towards forming aggregated structures that ultimately progress to form fibrillar structures. Seeds can be formed by the fragmentation of pre-fibrillar structures and they can induce fresh rounds of aggregation [Cremers et al., 2016].

Our seeding experiments address the seeding ability of the A β -ribosome co-aggregates and they demonstrate that the complexes can indeed induce the aggregation of fresh ribosome molecules that are not previously exposed to the presence of any peptides or inducers of aggregation. Previous studies with prion proteins [Cordeiro et al., 2019, Kovachev et al., 2019] and p53 protein [Kovachev et al., 2017], have demonstrated the ability of RNA-protein aggregates to seed *de novo* protein aggregation.

Since the eukaryotic ribosome is majorly constituted by the rRNA component, besides the presence of the ribosomal proteins, the A β -ribosome co-aggregation is likely to involve the formation of A β -rRNA as well as A β -ribosomal protein aggregates.

Thus, the rRNA component of the ribosome can be critical for the seeding behaviour exhibited by the A β -ribosome co-aggregates. In addition to this, the large number of intrinsically unstructured ribosomal proteins can also modulate this behaviour. The identification of the seeding component of the A β -ribosome co-aggregate as well as the potential of this phenomenon to threaten the ribosomal population of neurons requires further investigation.

Section B

Effect of RNA: protein stoichiometry and inhibitors on A β -ribosome co-aggregation

As discussed previously, in the “Introduction” section, nucleic acids can promote amyloid aggregate formation via the template effect, where the amyloid protein orientation is restricted along the nucleic acid chain, thereby increasing their local concentration as well as facilitating intermolecular hydrophobic interactions, that culminates in formation of amyloid aggregates [Jiang et al., 2007]. Studies by Rha et al. [2020], have proposed a model for nucleic acid-amyloid co-assembly where the peptides and the nucleic acids come together via electrostatic templating. Their studies suggested that a contributing factor towards the complementarity, structural integrity and homogeneity of the final cross β amyloid assembly is the nucleic acid phosphate periodicity. Thus, stretches on peptides with cationic nature can participate in complementary electrostatic interactions with nucleic acids with polyanionic nature. In addition, as mentioned previously, studies by Meli et al. [2018] proposed that RNA can interact with amyloid fibrils in a peptide sequence dependent manner where certain peptides sequences can sequester RNA and act as “RNA traps”. The role of polyphosphates as a modulator of amyloid aggregation and accelerator of fibril formation to prevent fragmentation of pre-formed fibrils has also been proposed and discussed before [Cremers et al., 2016]. This study is in agreement with a previous study demonstrating the stimulation of prion aggregation by host-encoded nucleic acids of variable sequences [Safar et al., 2005]. These studies imply at the sequence (nucleic acid) independent nature of the nucleic acid – mediated modulation of amyloid aggregation which can play a pivotal role in amyloid mediated toxicity. Previous studies revealed that Poly(A) RNA, Poly(U) RNA [Fichou et al., 2018] as well as cellular RNA can act as the polyanionic inducer of aggregation for the intrinsically unstructured Tau protein. Studies conducted in our laboratory demonstrated that

incubation of Tau protein (both full length Ht40 and 4 repeat microtubule binding subdomain K18) with total ribosomal RNA isolated from yeast 80S ribosome can lead to the formation of Tau-rRNA large co-aggregated complexes [Banerjee et al., 2020]. Previous studies with prion proteins have also demonstrated that their interaction with RNA can occur in a sequence and structure independent manner and the outcome of such interaction depends on the relative concentrations of the interacting partners [Cordeiro et al., 2019, Kovachev et al., 2019]. The selective binding of RNA to the positively charged N-terminus of the prion protein, which is a low complexity domain and its potential to modulate their aggregation propensity, has also been reported [Cordeiro et al., 2019]. Studies by Navarro et al. [2019] have suggested that about 30% of human proteins possessing prion-like domains have RNA-binding propensity and several intrinsically unstructured proteins with clinical implications possess RNA recognition motifs (RRMs). Another study showed that short basic peptides with alternating hydrophobic and hydrophilic residues that are unable to form amyloids on their own can be induced to undergo amyloid aggregation in the presence of Poly(A) RNA [Braun et al., 2011]. Taken together, all the studies discussed above ratify the role of RNA as an amyloid aggregation modulator.

A β peptides, which constitute the amyloid plaques associated with AD, can form amyloid fibrils in an inducer-independent manner [Lee et al., 2017]. Although these peptides are not predominantly positively charged, an analysis of their amino acid sequences (as discussed before; Section A, **Figure 3A**) reveals the presence of clusters of positively and negatively charged residues distributed along their length. This is significant in view of previous studies that have suggested that an overall net positive charge of the peptide is not essential for its interaction with a polyanion like RNA and the presence of clusters of positive and negative charges is sufficient to mediate such an interaction [Calamai et al., 2006]. Additionally, the presence of RNA in amyloid plaques [Stewart et al., 2017, Ginsberg et al., 1997, Ginsberg et

al., 1998, Ginsberg et al., 1999] was also detected. The ability of RNA to act as “pathological chaperones” and modulate A β aggregation intracellularly, have been reported in literature [Ginsberg et al.,1998]. Cumulatively these evidences imply that although A β peptides do not require RNA as an inducer of aggregation, RNA could imminently possess the ability to influence A β aggregation.

Our previous experiments (stated above: Section A; **Figures 7, 8 and 9**) have demonstrated the ability of A β peptides (both A β 40 and A β 42) to induce the co-aggregation of yeast 80S ribosomal components. A major proportion of the ribosomal surface is constituted by rRNA [Schavemaker et al., 2017]. The rRNA also constitutes a major proportion of the total cellular RNA [Kampers et al., 1996]. Hence the objectives of our next experiments were to explore the potential role of total rRNA isolated from yeast 80S ribosome in stimulating A β aggregation.

Previous studies conducted in the laboratory have confirmed the role of 80S rRNA as a stimulator of lysozyme aggregation [Pathak et al., 2017] and Tau aggregation (both full length Ht40 and 4 repeat microtubule binding subdomain K18) [Banerjee et al., 2020]. It was proposed that RNA on the ribosomal surface could act as a polyanionic interacting partner, with the potential to engage multiple molecules of Tau, subsequently leading to co-aggregation of ribosomal components. The aim of our current studies with A β 40, A β 42 and K18 and the RNA molecules Poly(A), Poly(U) and total 80S rRNA was to explore different aspects of RNA mediated stimulation of A β aggregation. A comparative study of the factors (stoichiometry and small molecule polyphenolic aggregation inhibitors) that influence A β -RNA or K18-RNA aggregation and the protein aggregate induced 80S ribosome co-aggregation process was also performed as described below.

B.1. Effect of Poly(A) RNA and Poly(U) RNA on A β 40, A β 42 and K18 aggregation

In order to assess the effects of Poly(A) RNA and Poly(U) RNA on the aggregation of the two A β peptides, A β 40 and A β 42, 10 μ M of each of the peptides was incubated with 0.2 μ M of each of Poly(A) and Poly(U) RNA over a period of 48 hours at 37 $^{\circ}$ C. The stoichiometry of the concentrations of the peptides and RNA molecules for the reactions was maintained at 1:50 (RNA: peptide). The determination of concentration of Poly(A) and Poly(U) RNA is described in details in the “Materials and Methods” section. The RNA: protein ratio of 1:50 has been reported to favour aggregation [Kovachev et al., 2017] and was hence selected for our studies. As discussed previously, light scattering intensity is directly proportional to the size of the scattering particle [Antoun et al., 2004]. Since aggregates are significantly larger in size compared to monomeric proteins, an increase in light scattering intensity at 450 nm wavelength over time would indicate formation of aggregates. Hence light scattering analysis at 450 nm was performed to investigate the effect of Poly(A) and Poly(U) RNA on A β -peptide aggregation. Since the stimulatory effect of RNA on Tau-K18 aggregation was already demonstrated by previous studies conducted in the laboratory [Banerjee et al., 2020], control experiments with K18 (10 μ M) and Poly(A) and Poly(U) RNA (0.2 μ M each) were also performed.

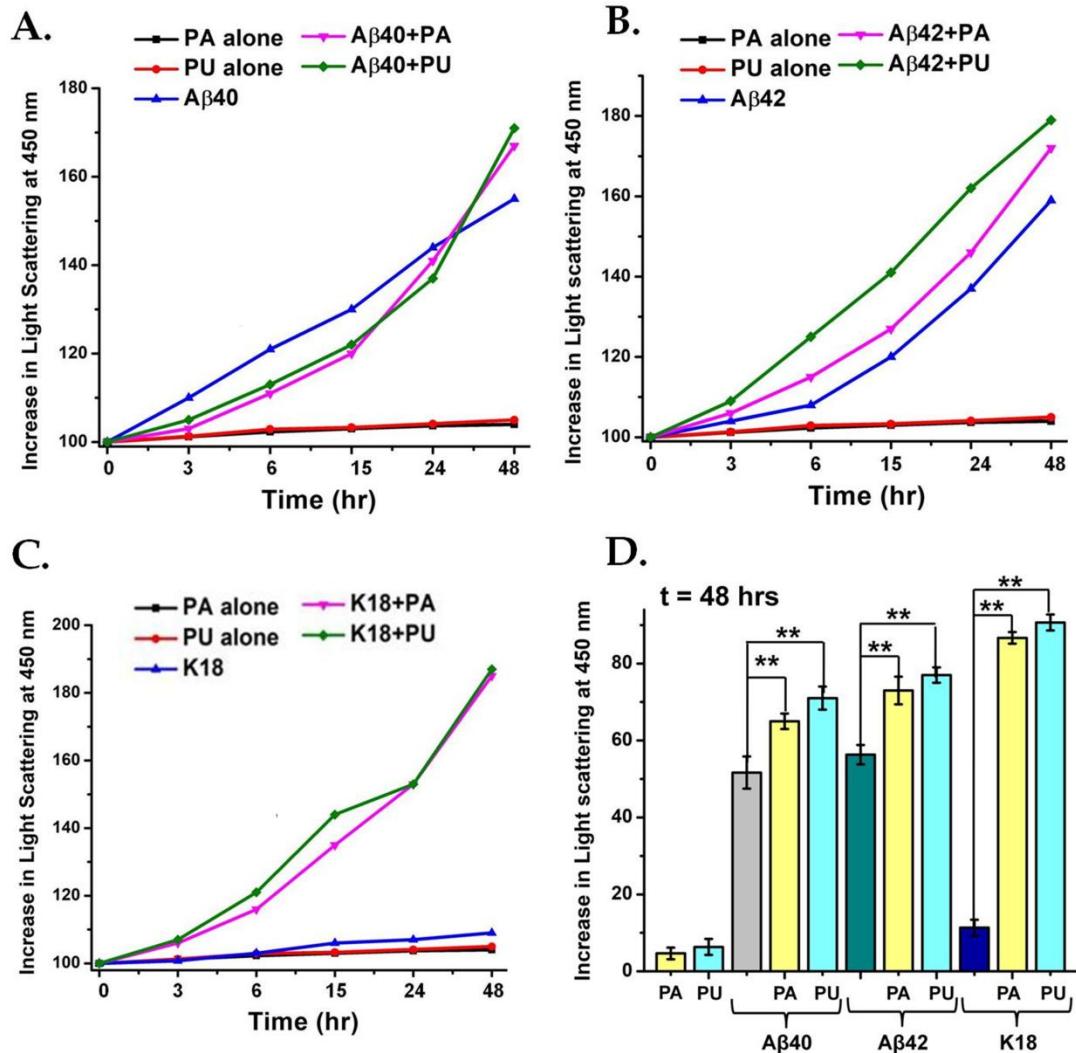


Figure 12: Poly(A) and Poly(U) RNA can stimulate aggregation of Aβ peptides

Aβ40, Aβ42 and K18 (10 μM) were incubated in the presence and absence of 50-fold less Poly(A) RNA (PA) and Poly(U) RNA (PU) (0.2 μM) over a period of 48 hours at 37 °C. The time course change in aggregation was monitored by recording the change in light scattering intensity at 450 nm at different time intervals (t=0 hr, t=3 hrs, t=6 hrs, t=15 hrs, t=24 hrs and t= 48 hrs) of peptide-RNA incubation. **A.** Light Scattering analysis: Time course change in light scattering intensity at 450 nm at different time intervals of Aβ40-RNA aggregation. PA alone (■), PU alone (●), Aβ40 alone (▲), Aβ40+PA (▼), Aβ40+PU (◆). **B.** Light Scattering analysis: Time course change in light scattering intensity at 450 nm at different time intervals of Aβ42-RNA aggregation. PA alone (■), PU alone (●), Aβ42 alone (▲), Aβ42+PA (▼), Aβ42+PU (◆). **C.** Light Scattering analysis: Time course change in light scattering intensity at 450 nm at different time intervals of K18-RNA aggregation. PA alone (■), PU alone (●), K18 alone (▲), K18+PA (▼), K18+PU (◆). **D.** Bar graph representing the net change in light scattering intensity at 450 nm at the end of 48 hours of incubation of Aβ40, Aβ42 and K18 in the presence of 50-fold less Poly(A) (PA) and Poly(U) (PU) RNA (1) PA alone (2) PU alone (3) Aβ40 alone (4) Aβ40 +PA (Aβ40:PA =50:1) (5) Aβ40 +PU (Aβ40:PU =50:1) (6) Aβ42 alone (7) Aβ42 +PA (Aβ42:PA =50:1) (8) Aβ42 +PU (Aβ42:PU =50:1) (9)K18 alone (10) K18 +PA (K18:PA =50:1) (11) K18 +PU (K18:PU =50:1). The experiments were repeated thrice and the data are presented as means± SEM; *P< 0.05 or **P< 0.001 in one-way ANOVA (N= 3).

The change in light scattering intensity at 450 nm (details in “Materials and Methods”) at different time intervals (t=0 hour, 3 hours, 6 hours, 15 hours, 24 hours and 48 hours) over a period of 48 hours was measured. **Figures 12A, B and C** include line graphs depicting the time course change in light scattering intensity at 450 nm for A β 40, A β 42 and K18 respectively, in the presence and absence of Poly(A) and Poly(U) RNA. The progressive increase in light scattering intensity over time indicates at the stimulatory effect of the RNA molecules towards aggregation of A β 40, A β 42 and K18. It is to be noted that a considerable increase in light scattering is observed even when the A β peptides, A β 40 (**Figure 12A**) and A β 42 (**Figure 12B**), are incubated alone. This is in agreement with the self-aggregating tendency of the A β peptides as reported in literature [Lee et al., 2017]. However, the results also clearly indicate at a stimulatory effect mediated by Poly(A) and Poly(U) RNA on the A β 40 and A β 42 aggregation. Further, no significant difference is observed between the stimulation of A β aggregation mediated by Poly(A) RNA from that mediated by Poly(U) RNA. As expected, although no significant increase in aggregation is observed upon incubation of K18 alone (since its aggregation is essentially dependent on the presence of a polyanionic inducer) [Ramachandran et al., 2011] (**Figure 12C**), a significant increase in aggregation is observed when RNA is present as the inducer.

Figure 12D includes a bar graph, representing the net increase in light scattering intensity at 450 nm at the end of 48 hours of incubation of A β 40, A β 42 and K18 with Poly(A) and Poly(U) RNA, which allows for a comparative analysis of the RNA-mediated stimulation of aggregation for each of the peptides. Though the A β peptides could aggregate on their own, the results confirm the nucleic acid sequence independent stimulatory effect mediated by the presence of Poly(A) and Poly(U) RNA on the A β aggregation process.

B.2. Effect of total ribosomal RNA isolated from yeast 80S ribosome (80S rRNA) on A β 40, A β 42 and K18 aggregation

B.2.a. Light scattering analysis of the effect of 80S rRNA on A β 40, A β 42 and K18 aggregation

In order to investigate whether the RNA could mediate its effect on A β 40, A β 42 and K18 aggregation in a sequence independent manner and whether 80S rRNA (the major cellular RNA as well as ribosomal component) also has the potential to stimulate aggregation of these peptides, the subsequent experiments were performed. In these experiments, 0.2 μ M of rRNA extracted from yeast 80S ribosome (80S rRNA) (Materials and Methods) was incubated with 10 μ M of A β 40, A β 42 and K18 over a period of 48 hours at 37 °C, and similar to our experiments performed with Poly(A) and Poly(U) RNA, the time course change in light scattering intensity at 450 nm was recorded at different time intervals (t=0 hour, 3 hours, 6 hours, 15 hours, 24 hours and 48 hours) over a period of 48 hours.

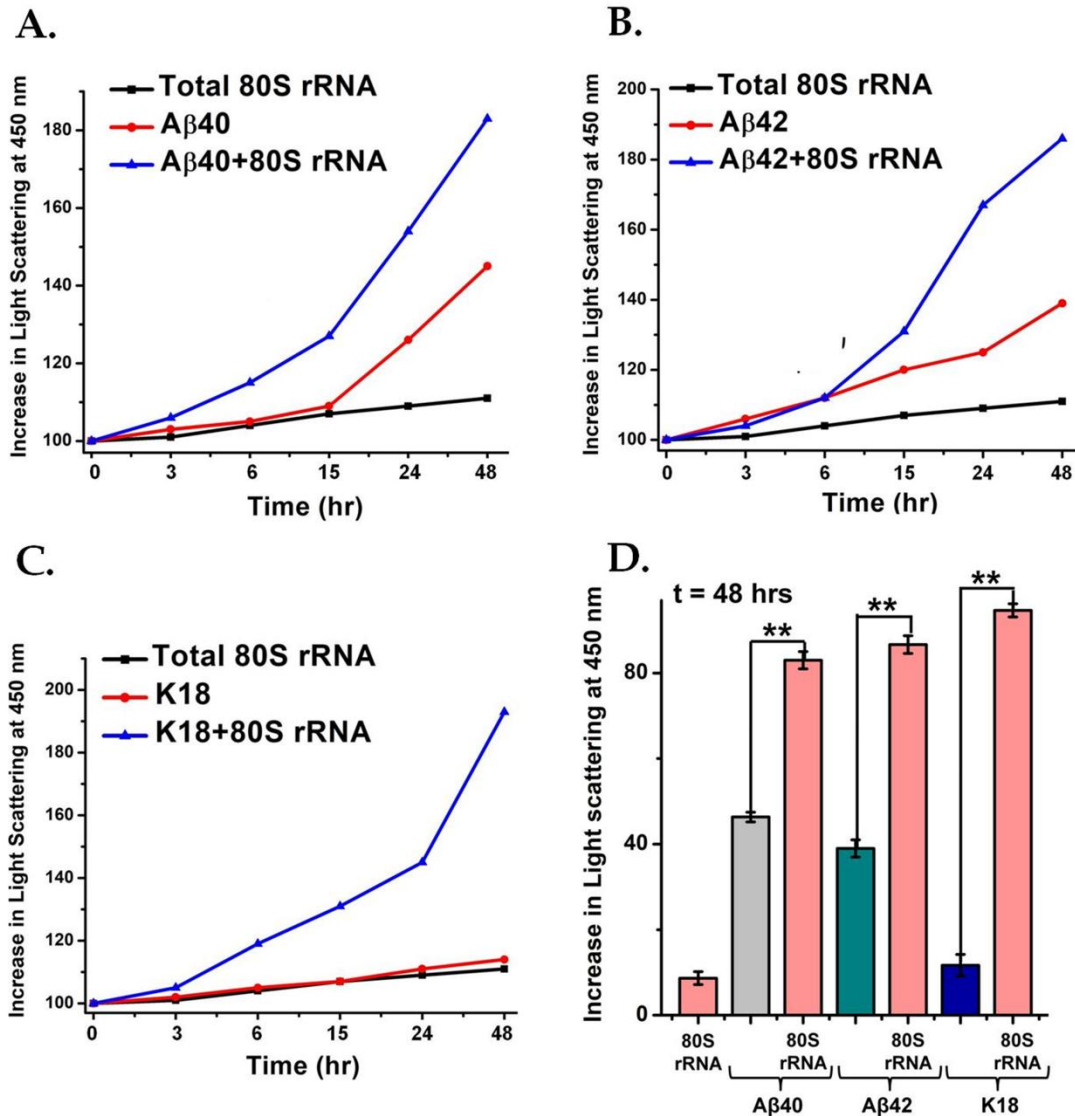


Figure 13: Yeast 80S rRNA can stimulate aggregation of Aβ peptides

Aβ40, Aβ42 and K18 (10 μM) were incubated in the presence and absence of 50-fold less 80S rRNA (0.2 μM) over a period of 48 hours at 37 °C. The time course change in aggregation was monitored by recording the change in light scattering intensity at 450 nm at different time intervals (t=0 hr, t=3 hrs, t=6 hrs, t=15 hrs, t=24 hrs and t= 48 hrs) of peptide-RNA incubation. **A.** Light Scattering analysis: Time course change in light scattering intensity at 450 nm at different time intervals of Aβ40-RNA aggregation. 80S rRNA alone (■), Aβ40 alone (●), Aβ40+80S rRNA (▲). **B.** Light Scattering analysis: Time course change in light scattering intensity at 450 nm at different time intervals of Aβ42-RNA aggregation. 80S rRNA alone (■), Aβ42 alone (●), Aβ42+80S rRNA (▲). **C.** Light Scattering analysis: Time course change in light scattering intensity at 450 nm at different time intervals of K18-RNA aggregation. 80S rRNA alone (■), K18 alone (●), K18+80S rRNA (▲). **D.** Bar graph representing the net change in light scattering intensity at 450 nm at the end of 48 hours of incubation of Aβ40, Aβ42 and K18 in the presence of 50-fold less 80S rRNA (1) 80S rRNA alone (2) Aβ40 alone (3) Aβ40 +80S rRNA (Aβ40:80S rRNA =50:1) (4) Aβ42 alone (5) Aβ42 +80S rRNA (Aβ42:80S rRNA =50:1) (6) K18 alone (7) K18 +80S rRNA (K18:80S rRNA =50:1). The experiments were repeated thrice and the data are presented as means± SEM; *P< 0.05 or **P< 0.001 in one –way ANOVA (N= 3).

Figure 13A, 13B and 13C include line graphs depicting the increase in light scattering intensity at 450 nm over time, exhibited by A β 40, A β 42 and K18 respectively in the presence and absence of 80S rRNA. With both A β 40 (**Figure 13A**) and A β 42 (**Figure 13B**) peptides, a significant stimulation of aggregation was observed, beyond their self-aggregation at similar time points during the course of their aggregation process. The 80S rRNA induced and stimulated the aggregation of K18 as well (**Figure 13C**), as was expected from earlier studies [Banerjee et al., 2020]. These results are also reflected in the bar graph depiction of the net increase in light scattering intensity at the end of 48 hours of incubation of A β 40, A β 42 and K18 with total 80S rRNA (**Figure 13D**).

B.2.b. Agarose gel electrophoretic analysis of the effect of 80S rRNA on A β 40, A β 42 and K18 aggregation

In addition to light scattering analysis, agarose gel electrophoretic analysis was also performed to investigate the outcome of incubation of A β 40, A β 42 and K18 with total 80S rRNA. For this purpose, 25 μ M of each of the peptides was incubated with 1 μ M of rRNA extracted from yeast 80S ribosome for a period of 6 hours. At the end of the incubation period, the resultant reaction mixtures were subjected to centrifugation at 21,380 g for 45 minutes in order to partition the aggregation mixture into supernatant and pellet and the presence of rRNA in the pellet was analyzed by 0.8% agarose gel electrophoresis.

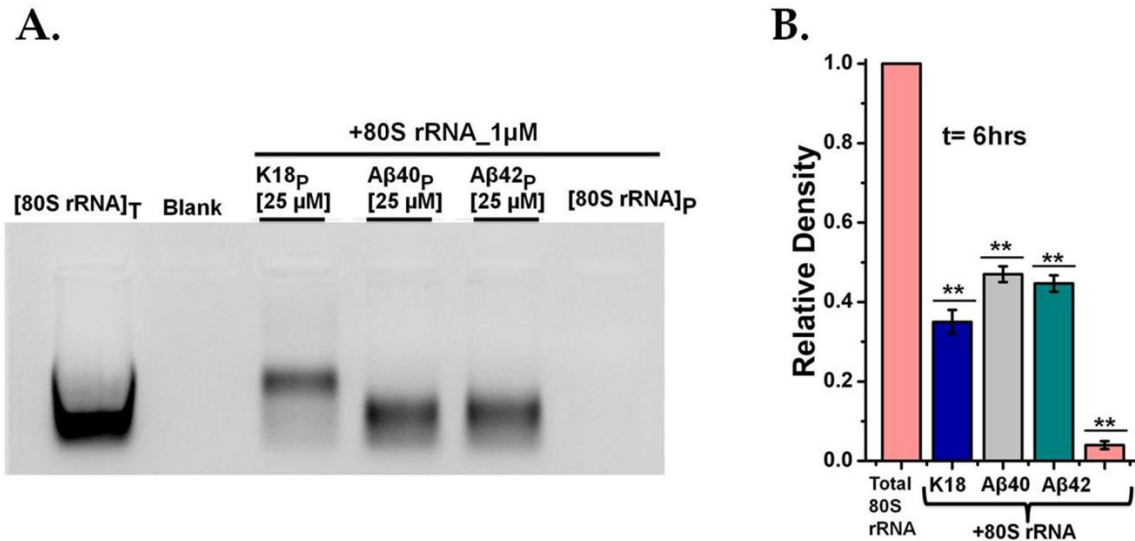


Figure 14: Yeast 80S rRNA can stimulate aggregation of Aβ peptides and lead to the formation of rRNA-Aβ co-aggregates

Aβ40 and Aβ42 (and K18, reduced with 1 mM DTT, as positive control) were incubated in the presence of 25-fold less (ratio of peptide: RNA = 25:1) 80S rRNA for 6 hours at 37 °C. The reaction mix, after 6 hours, was centrifuged and the pellet fractions were analyzed using 0.8% agarose gel electrophoresis for presence of rRNA. **A.** Agarose gel electrophoretic analysis: Lanes from left to right contain (1) Total 80S rRNA (80S rRNA)_T (2) Blank (3) (K18+80S rRNA)_{P,6h} (4) (Aβ40+80S rRNA)_{P,6h} (5) (Aβ42+80S rRNA)_{P,6h} (6) (80S rRNA)_{P,6h}. **B.** Bar graphs depicting the densitometric analysis of rRNA band intensities in the agarose gel for (1) Total 80S rRNA (2) (K18+80S rRNA)_{P,6h} (3) (Aβ40+80S rRNA)_{P,6h} (4) (Aβ42+80S rRNA)_{P,6h} (5) (80S rRNA)_{P,6h}. The band intensity of total 80S rRNA is assumed as 1 for calculations. The experiments were repeated thrice and the data are presented as means± SEM; *P< 0.05 or **P< 0.001 in one –way ANOVA (N= 3).

As shown in **Figure 14A**, the rRNA was indeed present in the pellet forming a major component of its constituents in case of all of the three peptides. No such presence of rRNA in the pellet was observed in the control experiment where the 80S rRNA was incubated alone in the absence of any peptides under similar conditions, indicating at the necessity of the presence of Aβ peptides or K18 for the formation of the large rRNA containing aggregates. The bar graph representing the relative densities of the rRNA bands obtained in the agarose gel is shown in **Figure 14B**. These results collectively imply at the stimulatory effect of rRNA towards Aβ40, Aβ42 and K18 aggregation and the subsequent formation of large RNA-protein co-aggregates.

B.3. Effect of stoichiometry on protein ribosome co-aggregation process

Previous studies conducted in the laboratory demonstrated that the outcomes of unfolded protein interaction with ribosomal RNA essentially depend on the relative stoichiometric ratios of the individual interacting partners [Pathak et al., 2014, Pathak et al., 2017]. While a super-stoichiometric concentration of unfolded protein with respect to the ribosome promotes co-aggregation of the ribosomal components [Pathak et al., 2017], stoichiometric concentrations of unfolded protein promote the chaperoning activity of the ribosome [Das et al., 2008]. The significance of stoichiometry has also been reported in a study with p53 protein and RNA [Kovachev et al., 2017]. This study reported that incubation of 50-fold excess concentration of the aggregation prone p53 protein with RNA resulted in stimulation of p53 aggregation. However, when p53 was incubated at an 8-fold excess concentration with respect to the RNA, suppression of its aggregation was observed. These observations indicated that at higher stoichiometric ratios (higher protein: RNA), the RNA might act as a scaffold for multiple p53 protein molecules and thereby provide spatial and energetic requirements for enhanced aggregation, while as the RNA concentration increases (lower protein: RNA), an increase in formation of smaller aggregates might be favoured [Kovachev et al., 2017]. Thus, the next objective of our study was to investigate whether such stoichiometry dependent outcomes are observed for A β 40, A β 42 and K18 aggregation.

B.3.a. Effect of stoichiometry on Poly(A) and Poly(U) RNA-mediated aggregation of A β 40, A β 42 and K18

In order to assess the effect of stoichiometry on Poly(A) and Poly(U) RNA-mediated aggregation of A β 40, A β 42 and K18, the two RNA: protein stoichiometric ratios that were used were 1:50 and 1:8 respectively [Kovachev et al., 2017]. In the aggregation reactions with RNA: protein ratio of 1:50, 10 μ M of A β 40, A β 42 and K18 (reduced with 1 mM DTT)

(described in detail in “Materials and Methods”) were incubated with 0.2 μM of each of Poly(A) and Poly(U) RNA for a period of 48 hours at 37 $^{\circ}\text{C}$. At the end of the incubation period, the net increase in light scattering intensity at 450 nm for each of the reaction sets was monitored. The increase was also recorded for all of the control reaction sets, where the individual peptides and the RNA molecules were incubated alone for 48 hours. Similar procedure was followed for reactions with RNA: protein ratio of 1:8 with the only exception of the concentration of RNA molecules used in these experiments, which was 1.25 μM . The net increase in light scattering intensities at the end of 48 hours for each of the peptides, A β 40, A β 42 and K18, incubated with two different stoichiometric concentrations of Poly(A) and Poly(U) RNA, is depicted as bar graphs in **Figure 15A, B and C** respectively.

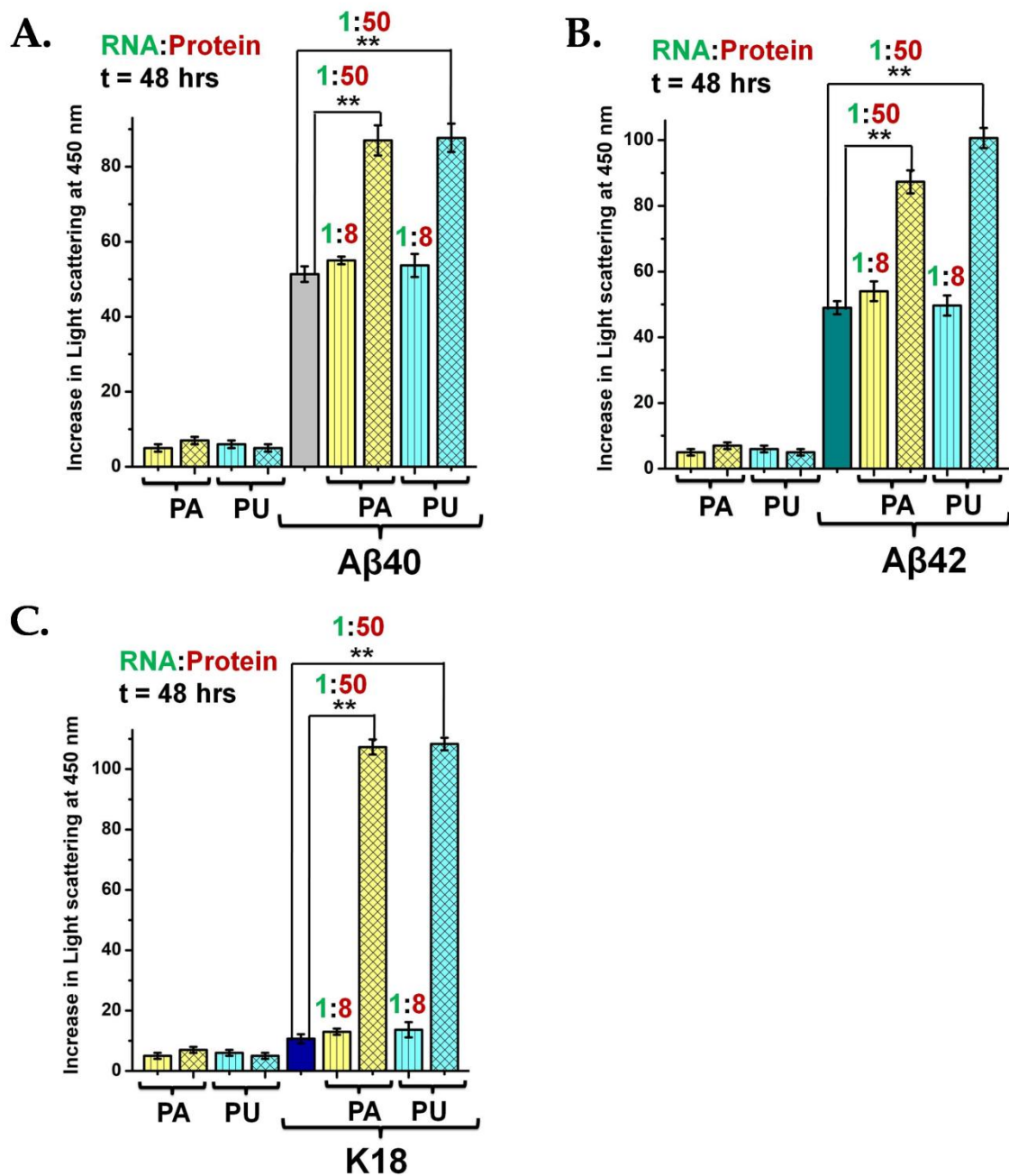


Figure 15: Effect of different stoichiometries of Poly(A) RNA and Poly(U) RNA with respect to the Aβ peptides on the aggregation of the Aβ peptides

Aβ40, Aβ42 and K18 were incubated in the absence and presence of 8-fold less (ratio of peptide: RNA = 8:1) and 50-fold less (ratio of peptide: RNA = 50:1) Poly(A) RNA (PA) and Poly(U) RNA (PU) for 48 hours at 37 °C, as described in “Materials and Methods”. The aggregation was monitored by recording the change in light scattering intensity at 450 nm. A. Bar graph representing net change in light scattering intensity at 450 nm after 48 hours of incubating Aβ40 (10 μM) in the presence of 8-fold less (1.25 μM) and 50-fold less (0.2 μM) PA and PU RNA (Materials and Methods). (1) PA alone (1.25 μM) (2) PA alone (0.2 μM) (3) PU alone (1.25 μM) (4) PU alone (0.2 μM) (5) Aβ40 alone (6) Aβ40+8-fold less PA (7) Aβ40+50-fold less PA (8) Aβ40+8-fold less PU (9) Aβ40+50-fold less PU.

B. Bar graph representing net change in light scattering intensity at 450 nm after 48 hours of incubating A β 42 (10 μ M) in the presence of 8-fold less (1.25 μ M) and 50-fold less (0.2 μ M) PA and PU RNA (Materials and Methods). (1) PA alone (1.25 μ M) (2) PA alone (0.2 μ M) (3) PU alone (1.25 μ M) (4) PU alone (0.2 μ M) (5) A β 42 alone (6) A β 42+8-fold less PA (7) A β 42+50-fold less PA (8) A β 42+8-fold less PU (9) A β 42+50-fold less PU. **C.** Bar graph representing net change in light scattering intensity at 450 nm after 48 hours of incubating K18 (10 μ M) in the presence of 8-fold less (1.25 μ M) and 50-fold less (0.2 μ M) PA and PU RNA (Materials and Methods). (1) PA alone (1.25 μ M) (2) PA alone (0.2 μ M) (3) PU alone (1.25 μ M) (4) PU alone (0.2 μ M) (5) K18 alone (6) K18+8-fold less PA (7) K18+50-fold less PA (8) K18+8-fold less PU (9) K18+50-fold less PU. The experiments were repeated thrice and the data are presented as means \pm SEM; *P< 0.05 or **P< 0.001 in one-way ANOVA (N= 3).

A significant stimulation of aggregation in the presence of Poly(A) and Poly(U) RNA is observed for A β 40 (**Figure 15A**), A β 42 (**Figure 15B**) and K18 (**Figure 15C**) at stoichiometric ratio of 1:50 (RNA: protein). However, at a 1:8 (RNA: protein) ratio, no significant stimulation of aggregation is noticed for any of the peptides including K18. In order to confirm this phenomenon with total 80S rRNA, subsequent experiments were performed with the proteins and the 80S rRNA.

B.3.b. Effect of stoichiometry on total 80S rRNA-mediated aggregation of A β 40, A β 42 and K18

In order to assess the effect of stoichiometry on 80S rRNA mediated aggregation of A β 40, A β 42 and K18, the RNA: protein stoichiometric ratios used were 1:50 and 1:8 [Kovachev et al., 2017], as in the earlier experiment. For reactions with RNA: protein ratio of 1:50, 10 μ M of each of A β 40, A β 42 and K18 (reduced with 1 mM DTT) (described in detail in “Materials and Methods”) was incubated with 0.2 μ M of 80S rRNA for a period of 48 hours at 37 $^{\circ}$ C. At the end of the incubation period, the net increase in light scattering intensity at 450 nm for each of the reaction sets was measured. The increase was also recorded for all of the control reaction sets where the individual peptides and the RNA molecule were incubated alone for 48 hours at 37 $^{\circ}$ C. Similar procedure was followed for reactions with RNA: protein ratio of 1:8 with the only exception of the concentration of RNA molecule used which was 1.25 μ M. The net increase in light scattering intensities at the end of 48 hours for each of the peptides,

A β 40, A β 42 and K18, incubated with two different stoichiometric concentrations of 80S rRNA, is depicted as bar graphs in **Figure 16A, B and C** respectively.

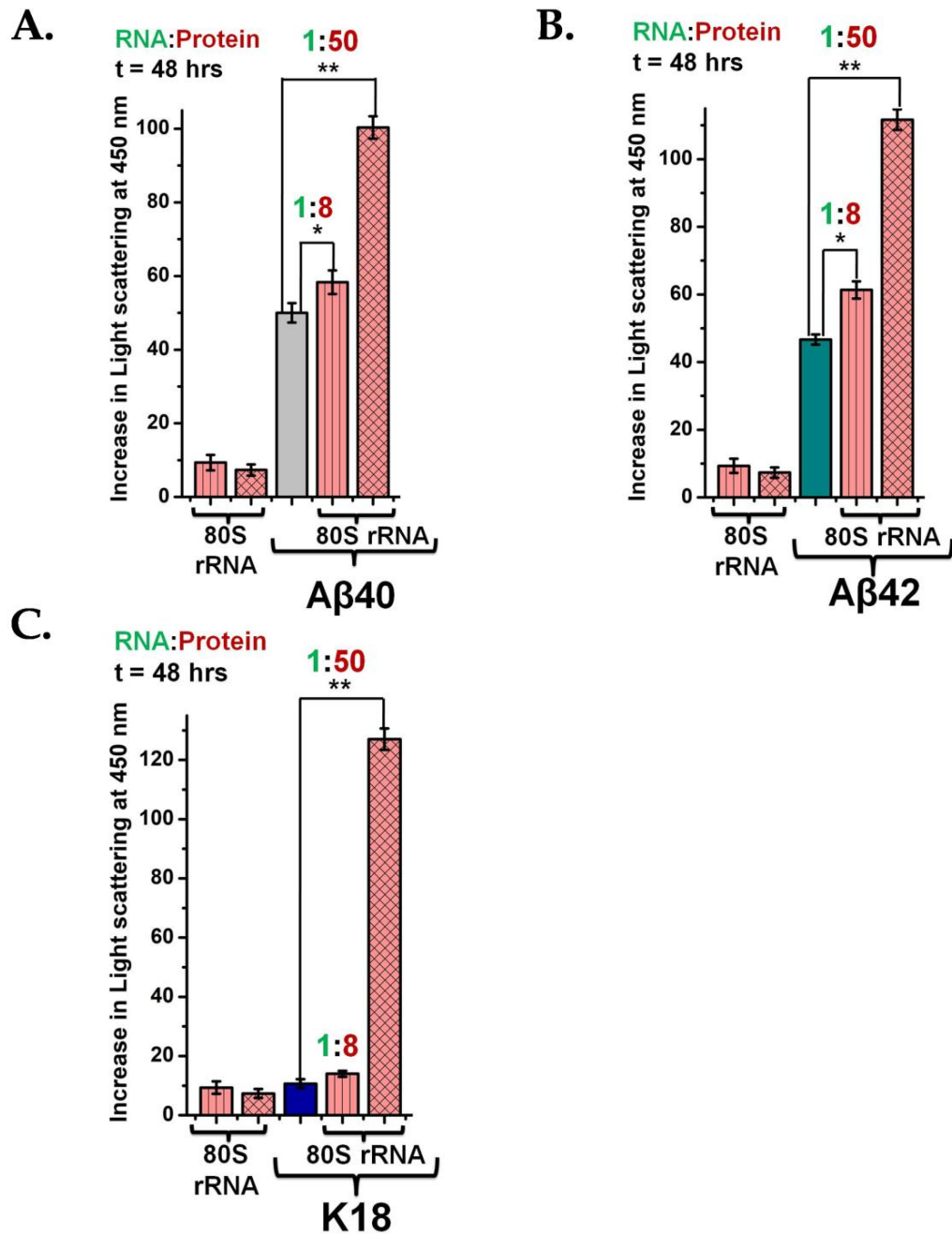


Figure 16: Effect of different stoichiometries of 80S rRNA with respect to the A β peptides on the aggregation of the A β peptides

A β 40, A β 42 and K18 were incubated in the absence and presence of 8-fold less (ratio of peptide: RNA = 8:1) and 50-fold less (ratio of peptide: RNA = 50:1) 80S rRNA for 48 hours at 37 °C, as described in “Materials and Methods”. The aggregation was monitored by recording the change in light scattering intensity at 450 nm.

A. Bar graph representing net change in light scattering intensity at 450 nm after 48 hours of incubating A β 40 (10 μ M) in the presence of 8-fold less (1.25 μ M) and 50-fold less (0.2 μ M) 80S rRNA (Materials and Methods). (1) 80S rRNA alone (1.25 μ M) (2) 80S rRNA alone (0.2 μ M) (3) A β 40 alone (4) A β 40+8-fold less 80S rRNA (5) A β 40+50-fold less 80S rRNA. **B.** Bar graph representing net change in light scattering intensity at 450 nm after 48 hours of incubating A β 42 (10 μ M) in the presence of 8-fold less (1.25 μ M) and 50-fold less (0.2 μ M) 80S rRNA (Materials and Methods). (1) 80S rRNA alone (1.25 μ M) (2) 80S rRNA alone (0.2 μ M) (3) A β 42 alone (4) A β 42+8-fold less 80S rRNA (5) A β 42+50-fold less 80S rRNA. **C.** Bar graph representing net change in light scattering intensity at 450 nm after 48 hours of incubating K18 (10 μ M) in the presence of 8-fold less (1.25 μ M) and 50-fold less (0.2 μ M) 80S rRNA (Materials and Methods). (1) 80S rRNA alone (1.25 μ M) (2) 80S rRNA alone (0.2 μ M) (3) K18 alone (4) K18+8-fold less 80S rRNA (5) K18+50-fold less 80S rRNA. The experiments were repeated thrice and the data are presented as means \pm SEM; *P< 0.05 or **P< 0.001 in one –way ANOVA (N= 3).

A significant stimulation of aggregation in the presence of 80S rRNA was observed for A β 40 (**Figure 16A**), A β 42 (**Figure 16B**) and K18 (**Figure 16C**) at stoichiometric ratio of 1:50 (RNA: protein), which is in agreement with our previously obtained results with Poly(A) and Poly(U) RNA. However, at a 1:8 (RNA: protein) ratio, no significant stimulation of aggregation is noticed for the A β peptides as well as the Tau variant K18. A possible explanation of this phenomenon is that a higher concentration of protein relative to that of RNA would increase the probability of multiple protein molecules interacting with a single RNA molecule, thereby highly increasing the localized concentration of the protein. Since increased concentration of proteins is a known promoter of aggregation, protein aggregation might be favoured by a low RNA: high protein ratio compared to the high RNA: low protein ratio.

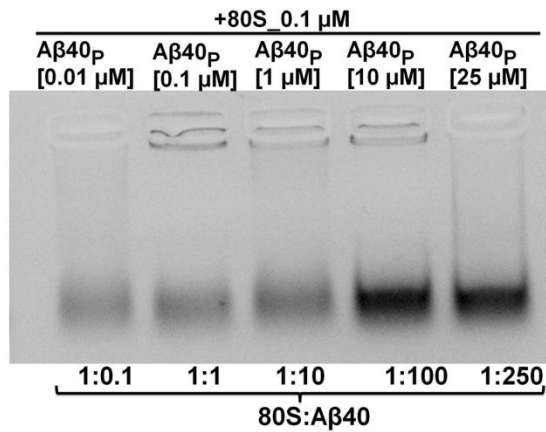
B.3.c. Effect of stoichiometry on co-aggregation of yeast 80S ribosome with A β 40, A β 42 and K18

Our next objective was to examine the effect of protein: ribosome stoichiometries on the phenomenon of co-aggregation of 80S ribosome with A β 40, A β 42 and K18. The aim was to assess, if similar effect of stoichiometry, as that observed with RNA and protein, would also be reflected in the protein-ribosome co-aggregation process. In these experiments, increasing concentrations of A β 40, A β 42 and K18 (reduced with 1 mM DTT) were incubated with 0.1

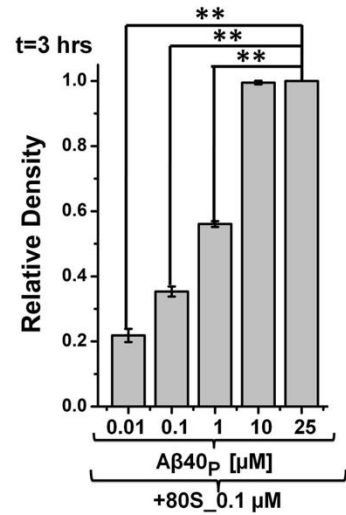
μM of the intact yeast 80S ribosome at 37°C for a period of 3 hours. The ribosome: protein ratios used for 80S ribosome and both the $\text{A}\beta$ peptides were 1:0.1, 1:1, 1:10, 1:100 and 1:250, whereas that used for K18 was 1:10, 1:100 and 1:250. The selection of the lowest protein concentration was based on the critical concentration of aggregation for each of the proteins [Hu et al., 2009]. While the critical concentration for oligomerization of the $\text{A}\beta$ peptides resides in the lower nanomolar range [Novo et al., 2018], that for K18 lies between 1-3 μM [Ramachandran et al., 2011]. Hence, the ribosome: protein ratios for this study were selected accordingly.

At the end of the incubation period, the reaction mixtures were centrifuged at 21,380 g for 45 minutes to separate the supernatant from the large insoluble aggregate containing pellets. The presence of ribosomal RNA in the pellets was analyzed using 0.8% agarose gel electrophoresis, as discussed previously.

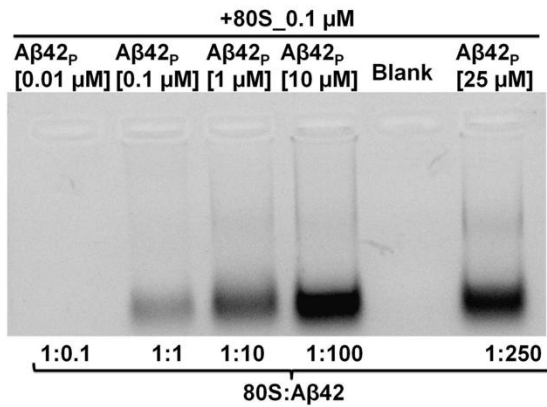
A.i)



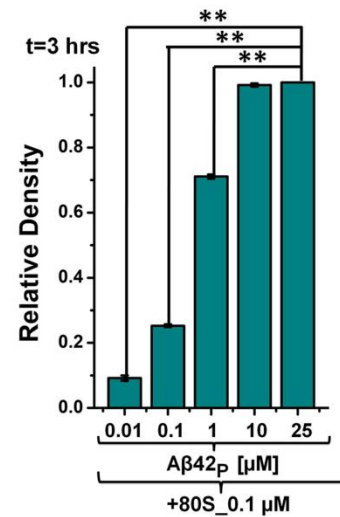
B.i)



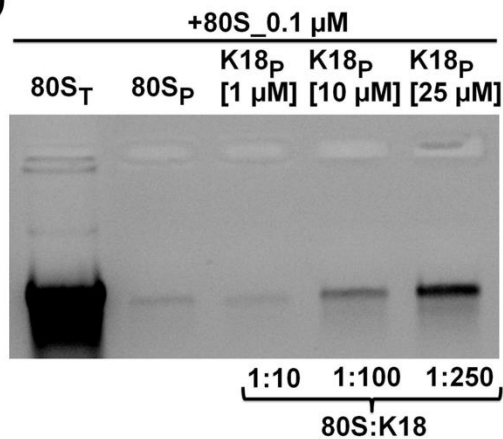
A.ii)



B.ii)



A.iii)



B.iii)

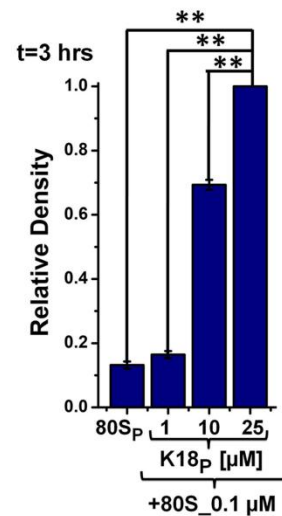


Figure 17: Effect of different stoichiometries of $A\beta$ peptides with respect to the yeast 80S ribosome on the $A\beta$ -ribosome co-aggregation process

0.1 μM of yeast 80S ribosome was incubated with different concentrations of A β 40, A β 42 and K18 (as positive control) for 3 hours at 37 $^{\circ}\text{C}$ and centrifuged to obtain the large insoluble aggregate containing pellets. The pellets were analyzed using 0.8% agarose gel electrophoresis. **A.** Agarose gel electrophoretic analysis of (i) A β 40-80S aggregation pellet for the presence of ribosomal RNA. Lanes from left to right contain: (1) (0.01 μM A β 40+80S)_{P_3h} (2) (0.1 μM A β 40+80S)_{P_3h} (3) (1 μM A β 40+80S)_{P_3h} (4) (10 μM A β 40+80S)_{P_3h} (5) (25 μM A β 40+80S)_{P_3h}. (ii) A β 42-80S aggregation pellet for the presence of ribosomal RNA. Lanes from left to right contain: (1) (0.01 μM A β 42+80S)_{P_3h} (2) (0.1 μM A β 42+80S)_{P_3h} (3) (1 μM A β 42+80S)_{P_3h} (4) (10 μM A β 42+80S)_{P_3h} (5) Blank (6) (25 μM A β 42+80S)_{P_3h}. (iii) K18-80S aggregation pellet for the presence of ribosomal RNA. Lanes from left to right contain: (1) Total 80S (80S)_T (2) (80S)_{P_3h} (3) (1 μM K18+80S)_{P_3h} (4) (10 μM K18+80S)_{P_3h} (5) (25 μM K18+80S)_{P_3h}. **B.** Bar graphs depicting the densitometric analysis of rRNA band intensities showing stimulation of co-aggregation with increasing concentrations of (i) A β 40. (25 μM A β 40+80S)_{P_3h} assumed as 1 for calculations. (ii) A β 42. (25 μM A β 42+80S)_{P_3h} assumed as 1 for calculations and (iii) K18. (25 μM K18+80S)_{P_3h} assumed as 1 for calculations. The experiments were repeated thrice and the data are presented as means \pm SEM; *P < 0.05 or **P < 0.001 in one –way ANOVA (N = 3).

As shown in **Figure 17Ai, Aii and Aiii**, a distinct dose-dependent increase in the appearance of 80S rRNA in the pellet occurs with increasing concentrations of A β 40 (**Figure 17Ai**), A β 42 (**Figure 17Aii**) and K18 (**Figure 17Aiii**) respectively. This is also reflected in the bar graphs representing the relative densities of the rRNA bands obtained in the agarose gel with A β 40 (**Figure 17Bi**), A β 42 (**Figure 17Bii**) and K18 (**Figure 17Biii**). These results imply that the interaction of multiple molecules of A β 40, A β 42 and K18 on the ribosomal surface (rRNA exposed surface) that is favored at higher protein: 80S stoichiometric ratios and their subsequent aggregation might be the underlying cause of co-aggregation of ribosomal components.

B.4. Effect of polyphenols on RNA-mediated stimulation of A β and Tau aggregation

As discussed in the “Introduction” section, polyphenols are naturally occurring compounds which possess neuroprotective properties largely owing to their anti-amyloidogenic activities *in vitro* [Freyssin et al., 2018]. They are known to mediate their inhibitory effect on aggregation, by either directly binding to the peptide oligomers and preventing their further maturation into fibrils or by interfering with the action of metal ions that promote aggregation

[Freyssin et al., 2018]. These molecules are also capable of destabilizing fibrillar aggregates [Freyssin et al., 2018].

The next objective of our study, thus, aimed at investigating the ability of such polyphenolic compounds to exert their inhibitory effect on the RNA-mediated stimulation of A β peptides and Tau protein aggregation that was demonstrated in our previous experiments and in previous works with Tau conducted in the laboratory [Banerjee et al., 2020]. For this purpose, the two polyphenols, rosmarinic acid (RA) and myricetin (Myr) were selected, since their inhibitory effect on the self-aggregation of A β peptides, in a concentration dependent manner, has been previously demonstrated [Ono et al., 2012]. Similar to our previous experiments studying the effects of RNA on A β 40, A β 42 and K18 in this section, the RNA molecules used in this case were also Poly(A) RNA, Poly(U) RNA and total ribosomal RNA extracted from yeast 80S ribosome (80S rRNA).

In order to examine the effect of rosmarinic acid (RA) and myricetin (Myr) on Poly(A), Poly(U) and 80S rRNA-mediated stimulation of A β 40, A β 42 and K18 aggregation, subsequent experiments were performed. In this study A β 40, A β 42 and K18 (10 μ M) (reduced with 1 mM DTT) were incubated in the presence and absence of 0.2 μ M of each of Poly(A), Poly(U) and 80S rRNA along with the presence or absence of 40 μ M of RA and Myr. The concentrations of the polyphenolic inhibitors were maintained at a 4-fold excess to that of the peptides, which have been previously shown to completely inhibit the self-aggregation of both A β 40 and A β 42 peptides [Ono et al., 2012]. The incubation was done at 37 $^{\circ}$ C over a period of 48 hours and the net change in light scattering intensity at 450 nm was monitored at the end of the incubation period, to ascertain the extent of aggregation (as described earlier in studies on the effect of RNA on A β aggregation) [Antoun et al., 2004].

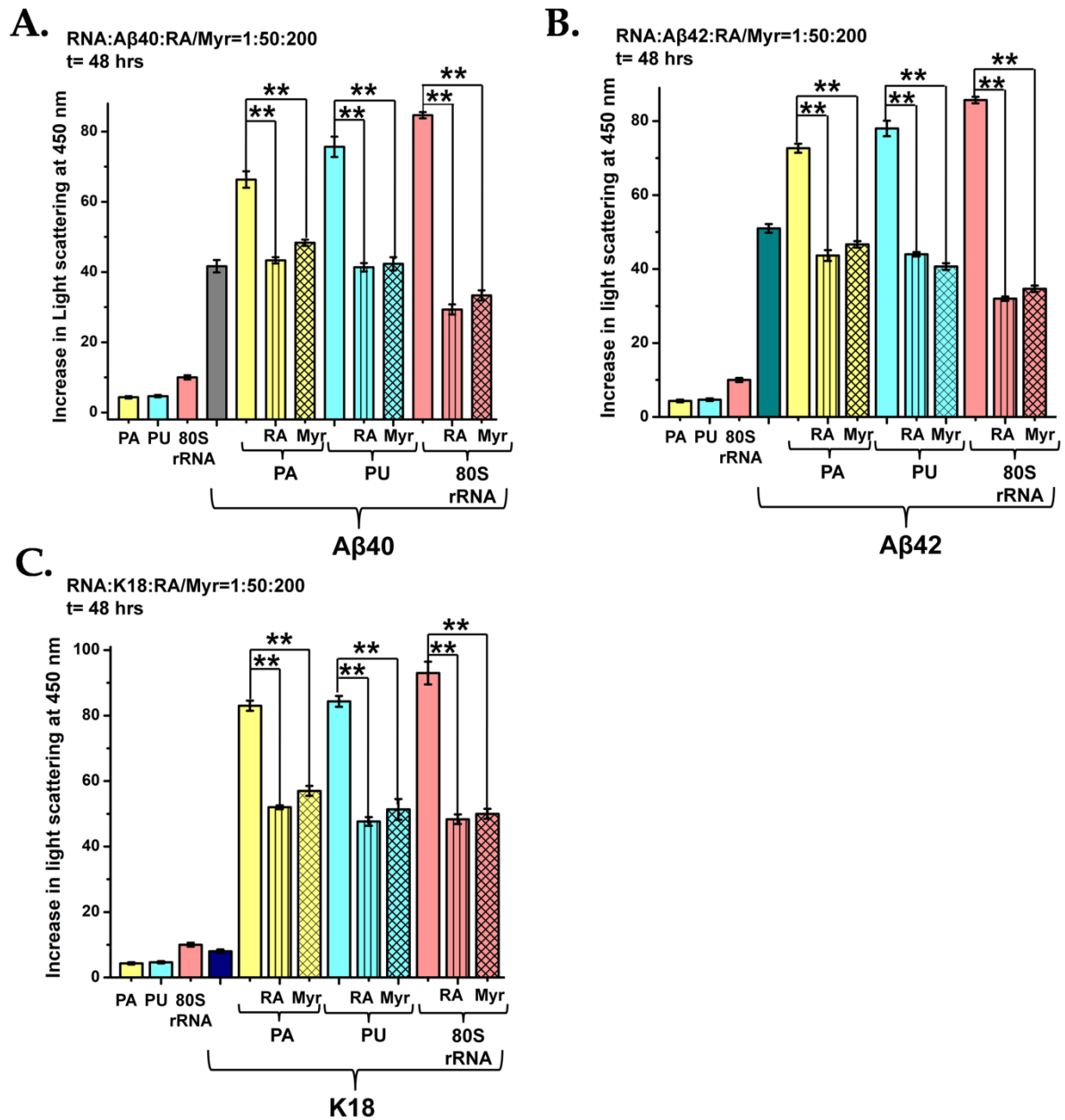


Figure 18: Effect of rosmarinic acid (RA) and myricetin (Myr) on aggregation of Aβ40, Aβ42 and Tau-K18 with Poly(A) RNA (PA), Poly(U) RNA (PU) and 80S rRNA

Aβ40, Aβ42 and K18 (10 μM) were incubated in the presence and absence of 50-fold less Poly(A) (PA), Poly(U) (PU) and 80S rRNA (0.2 μM) along with the presence and absence of 40 μM of rosmarinic acid (RA) and myricetin (Myr) over a period of 48 hours at 37 °C. The aggregation was monitored by recording the change in light scattering intensity after 48 hours of peptide-RNA incubation.

A. Bar graph representing net change in light scattering intensity at 450 nm at the end of 48 hours of incubation of A β 40 with PA, PU and 80S rRNA in the presence and absence of RA and Myr. (1) PA alone, (2) PU alone, (3) 80S rRNA alone, (4) A β 40 alone, (5) A β 40+PA, (6) A β 40+PA+RA, (7) A β 40+PA+Myr, (8) A β 40+PU, (9) A β 40+PU+RA, (10) A β 40+PU+Myr, (11) A β 40+80S rRNA, (12) A β 40+80S rRNA+RA and (13) A β 40+80S rRNA+Myr. **B.** Bar graph representing net change in light scattering intensity at 450 nm at the end of 48 hours of incubation of A β 42 with PA, PU and 80S rRNA in the presence and absence of RA and Myr. (1) PA alone, (2) PU alone, (3) 80S rRNA alone, (4) A β 42 alone, (5) A β 42+PA, (6) A β 42+PA+RA, (7) A β 42+PA+Myr, (8) A β 42+PU, (9) A β 42+PU+RA, (10) A β 42+PU+Myr, (11) A β 42+80S rRNA, (12) A β 42+80S rRNA+RA and (13) A β 42+80S rRNA+Myr. **C.** Bar graph representing net change in light scattering intensity at 450 nm at the end of 48 hours of incubation of K18 with PA, PU and 80S rRNA in the presence and absence of RA and Myr. (1) PA alone, (2) PU alone, (3) 80S rRNA alone, (4) K18 alone, (5) K18+PA, (6) K18+PA+RA, (7) K18+PA+Myr, (8) K18+PU, (9) K18+PU+RA, (10) K18+PU+Myr, (11) K18+80S rRNA, (12) K18+80S rRNA+RA and (13) K18+80S rRNA+Myr.

Figure 18 includes, bar graphical depictions of the net increase in light scattering intensity at 450 nm at the end of 48 hours of incubation of the respective peptides (A β 40, A β 42 and K18), RNA [Poly(A), Poly(U) and 80S rRNA] and inhibitor molecules (RA and Myr) at 37 °C. It shows the effect of RA and Myr on Poly(A) RNA (designated as PA in **Figure 18**), Poly(U) RNA (designated as PU in **Figure 18**) and 80S rRNA mediated stimulation of aggregation of A β 40 (**Figure 18A**), A β 42 (**Figure 18B**) and K18 (**Figure 18C**). The presence of both RA and Myr resulted in the suppression of Poly(A), Poly(U) and 80S rRNA mediated stimulation of aggregation of A β 40 (**Figure 18A**), A β 42 (**Figure 18B**) and K18 (**Figure 18C**). RA and Myr were also able to suppress the self-aggregation of A β 40 (**Figure 18A**) and A β 42 (**Figure 18B**), which is in agreement with previous studies [Ono et al., 2012]. This clearly indicates at the inhibitory effect mediated by RA and Myr on the self-aggregation of A β peptides as well as on the RNA mediated stimulation of aggregation of A β 40, A β 42 and K18.

Cumulatively, these studies imply that the RNA-mediated stimulation of A β 40, A β 42 and K18 aggregation could be suppressed in the presence of polyphenolic inhibitors like rosmarinic acid (RA) and myricetin (Myr) under the conditions used in our experiments.

B.5. Inhibition of A β and Tau mediated co-aggregation of ribosomal components

As discussed previously and demonstrated in our previous experiments (Chapter 3, Section B.4) polyphenolic compounds like rosmarinic acid (RA) and myricetin (Myr) can inhibit the stimulation of aggregation of A β 40, A β 42 and K18 mediated by Poly(A) RNA, Poly(U) RNA as well as 80S rRNA. If indeed the engagement of rRNA on the ribosomal surface during protein aggregation is the underlying cause of protein ribosome co-aggregation process, the question arises whether the inhibition of RNA-stimulated aggregation could also lead to the inhibition of co-aggregation of ribosomal components. Our subsequent experiments were aimed at exploring the effect of RA and Myr on the protein-ribosome co-aggregation process. For this purpose, 0.1 μ M of intact 80S ribosome was incubated with 25 μ M of each of A β 40, A β 42 and K18 (reduced with 1 mM DTT) in the presence and absence of 100 μ M of RA and Myr. A 4-fold excess concentration of RA and Myr compared to that of the peptides was selected for our study, since at this stoichiometry their inhibitory effect exerted on the self-aggregation of A β peptides was shown to be maximum, in previous studies [Ono et al., 2012]. The incubation was proceeded for 3 hours at 37 °C after which the resultant reaction mixtures were subjected to centrifugation at 21,380 g for 45 minutes to separate the supernatant and pellet. The supernatant and pellet fractions were analyzed separately as discussed below.

B.5.a. Analysis of insoluble pellet obtained after protein-ribosome co-aggregation in the presence of rosmarinic acid (RA) and myricetin (Myr) using agarose gel electrophoresis

The pellet fractions obtained after centrifugation were analyzed using 0.8% agarose gel electrophoresis to investigate the presence of rRNA in the large aggregates. Control experiments performed (**Figure 19A**) showed that the presence of rRNA in the pellets is insignificant when the 80S ribosome is incubated alone in the presence of different concentrations of the inhibitor molecules RA and Myr. This is also reflected in the bar graph

(Figure 19B) which represents the relative densities of the rRNA bands obtained in the agarose gel (as shown in Figure 19A). This implied that both RA and Myr themselves do not induce the aggregation of ribosomal components.

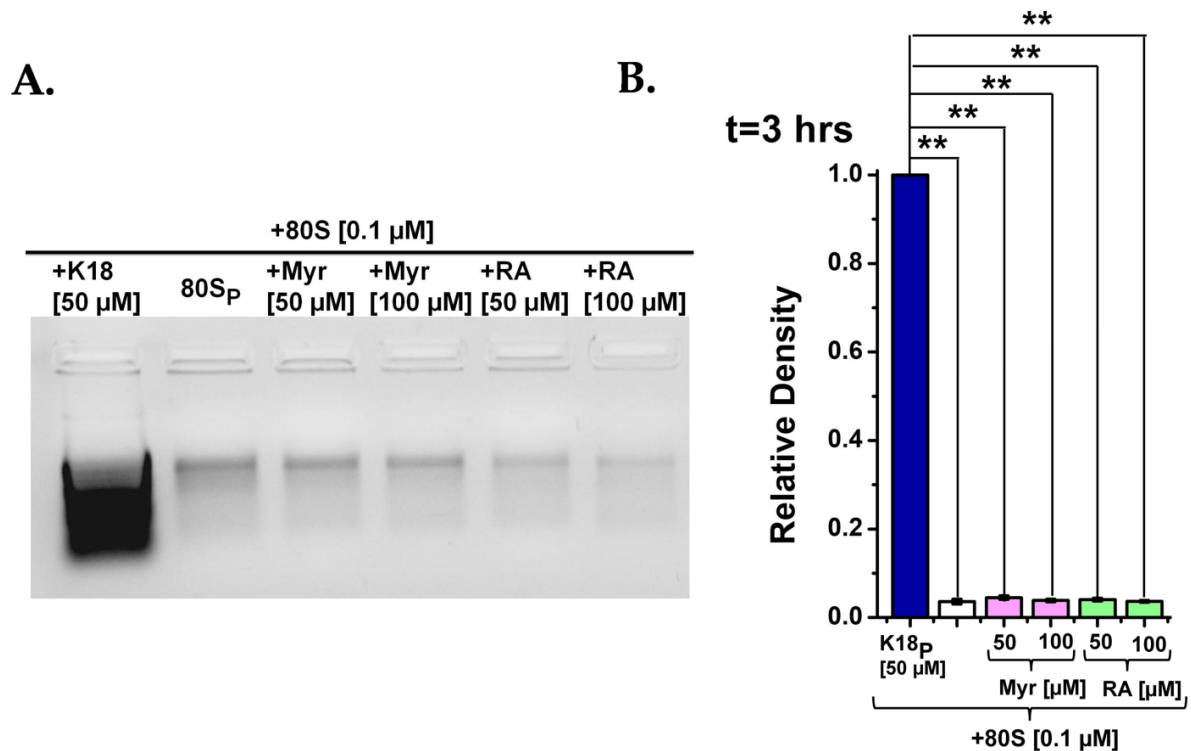
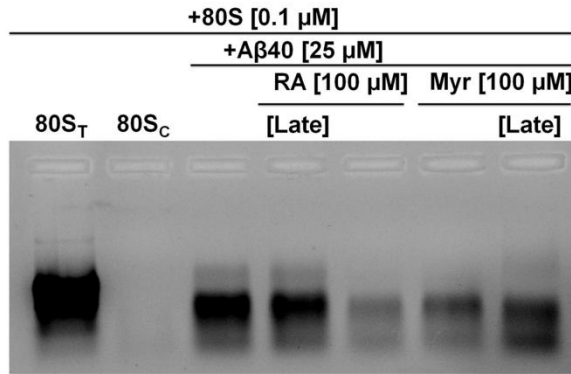


Figure 19: Effect of rosmarinic acid (RA) and myricetin (Myr) on the yeast 80S ribosome

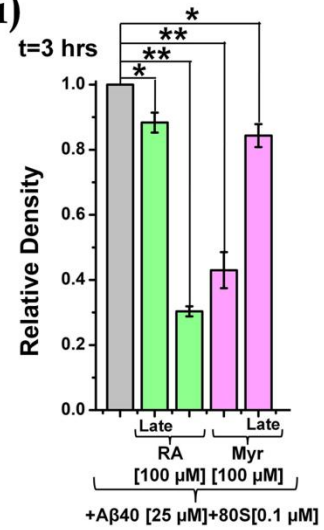
0.1 μM of yeast 80S ribosome was incubated with different concentrations of rosmarinic acid (RA) and myricetin (Myr) for 3 hours at 37 °C. As positive control, 50 μM of K18 was incubated with 0.1 μM of 80S and as negative control the 80S ribosome was incubated alone under similar conditions. The resultant reaction mixtures were centrifuged and the pellets were analyzed using 0.8% agarose gel electrophoresis for the presence of rRNA in the large insoluble aggregates. **A.** Agarose gel electrophoretic analysis of the pellets. Lanes from left to right contain: (1) (80S+50 μM K18)_{P_3h} (2) (80S)_{P_3h} (3) (80S+50 μM Myr)_{P_3h} (4) (80S+100 μM Myr)_{P_3h} (5) (80S+50 μM RA)_{P_3h} (6) (80S+100 μM RA)_{P_3h}. **B.** Bar graph depicting the densitometric analysis of rRNA band intensities present in the agarose gel for pellets formed with (1) (80S+50 μM K18)_{P_3h} (2) (80S)_{P_3h} (3) (80S+50 μM Myr)_{P_3h} (4) (80S+100 μM Myr)_{P_3h} (5) (80S+50 μM RA)_{P_3h} (6) (80S+100 μM RA)_{P_3h}. The rRNA band intensity obtained with (80S+50 μM K18)_{P_3h} has been assumed as 1 for calculations. The experiments were repeated thrice and the data are presented as means± SEM; *P< 0.05 or **P< 0.001 in one –way ANOVA (N= 3).

Agarose gel electrophoretic analysis of the pellets obtained after incubation of A β 40, A β 42 and K18 with 80S ribosome in the presence of RA and Myr revealed a significant reduction in the intensity of sequestered rRNA, when the inhibitor molecules are present from the initiation of reaction (**Figure 20Ai, Aii, Aiii**). Our next objective was to study whether the presence of the aggregation inhibitor was necessary from the initiation of the co-aggregation process. In this experiment (**Figure 20**), the analysis of the pellets obtained from the reaction sets, where RA and Myr were added to the reaction mixture 45 minutes after the initiation of aggregation reaction, showed that a delayed addition of the inhibitor molecules was incapable of suppressing the rRNA sequestration into the pellet fractions obtained with all three peptides, A β 40 (**Figure 20Ai**), A β 42 (**Figure 20Aii**) and K18 (**Figure 20Aiii**). This is also reflected in the bar graphs representing the relative densities of the rRNA bands for A β 40-80S pellet (**Figure 20Bi**), A β 42-80S pellet (**Figure 20Bii**) and the K18-80S pellet (**Figure 20Biii**), as shown in **Figure 20Ai, 20Aii and 20Aiii** respectively.

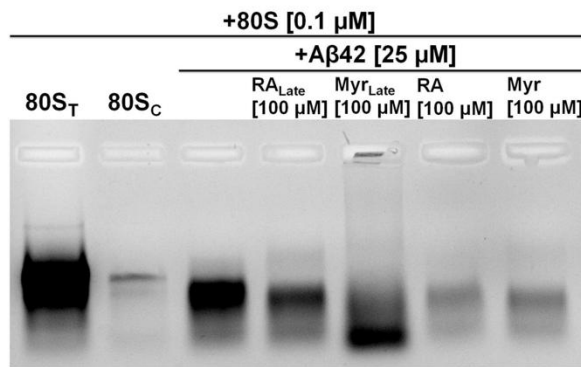
A.i)



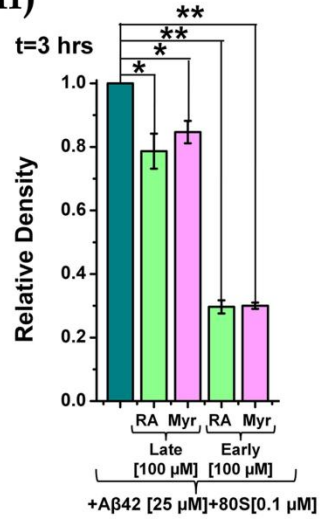
B.i)



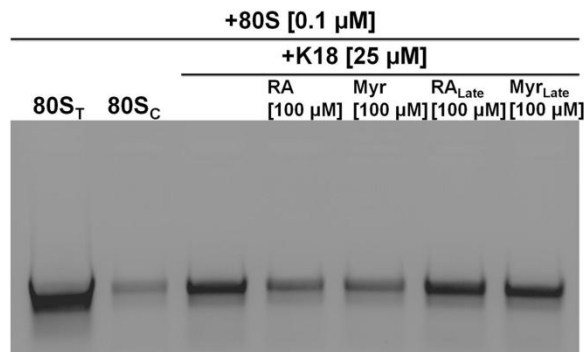
A.ii)



B.ii)



A.iii)



B.iii)

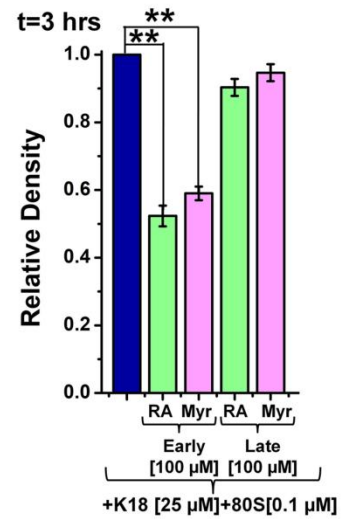


Figure 20: Effect of rosmarinic acid (RA) and myricetin (Myr) on Aβ-80S co-aggregation: Agarose gel electrophoretic analysis of the large insoluble aggregate containing pellets

A β 40, A β 42 and K18 (25 μ M each) were incubated with 80S ribosome (0.1 μ M) in the presence and absence of rosmarinic acid (RA) and myricetin (Myr) (100 μ M each) for 3 hours at 37 $^{\circ}$ C. In two experimental sets with RA and Myr, the polyphenols were added 45 minutes after the initiation of reaction. The resultant reaction mixtures were centrifuged to separate supernatant and pellet. The pellets were analyzed using agarose gel electrophoresis. **A.** Agarose gel electrophoretic analysis of (i) A β 40-80S aggregation pellets, in the presence and absence of RA and Myr, for presence of ribosomal RNA: lanes from left to right contain: (1) Total 80S (80S)_T (2) (80S)_{P_3h} (80S)_C (3) (A β 40+80S)_{P_3h} (4) (A β 40+80S+RA_{Late})_{P_3h} (5) (A β 40+80S+RA)_{P_3h} (6) (A β 40+80S+Myr)_{P_3h} (7) (A β 40+80S+Myr_{Late})_{P_3h} (ii) A β 42-80S aggregation pellets, in the presence and absence of RA and Myr, for presence of ribosomal RNA: lanes from left to right contain: (1) Total 80S (80S)_T (2) (80S)_{P_3h} (80S)_C (3) (A β 42+80S)_{P_3h} (4) (A β 42+80S+RA_{Late})_{P_3h} (5) (A β 42+80S+Myr_{Late})_{P_3h} (6) (A β 42+80S+RA)_{P_3h} (7) (A β 42+80S+Myr)_{P_3h}. (iii) K18-80S aggregation pellets, in the presence and absence of RA and Myr, for presence of ribosomal RNA: lanes from left to right contain: (1) Total 80S (80S)_T (2) (80S)_{P_3h} (80S)_C (3) (K18+80S)_{P_3h} (4) (K18+80S+RA)_{P_3h} (5) (K18+80S+Myr)_{P_3h} (6) (K18+80S+RA_{Late})_{P_3h} (7) (K18+80S+Myr_{Late})_{P_3h}. **B.** Bar graphs depicting the densitometric analysis of rRNA band intensities showing inhibition of co-aggregation in the presence of RA and Myr (for addition at the initiation of reaction) and no inhibition of co-aggregation upon delayed addition of RA and Myr for (i) A β 40-80S. (A β 40+80S)_{P_3h} is assumed as 1 for calculation. (ii) A β 42-80S. (A β 42+80S)_{P_3h} is assumed as 1 for calculation. (iii) K18-80S. (K18+80S)_{P_3h} is assumed as 1 for calculation. The experiments were repeated thrice and the data are presented as means \pm SEM; *P< 0.05 or **P< 0.001 in one –way ANOVA (N= 3).

These results implied that the presence of inhibitors of aggregation, rosmarinic acid (RA) and myricetin (Myr) could effectively inhibit the co-aggregation of 80S ribosomal components with A β 40, A β 42 and K18. This study supports our earlier conclusion that indeed protein aggregation in the vicinity of ribosome leads to the co-aggregation of ribosomal components. This study also suggests that presence of the aggregation inhibitors is necessary from the initiation of aggregation in order to exert their inhibitory activity towards the co-aggregation process.

B.5.b. Analysis of supernatant obtained after protein ribosome co-aggregation in the presence of rosmarinic acid (RA) and myricetin (Myr) using sucrose density gradient centrifugation (SDGC)

For further analysis, the supernatant fractions obtained after centrifugation of the reaction mixtures were subjected to sucrose density gradient centrifugation. The aim was to examine the 80S ribosomal profile after its incubation with A β 40, A β 42 and K18 (reduced with 1mM DTT) in the presence and absence of RA and Myr. The reduction in the 80S ribosomal peak when the 80S ribosome is incubated with A β 40, A β 42 and K18 alone indicates loss of ribosome integrity in the presence of the aggregating proteins (**Figures 21A, B and C** respectively). However, when the incubation of A β 40, A β 42 and K18 with the 80S ribosome is performed in the presence of RA and Myr, the ribosomal peak is significantly retained even in the presence of A β 40 (**Figure 21A**), A β 42 (**Figure 21B**) and K18 (**Figure 21C**).

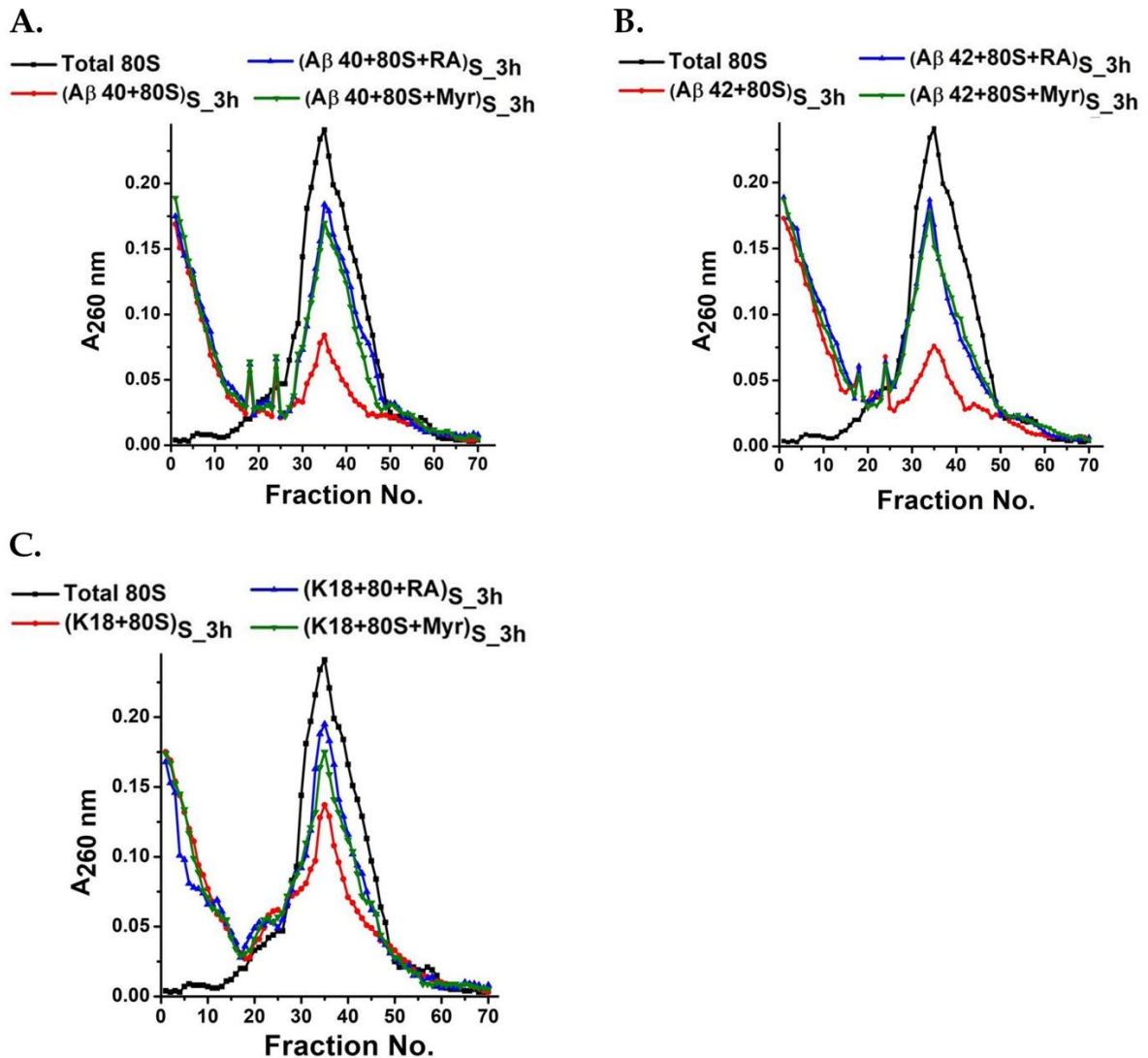


Figure 21: Effect of rosmarinic acid (RA) and myricetin (Myr) on $A\beta$ -80S co-aggregation: Sucrose density gradient centrifugation analysis of the supernatants

$A\beta$ 40, $A\beta$ 42 and K18 (25 μ M each) were incubated with 80S ribosome (0.1 μ M) in the presence and absence of rosmarinic acid (RA) and myricetin (Myr) (100 μ M each) for 3 hours at 37 $^{\circ}$ C and centrifuged to separate supernatant and pellet. The supernatants were analyzed using sucrose density gradient centrifugation. **A.** Sedimentation profile of the supernatant obtained after $A\beta$ 40-80S aggregation in the presence and absence of RA and Myr. (1) Total 80S (■) (2) ($A\beta$ 40+80S)_{S_3h} (●) (3) ($A\beta$ 40+80S+RA)_{S_3h} (▲) (4) ($A\beta$ 40+80S+Myr)_{S_3h} (▼) **B.** Sedimentation profile of the supernatant obtained after $A\beta$ 42-80S aggregation in the presence and absence of RA and Myr. (1) Total 80S (■) (2) ($A\beta$ 42+80S)_{S_3h} (●) (3) ($A\beta$ 42+80S+Myr)_{S_3h} (▼) (4) ($A\beta$ 42+80S+RA)_{S_3h} (▲) **C.** Sedimentation profile of the supernatant obtained after K18-80S aggregation in the presence and absence of RA and Myr. (1) Total 80S (■) (2) (K18+80S)_{S_3h} (●) (3) (K18+80S+Myr)_{S_3h} (▼) (4) (K18+80S+RA)_{S_3h} (▲)

Figure 22 includes a bar graph representing the area under the 80S ribosomal peaks, when the ribosome is subjected to the presence of A β 40, A β 42 and K18, with or without the additional presence of RA and Myr. This also reflects the retention of 80S ribosomal peak upon incubation of the ribosome with the peptides in the presence of RA and Myr.

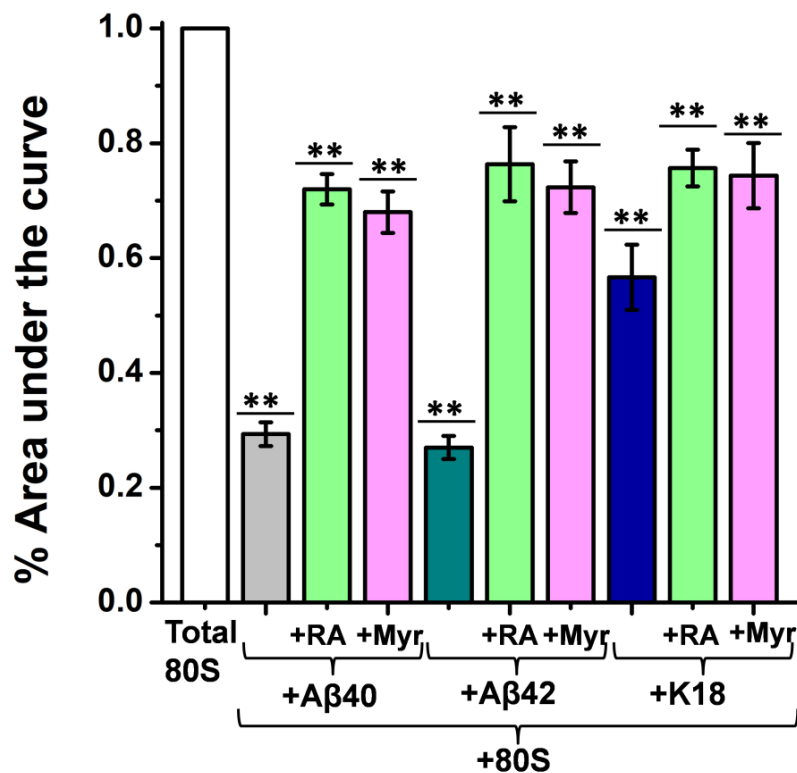


Figure 22: Retention of ribosomal peak upon incubation of 80S ribosome with A β 40, A β 42 and K18 in the presence of rosmarinic acid (RA) and myricetin (Myr)

Bar graph depicting the relative area under the peak of 80S ribosome present in the soluble fraction after 3 hours of incubation of A β 40, A β 42 and K18 with 80S ribosome, in the absence and presence of RA and Myr. Area under the total 80S peak at 0 hrs has been assumed as 1 for area under the 80S peak calculation. The experiments were repeated thrice and the data are presented as means \pm SEM; *P< 0.05 or **P< 0.001 in one –way ANOVA (N= 3).

These results collectively indicate that the aggregation of A β 40, A β 42 and K18 in the vicinity of the 80S ribosome can induce the loss of physical integrity of the ribosome and co-aggregation of the ribosomal components which can be mitigated in the presence of inhibitors of protein aggregation.

Conclusion:

As discussed in the “Introduction” section of this chapter, the onset of Alzheimer’s disease (AD) is marked by the appearance of extracellular senile plaques that are composed of A β fibrils and the accumulation of A β aggregates closely follows the progression of the disease [Cuello et al., 2017]. The disease progression is also accompanied by a progressive loss in the neuronal ribosomal population in AD afflicted individuals [Ding et al., 2006, Ding et al., 2007].

Despite being majorly implicated in constituting extracellular plaques, the intracellular localization of A β oligomers is widely reported [Lee et al., 2017, LaFerla et al., 2007, Stewart et al., 2017, Ginsberg et al., 1998]. This brings these toxic oligomeric peptides in the vicinity of several cellular organelles [Lee et al., 2017] including the ribosome. The presence of non-proteinaceous biological macromolecules like glycosaminoglycans, lipids and nucleic acids within the amyloid plaques along with the A β peptides, as well as their modulatory role towards amyloid aggregation is also extensively reported [Stewart et al., 2017, Calamai et al., 2006, Castillo et al., 1999, Ginsberg et al., 1998, Ginsberg et al., 1999, Jiang et al., 2007] and discussed in the “Introduction” section of this chapter. This therefore raises the possibility that cellular organelles constituting of these modulators might become engaged during the aggregation process which can lead to their sequestration within the aggregates that in turn might underlie their neurotoxicity.

Our *in vitro* experiments demonstrate that incubation of super-stoichiometric concentrations of A β peptides (both the abundant A β 40 variant and the aggregation-prone A β 42 variant) with intact purified non-translating yeast 80S ribosome (under conditions that favour A β aggregation) induces the loss of physical integrity of the ribosome and co-aggregation of the ribosomal components. The A β peptides could also lead to loss of function of human ribosomes present in the HeLa cell lysate. Further studies with purified human 80S ribosome

and *in vivo* experiments using neuronal cell lines and mouse-models of AD might provide further evidence in support of our *in vitro* observations.

A schematic outlining the observations made in our studies with the A β peptides (A β 40 and A β 42) is included as **Figure 23**. The A β peptides, when subjected to aggregating conditions, can engage with the eukaryotic 80S ribosome present in their vicinity and disrupt its physical integrity leading to co-aggregation of the ribosomal components with the peptides. The aggregation of A β peptides also occurs in a stimulated manner in the presence of ribosomal RNA and the aggregating peptides are capable of associating with the extracted ribosomal RNA component of the 80S ribosome leading to the formation of rRNA-A β co-aggregates. Similar stimulation of A β aggregation is also observed in the presence of small RNA molecules like the Poly(A) RNA and Poly(U) RNA molecules. Our observations also indicate that stoichiometry indeed has an effect on the RNA-mediated stimulation of A β aggregation as well as formation of A β -ribosome or A β -RNA co-aggregates. A low RNA or low ribosome stoichiometric concentration with respect to the peptides promotes stimulation of A β aggregation as well as formation of the co-aggregated structures. The increased aggregation observed in the presence of high protein: RNA ratio might imply that multiple molecules of the protein interacting with the same RNA molecule lead to the enhanced aggregation, as has been reported earlier [Kovachev et al., 2017] (as discussed below). The formation of ribosome-A β co-aggregates as well as the RNA-A β co-aggregates is effectively inhibited in the presence of polyphenolic inhibitors of amyloid aggregation, rosmarinic acid (RA) and myricetin (Myr).

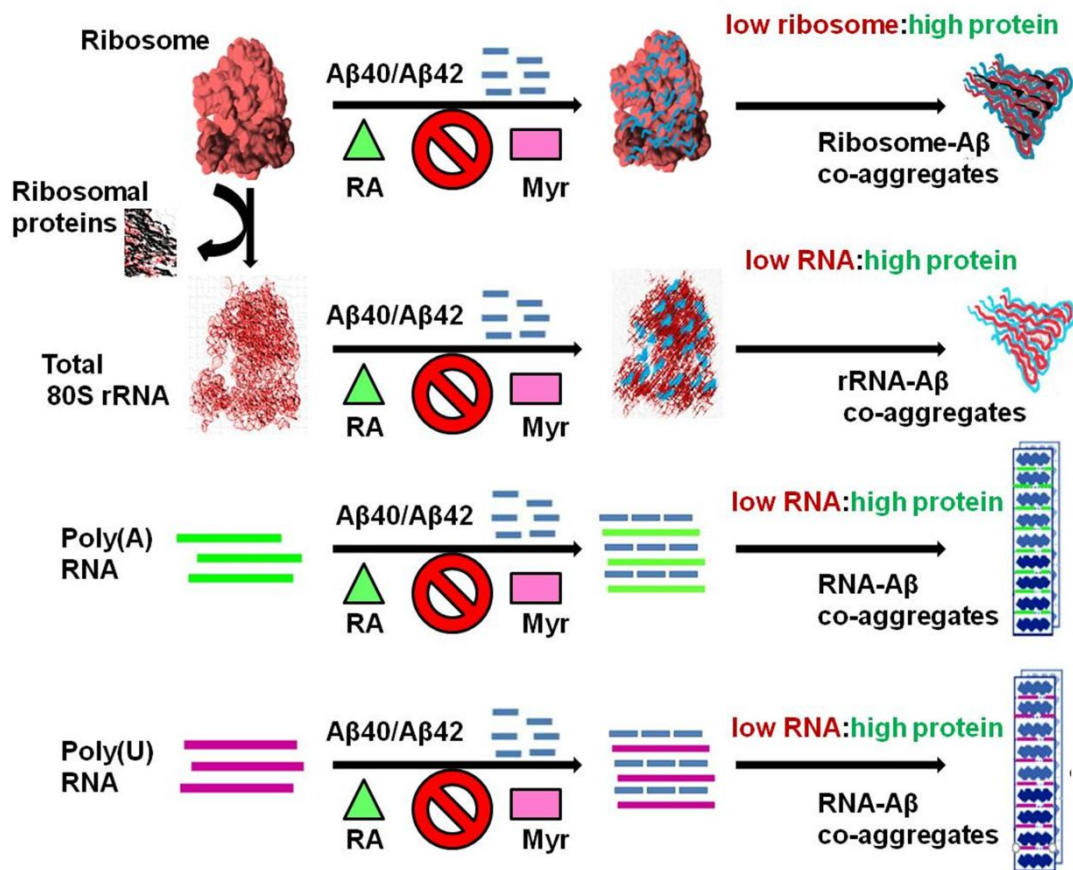


Figure 23: Schematic outlining the outcomes of Aβ peptides and eukaryotic ribosome and RNA interactions.

Aggregation of the Aβ peptides, Aβ40 and Aβ42 on the rRNA rich ribosomal surface can lead to co-aggregation of the ribosomal components. The aggregating Aβ peptides can also engage with RNA molecules like the extracted total rRNA from yeast 80S ribosome or the Poly(A) and Poly(U) RNA, resulting in stimulation of their aggregation and formation of RNA-protein co-aggregates. This RNA mediated stimulation of aggregation and formation of co-aggregates is essentially dependent on the stoichiometry of the protein with respect to the RNA or ribosome. A low RNA or low ribosome stoichiometry, with respect to the protein, favours the stimulation of aggregation and formation of co-aggregates. The presence of polyphenolic inhibitors of amyloid aggregation, rosmarinic acid (RA) and myricetin (Myr), mitigates RNA-mediated stimulation of aggregation as well as ribosome-protein co-aggregation.

Another interesting observation made in our studies is the seeding ability of A β -ribosome co-aggregates that can induce the aggregation of new ribosome without the addition of fresh peptides. Recent studies in the laboratory also demonstrated the seeding ability of Tau-ribosome co-aggregates in inducing the aggregation of untreated ribosome [Banerjee et al., 2020]. Further studies might help to delineate the intricacies of this phenomenon and its potential to influence the intraneuronal ribosomal population of AD-afflicted neurons.

In contrast to Tau, the A β peptides are capable of aggregating on their own in an inducer-independent manner [Chen et al., 2017, Stewart et al., 2017]. However, RNA-mediated stimulation of A β aggregation has been reported earlier [Ginsberg et al., 1998] and also is observed in our studies. This indicates that even though A β does not require RNA as a polyanionic inducer of aggregation, it can engage with RNA during the course of its aggregation.

Previous studies conducted by Kovachev et al.[2017 and 2019] and Cordeiro et al.[2019] have demonstrated the role of RNA as a scaffold for amyloid aggregation of proteins like p53 and PrP respectively, where the RNA provides the spatial and energetic requirements for increased intermolecular interactions of the proteins. They also emphasized the importance of RNA: protein stoichiometry in dictating the outcome of their interaction. A low RNA: high protein ratio was shown to favour aggregation and accumulation of aggregates.

This was reflected in our experimental observations while studying the effect of stoichiometry on RNA-mediated stimulation of A β aggregation, as well as on A β -ribosome co-aggregation. A high protein: RNA stoichiometry leads to stimulation of A β aggregation that is also reflected in the case of A β ribosome co-aggregation, where the extent of co-aggregation of ribosomal components increases with increasing concentrations of the peptides with respect to the ribosome. The probability of multiple protein molecules

interacting with a single RNA molecule is significantly higher at a high protein: RNA stoichiometric ratio. This would allow for a localized increase in protein concentration, which in turn would result in enhanced aggregation. Since rRNA is the major ribosomal component, super-stoichiometric concentrations of the A β peptides, when present in the vicinity of the ribosome, could allow multiple peptide molecules to engage with rRNA on the ribosomal surface, subsequently inducing co-aggregation of the ribosomal components.

Our studies with the polyphenolic inhibitor molecules, rosmarinic acid (RA) and myricetin (Myr), demonstrated that these molecules are able to mediate their aggregation inhibitory activity towards RNA-mediated stimulation of A β aggregation as well as co-aggregation of ribosomal components. The suppression of A β aggregation in the presence of the inhibitors was also shown to mitigate the effect of the peptides on the integrity of the translational machinery.

Previous studies conducted in the laboratory have demonstrated that the super-stoichiometric presence of aggregating Tau protein (both full length Ht40 and the 4 repeat microtubule binding subdomain K18) can sequester the eukaryotic ribosome present in its vicinity and hence can be a potential mediator of ribosome dysfunction observed in AD [Banerjee et al., 2020]. A recent study with the amyloid forming protein Huntingtin demonstrated that its interaction with the ribosome can lead to translational down-regulation [Eshraghi et al., 2021]. These studies imply that the potential to target the translational machinery could be universal to all amyloid forming proteins. The possibility of aberrant A β -ribosome interactions might be further increased by ageing associated reduction in activity of the cellular chaperones [Jinwal et al., 2010].

Our present studies indicate that A β -ribosome co-aggregation might be an underlying phenomenon contributing towards the disruption of ribosomal profile associated with AD.

The observed mitigation of A β -ribosome co-aggregation by polyphenolic inhibitors (rosmarinic acid and myricetin), indicate that their anti-amyloidogenic activity towards A β peptides [Ono et al., 2012] can in turn have a protective effect on the neuronal translational machinery. Although further *in vivo* studies are necessary to corroborate our results obtained *in vitro*, these observations indicate at the therapeutic potential possessed by the polyphenolic inhibitors, towards curbing the neurotoxicity associated with the loss of intraneuronal ribosomal population observed in Alzheimer's disease.

References:

1. **Antoun, A.**, Pavlov, M. Y., Tenson, T., & Ehrenberg, M. (2004). Ribosome formation from subunits studied by stopped-flow and Rayleigh light scattering. *Biological Procedures Online*, 6(1), 35-54.
2. **Arispe, N.**, Pollard, H. B., & Rojas, E. (1993). Giant multilevel cation channels formed by Alzheimer disease amyloid beta-protein [A beta P-(1-40)] in bilayer membranes. *Proceedings of the National Academy of Sciences*, 90(22), 10573-10577.
3. **Assarsson, A.**, Hellstrand, E., Cabaleiro-Lago, C., & Linse, S. (2014). Charge dependent retardation of amyloid β aggregation by hydrophilic proteins. *ACS chemical neuroscience*, 5(4), 266-274.
4. **Banerjee, S.**, Ferdosh, S., Ghosh, A. N., & Barat, C. (2020). Tau protein-induced sequestration of the eukaryotic ribosome: Implications in neurodegenerative disease. *Scientific reports*, 10(1), 1-15.
5. **Bourhim, M.**, Kruzel, M., Srikrishnan, T., & Nicotera, T. (2007). Linear quantitation of A β aggregation using Thioflavin T: Reduction in fibril formation by colostrinin. *Journal of neuroscience methods*, 160(2), 264-268.
6. **Braun, S.**, Humphreys, C., Fraser, E., Brancale, A., Bochtler, M., & Dale, T. C. (2011). Amyloid-associated nucleic acid hybridisation. *Plos one*, 6(5), e19125.
7. **Buell, A. K.**, Hung, P., Salvatella, X., Welland, M. E., Dobson, C. M., & Knowles, T. P. (2013). Electrostatic effects in filamentous protein aggregation. *Biophysical journal*, 104(5), 1116-1126.
8. **Butterfield, S. M.**, & Lashuel, H. A. (2010). Amyloidogenic protein–membrane interactions: mechanistic insight from model systems. *Angewandte Chemie International Edition*, 49(33), 5628-5654.
9. **Calamai, M.**, Kumita, J. R., Mifsud, J., Parrini, C., Ramazzotti, M., Ramponi, G., ... & Dobson, C. M. (2006). Nature and significance of the interactions between amyloid fibrils and biological polyelectrolytes. *Biochemistry*, 45(42), 12806-12815.

10. **Castillo, G. M.**, Lukito, W., Wight, T. N., & Snow, A. D. (1999). The sulfate moieties of glycosaminoglycans are critical for the enhancement of β - amyloid protein fibril formation. *Journal of neurochemistry*, 72(4), 1681-1687.
11. **Chakraborty, B.**, Bhakta, S., & Sengupta, J. (2016). Disassembly of yeast 80S ribosomes into subunits is a concerted action of ribosome-assisted folding of denatured protein. *Biochemical and biophysical research communications*, 469(4), 923-929.
12. **Chen, G. F.**, Xu, T. H., Yan, Y., Zhou, Y. R., Jiang, Y., Melcher, K., & Xu, H. E. (2017). Amyloid beta: structure, biology and structure-based therapeutic development. *Acta Pharmacologica Sinica*, 38(9), 1205-1235.
13. **Commenges, D.**, Scotet, V., Renaud, S., Jacqmin-Gadda, H., Barberger-Gateau, P., & Dartigues, J. F. (2000). Intake of flavonoids and risk of dementia. *European journal of epidemiology*, 16(4), 357-363.
14. **Cordeiro, Y.**, Vieira, T., Kovachev, P. S., Sanyal, S., & Silva, J. L. (2019). Modulation of p53 and prion protein aggregation by RNA. *Biochimica et Biophysica Acta (BBA)- Proteins and Proteomics*, 1867(10), 933-940.
15. **Coronel, R.**, Lachgar, M., Bernabeu-Zornoza, A., Palmer, C., Domínguez-Alvaro, M., Revilla, A., ... & Liste, I. (2019). Neuronal and glial differentiation of human neural stem cells is regulated by amyloid precursor protein (APP) levels. *Molecular neurobiology*, 56(2), 1248-1261.
16. **Cremers, C. M.**, Knoefler, D., Gates, S., Martin, N., Dahl, J. U., Lempart, J., ... & Jakob, U. (2016). Polyphosphate: a conserved modifier of amyloidogenic processes. *Molecular cell*, 63(5), 768-780.
17. **Cuello, A. C.** (2017). Early and late CNS inflammation in Alzheimer's disease: two extremes of a continuum?. *Trends in pharmacological sciences*, 38(11), 956-966.
18. **Ding, Q.**, Dimayuga, E., & Keller, J. N. (2007). Oxidative damage, protein synthesis, and protein degradation in Alzheimer's disease. *Current Alzheimer Research*, 4(1), 73-79.

19. **Ding, Q.**, Markesbery, W. R., Cecarini, V., & Keller, J. N. (2006). Decreased RNA, and increased RNA oxidation, in ribosomes from early Alzheimer's disease. *Neurochemical research*, *31*(5), 705-710.
20. **Dinkel, P. D.**, Holden, M. R., Matin, N., & Margittai, M. (2015). RNA binds to Tau fibrils and sustains template-assisted growth. *Biochemistry*, *54*(30), 4731-4740.
21. **Eichner, T.**, & Radford, S. E. (2011). A diversity of assembly mechanisms of a generic amyloid fold. *Molecular cell*, *43*(1), 8-18.
22. **Eshraghi, M.**, Karunadharma, P. P., Blin, J., Shahani, N., Ricci, E. P., Michel, A., ... & Subramaniam, S. (2021). Mutant Huntingtin stalls ribosomes and represses protein synthesis in a cellular model of Huntington disease. *Nature communications*, *12*(1), 1-20.
23. **Fichou, Y.**, Lin, Y., Rauch, J. N., Vigers, M., Zeng, Z., Srivastava, M., ... & Han, S. (2018). Cofactors are essential constituents of stable and seeding-active Tau fibrils. *Proceedings of the National Academy of Sciences*, *115*(52), 13234-13239.
24. **Fitzpatrick, A. W.**, Falcon, B., He, S., Murzin, A. G., Murshudov, G., Garringer, H. J., ... & Scheres, S. H. (2017). Cryo-EM structures of Tau filaments from Alzheimer's disease. *Nature*, *547*(7662), 185-190.
25. **Freyssin, A.**, Page, G., Fauconneau, B., & Bilan, A. R. (2018). Natural polyphenols effects on protein aggregates in Alzheimer's and Parkinson's prion-like diseases. *Neural regeneration research*, *13*(6), 955.
26. **Ge, J. F.**, Qiao, J. P., Qi, C. C., Wang, C. W., & Zhou, J. N. (2012). The binding of resveratrol to monomer and fibril amyloid beta. *Neurochemistry international*, *61*(7), 1192-1201.
27. **Ginsberg, S. D.**, Crino, P. B., Hemby, S. E., Weingarten, J. A., Lee, V. M. Y., Eberwine, J. H., & Trojanowski, J. Q. (1999). Predominance of neuronal mRNAs in individual Alzheimer's disease senile plaques. *Annals of Neurology: Official Journal of the American Neurological Association and the Child Neurology Society*, *45*(2), 174-181.

28. **Ginsberg, S. D.**, Crino, P. B., Lee, V. M. Y., Eberwine, J. H., & Trojanowski, J. Q. (1997). Sequestration of RNA in Alzheimer's disease neurofibrillary tangles and senile plaques. *Annals of Neurology: Official Journal of the American Neurological Association and the Child Neurology Society*, 41(2), 200-209.
29. **Ginsberg, S. D.**, Galvin, J. E., Chiu, T. S., Lee, V. M. Y., Masliah, E., & Trojanowski, J. Q. (1998). RNA sequestration to pathological lesions of neurodegenerative diseases. *Acta neuropathologica*, 96(5), 487-494.
30. **Hare, D. J.**, Faux, N. G., Roberts, B. R., Volitakis, I., Martins, R. N., & Bush, A. I. (2016). Lead and manganese levels in serum and erythrocytes in Alzheimer's disease and mild cognitive impairment: results from the Australian Imaging, Biomarkers and Lifestyle Flagship Study of Ageing. *Metallomics*, 8(6), 628-632.
31. **Holehouse, A. S.**, Das, R. K., Ahad, J. N., Richardson, M. O., & Pappu, R. V. (2017). CIDER: resources to analyze sequence-ensemble relationships of intrinsically disordered proteins. *Biophysical journal*, 112(1), 16-21.
32. **Hu, X.**, Crick, S. L., Bu, G., Frieden, C., Pappu, R. V., & Lee, J. M. (2009). Amyloid seeds formed by cellular uptake, concentration, and aggregation of the amyloid-beta peptide. *Proceedings of the National Academy of Sciences*, 106(48), 20324-20329.
33. **Inoue, S.** (2008). In situ A beta pores in AD brain are cylindrical assembly of A beta protofilaments. *Amyloid*, 15(4), 223-233.
34. **Jiang, W.**, Han, Y., Zhou, R., Zhang, L., & Liu, C. (2007). DNA is a template for accelerating the aggregation of copper, zinc superoxide dismutase. *Biochemistry*, 46(20), 5911-5923.
35. **Jinwal, U. K.**, O'Leary, J. C., Borysov, S. I., Jones, J. R., Li, Q., Koren, J., ... & Dickey, C. A. (2010). Hsc70 rapidly engages Tau after microtubule destabilization. *Journal of biological chemistry*, 285(22), 16798-16805.
36. **Kampers, T.**, Friedhoff, P., Biernat, J., Mandelkow, E. M., & Mandelkow, E. (1996). RNA stimulates aggregation of microtubule-associated protein Tau into Alzheimer-like paired helical filaments. *FEBS letters*, 399(3), 344-349.

37. **Kim, S. I.**, Yi, J. S., & Ko, Y. G. (2006). Amyloid β oligomerization is induced by brain lipid rafts. *Journal of cellular biochemistry*, 99(3), 878-889.
38. **Kim, W.**, & Hecht, M. H. (2006). Generic hydrophobic residues are sufficient to promote aggregation of the Alzheimer's A β 42 peptide. *Proceedings of the National Academy of Sciences*, 103(43), 15824-15829.
39. **Kiskis, J.**, Fink, H., Nyberg, L., Thyr, J., Li, J. Y., & Enejder, A. (2015). Plaque-associated lipids in Alzheimer's diseased brain tissue visualized by nonlinear microscopy. *Scientific reports*, 5(1), 1-9.
40. **Kovachev, P. S.**, Banerjee, D., Rangel, L. P., Eriksson, J., Pedrote, M. M., Martins-Dinis, M. M. D., ... & Sanyal, S. (2017). Distinct modulatory role of RNA in the aggregation of the tumor suppressor protein p53 core domain. *Journal of Biological Chemistry*, 292(22), 9345-9357.
41. **Kovachev, P. S.**, Gomes, M. P., Cordeiro, Y., Ferreira, N. C., Valadão, L. P. F., Ascari, L. M., ... & Sanyal, S. (2019). RNA modulates aggregation of the recombinant mammalian prion protein by direct interaction. *Scientific reports*, 9(1), 1-12.
42. **LaFerla, F. M.**, Green, K. N., & Oddo, S. (2007). Intracellular amyloid- β in Alzheimer's disease. *Nature Reviews Neuroscience*, 8(7), 499-509.
43. **Lee, S. J. C.**, Nam, E., Lee, H. J., Savelieff, M. G., & Lim, M. H. (2017). Towards an understanding of amyloid- β oligomers: characterization, toxicity mechanisms, and inhibitors. *Chemical Society Reviews*, 46(2), 310-323.
44. **Li, H.**, Rahimi, F., Sinha, S., Maiti, P., Bitan, G., & Murakami, K. (2009). Amyloids and protein aggregation—analytical methods. *Encyclopedia of analytical chemistry*, 1-32.
45. **Li, W.**, Yu, J., Liu, Y., Huang, X., Abumaria, N., Zhu, Y., ... & Liu, G. (2013). Elevation of brain magnesium prevents and reverses cognitive deficits and synaptic loss in Alzheimer's disease mouse model.
46. **Louka, A.**, Zacco, E., Temussi, P. A., Tartaglia, G. G., & Pastore, A. (2020). RNA as the stone guest of protein aggregation. *Nucleic Acids Research*, 48(21), 11880-11889.

47. **Meli, M.**, Gasset, M., & Colombo, G. (2018). Are amyloid fibrils RNA-traps? a Molecular Dynamics perspective. *Frontiers in molecular biosciences*, 5, 53.
48. **Mylonas, E.**, Hascher, A., Bernado, P., Blackledge, M., Mandelkow, E., & Svergun, D. I. (2008). Domain conformation of Tau protein studied by solution small-angle X-ray scattering. *Biochemistry*, 47(39), 10345-10353.
49. **Navarro, M. G. J.**, Kashida, S., Chouaib, R., Souquere, S., Pierron, G., Weil, D., & Gueroui, Z. (2019). RNA is a critical element for the sizing and the composition of phase-separated RNA–protein condensates. *Nature communications*, 10(1), 1-13.
50. **Novo, M.**, Freire, S., & Al-Soufi, W. (2018). Critical aggregation concentration for the formation of early Amyloid- β (1–42) oligomers. *Scientific reports*, 8(1), 1-8.
51. **Ono, K.**, Li, L., Takamura, Y., Yoshiike, Y., Zhu, L., Han, F., ... & Yamada, M. (2012). Phenolic compounds prevent amyloid β -protein oligomerization and synaptic dysfunction by site-specific binding. *Journal of Biological Chemistry*, 287(18), 14631-14643.
52. **Pathak, B. K.**, Banerjee, S., Mondal, S., Chakraborty, B., Sengupta, J., & Barat, C. (2017). Unfolded protein exhibits antiassociation activity toward the 50S subunit facilitating 70S ribosome dissociation. *The FEBS journal*, 284(22), 3915-3930.
53. **Pathak, B. K.**, Mondal, S., Banerjee, S., Ghosh, A. N., & Barat, C. (2017). Sequestration of ribosome during protein aggregate formation: contribution of ribosomal RNA. *Scientific reports*, 7(1), 1-14.
54. **Pathak, B. K.**, Mondal, S., Ghosh, A. N., & Barat, C. (2014). The ribosome can prevent aggregation of partially folded protein intermediates: studies using the Escherichia coli ribosome. *PloS one*, 9(5), e96425.
55. **Piir, K.**, Tamm, T., Kisly, I., Tammsalu, T., & Remme, J. (2014). Stepwise splitting of ribosomal proteins from yeast ribosomes by LiCl. *PLoS One*, 9(7), e101561.
56. **Preston, G. W.**, Radford, S. E., Ashcroft, A. E., & Wilson, A. J. (2012). Covalent cross-linking within supramolecular peptide structures. *Analytical chemistry*, 84(15), 6790-6797.

57. **Ramachandran, G.**, & Udgaonkar, J. B. (2011). Understanding the kinetic roles of the inducer heparin and of rod-like protofibrils during amyloid fibril formation by Tau protein. *Journal of biological chemistry*, 286(45), 38948-38959.
58. **Rha, A. K.**, Das, D., Taran, O., Ke, Y., Mehta, A. K., & Lynn, D. G. (2020). Electrostatic Complementarity Drives Amyloid/Nucleic Acid Co- Assembly. *Angewandte Chemie International Edition*, 59(1), 358-363.
59. **Roy, A.**, Kucukural, A., & Zhang, Y. (2010). I-TASSER: a unified platform for automated protein structure and function prediction. *Nature protocols*, 5(4), 725-738.
60. **Safar, J. G.**, Kellings, K., Serban, A., Groth, D., Cleaver, J. E., Prusiner, S. B., & Riesner, D. (2005). Search for a prion-specific nucleic acid. *Journal of virology*, 79(16), 10796-10806.
61. **Schavemaker, P. E.**, Śmigiel, W. M., & Poolman, B. (2017). Ribosome surface properties may impose limits on the nature of the cytoplasmic proteome. *Elife*, 6, e30084.
62. **Stewart, K. L.**, & Radford, S. E. (2017). Amyloid plaques beyond A β : a survey of the diverse modulators of amyloid aggregation. *Biophysical reviews*, 9(4), 405-419.
63. **Sung, J. J.**, Pardeshi, N. N., Mulder, A. M., Mulligan, S. K., Quispe, J., On, K., ... & Schneemann, A. (2015). Transmission electron microscopy as an orthogonal method to characterize protein aggregates. *Journal of pharmaceutical sciences*, 104(2), 750-759.
64. **Taguchi, R.**, Hatayama, K., Takahashi, T., Hayashi, T., Sato, Y., Sato, D., ... & Uwai, K. (2017). Structure–activity relations of rosmarinic acid derivatives for the amyloid β aggregation inhibition and antioxidant properties. *European journal of medicinal chemistry*, 138, 1066-1075.
65. **Tenreiro, S.**, & Outeiro, T. F. (2010). Simple is good: yeast models of neurodegeneration. *FEMS yeast research*, 10(8), 970-979.
66. **Tenreiro, S.**, Munder, M. C., Alberti, S., & Outeiro, T. F. (2013). Harnessing the power of yeast to unravel the molecular basis of neurodegeneration. *Journal of neurochemistry*, 127(4), 438-452.

67. **Trazzi, S.**, Fuchs, C., Valli, E., Perini, G., Bartesaghi, R., & Ciani, E. (2013). The amyloid precursor protein (APP) triplicated gene impairs neuronal precursor differentiation and neurite development through two different domains in the Ts65Dn mouse model for Down syndrome. *Journal of Biological Chemistry*, 288(29), 20817-20829.
68. **Vandersteen, A.**, Masman, M. F., De Baets, G., Jonckheere, W., Van Der Werf, K., Marrink, S. J., ... & Broersen, K. (2012). Molecular plasticity regulates oligomerization and cytotoxicity of the multi-peptide-length amyloid- β peptide pool. *Journal of biological chemistry*, 287(44), 36732-36743.
69. **Walsh, D. M.**, Thulin, E., Minogue, A. M., Gustavsson, N., Pang, E., Teplow, D. B., & Linse, S. (2009). A facile method for expression and purification of the Alzheimer's disease-associated amyloid β - peptide. *The FEBS journal*, 276(5), 1266-1281.
70. **Wang, M.**, Law, M., Duhamel, J., & Chen, P. (2007). Interaction of a self-assembling peptide with oligonucleotides: complexation and aggregation. *Biophysical journal*, 93(7), 2477-2490.
71. **Wang, X. S.**, Wang, D. L., Zhao, J., Qu, M. H., Zhou, X. H., He, H. J., & He, R. Q. (2006). The proline-rich domain and the microtubule binding domain of protein Tau acting as RNA binding domains. *Protein and peptide letters*, 13(7), 679-685.
72. **Wiltfang, J.**, Esselmann, H., Bibl, M., Hüll, M., Hampel, H., Kessler, H., ... & Lewczuk, P. (2007). Amyloid β peptide ratio 42/40 but not A β 42 correlates with phospho-Tau in patients with low- and high- CSF A β 40 load. *Journal of neurochemistry*, 101(4), 1053-1059.
73. **Yang, J.**, Yan, R., Roy, A., Xu, D., Poisson, J., & Zhang, Y. (2015). The I-TASSER Suite: protein structure and function prediction. *Nature methods*, 12(1), 7-8.
74. **Yang, X.**, Meisl, G., Frohm, B., Thulin, E., Knowles, T. P., & Linse, S. (2018). On the role of sidechain size and charge in the aggregation of A β 42 with familial mutations. *Proceedings of the National Academy of Sciences*, 115(26), E5849-E5858.
75. **Zhang, X.**, Lin, Y., Eschmann, N. A., Zhou, H., Rauch, J. N., Hernandez, I., ... & Han, S. (2017). RNA stores Tau reversibly in complex coacervates. *PLoS biology*, 15(7), e2002183.

76. **Zhang, Y.** (2008). I-TASSER server for protein 3D structure prediction. *BMC bioinformatics*, 9(1), 1-8.
77. **Zheng, H., & Koo, E. H.** (2006). The amyloid precursor protein: beyond amyloid. *Molecular neurodegeneration*, 1(1), 1-12.
78. **Zhigalova, E. A.,** Izosimova, A. I., Yuzhakova, D. V., Volchkova, L. N., Shagina, I. A., Turchaninova, M. A., ... & Sharonov, G. V. (2020). RNA-Seq-based TCR profiling reveals persistently increased intratumoral clonality in responders to anti-PD-1 therapy. *Frontiers in oncology*, 10, 385.

Chapter 4

General Materials and Methods

Materials

Bacterial strains and plasmid

For transformation of cloned plasmids, XL1-Blue strain of *Escherichia coli* (*E.coli*) cells was used. BL21 (DE3) strain of *E.coli* cells, obtained from Dr. Jayant Udgaonkar's laboratory (formerly in NCBS, Bangalore, currently in IISER, Pune), was used as host for protein expression. MRE600 (RNaseI-) strain of *E.coli* cells was used for isolation of 70S ribosome. In order to isolate 70S ribosome as well as 100S ribosome from *Staphylococcus aureus*, the MTCC 3160 strain was used (obtained from Microbial Type Culture Collection and Genebank, MTCC, CSIR Institute of Microbial Technology, Chandigarh, India). The 100S ribosome from *E.coli* cells was isolated from the *E.coli* BW25113 Δ *yfiA* [Beckert et al., 2018] (purchased from Keio Knockout Collection of the Coli Genetic Stock Centre (CGSC), Yale University, USA [Baba et al., 2006]). The *E.coli hpf* gene was cloned into the pET28a (+) plasmid vector.

Yeast strain

The MAT a/ α strain of *Saccharomyces cerevisiae*, obtained from Dr. Jayati Sengupta's laboratory (IICB, Kolkata) was used for isolation of 80S ribosome.

Chemicals

Acrylamide, bis-acrylamide, ammonium persulphate, Ethidium bromide, Diethyl pyrocarbonate (DEPC), IPTG, DTT, DEAE-cellulose, guanidine hydrochloride, Ethylene diamine tetra-acetic acid (EDTA), Sodium chloride (NaCl) and antibiotics (Blasticidine S, Ampicillin, Kanamycin), 6-Aminophenanthridine (6AP), magnesium chloride (MgCl₂) were purchased from Sigma Aldrich. Agarose was purchase from Loba Chemie Pvt. Ltd. Ribonucleoside triphosphates (ATP, CTP, GTP and UTP) and deoxyribonucleoside

triphosphates (dATP, dCTP, dGTP and dTTP) were purchased from Fermentas ThermoScientific. cOmplete™ Mini, EDTA-free Protease Inhibitor Cocktail was purchased from Roche. All other chemicals used for experiments were local products of analytical grade or equivalent.

Enzymes

Restriction enzymes BamHI, HindIII and EcoRI and DreamTaq DNA polymerase were purchased from Fermentas, ThermoScientific. Bovine carbonic anhydrase II (BCAII), chicken egg white lysozyme, RNase A and DNase I were purchased from Sigma Aldrich. T4 DNA ligase was obtained from Genei, Bangalore.

Markers

DNA ladders (1Kbp) and PageRuler™ unstained protein ladder were purchased from ThermoFisher Scientific.

Media compositions

The media for bacterial and yeast cell culture were prepared by dissolving the components in distilled water followed by sterilization through autoclaving or filtration through 0.22 micron filter (Whatman).

Culture media used in experiments and their composition

Media	Composition
Luria-Bertani broth (LB) (For purification of HPF and 70S ribosome from <i>E.coli</i>)	1% NaCl, 1% bacto-tryptone, 0.5% yeast extract. pH adjusted to 7.5 with 1N NaOH
Luria-Bertani Agar (LA)	1.5% agar in Luria broth (LB)
Yeast extract-Peptone-Dextrose (YPD) (For purification of 80S ribosome from <i>S.cerevisiae</i>)	Bacto-peptone (1%), yeast extract (0.5%), dextrose (2%). pH adjusted to 7 using 1 N NaOH
Terrific Broth (TB) (for purification of A β peptides)	2.4% yeast extract, 1.2% tryptone, 0.231% KH ₂ PO ₄ , 1.254% K ₂ HPO ₄ , 0.4% glycerol. The final pH comes to 7.2+/-0.2
Tryptic Soy Broth (TSB) (For purification of 70S and 100S ribosomes from <i>S.aureus</i>) [Ueta et al., 2010]	1.7% pancreatic digest casein, 0.3% papaic digest soyabean meal, 0.5% NaCl, 0.25% Dextrose, 0.25% K ₂ HPO ₄ . pH adjusted to 7.5+/- 0.2 with 1N NaOH

Buffer compositions

The buffers and solutions used in the experiments were prepared by dissolving the components in distilled water and were sterilized by autoclaving or through filtration using 0.22 micron filters (Whatman).

Buffers used in experiments and their composition

Buffer	Composition
Refolding buffer (for 70S dissociation studies)	50 mM Tris-HCl pH 7.5, 100 mM NaCl, 1 or 7.5 mM MgCl ₂
HPF binding buffer	5 mM Tris-HCl pH 7.5, 50 mM KCl, 100 mM NH ₄ Cl, 7.5 mM MgCl ₂
Refolding buffer (for refolding and aggregation studies)	50 mM Tris-HCl pH 7.5, 100 mM NaCl, 7.5 or 10 mM MgCl ₂
Blasticidine S binding buffer (for 70S)	100 mM Tris-HCl pH 7.2, 10 mM MgCl ₂ , 100 mM NH ₄ Cl pH 7.2, 6mM β-Mercaptoethanol
Buffer A for Aβ purification [Walsh et al., 2009]	10 mM Tris-HCl pH 8, 1 mM EDTA pH 8 (with added 5 mM DTT and 1 mM PMSF during cell lysis)
Buffer B for final buffer exchange and storage of Aβ	25 mM Tris-HCl pH 8
Buffer C for aggregation reactions with Aβ peptides [Banerjee et al., 2020]	25 mM Tris-HCl pH 7.5, 50 mM NaCl, 5 mM MgCl ₂
Buffer for harvesting bacterial cells	20 mM Tris-HCl pH 7.5, 10 mM MgCl ₂ , 100 mM NH ₄ Cl, 5mM β-Mercaptoethanol
TMA 10 for 70S purification	20 mM Tris-HCl pH 7.5, 10 mM MgCl ₂ , 30 mM NH ₄ Cl, 5mM β-Mercaptoethanol
Ribosome Buffer for yeast 80S purification	100 mM KOAc, 20 mM HEPES-KOH pH 7.6, 10 mM Mg(OAc) ₂ , 1 mg/ml heparin, 2 mM DTT, 0.5 mM PMSF
High salt Buffer for yeast 80S purification	100 mM KOAc, 20 mM HEPES-KOH pH 7.6, 10 mM Mg(OAc) ₂ , 1 mg/ml heparin, 2 mM DTT, 0.5 mM PMSF, 1 M KCl
Storage buffer for 80S	10 mM Tris-HCl pH 7.5, 12.5 mM Mg(OAc) ₂ , 80 mM KCl, 5mM β-Mercaptoethanol, 0.5 mM PMSF
B100S buffer for 100S purification [Beckert et al., 2018]	25 mM HEPES-KOH pH 7.5, 100 mM KOAc, 15 mM Mg(OAc) ₂ , 1 mM DTT
Buffer G for 100S dissociation and refolding studies [Beckert et al., 2017, Khusainov et al., 2017]	10 mM Tris-HCl pH 7.5, 50 mM KCl, 10 mM NH ₄ Cl, 7.5 mM MgCl ₂
Buffer G for 100S enrichment and storage [Beckert et al., 2017, Khusainov et al., 2017]	10 mM Tris-HCl pH 7.5, 50 mM KCl, 10 mM NH ₄ Cl, 25 mM MgCl ₂
TAE buffer (1X) (for agarose gel)	40 mM Tris-HCl pH 7.5, 40 mM Acetic acid, 2 mM EDTA pH 8.
Tris-Glycine buffer (Running buffer for SDS-PAGE)	Tris base 1.5 gm, Glycine 7 gm , SDS 500 mg in 500 ml distilled water
Gel loading dye (6X)	0.25% Bromophenol blue , 30% w/v glycerol
Phosphate Buffered Saline with Tween 20 (1X)	137 mM NaCl, 2.7 mM KCl, 10 mM Na ₂ HPO ₄ , 1.8 mM KH ₂ PO ₄ + 0.1% Tween 20
SDS-gel loading dye (1x) (Laemmli buffer)	50 mM Tris HCl pH 6.8, 10 mM DTT , 2% SDS, 0.1% bromophenol blue, 10% glycerol

Methods

Purification of E.coli 70S ribosome

The *E. coli* 70S ribosome (70S_{Ec}) was purified from MRE600 cells [Das et al., 1996] and the purification was performed as reported earlier. *E. coli* MRE600 cells were grown in Luria Bertani medium supplemented with 0.1% glucose until the A_{600 nm} was approximately 0.8. Cells were then slowly cooled to 4 °C to produce run-off ribosome particles [Chattopadhyay et al., 1996, Mondal et al., 2014] and harvested in 20 mM Tris-HCl pH 7.5, 10 mM MgCl₂, 100 mM NH₄Cl and 5 mM β-mercaptoethanol. Frozen cells were lysed in the same buffer containing 2 µg/ml DNase I, using French Pressure lysis cell. Cell debris was removed by centrifuging the suspension twice at 12,000 g for 30 mins in a Sigma 12158-H rotor. The supernatant was centrifuged at 1,54,000 g for 2 hours in a Beckman Ti50 rotor and the pellet containing ribosome was resuspended in TMA-10 buffer (20 mM Tris-HCl pH 7.5, 10 mM MgCl₂, 30 mM NH₄Cl, 5mM β-mercaptoethanol) [Chattopadhyay et al., 1996, Mondal et al., 2014]. 1 M NH₄Cl was added and the suspension was kept at 0 °C for 1 hour. The ribosomal preparation was clarified by centrifugation at 12,000 g for 20 minutes in a Sigma 12158-H rotor. The supernatant was centrifuged at 1,54,000 g for 2 hours in a Beckman Ti50 rotor and the pellet was resuspended in TMA-10. About 7.5 A_{260 nm} units (one A_{260 nm} unit is the amount of material that, when contained in 1 ml of solution, gives an absorbance value of 1 at 260 nm, in a 1 cm path-length cell) of this ribosomal preparation was loaded on top of a 5% to 30% linear sucrose (RNase-free) gradient in the same buffer and centrifuged at 1,54,000 g for 90 minutes in a Beckman SW40.1 rotor at 4 °C. The gradient was monitored at 260 nm and appropriate fractions containing 70S_{Ec} particles were pooled. The pooled fractions containing the purified 70S_{Ec} ribosome particles were concentrated using Amicon Ultra 10 KDa molecular weight cut-off filters and the sucrose from the fractions was removed by centrifugation filtration using the same filters and TMA-10 buffer at 4 °C. The concentrated

70S_{Ec} ribosome was stored at -80 °C until further use [Chattopadhyay et al., 1996, Mondal et al., 2014].

Purification of 80S ribosome from *Saccharomyces cerevisiae*

80S ribosome from *Saccharomyces cerevisiae* was purified following the protocol outlined by Chakraborty et al. [2016]. *S. cerevisiae* (MAT a/a strain, a kind gift from Dr. Jayati Sengupta's laboratory, IICB, Kolkata) was cultured overnight in Yeast extract-Peptide-Dextrose (YPD) complete media. The temperature for incubation was maintained at 25 °C. The cells were cooled for about 1 hour at 4 °C, after they reached log phase (OD_{600 nm} ~ 2.5) after approximately 18 hours of incubation. After cooling, the cells were harvested by centrifugation at 6,100 g for 10 minutes at 4 °C. Yeast cell pellets were stored at -80 °C until further use. Isolation of ribosome from these yeast cell pellets was conducted according to the protocol of purification of salt washed yeast 80S ribosome as described previously [Algire et al., 2002] with minor modifications. Briefly, the pellets were resuspended in ribosome buffer (composition enlisted in the table given earlier) and lysed by passage through a French Pressure cell twice. The resulting lysate was centrifuged at 17,000 g for 30 minutes at 4 °C. The cleared supernatant was subjected to ultracentrifugation at 3, 50, 000 g for 1 hour at 4 °C. The supernatant was removed and the pellet was dissolved in minimal volume of ribosome buffer (~ 1 ml). High salt buffer (composition enlisted in the table given earlier) was added to the dissolved pellet and volume was made up to 18 ml. This was kept on ice for about 1 hour with gentle stirring. The salt washed solution was centrifuged at 17,000 g for 10 minutes at 4 °C. This centrifugation was performed 3-4 times until the size of the pellet became indistinguishable. The resulting supernatant was then layered over a 34% sucrose cushion and centrifuged at 3, 50, 000 g for 1 hour at 4 °C. The supernatant was discarded and the clear ribosome pellet was dissolved in storage buffer for 80S ribosome (composition enlisted in the table given earlier). The ribosome was stored at -80 °C.

Transformation of bacterial cells

Transformation of plasmid DNA into *E. coli* XL1-Blue or BL21(DE3) cells was performed following the procedure described in “Molecular cloning-A Laboratory Manual” by Sambrook, Fritsch and Maniatis (2nd edition), with minor modifications. 5 ml LB was inoculated with bacterial cells and these cells were grown to 0.4-0.6 O.D_{600 nm}, followed by chilling on ice for 30 minutes. The cells were then harvested by centrifugation at 6,100 g for 6 minutes at 4°C. The supernatant was discarded and pellets containing the cells were resuspended in 100 µl of chilled CaCl₂ (100 mM) and kept on ice for 2.5 hours in order for them to become sufficiently competent. 100-200 ng of plasmid DNA or 7 µl of ligation mixture was gently added to the competent cells (100 µl) and incubated on ice for 30 minutes. This was followed by heat shock at 37 °C for 5 minutes. After heat shock, the cells were immediately cooled on ice for 30 minutes and then diluted in 1 ml of LB. The cells were then recovered for 1.5 hours at 37°C and added in appropriate quantity on LA plates containing selective antibiotic and spread. The plates were incubated at 37 °C overnight.

Plasmid and genomic DNA isolation

Bacterial cells with the desired plasmid were grown in 5 ml LB at 37 °C overnight and harvested using centrifugation at 6,100 g for 6 minutes at 4 °C. For plasmid DNA isolation the GeneElute™ Plasmid Miniprep Kit from Sigma Aldrich was used routinely in the laboratory. The procedure followed was according to that described in the manufacturer’s protocol. Genomic DNA isolation from *E.coli* MG1655 cells was performed using the GeneElute™ Bacterial Genomic DNA kits (purchased from Sigma Aldrich) and according to the procedure described in the manufacturer’s protocol.

The DNA was finally eluted with nuclease free water or with 10 mM Tris-HCl pH 8.0 (along with the presence of 1 mM EDTA). DNA concentration was determined spectrophotometrically or by running agarose gel with suitable standards.

Agarose Gel Electrophoresis of DNA

1% agarose gel (in 1X TAE buffer; composition enlisted in table given before) was melted in a microwave or on a hot plate and cooled to approximately 50 °C after which it was poured on a gel casting trough. The comb was placed near one end of the gel to define the lanes for loading samples. After solidification of the gel, the comb was carefully lifted and the gel was transferred to an electrophoresis tank containing 1X TAE so as to submerge the gel completely. The DNA samples (0.2-1 µg) were mixed with DNA loading buffer and carefully loaded into the gel lanes. The electrophoresis was conducted at a constant voltage of 1-5 V/cm for 1-2 hours. The DNA was visualized using Ethidium bromide staining (0.5 µg/ml solution) and over a UV-transilluminator.

Elution of DNA from agarose Gel

The DNA bands were first appropriately resolved on an agarose gel after which the band of interest was excised out of the gel with a sterile and sharp scalpel. The DNA was eluted from the excised gel fragment using Promega Wizard® SV Gel and PCR Clean-Up System kit.

SDS-Polyacrylamide gel electrophoresis

SDS-Polyacrylamide gel was prepared as per the procedure described in “Molecular cloning- A Laboratory Manual” by Sambrook, Fritsch and Maniatis (2nd edition). For the resolving and stacking gels, a 12% and 5% gel mix was used respectively. Running buffer for SDS-PAGE was Tris-Glycine buffer. The protein samples were mixed with 1X SDS gel loading buffer (Laemmli buffer; composition enlisted in table given before) and heated for 3 minutes at 100 °C. The samples were cooled to room temperature and loaded carefully. The gel was run at appropriate voltage till the bromophenol blue reached the bottom of the gel. The gels were stained with Coomassie Brilliant Blue R250, followed by destaining and visualization using Gel-Doc imaging system (MEGA BIO-PRINT1100/20 M).

References

1. **Algire, M. A.**, Maag, D., Savio, P., Acker, M. G., Tarun, S. Z., Sachs, A. B., ... & Lorsch, J. R. (2002). Development and characterization of a reconstituted yeast translation initiation system. *Rna*, 8(3), 382-397.
2. **Baba, T.**, Ara, T., Hasegawa, M., Takai, Y., Okumura, Y., Baba, M., ... & Mori, H. (2006). Construction of Escherichia coli K-12 in-frame, single-gene knockout mutants: the Keio collection. *Molecular systems biology*, 2(1), 2006-0008.
3. **Banerjee, S.**, Ferdosh, S., Ghosh, A. N., & Barat, C. (2020). Tau protein-induced sequestration of the eukaryotic ribosome: Implications in neurodegenerative disease. *Scientific reports*, 10(1), 1-15.
4. **Beckert, B.**, Abdelshahid, M., Schäfer, H., Steinchen, W., Arenz, S., Berninghausen, O., ... & Wilson, D. N. (2017). Structure of the Bacillus subtilis hibernating 100S ribosome reveals the basis for 70S dimerization. *The EMBO journal*, 36(14), 2061-2072.
5. **Beckert, B.**, Turk, M., Czech, A., Berninghausen, O., Beckmann, R., Ignatova, Z., ... & Wilson, D. N. (2018). Structure of a hibernating 100S ribosome reveals an inactive conformation of the ribosomal protein S1. *Nature microbiology*, 3(10), 1115-1121.
6. **Chakraborty, B.**, Bhakta, S., & Sengupta, J. (2016). Mechanistic insight into the reactivation of BCAII enzyme from denatured and molten globule states by eukaryotic ribosomes and domain V rRNAs. *PloS one*, 11(4), e0153928.
7. **Chattopadhyay, S. U. B. R. A. T. A.**, Das, B. I. S. W. A. D. I. P., Bera, A. K., Dasgupta, D. I. P. A. K., & Dasgupta, C. H. A. N. C. H. A. L. (1994). Refolding of denatured lactate dehydrogenase by Escherichia coli ribosomes. *Biochemical Journal*, 300(3), 717-721.
8. **Chattopadhyay, S.**, Das, B., & Dasgupta, C. (1996). Reactivation of denatured proteins by 23S ribosomal RNA: role of domain V. *Proceedings of the National Academy of Sciences*, 93(16), 8284-8287.
9. **Das, B.**, Chattopadhyay, S., Bera, A. K., & DasGupta, C. (1996). In vitro protein folding by ribosomes from Escherichia coli, wheat germ and rat liver: the role of the 50S particle and its 23S rRNA. *European journal of biochemistry*, 235(3), 613-621.

10. **Khusainov, I.**, Vicens, Q., Ayupov, R., Usachev, K., Myasnikov, A., Simonetti, A., ... & Hashem, Y. (2017). Structures and dynamics of hibernating ribosomes from *Staphylococcus aureus* mediated by intermolecular interactions of HPF. *The EMBO journal*, 36(14), 2073-2087.
11. **Mondal, S.**, Pathak, B. K., Ray, S., & Barat, C. (2014). Impact of P-Site tRNA and antibiotics on ribosome mediated protein folding: studies using the *Escherichia coli* ribosome. *PLoS One*, 9(7), e101293.
12. **Sambrook, J.**, Fritsch, E. F., & Maniatis, T. (1989). *Molecular cloning: a laboratory manual* (No. Ed. 2). Cold spring harbor laboratory press.
13. **Ueta, M.**, Wada, C., & Wada, A. (2010). Formation of 100S ribosomes in *Staphylococcus aureus* by the hibernation promoting factor homolog SaHPF. *Genes to Cells*, 15(1), 43-58.
14. **Walsh, D. M.**, Thulin, E., Minogue, A. M., Gustavsson, N., Pang, E., Teplow, D. B., & Linse, S. (2009). A facile method for expression and purification of the Alzheimer's disease- associated amyloid β - peptide. *The FEBS journal*, 276(5), 1266-1281.

List of publications

- **Ferdosh, S.**, Banerjee, S., Pathak, B. K., Sengupta, J., & Barat, C. (2021). Hibernating ribosomes exhibit chaperoning activity but can resist unfolded protein- mediated subunit dissociation. *The FEBS Journal*, 288(4), 1305-1324.
- Banerjee, S., **Ferdosh, S.**, Ghosh, A. N., & Barat, C. (2020). Tau protein-induced sequestration of the eukaryotic ribosome: Implications in neurodegenerative disease. *Scientific reports*, 10(1), 1-15.

Hibernating ribosomes exhibit chaperoning activity but can resist unfolded protein-mediated subunit dissociation

Sehnaz Ferdosh¹, Senjuti Banerjee¹, Bani K. Pathak², Jayati Sengupta²  and Chandana Barat¹ 

¹ Department of Biotechnology, St. Xavier's College, Kolkata, India

² Structural Biology and Bio-Informatics Division, Indian Institute of Chemical Biology (Council of Scientific and Industrial Research), Kolkata, India

Keywords

chaperoning activity; hibernating ribosomes; ribosome degradation; stationary phase; unfolded protein-mediated dissociation

Correspondence

C. Barat, Department of Biotechnology, St. Xavier's College (Autonomous), Under the University of Calcutta, Kolkata-700016, India

Tel: (033)2255-1101

E-mail: cbarat@sxccal.edu

Sehnaz Ferdosh and Senjuti Banerjee contributed equally

(Received 25 February 2020, revised 24 June 2020, accepted 7 July 2020)

doi:10.1111/febs.15479

Ribosome hibernation is a prominent cellular strategy to modulate protein synthesis during starvation and the stationary phase of bacterial cell growth. Translational suppression involves the formation of either factor-bound inactive 70S monomers or dimeric 100S hibernating ribosomal complexes, the biological significance of which is poorly understood. Here, we demonstrate that the *Escherichia coli* 70S ribosome associated with stationary phase factors hibernation promoting factor or protein Y or ribosome-associated inhibitor A and the 100S ribosome isolated from both Gram-negative and Gram-positive bacteria are resistant to unfolded protein-mediated subunit dissociation and subsequent degradation by cellular ribonucleases. Considering that the increase in cellular stress is accompanied by accumulation of unfolded proteins, such resistance of hibernating ribosomes towards dissociation might contribute to their maintenance during the stationary phase. Analysis of existing structures provided clues on the mechanism of inhibition of the unfolded protein-mediated disassembly in case of hibernating factor-bound ribosome. Further, the factor-bound 70S and 100S ribosomes can suppress protein aggregation and assist in protein folding. The chaperoning activity of these ribosomes is the first evidence of a potential biological activity of the hibernating ribosome that might be crucial for cell survival under stress conditions.

Introduction

The microorganisms possess diverse mechanisms to recognize adverse environmental conditions, and their ability to control the pace of protein synthesis is essential for cell survival under such conditions [1,2]. For heterotrophic bacteria, the transition into the stationary phase might be accompanied by limitation of carbon and energy supply due to the depletion of nutrients in the growth medium. Ribosome

hibernation is one prominent molecular strategy to modulate protein synthesis during the stationary phase [3]. Such translation-suppressing mechanism involves the formation of either the factor-bound inactive 70S monomers or the dimerization of two ribosomes into the 'hibernating' 100S inactive ribosomal complexes. In *Escherichia coli*, a clinically important Gram-negative bacterium, ribosome hibernation through 100S

Abbreviations

6AP, 6-aminophenanthridine; ATP, adenosine triphosphate; BCaII, bovine carbonic anhydrase II; BLS, blasticidin S; GTP, guanosine triphosphate; HPF, hibernation promoting factor; HRP, horseradish peroxidase; mBCaII, molten globule bovine carbonic anhydrase II; nBCaII, native bovine carbonic anhydrase II; PTC, peptidyl transferase centre; PVDF, polyvinylidene difluoride; SDGC, sucrose density gradient centrifugation; uBCaII, unfolded bovine carbonic anhydrase II; YfiA, protein Y or ribosome-associated inhibitor A.

(100S_{Ec}) formation in the stationary phase, is mediated by a short form of hibernation promoting factor (HPF) which acts in concert with the ribosome modulation factor (RMF) [4]. The *E. coli* cells also express an additional hibernation factor, ribosome-associated inhibitor A [also known as protein Y or ribosome-associated inhibitor A (YfiA) or pY], which accumulates in the stationary phase like HPF, inhibits translation and stabilizes 70S ribosomes (70S_{Ec}) against subunit dissociation [5,6]. However, while HPF assists in the formation of the 100S ribosomes, YfiA could only be found associated with the 70S particles and acts as an antagonist to HPF-mediated 100S formation [7]. The induction of expression of the YfiA protein is also observed during cold shock and during stringent response due to carbon and amino acid starvation [1,8]. In contrast to *E. coli*, the 100S ribosome formation in the clinically important Gram-positive bacterium *Staphylococcus aureus* (100S_{Sa}) is mediated by the long form of HPF (HPF_{Sa}) and such dimeric ribosomes are present in all growth phases even when the nutrients are abundant [4]. Recent studies have confirmed that in both *E. coli* and *S. aureus*, the formation of the 100S ribosome is essential for long-term cell viability and stress tolerance [9–11]. The actively translating ribosomes in *E. coli* are stable under normal growth conditions. However, under adverse conditions like starvation, the cellular ribosomes become prone towards degradation and such ribosomal metabolism might be expensive for growing cells [12–15].

The HPF_{Sa} knockout in *S. aureus* indeed causes ribosome breakdown upon entering the stationary phase that correlates with the onset of cell death and attenuated virulence [16]. However, the factors that might initiate ribosome degradation are still unknown. It has been speculated that the resistance of the translationally silent ribosomes towards degradation or a possible biological role of the hibernating ribosomes could contribute to the increased viability associated with their formation [9].

The ability of the cell to respond to the increase in protein unfolding determines its resilience under stress conditions. Since the accumulation of unfolded proteins would increase the possibility of their encounter with the ribosome, two important aspects of ribosome-unfolded protein interaction that are well documented in literature become especially relevant: (a) the isolated subunits formed due to unfolded protein-mediated ribosome subunit dissociation [17,18] have increased susceptibility towards degradation by cellular ribonucleases [19] and (b) the ability of the ribosomes from diverse origins to assist in the folding of proteins with

a wide range of folds and functions which is widely reported in the literature [20] and references therein]. Such noncanonical chaperoning activity of the translation machine could be effectively inhibited in an actively translating ribosome due to the tRNA positioned at the P-site [21] thus ensuring that an actively translating ribosome does not engage in chaperoning function. Extensive studies have demonstrated that the protein folding ability of the ribosome arises due to the interaction of unfolded protein with the peptidyl transferase centre (PTC) of the ribosome. The subsequent release of the protein in a folding competent state completes the chaperoning cycle, thereby enabling the ribosome to act as a protein folding modulator [22,23]. It has also been reported that the ribosome can also behave like a 'holdase' chaperone and can prevent aggregation of partially folded proteins [24]. Structural studies of the hibernating 70S_{Ec}-HPF and 70S_{Ec}-YfiA complexes have shown that both of these factors inhibit translation by binding exclusively to the 30S subunit, that is distinct from the PTC of the ribosome residing in the 50S subunit [20,25]. Hence, the possibility arises that the factor-bound ribosomes might retain their chaperoning activity. The objective of the present investigation was to study whether the factor-bound (HPF or YfiA) inactive 70S monomeric or 100S dimeric ribosome could be dissociated in the presence of unfolded proteins and whether such hibernating ribosomes could assist in protein folding and prevent protein aggregation.

Our *in vitro* studies demonstrate that the 70S_{Ec} ribosome bound to YfiA or HPF (70S_{Ec}-YfiA and 70S_{Ec}-HPF, respectively) and the 100S_{Ec} ribosome are resistant towards unfolded bovine carbonic anhydrase II (uBCAII)-mediated subunit dissociation and subsequent degradation by cellular nucleases. The 100S_{Sa} ribosomes also showed resistance towards uBCAII-mediated subunit dissociation. Further, the 70S_{Ec}-YfiA and 70S_{Ec}-HPF complexes and the 100S_{Ec} and the 100S_{Sa} dimeric ribosomes isolated from *E. coli* and *S. aureus*, respectively, were capable of assisting in the folding of uBCAII and suppressing the aggregation of the molten globule form of BCAII (mBCAII). The *E. coli* ribosomal complexes were also capable of suppressing the aggregation of reduced and denatured lysozyme (R/D Lyso). Our studies therefore provide the first evidence of a potential biological activity of the hibernating ribosome and also provide a possible explanation of how ribosome hibernation might render the translational machine immune towards unfolded protein-mediated dissociation and hence towards subsequent degradation under stress conditions.

Results

Effect of HPF and YfiA on unfolded protein-mediated ribosome dissociation into subunits

As discussed in the 'Introduction' section, light scattering experiments were performed to study the effect of recombinant hibernation factors HPF and YfiA on unfolded protein-mediated ribosome subunit dissociation. The ability of 0.5 μM uBCAII protein to dissociate 70S_{Ec} ribosomes (0.1 μM) when incubated with increasing concentrations of the factors (ribosome: factor ratios are 1 : 1, 1 : 3 and 1 : 10) was analysed under conditions reported in the literature [11] and stated in the 'Materials and methods'. As shown in Fig. 1Ai, an increase in the inhibition of unfolded protein-mediated subunit dissociation is observed in the presence of increasing concentration of both the factors HPF and YfiA. The extent of dissociation in the presence of similar concentration of the two factors was, however, different, and HPF was more effective than YfiA in inhibiting uBCAII-mediated ribosome splitting (Fig. 1Aii). It might be argued that the inability of the unfolded protein to associate with the HPF or YfiA bound 70S_{Ec} ribosome could have prevented the initiation of ribosome splitting. In our earlier studies, the ribosome-uBCAII complexes were separated from the unassociated protein by ultrafiltration and detected by western blot analysis using anti-BCAII antibody [19]. Similar experiments were performed to analyse whether uBCAII and the factors HPF and YfiA could simultaneously bind to the ribosome under our experimental conditions. Dot blot analysis (Fig. 1Bi-ii) using anti-BCAII and anti-His-tag antibodies performed at ribosome: uBCAII and ribosome: HPF/YfiA ratios of 1 : 5 and 1 : 10, respectively, are shown in Fig. 1Bi-ii. This experiment demonstrates that it is likely that both the BCAII protein and the factors are bound to a ribosome simultaneously. However, the methods used cannot unequivocally prove this. The dose-dependent inhibition of unfolded protein-mediated ribosome subunit dissociation was also confirmed by equilibrium sucrose density gradient centrifugation (SDGC) (Fig. 1Ci-ii).

Further studies were performed to understand the basis of the resistance of factor-bound ribosome towards unfolded protein-mediated dissociation. Earlier studies have demonstrated that the factor YfiA is capable of acting as a ribosome association factor that is capable of stabilizing the 70S_{Ec} ribosomes against dissociation [6]. Hence, experiments were performed to study whether the inability of chemically denatured BCAII to dissociate the 70S_{Ec} ribosomes arises due to

increased association between the ribosomal subunits in the presence of the factors HPF or YfiA. Light scattering experiments and SDGC studies indeed showed that, while the empty 70S_{Ec} ribosome (70S_{Ec}-free; 0.1 μM) is dissociated into its subunits at low concentrations of magnesium (1 mM), the 70S_{Ec} ribosome shows resistance towards dissociation in the presence of 10-fold concentrations of HPF or YfiA (1 μM ; Fig. 1Di). The SDGC profile also showed that in the presence of the factors, there is negligible presence of isolated ribosomal subunits even at Mg²⁺ ion concentration as low as 1 mM (Fig. 1Dii). In this case also, HPF was observed to be more capable than YfiA in preventing low Mg²⁺ concentration-induced 70S_{Ec} dissociation. The reasons underlying this observation need to be further investigated. Further experiments were also performed to assess whether the factor HflX, which acts as a dissociation factor in the presence of guanosine triphosphate (GTP) during stress conditions, could dissociate the HPF or YfiA-stabilized ribosome as well. The light scattering experiments shown in Fig. 1E demonstrated that HflX-GTP was able to dissociate the factor-bound ribosome although uBCAII could not, under the conditions used in our experiment.

Our earlier *ex-vivo* studies performed using *E. coli* cell lysate had demonstrated that, the isolated ribosomal subunits formed due to the unfolded protein-mediated 70S_{Ec}-free dissociation, increased the susceptibility of the ribosome towards degradation by cellular ribonucleases [19]. In the present study, similar assays were performed in which 0.1 μM 70S_{Ec} was incubated with a 10-fold stoichiometric excess of HPF and YfiA in the presence of 0.5 μM uBCAII. The reaction mixture was subjected to degradation with *E. coli* mS30 cell lysate. SDGC was performed to study the outcome of the reaction (Fig. 1F). This study demonstrated that while the 70S_{Ec}-free ribosome was degraded when incubated with uBCAII and mS30 extract, the peak corresponding to 70S_{Ec} was retained in the presence of 10-fold concentrations of the factors HPF or YfiA. The ribosome-associated stress factors could therefore influence the unfolded protein-mediated ribosome dissociation and subsequent degradation by cellular nucleases.

Ribosome bound to HPF and YfiA can assist in protein folding and inhibit protein aggregation

The ability of hibernation factor-bound 70S_{Ec} ribosome to assist in protein folding, as stated in the 'Introduction' section, was assessed in the subsequent studies. The ability of the 70S_{Ec} ribosomes (0.3 μM) to

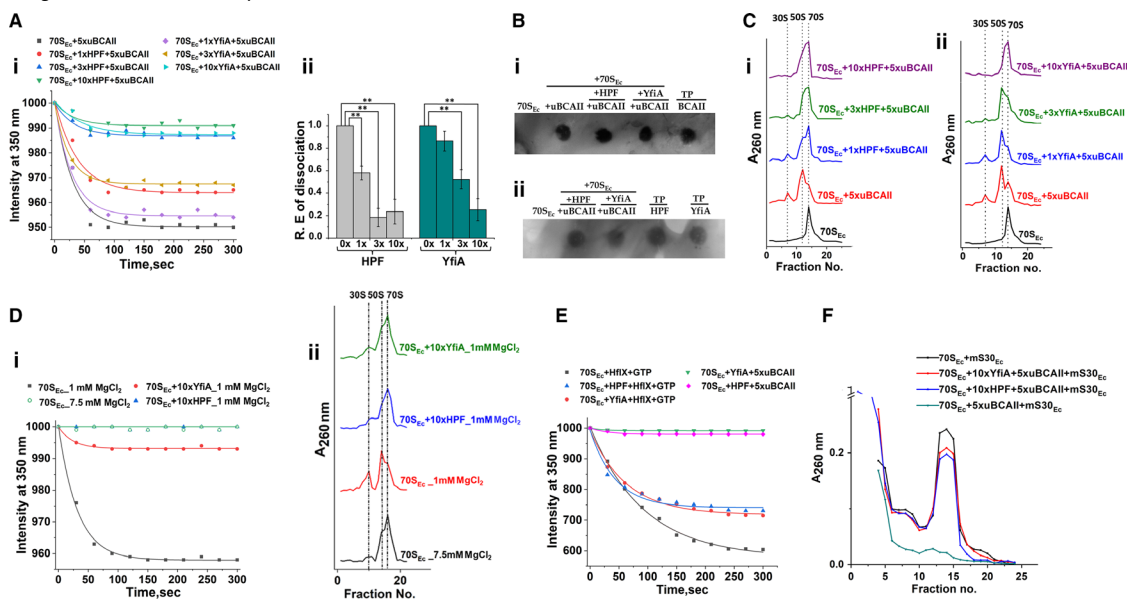


Fig. 1. Effect of HPF and YfiA on *E. coli* 70S ribosome (70S_{Ec}) subunit dissociation and degradation. (A) (i) Light scattering analysis of uBCAII-mediated 70S_{Ec} dissociation in the presence of HPF and YfiA: Time course change in light scattering at 350 nm upon interaction of 70S_{Ec} ribosome (1x = 0.1 μM) with uBCAII (5x), in the presence of different stoichiometric concentrations of HPF and YfiA. 70S_{Ec} + 5x uBCAII (■), 70S_{Ec} + 1x HPF + 5x uBCAII (●), 70S_{Ec} + 3x HPF + 5x uBCAII (▲), 70S_{Ec} + 10x HPF + 5x uBCAII, 70S_{Ec} + 1x YfiA + 5x uBCAII (◆), 70S_{Ec} + 3x YfiA + 5x uBCAII (◀), 70S_{Ec} + 10x YfiA + 5x uBCAII. (ii) Bar graphs representing the extent of dissociation of 0.1 μM 70S_{Ec} (x = 0.1 μM) in the presence of 5x concentration of unfolded BCAII and different stoichiometric concentrations of HPF and YfiA (1x, 3x and 10x). The calculation for the extent of dissociation of 70S_{Ec} was performed assuming the uBCAII-mediated 70S_{Ec} dissociation at 70S_{Ec}: uBCAII = 1 : 5 to be 1. The experiments were repeated thrice, and the data are presented as means ± SEM; *P < 0.05 or **P < 0.001 in one-way ANOVA (N = 3). (B) Dot blot analysis for the presence of uBCAII, HPF and YfiA in the ribosome-bound fraction: 0.1 μM of *E. coli* 70S ribosome, empty or bound to 1 μM HPF or 1 μM YfiA was incubated with 0.5 μM uBCAII for 5 min at room temperature. The reaction mix was loaded on a 100 K Amicon Ultra filter, centrifuged and washed, and dot blot analysis was performed with the 70S_{Ec} bound fraction retained on the filter using (i) carbonic anhydrase II polyclonal antibody to detect the presence of uBCAII and (ii) anti-His tag antibody to detect the presence of factors HPF and YfiA. The total amount of unfolded protein, HPF and YfiA used in the experiment has been included as controls. (i) Dots from left to right contain: (1) total 70S_{Ec} (0.1 μM), uBCAII retained for; (2) 70S_{Ec} (0.1 μM) + uBCAII (0.5 μM), (3) 70S_{Ec} (0.1 μM) + HPF (1 μM) + uBCAII (0.5 μM), (4) 70S_{Ec} (0.1 μM) + YfiA (1 μM) + uBCAII (0.5 μM) and (5) total protein (T.P.) uBCAII (0.5 μM) (TP). (ii) Dots from left to right contain: (1) total 70S_{Ec} (0.1 μM), (2) HPF retained for 70S_{Ec} (0.1 μM) +HPF (1 μM) + uBCAII (0.5 μM), (3) YfiA retained for 70S_{Ec} (0.1 μM) +YfiA (1 μM) + uBCAII (0.5 μM), (4) T.P. HPF (1 μM), (5) T.P. YfiA (1 μM). (C) (i) Sedimentation analysis of dissociation of 70S_{Ec} ribosome (1x = 0.1 μM); (1) alone, (2) upon interaction with uBCAII (5x), (3) upon interaction with uBCAII (5x) in the presence of HPF (1x), (4) upon interaction with uBCAII (5x) in the presence of HPF (3x), (5) upon interaction with uBCAII (5x) in the presence of HPF (10x). The dotted lines represent the positions of the 70S_{Ec} ribosome peak as well as the positions of the 50S and 30S subunits. (ii) Sedimentation analysis of dissociation of 70S_{Ec} ribosome (1x = 0.1 μM); (1) alone, (2) upon interaction with uBCAII (5x), (3) upon interaction with uBCAII (5x) in the presence of YfiA (1x), (4) upon interaction with uBCAII (5x) in the presence of YfiA (3x), (5) upon interaction with uBCAII (5x) in the presence of YfiA (10x). The dotted lines represent the positions of the 70S_{Ec} ribosome peak as well as the positions of the 50S and 30S subunits. (D) (i) Light scattering analysis of 70S_{Ec} dissociation at 1 mM MgCl₂ in the presence of HPF and YfiA: Time course change in light scattering at 350 nm of 0.1 μM (x) 70S_{Ec} ribosome bound to 10x HPF and YfiA (binding was performed at 7.5 mM MgCl₂: 'Materials and methods') at MgCl₂ concentration of 1 mM. 70S_{Ec} ribosome in 1 mM MgCl₂ (■), 70S_{Ec} ribosome in 7.5 mM MgCl₂ (○), 70S_{Ec} ribosome + 10x YfiA in 1 mM MgCl₂ (●), 70S_{Ec} ribosome + 10x HPF in 1 mM MgCl₂ (▲). (ii) Sedimentation analysis of 70S_{Ec} ribosome profile the in presence of HPF and YfiA at 1 mM MgCl₂: Sedimentation profile of (1) 70S_{Ec} in 7.5 mM MgCl₂, (2) 70S_{Ec} in 1 mM MgCl₂, (3) 70S_{Ec} + 10xHPF in 1 mM MgCl₂ and (4) 70S_{Ec} + 10x YfiA in 1 mM MgCl₂. The dotted lines represent the positions of the 70S_{Ec} ribosome peak as well as the positions of the 50S and 30S subunits. (E) Light Scattering analysis of 70S_{Ec} dissociation by HflX-GTP in presence of HPF or YfiA: 0.1 μM (x) 70S_{Ec} ribosome in the presence and absence of 10x (1 μM) HPF or YfiA was rapidly mixed with 1 μM HflX and 100 μM GTP in 7.5 mM MgCl₂ (Materials and methods). Time course change in the intensity of light scattering at 350 nm of the reaction mixtures was measured. 70S_{Ec} + HflX+GTP (■), 70S_{Ec} + HPF+HflX + GTP (▲), 70S_{Ec} + YfiA+HflX + GTP (●), 70S_{Ec} + YfiA+5x uBCAII, 70S_{Ec} + HPF+5x uBCAII. (F) Sedimentation analysis of degradation of *E. coli* 70S ribosome (1x = 0.1 μM) in the presence of HPF and YfiA (10x) upon incubation with *E. coli* mS30 (mS30_{Ec}) extract for 90 min in the presence of 5x uBCAII. As control sets, 70S_{Ec} ribosome alone was incubated with mS30_{Ec} extract and 70S_{Ec} ribosome was incubated with mS30_{Ec} extract in the presence of 5x uBCAII in the absence of either of the factors HPF and YfiA. Gradient profile when 70S_{Ec} alone was incubated with mS30_{Ec} extract (■), 70S_{Ec} was incubated in the presence of 10x YfiA and 5x uBCAII with mS30_{Ec} extract (●), 70S_{Ec} was incubated in the presence of 10x HPF and 5x uBCAII with mS30_{Ec} extract (▲), and 70S_{Ec} was incubated in the presence of 5x uBCAII with mS30_{Ec} extract (▼).

assist in the refolding of uBCAII ($0.3 \mu\text{M}$) in the presence of 10-fold concentration ($3 \mu\text{M}$) of HPF or YfiA was analysed. As shown in Fig. 2A, the increase in reactivation of uBCAII in the presence of the

70S_{Ec} -free ribosome was comparable to that of the 70S_{Ec} ribosome in the presence of HPF and YfiA. Control experiments confirmed that uBCAII reactivation yield in the presence of similar concentrations of

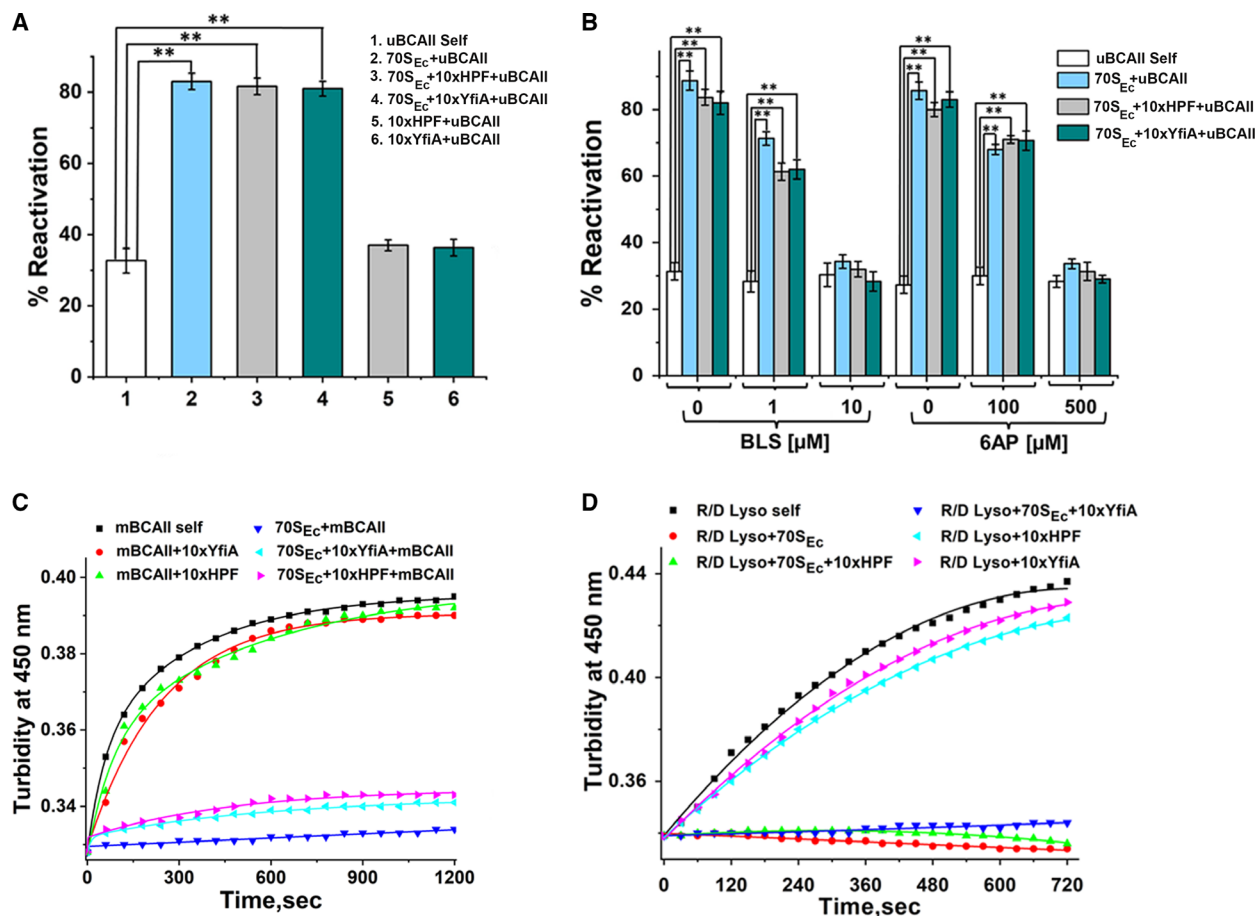


Fig. 2. Chaperoning activity of factor-bound *E. coli* 70S ribosome. (A) Refolding assay of uBCAII in the presence of 70S_{Ec} with 10x ($x = 0.3 \mu\text{M}$) concentrations of HPF and YfiA: $0.3 \mu\text{M}$ of uBCAII was refolded in the presence and absence of 1x 70S_{Ec} alone ($x = 0.3 \mu\text{M}$), 70S_{Ec} in the presence 10x concentration of HPF and YfiA. Bar graphs showing percentage of reactivation of (1) uBCAII self, (2) 70S_{Ec} + uBCAII, (3) 70S_{Ec} + 10x HPF + uBCAII, (4) 70S_{Ec} + 10xYfiA+uBCAII, (5) 10xHPF + uBCAII and (6) 10xYfiA + uBCAII. The experiments were repeated thrice, and the data are presented as means \pm SEM; $*P < 0.05$ or $**P < 0.001$ in one-way ANOVA ($N = 3$). (B) Refolding assay of uBCAII in the presence of 70S_{Ec} and 10x ($x = 0.3 \mu\text{M}$) concentrations of HPF and YfiA with BLS and 6AP: $0.3 \mu\text{M}$ of uBCAII was refolded in the presence and absence of 1x 70S_{Ec} alone ($x = 0.3 \mu\text{M}$), 70S_{Ec} in the presence of 10x concentrations of HPF and YfiA, along with the presence of 0, 1 and 10 μM BLS (Materials and methods). $0.3 \mu\text{M}$ of uBCAII was also refolded in the presence and absence of 70S_{Ec} alone ($x = 0.3 \mu\text{M}$), 70S_{Ec} in the presence of 10x concentrations of HPF and YfiA, along with the presence of 0, 100 and 500 μM 6AP (Materials and methods). Bar graphs showing percentage of reactivation of uBCAII self, 70S_{Ec} + uBCAII, 70S_{Ec} + 10x HPF + uBCAII and 70S_{Ec} + 10x YfiA + uBCAII in the presence of (1) 0 μM BLS, (2) 1 μM BLS, (3) 10 μM BLS, (4) 0 μM 6AP, (5) 100 μM 6AP and (6) 500 μM 6AP. The experiments were repeated thrice, and the data are presented as means \pm SEM; $*P < 0.05$ or $**P < 0.001$ in one-way ANOVA ($N = 3$). (C) Time course change in the aggregation of mBCAII in the presence of 70S_{Ec} with 10x ($x = 0.9 \mu\text{M}$) HPF and YfiA: The time course change in turbidity at 450 nm was measured for 0.9 μM mBCAII (Materials and methods) for 1200 s in the presence and absence of 1x 70S_{Ec} alone ($x = 0.9 \mu\text{M}$), 70S_{Ec} + 10xHPF, 70S_{Ec} + 10xYfiA: mBCAII self (■), mBCAII + 10x YfiA (●), mBCAII + 10xHPF (▲), 70S_{Ec} + mBCAII (▼), 70S_{Ec} + 10x YfiA + mBCAII (◀), 70S_{Ec} + 10x HPF + mBCAII. (D) Time course change in the aggregation of reduced-denatured lysozyme in the presence of 70S_{Ec} with 10x ($x = 2 \mu\text{M}$) HPF and YfiA: The time course change in turbidity at 450 nm was measured for 2 μM of reduced-denatured lysozyme (R/D Lyso) (Materials and methods) for 720 s in the presence and absence of 1x 70S_{Ec} alone ($x = 2 \mu\text{M}$), 70S_{Ec} + 10xHPF, 70S_{Ec} + 10xYfiA: R/D Lyso self (■), R/D Lyso + 70S_{Ec} (●), R/D Lyso + 70S_{Ec} +10x HPF (▲), R/D Lyso + 70S_{Ec} +10x YfiA (▼), R/D Lyso + 10xHPF (◀), R/D Lyso + 10x YfiA.

the factors alone was comparable to the self-reactivation of uBCAII. Taken together, these studies imply that the ability of the ribosome to act as a protein folding modulator remains unaffected in the presence of the factors.

The question regarding whether the chaperoning ability of the factor-bound ribosome originated in its PTC was addressed using the PTC antibiotic blastidicin S (BLS) and the antiprion drug 6-aminophenanthridine (6AP). Earlier studies have demonstrated that BLS, a PTC substrate analog that mimics the binding of the 3'-CCA end of the P-site tRNA [21], inhibits the ribosome-assisted reactivation of uBCAII. Further, it has been demonstrated that the antiprion drug 6AP also inhibits protein folding activity associated with the ribosome [26] by inhibiting the specific interactions between the five sites on the PTC and the unfolded protein that is necessary for the ribosome chaperoning activity. Experiments were performed in which the 70S_{Ec} ribosome (0.3 μM) was incubated in the presence of 10-fold excess of HPF or YfiA (3 μM) and increasing concentrations of BLS (0, 1 and 10 μM) in BLS binding buffer. To this reaction mixture, 0.3 μM of uBCAII was added and BCAII reactivation yield was measured. In each set, control experiments were performed in which the self-reactivation of uBCAII was studied in the presence of equivalent amounts of BLS in BLS binding buffer. As shown in Fig. 2B, the ability of the 70S_{Ec}-HPF and 70S_{Ec}-YfiA to assist in folding and reactivation of uBCAII shows a dose-dependent suppression by the antibiotic BLS. Similar experiments were performed to study the effect of the antiprion drug 6AP on the refolding ability of 70S_{Ec} ribosome in the presence of these stationary phase factors. A similar dose-dependent inhibition of the refolding ability of factor-bound ribosome was observed in the presence of increasing concentrations of 6AP (Fig. 2B). These studies indicate at the involvement of the PTC of the ribosome and imply that the mechanism of chaperoning action of the factor-bound ribosome might be similar to that of the empty ribosome.

Our earlier studies have shown that the 70S_{Ec} free is capable of suppressing aggregation of the mBCAII or R/D Lyso [24]. Similar studies were performed in which the ribosome (0.9 μM), incubated with 10-fold excess concentration of HPF or YfiA, was added to 0.9 μM of mBCAII. Turbidity measurements at 450 nm were performed as outlined in 'Materials and methods'. An increase in turbidity at 450 nm, indicative of increase in protein aggregation, was observed when mBCAII is incubated alone under our experimental conditions. This increase in turbidity was suppressed when mBCAII was incubated with 70S_{Ec} free

or the 70S_{Ec} ribosomes in the presence of HPF or YfiA (Fig. 2C). In control experiments, no significant aggregation suppression was observed in the presence of similar concentrations of the factors alone. The 70S_{Ec} ribosomes bound to the factors HPF and YfiA showed similar inhibition of aggregation of reduced and denatured lysozyme (Fig. 2D). The ability of the stress factor-bound ribosome to assist in protein folding and suppress protein aggregation might play a significant role in the maintenance of an active cellular proteome under stress conditions.

Comparison of uBCAII-mediated subunit dissociation and chaperoning activity of the *E. coli* 70S and 100S ribosomes

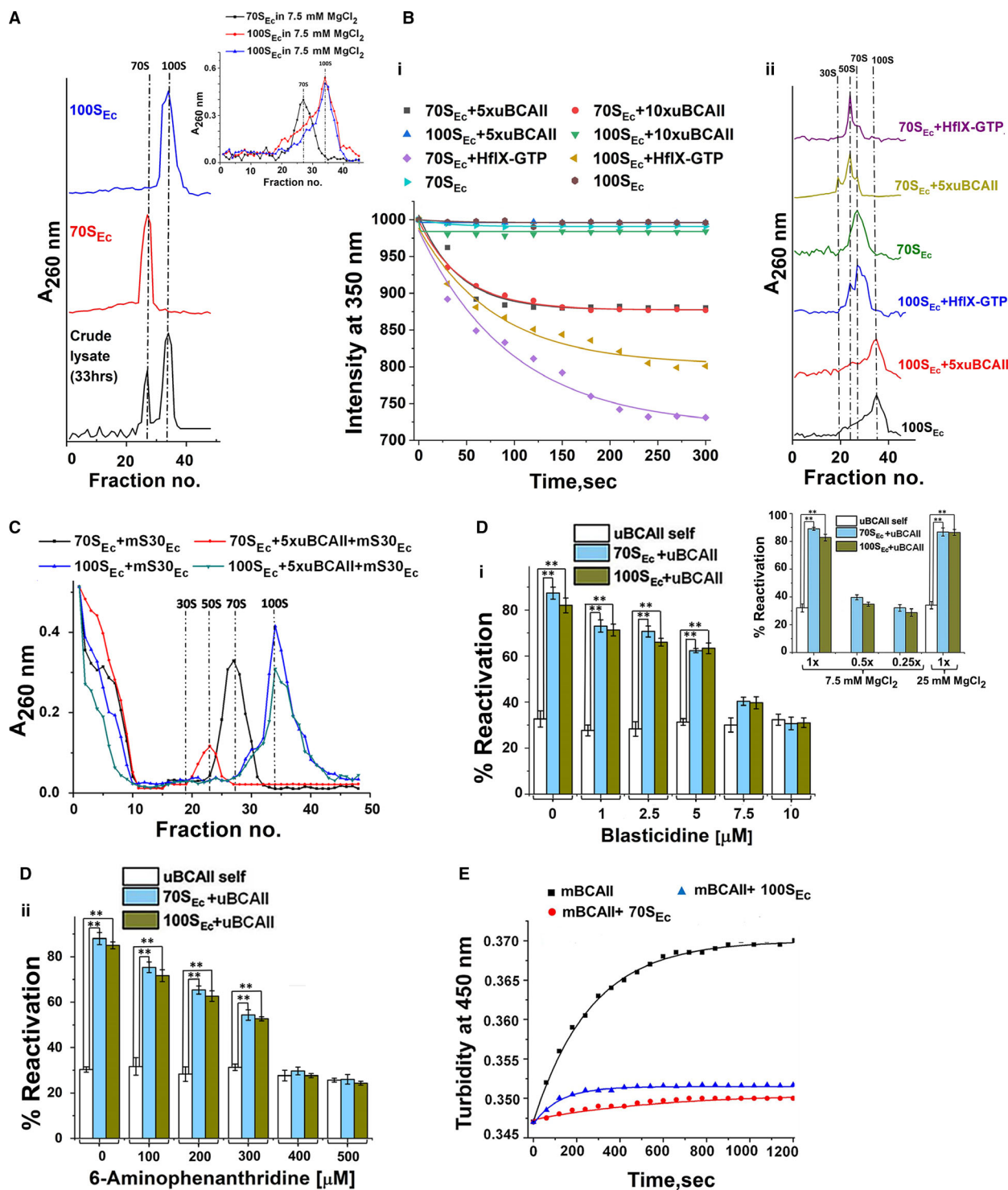
As discussed above, further experiments were performed to compare (a) uBCAII-mediated dissociation and (b) chaperoning activity of the 100S_{Ec} and the 70S_{Ec} ribosome. The 100S_{Ec} ribosomes were isolated from BW25113 $\Delta yfiA$ strain of *E. coli*, enriched and purified as reported earlier [27] (Fig. 3A). It should be noted that our earlier light scattering experiments had demonstrated that unfolded protein-mediated ribosome subunit dissociation occurs optimally at 7.5 mM magnesium ion concentration [19]. Since the uBCAII-mediated ribosome splitting had to be performed at Mg²⁺ concentration of 7.5 mM, the sucrose density gradient profile of the 100S_{Ec} ribosomes was compared in the presence of 7.5 and 25 mM Mg²⁺ ion concentrations. Due to the reduced stability of the dimeric ribosome at low Mg²⁺ concentration [9], there is a variable overlap between the 100S_{Ec} and 70S_{Ec} ribosomal peaks in different experiments. This is indicative of contribution (~30–40%) of the 70S_{Ec} ribosome in the 100S_{Ec} preparation (inset of Fig. 3A). Light scattering experiments were performed to compare the effect of unfolded protein on 70S_{Ec}-free and the 100S_{Ec} ribosomal preparation. As shown in Fig. 3Bi, a reduction in light scattering was observed when the 70S_{Ec} free was treated with 5-fold excess of uBCAII. However, no similar reduction was observed upon treatment of 100S_{Ec} ribosomes with 5-fold or even 10-fold excess of the unfolded protein. This experiment suggests that unlike the 70S_{Ec} free, the unfolded protein is incapable of dissociating the dimeric 100S_{Ec} ribosome under the conditions used in our experiments. SDGC studies also confirmed that the peak corresponding to the 100S_{Ec} ribosomes remains intact in the presence of uBCAII (Fig. 3Bii). As stated above, the 100S_{Ec} ribosome preparation also contains a population of 70S_{Ec} ribosomes. The inability of the unfolded protein to dissociate even the 70S_{Ec} ribosome present in the 100S_{Ec}

preparation therefore implies that the 70S_{Ec} monomers which originate from the 100S_{Ec} ribosome might still remain bound to the hibernation factor HPF. As shown in Fig. 1Ai,Ci, HPF itself can inhibit the uBCAII-mediated subunit dissociation of 70S_{Ec}. Earlier studies performed *in vivo* have indeed demonstrated that when the stationary phase cells are transferred into fresh medium, although 100S_{Ec} ribosomal dimers dissociated into 70S_{Ec} ribosomes, HPF still remained associated with these monomeric ribosomes [28].

It has been shown that HflX in the presence of GTP is capable of dissociating the 100S_{Ec} ribosome [29] and 70S_{Ec} ribosome bound to the factors (studies stated

above, Fig. 1E). Hence, further experiments were performed to study the ability of HflX-GTP to dissociate the 100S_{Ec} ribosomes. Light scattering experiments demonstrated that HflX-GTP is capable of dissociating the 70S_{Ec}-free and the 100S_{Ec} ribosomes under the conditions used in our experiment (Fig. 3Bi). SDGC experiments also showed that the treatment of the ribosomes with HflX-GTP leads to dissociation of the 70S_{Ec}-free and the disappearance of the 100S_{Ec} ribosomal peak (Fig. 3Bii). Taken together, these studies suggest that the dissociation of the 100S_{Ec} ribosome is necessarily factor-mediated and these dimeric ribosomes remain protected from unfolded protein-mediated subunit dissociation. Therefore, as expected, when

Fig. 3. Comparison of unfolded protein (uBCAII)-mediated subunit dissociation, stability in the presence of HflX + GTP and chaperoning activity of the 70S (70S_{Ec}) and 100S (100S_{Ec}) ribosomes isolated and enriched from Gram-negative bacteria *E. coli*. (A) Purification and enrichment of 100S ribosomes from BW25113Δyfia strain of *E. coli* (100S_{Ec}). Purification and enrichment of 100S_{Ec} ribosomes from BW25113Δyfia strain of *E. coli* was performed as described in 'Materials and methods'. (1) SDGC profile (in 10–60% gradient in Buffer G containing 25 mM MgCl₂) of crude cell lysate of BW25113Δyfia strain of *E. coli* after 33 h of incubation at 37 °C, containing a major proportion of 100S_{Ec}, (2) 70S_{Ec} isolated from MRE600 strain of *E. coli* run on gradient and plotted to mark the position of the 70S_{Ec} ribosome and (3) 100S_{Ec} ribosome obtained after enrichment through sequential SDGC. The dotted lines represent the position of the 70S_{Ec} and 100S_{Ec} ribosome peaks. The inset graph shows the varying levels of overlap that is obtained between the 70S_{Ec} and 100S_{Ec} peaks when the respective ribosomes are exposed to 7.5 mM MgCl₂ concentration and run on the 10–60% sucrose density gradient in different ultracentrifugation runs under the same conditions as stated in 'Materials and methods'. (B) (i) Light scattering analysis of uBCAII and HflX-GTP mediated 70S_{Ec} and 100S_{Ec} ribosome subunit dissociation: Time course change in light scattering at 350 nm upon interaction of 70S_{Ec} (0.1 μM) and 100S_{Ec} (A_{260 nm} units equivalent of 0.1 μM) ribosome (1x = 0.1 μM or A_{260 nm} units equivalent of 0.1 μM) with uBCAII (5x) and uBCAII (10x) concentrations or with 10x HflX (1 μM) in presence of 100 μM GTP (Materials and methods). 70S_{Ec} + 5x uBCAII (■), 100S_{Ec} + 5x uBCAII (▲), 70S_{Ec} + HflX + GTP (◆), 70S_{Ec} + 10x uBCAII (●), 100S_{Ec} + 10x uBCAII, 100S_{Ec} + HflX + GTP (◀), 70S_{Ec} and 100S_{Ec} (●) in Buffer G containing 7.5 mM Mg²⁺ ion concentration. (ii) Sedimentation analysis of uBCAII and HflX-GTP mediated 70S_{Ec} and 100S_{Ec} ribosome (1x = 0.1 μM) subunit dissociation: Sucrose gradient profile of (1) 100S_{Ec} in Buffer G containing 7.5 mM MgCl₂, (2) 100S_{Ec} + 5x uBCAII in Buffer G containing 7.5 mM MgCl₂, (3) 100S_{Ec} + 10x HflX + 1000x GTP in Buffer G containing 7.5 mM MgCl₂, (4) 70S_{Ec} in Buffer G containing 7.5 mM MgCl₂, (5) 70S_{Ec} + 5x uBCAII in Buffer G containing 7.5 mM MgCl₂ and (6) 70S_{Ec} + 10x HflX + 1000x GTP in Buffer G containing 7.5 mM MgCl₂. The dotted lines represent the positions of the 100S_{Ec} and 70S_{Ec} ribosome peak as well as the positions of the respective 50S and 30S subunits. (C) Sedimentation analysis of the degradation of 70S_{Ec} and 100S_{Ec} ribosome (1x = 0.1 μM or A_{260 nm} units equivalent of 0.1 μM) upon incubation with *E. coli* mS30 extract (mS30_{Ec}) for 90 min in the presence of 5x uBCAII (Materials and methods). As control sets, 70S_{Ec} ribosome and 100S_{Ec} ribosome alone were incubated with mS30_{Ec} extract for the same period of time. Gradient profile shown are 70S_{Ec} + mS30_{Ec} extract (■), 100S_{Ec} + mS30_{Ec} extract (▲), 70S_{Ec} + 5xuBCAII + mS30_{Ec} extract (●) and 100S_{Ec} + 5x uBCAII + mS30_{Ec} extract (▼). The dotted lines represent the positions of the 100S_{Ec} and 70S_{Ec} ribosome peaks as well as the positions of the respective 50S and 30S subunits. (D) (i) Refolding assay of uBCAII in the presence of 70S_{Ec} and 100S_{Ec} with BLS: Bar graphs showing percentage reactivation of uBCAII self (0.3 μM), uBCAII assisted by 70S_{Ec} (0.3 μM) or 100S_{Ec} (A_{260 nm} units equivalent of 0.3 μM) in the presence of (1) 0 μM BLS (2) 1 μM BLS, (3) 2.5 μM BLS, (4) 5 μM BLS, (5) 7.5 μM BLS and (6) 10 μM BLS. The inset graph represents the refolding assay of uBCAII (0.3 μM) in the presence and absence of different stoichiometric concentrations of 70S_{Ec} and 100S_{Ec} (Materials and methods). Bar graphs showing percentage reactivation of uBCAII self, 70S_{Ec} + uBCAII and 100S_{Ec} + uBCAII when 70S_{Ec} (0.3, 0.15 and 0.075 μM) and 100S_{Ec} (equivalent A_{260 nm} units corresponding to 0.3, 0.15 and 0.075 μM) are present in concentrations (1) 1x (0.3 μM or equivalent A_{260 nm} units corresponding to 0.3 μM in Buffer G containing 7.5 mM MgCl₂), (2) 0.5x (0.15 μM or equivalent A_{260 nm} units corresponding to 0.15 μM in Buffer G containing 7.5 mM MgCl₂), (3) 0.25x (0.075 μM or equivalent A_{260 nm} units corresponding to 0.075 μM in Buffer G containing 7.5 mM MgCl₂) and (4) 1x (0.3 μM or equivalent A_{260 nm} units corresponding to 0.3 μM in Buffer G containing 25 mM MgCl₂). The experiments were repeated thrice, and the data are presented as means ± SEM; *P < 0.05 or **P < 0.001 in one-way ANOVA (N = 3). (ii) Refolding assay of uBCAII in the presence of 70S_{Ec} and 100S_{Ec} with 6AP: Bar graphs showing percentage reactivation of uBCAII self (0.3 μM), uBCAII assisted by 70S_{Ec} (0.3 μM) or 100S_{Ec} (A_{260 nm} units equivalent of 0.3 μM) in the presence of (1) 0 μM 6AP, (2) 100 μM 6AP, (3) 200 μM 6AP, (4) 300 μM 6AP, (5) 400 μM 6AP and (6) 500 μM 6AP. The experiments were repeated thrice, and the data are presented as means ± SEM; *P < 0.05 or **P < 0.001 in one-way ANOVA (N = 3). (E) Time course of aggregation of mBCAII in the presence of 70S_{Ec} and 100S_{Ec} ribosome: The time course of change in turbidity at 450 nm was measured for 0.9 μM of mBCAII (Materials and methods) for 1200 s in the presence and absence of 0.9 μM of 70S_{Ec} ribosome and A_{260 nm} units equivalent of 0.9 μM of 100S_{Ec} ribosome. mBCAII self (■), mBCAII + 70S_{Ec} (●), mBCAII + 100S_{Ec}.



the 70S_{Ec}-free and the 100S_{Ec} ribosomes were treated with unfolded protein and incubated with the mS30 extract (prepared from MG1655 *E. coli* cells), the nucleases present in the extract were capable of degrading subunits formed from the 70S_{Ec}-free, while

the undissociated 100S_{Ec} ribosome was resistant to similar degradation in the presence of the unfolded protein (Fig. 3C).

Subsequent experiments were performed to compare the chaperoning activity of the dimeric 100S_{Ec} and the

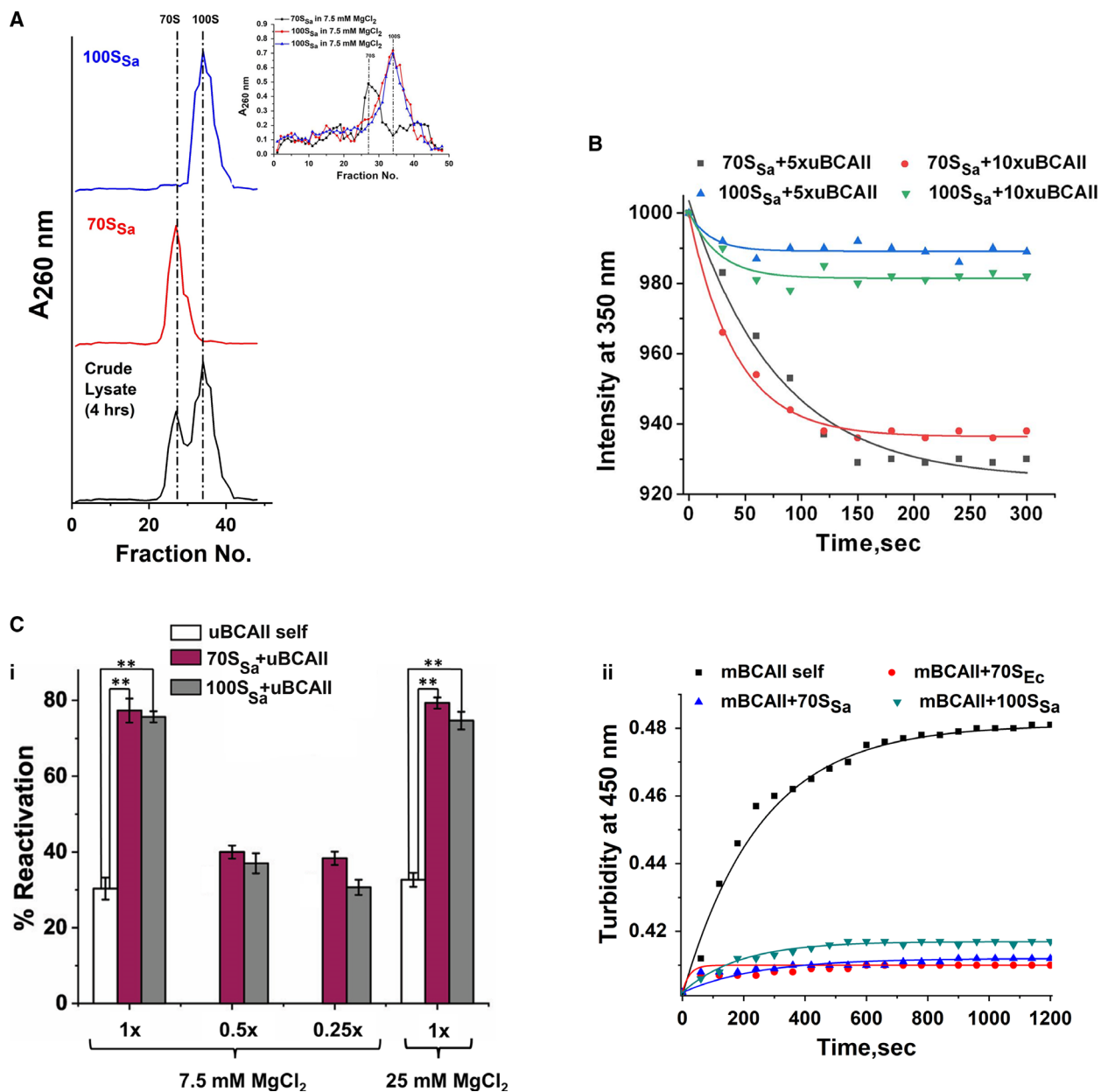
70S_{Ec} ribosome. The 70S_{Ec}-free and the 100S_{Ec} ribosome preparation (0.3 μM based on $A_{260\text{ nm}}$) were incubated at stoichiometric concentrations with uBCAII, and the chaperoning activity was measured. As shown in Fig. 3Di, the 70S_{Ec}-free and the 100S_{Ec} ribosomes showed comparable chaperoning ability. To test whether the chaperoning activity observed could originate from the residual population of the 70S_{Ec} ribosome present in the 100S_{Ec} preparation, refolding of 0.3 μM uBCAII was performed with substoichiometric (uBCAII: ribosome ratios of 1 : 0.5, 1 : 0.25) concentrations of the 70S_{Ec}-free and 100S_{Ec} ribosomes with respect to the unfolded protein. As shown in the inset of Fig. 3Di, the contribution of the residual 70S_{Ec} ribosome present in the 100S_{Ec} preparation towards the chaperoning activity observed could be considered insignificant. Further studies also showed that the 100S_{Ec} and 70S_{Ec}-free have comparable chaperoning activity at higher Mg^{2+} concentration (25 mM) (inset of Fig. 3Di) at which there is negligible contribution of 70S_{Ec} in the 100S_{Ec} preparation (Fig. 3A). These studies imply that the 100S_{Ec} dimeric ribosome exhibits chaperoning activity that is comparable to that of the 70S_{Ec}-free. Subsequent refolding experiments were performed with the 70S_{Ec} and the 100S_{Ec} ribosomes in the presence of increasing concentrations of the PTC binding substrates like BLS and 6AP that are known inhibitors of ribosome chaperoning activity. A dose-dependent suppression of chaperoning activity in the presence of increasing concentrations BLS (Fig. 3Di) and 6AP (Fig. 3Dii) was observed. This could imply that the ability of both 70S_{Ec} and the 100S_{Ec} ribosomes to act as protein folding modulators originated from the PTC of the ribosomes. These observations suggest that the chaperoning action of the 70S_{Ec} and the 100S_{Ec} ribosomes could occur following a similar mechanism [20]. Additionally, in studies performed with the mBCAII, both the 70S_{Ec}-free and the 100S_{Ec} ribosomes were capable of suppressing protein aggregation (Fig. 3E). Considering the large number of ribosomes present in the cell, our present studies suggest that the chaperoning activity of the translationally suppressed ribosomes might be capable of assisting in protein folding and mitigating protein aggregation under stress conditions.

Comparison of uBCAII-mediated subunit dissociation and chaperoning activity of the *Staphylococcus aureus* 70S and 100S ribosomes

As discussed in the 'Introduction' in the Gram-positive bacterium *S. aureus*, the 100S ribosomes are present through all growth phases although the physiological

relevance of the formation of the dimeric ribosomes remains unclear. Hence based on our present studies on the *E. coli* 100S ribosome, preliminary studies were performed on the unfolded protein-mediated subunit dissociation and chaperoning activity of the 70S (70S_{Sa}) and 100S_{Sa} ribosomes isolated from *S. aureus*. The 100S_{Sa} ribosomes and the 70S_{Sa} ribosomes were prepared from the MTCC 3160 strain of *S. aureus* cells in their mid-log-phase [30]. The cell extract was subjected to SDGC, and subsequent enrichment of the corresponding 100S and 70S peaks was performed as reported earlier and as shown in Fig. 4A. It should be noted that as in the studies with the *E. coli* ribosomes (stated above), light scattering and refolding experiments with the *S. aureus* ribosomes were also performed at Mg^{2+} concentration of 7.5 mM. The variable overlap between the 100S and 70S ribosomal peaks that is observed in sucrose density gradient profiles at 7.5 mM Mg^{2+} concentration (inset of Fig. 4A) indicates that at the lower Mg^{2+} ion concentration, there is a contribution of 70S_{Sa} ribosomes in the 100S_{Sa} preparation. A comparative study of the unfolded protein-mediated dissociation of the 70S_{Sa} (70S_{Sa}-free) and the 100S_{Sa} ribosomes was performed using light scattering analysis in which the ribosomes ($A_{260\text{ nm}}$ units equivalent of 0.1 μM) were treated with a 5-fold and 10-fold stoichiometric excess of uBCAII. Preliminary light scattering studies show that while a reduction in light scattering, indicative of ribosome subunit dissociation, is observed when 70S_{Sa}-free is treated with uBCAII, no significant reduction in scattering was observed with the ribosomes present in the 100S_{Sa} preparation (Fig. 4B). These studies therefore indicate that, similar to that observed with the ribosomes isolated from Gram-negative bacteria, the dimeric ribosome isolated from Gram-positive bacteria is more resistant towards dissociation by unfolded proteins than the 70S monomeric ribosome.

Preliminary experiments were also performed to assess the chaperoning activity of ribosomes isolated from *S. aureus*. In these experiments, 0.3 μM of uBCAII was incubated with or without the 70S_{Sa}-free and the 100S_{Sa} ribosomes ($A_{260\text{ nm}}$ units equivalent of 0.3 μM) and the reactivation of the uBCAII was assayed in refolding buffer (7.5 mM Mg^{2+}). As shown in Fig. 4Ci, both the 100S_{Sa} and the 70S_{Sa}-free ribosomes could assist in the refolding and reactivation of the BCAII protein. The outcome of the ribosome-assisted BCAII refolding was, as with *E. coli* ribosomes, influenced by the different stoichiometry of unfolded protein: ribosome present during the experiment (Fig. 4Ci). This experiment also implies that the contribution to chaperoning activity of residual 70S_{Sa}



present in the 100S_{Sa} preparation is negligible. The chaperoning activity of 70S_{Sa}-free and 100S_{Sa} was comparable in refolding buffer containing 25 mM Mg²⁺ concentration (Fig. 4Ci), at which there is negligible contribution of 70S_{Sa} in the 100S_{Sa} preparation (Fig. 4A). These studies therefore demonstrated the ability of both 70S_{Sa}-free and 100S_{Sa} to act as a protein folding modulator. The 70S_{Sa}-free and the 100S_{Sa} ribosomes were also capable of suppressing aggregation of mBCAII (Fig. 4Cii). The implications of these experimental observations are discussed below.

Discussion

As stated above, earlier studies have shown that the unfolded proteins are capable of mediating dissociation of the ribosome into its subunits [17–19]. Our present study demonstrates that the *E. coli* 70S ribosome that is associated with stationary phase factors HPF or YfiA and the 100S dimeric ribosomes, isolated from both Gram-negative and Gram-positive bacteria, are resistant to unfolded protein-mediated subunit dissociation. The *E. coli* 100S ribosomes were also resistant towards subsequent degradation by cellular

Fig. 4. Comparison of uBCAII-mediated subunit dissociation and chaperoning activity of the 70S (70S_{Sa}) and 100S (100S_{Sa}) ribosomes isolated and enriched from the Gram-positive bacteria *S. aureus*. (A) Purification and enrichment of 70S_{Sa} and 100S_{Sa} ribosomes from *S. aureus* was performed using the MTCC 3160 strain of *S. aureus* cells that were harvested after 4 h of incubation at 37° C in TSB media. The crude lysate from the cells was prepared and subjected to sucrose cushion, the pellet obtained dissolved in B100S buffer (Materials and methods) and purification and enrichment of 70S_{Sa} and 100S_{Sa} was performed on a sucrose density gradient (Materials and methods). SDGC profile of (in 10–60% gradient in Buffer G containing 25 mM MgCl₂). (1) Crude lysate pellet of MTCC 3160 strain of *S. aureus*, prepared after 4 h of incubation at 37° C in TSB media, (2) 70S_{Sa} ribosome isolated, purified and enriched from crude lysate pellet via sequential SDGC, (3) 100S_{Sa} ribosome isolated, purified and enriched from the crude lysate pellet via sequential SDGC. The dotted lines represent the positions of the 70S_{Sa} and 100S_{Sa} ribosome peaks. The inset graph shows the varying levels of overlap that is obtained between the 70S_{Sa} and 100S_{Sa} peaks when the respective ribosomes are exposed to 7.5 mM MgCl₂ concentration and run on the 10–60% sucrose density gradient in different ultracentrifugation runs under the same conditions as stated in 'Materials and methods'. (B) Light scattering analysis of uBCAII-mediated 70S_{Sa} and 100S_{Sa} ribosome subunit dissociation: Time course change in light scattering at 350 nm upon interaction of 70S_{Sa} (1x = A_{260 nm} units equivalent 0.1 μM) and 100S_{Sa} (A_{260 nm} units equivalent of 0.1 μM) ribosome with 5x and 10x concentrations of uBCAII, denatured with 6 M GuHCl. 70S_{Sa} + 5x uBCAII (■), 100S_{Sa} + 5x uBCAII (▲), 70S_{Sa} + 10x uBCAII (●) and 100S_{Sa} + 10x uBCAII. (C) (i) Refolding assay of uBCAII in the presence of 70S_{Sa} and 100S_{Sa} ribosomes: 0.3 μM of uBCAII was refolded in the presence and absence of different stoichiometric concentrations of 70S_{Sa} and 100S_{Sa} ribosomes. The chaperoning activity of the ribosomes was measured by monitoring the recovery of BCAII enzyme activity (Materials and methods). Bar graphs showing percentage reactivation of uBCAII self, uBCAII + 70S_{Sa} and uBCAII + 100S_{Sa} when 70S_{Sa} (equivalent A_{260 nm} units corresponding to 0.3, 0.15 and 0.075 μM) and 100S_{Sa} (equivalent A_{260 nm} units corresponding to 0.3, 0.15 and 0.075 μM) are present in concentrations (1) 1x (0.3 μM equivalent A_{260 nm} units in Buffer G containing 7.5 mM MgCl₂), (2) 0.5x (0.15 μM equivalent A_{260 nm} units in Buffer G containing 7.5 mM MgCl₂), (3) 0.25x (0.075 μM equivalent A_{260 nm} units in Buffer G containing 7.5 mM MgCl₂) and (4) 1x (0.3 μM equivalent A_{260 nm} units in Buffer G containing 25 mM MgCl₂). The experiments were repeated thrice, and the data are presented as means ± SEM; **P* < 0.05 or ***P* < 0.001 in one-way ANOVA (*N* = 3). (ii) Time course of aggregation of mBCAII in presence of 70S_{Sa} and 100S_{Sa} ribosome: The time course change in turbidity at 450 nm of 0.9 μM of mBCAII was measured for 1200 s in the absence and presence of stoichiometric concentrations (1x = 0.9 μM equivalent A_{260 nm} units) of 70S_{Sa} ribosome and 100S_{Sa} ribosome: mBCAII self (■), mBCAII + 70S_{Sa} (▲), mBCAII + 70S_{Ec} (●), mBCAII + 100S_{Sa}.

ribonucleases. Further, the factor-bound 70S and 100S ribosomes exhibit chaperoning activity and can suppress protein aggregation and assist in protein folding.

Studies were also conducted to investigate the mechanism underlying the resistance of the factor-bound ribosomes towards unfolded protein-mediated subunit dissociation. An analysis of the structure of 70S ribosome bound to the stationary phase factors [25] indicates that the restricted movement of helix 44 of 16S rRNA of the 30S subunit could stabilize the central inter-subunit bridge B2a, that is implicated in unfolded protein-mediated ribosome splitting. It is well documented in literature that the physical factors like low Mg²⁺ concentrations can lead to ribosome subunit dissociation [31]. The factor YfiA is also capable of acting as a ribosome association factor, and the binding of YfiA protein to the ribosome inhibits the dissociation of the 70S_{Ec} at a low concentration of Mg²⁺ [6]. Our present studies suggest that, like YfiA, the factor HPF can also prevent low Mg²⁺ concentration-induced dissociation of 70S_{Ec} (Fig. 1Di-ii). HPF also appears to be more effective than YfiA as a ribosome subunit association factor, although the reasons underlying this observation need to be further investigated. As stated earlier, sustained interaction of the unfolded protein to the large subunit of the ribosome forms the basis of its 50S subunit antiassociation activity [19]. The ability of

HPF and YfiA to act as a ribosome association factor would reduce the presence of isolated subunits in a factor-bound ribosomal population, thereby rendering the 50S subunit antiassociation activity of the unfolded protein ineffective.

The cellular recycling factors like ribosome recycling factor and HflX are the classical 70S_{Ec} recycling factors in *E. coli* [32,33]. The stress factor HflX in concert with GTP can also recycle subunits of the stalled 70S_{Ec} ribosome and the 100S_{Ec} dimeric ribosome [33,29]. Our studies also demonstrate that under the conditions used in our experiments, HflX and GTP are capable of dissociating the stationary phase factor-bound ribosomes (Fig. 1E). These studies imply that the recycling of YfiA and HPF stabilized 70S_{Ec} ribosomes, for new rounds of translation, is necessarily dependent on active factor-mediated dissociation by HflX-GTP. Our subsequent studies also demonstrated that the hibernating dimeric 100S_{Ec} ribosome, although resistant to dissociation by unfolded proteins (Fig. 3B), could be dissociated by recycling factor HflX-GTP (Fig. 3B). The dimeric 100S_{Sa} ribosomes isolated from the Gram-positive *S. aureus* were also resistant towards unfolded protein-mediated subunit dissociation (Fig. 4B).

As stated earlier, the stable dissociation of ribosomal subunits in the presence of unfolded proteins

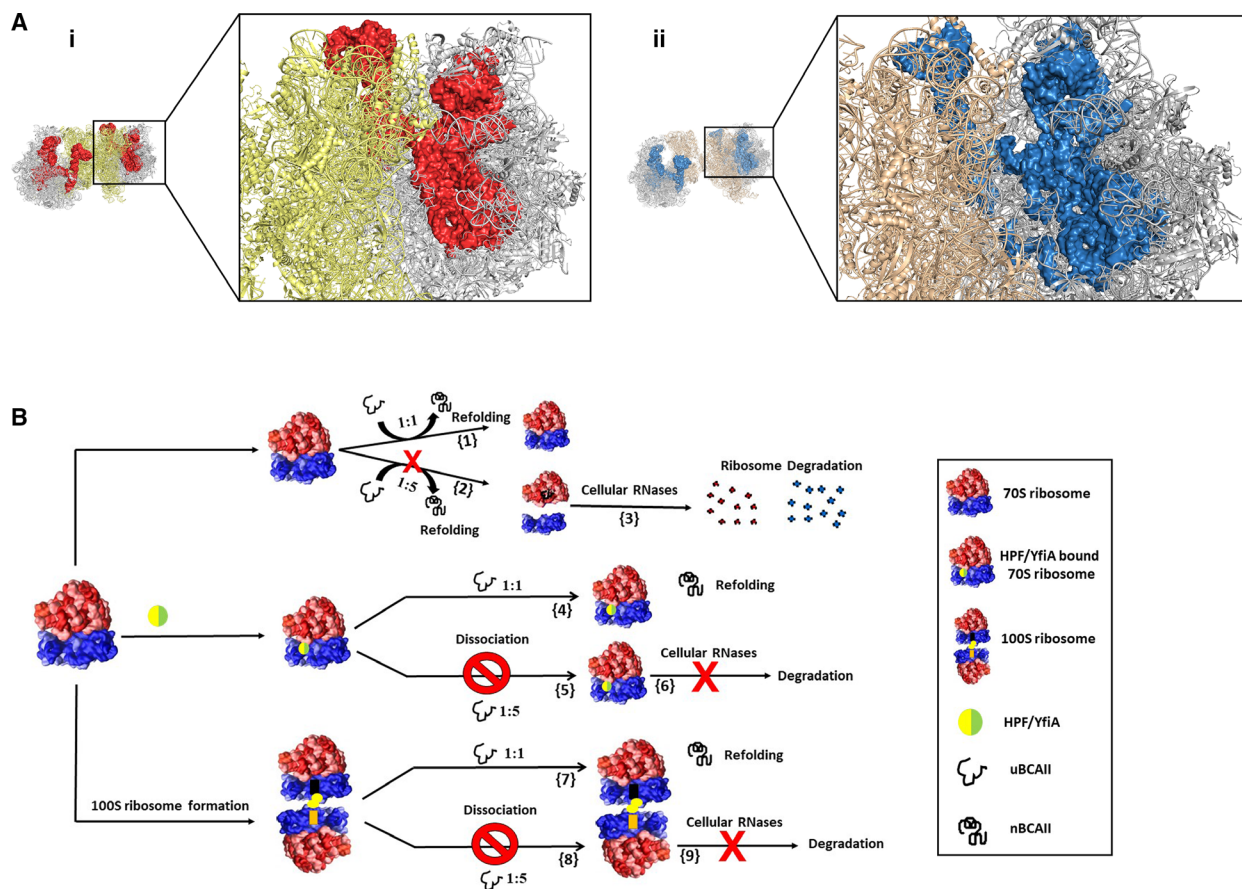


Fig. 5. Structural representations of the availability of the domain V region of the *E. coli* and *S. aureus* 100S ribosomes and a model depicting the outcomes of interaction of unfolded protein with ribosome. (A) (i) Crystal structure of the *E. coli* 100S ribosome (100S_{Ec}) (Protein Data Bank: 6H58) is shown with the close-up view of one 70S_{Ec} counterpart in the right panel. Light yellow represents the 30S subunit, grey represents the 50S subunit, and red represents the domain V region of the 23S rRNA. (ii) Crystal structure of the *S. aureus* 100S ribosome (100S_{Sa}) (Protein Data Bank: 6FXC), and the close-up view of one 70S_{Sa} counterpart in the right panel are shown. Light orange represents the 30S subunit, grey represents the 50S subunit, and the domain V region of the 23S rRNA is presented in blue. Clearly, RNA1 part of the domain V rRNA is quite accessible to the unfolded protein encountered by the 100S ribosomes in both the structures (i and ii). Structural illustrations have been made using PYMOL 2008 (De Lano Scientific, available at: <https://pymol.org/2/>). (B) Model depicting the outcomes of unfolded protein–ribosome interaction: The possible outcomes of unfolded protein interaction with HPF and YfiA bound 70S_{Ec} ribosome and the 100S ribosomes isolated from *E. coli* (100S_{Ec}) and *S. aureus* (100S_{Sa}). {1} chaperoning activity of empty 70S_{Ec} or 70S_{Sa} ribosome in the presence of equimolar concentrations of the unfolded protein (uBCAII) to yield folded BCAII (nBCAII), {2} dissociation of 70S_{Ec} or 70S_{Sa} ribosome into its subunits in the presence of 5-fold excess concentration of uBCAII, {3} degradation by cellular nucleases of dissociated subunits formed due to 70S_{Ec}-uBCAII interaction, {4} chaperoning activity of HPF or YfiA bound 70S_{Ec} in the presence of equimolar concentrations of the uBCAII to yield nBCAII, {5} resistance of 70S_{Ec}-HPF or 70S_{Ec}-YfiA to ribosome subunit dissociation in the presence of 5-fold excess concentration of uBCAII, {6} resistance to degradation by cellular nucleases of 70S_{Ec}-HPF or 70S_{Ec}-YfiA in the presence of 5-fold excess concentration of uBCAII due to restricted uBCAII-mediated subunit dissociation. {7} Chaperoning activity of 100S_{Ec} or 100S_{Sa} in the presence of equimolar concentrations of the uBCAII to yield nBCAII, {8} resistance of 100S_{Ec} or 100S_{Sa} to ribosome subunit dissociation in the presence of 5-fold excess concentration of uBCAII, {9} resistance to degradation by cellular nucleases of 100S_{Ec} in the presence of 5-fold excess concentration of uBCAII due to restricted uBCAII-mediated subunit dissociation.

renders the ribosome vulnerable to cellular ribonucleases. Our studies demonstrate that HPF or YfiA-stabilized 70S_{Ec} ribosomes and the 100S_{Ec} dimeric ribosomes are resistant to unfolded protein-mediated subunit dissociation and subsequent degradation by cellular ribonucleases (Figs 1F and 3C). The

dissociation of the ribosome into its subunits is an initial step in the ribosome degradation process [34]. The increasing concentration of unfolded protein under stress conditions [35] and its ability to dissociate the ribosome can therefore influence cellular ribosome metabolism by acting as a potential trigger of

ribosomal dissociation and subsequent degradation. It has been reported that 50% of the cellular ribosomes undergo degradation during transition from log-phase to stationary phase of bacterial cell growth [15]. The preservation of the residual ribosomes might play an important role in long-term cell viability. Our studies imply that ribosome hibernation in the stationary phase could render the ribosome immune to unfolded protein-mediated dissociation, and these hibernating ribosomes can thus function as a stable ribosomal repository during the stationary phase resulting in increased viability after removal of starvation or stress conditions [36,37].

Our studies also indicate that the chaperoning ability of the hibernating ribosomes might be a potential biological activity of such nontranslating ribosomes. Recent studies suggest that RNA molecules can function as protein folding chaperones and are very effective in executing folding of a variety of proteins, both *in vivo* and *in vitro* [38–40]. The potential role of RNA in modulating aggregation and amyloid formation of the p53 protein has also been reported [41]. Chaperone activities of RNA have been also shown to be intrinsic to some ribozymes such as the M1 RNA ribozyme responsible for tRNA maturation [42] and the 23S rRNA that catalyses the peptidyl transferase activity of the ribosome [20,22]. Our studies suggest that the stationary phase factor-bound 70S_{Ec} ribosomes or 100S dimeric ribosomes isolated from both Gram-negative and Gram-positive bacteria retain their ability to act as a protein folding modulator (Figs 2A, 3D, 4Ci). Studies using PTC substrates like BLS and 6AP (Figs 2B and 3D) confirmed that the ability of the hibernating *E. coli* ribosomes to assist in protein folding originates from the PTC of the ribosomes. The structure of the 70S_{Ec}-HPF ribosome from *Thermus thermophilus* (PDB: 4V8H) [25], the 100S_{Ec} ribosome (PDB: 6H58) (Fig. 5Ai) and the 100S_{Sa} ribosome (PDB: 6FXC) (Fig. 5Aii) also shows that domain V of 23S rRNA is accessible for binding to the unfolded protein in the factor-bound 70S ribosomes and in the 70S_{Ec} or 70S_{Sa} monomers that constitutes the 100S dimeric ribosomes. This might imply a similar mechanism for chaperoning activity of the *S. aureus* and *E. coli* 70S and 100S ribosomes. The factor-bound 70S_{Ec}, the 70S_{Sa} ribosome and the dimeric ribosomes (100S_{Sa} and 100S_{Ec}) were also capable of suppressing aggregation of molten globule form of the BCaII protein (Figs 2C, 3E and 4Cii).

The increase in protein misfolding and unfolding under stress conditions increases the propensity of aggregation of the cellular proteins. The cell utilizes its molecular chaperone network to minimize the

accumulation of the cytotoxic protein aggregates [43,44]. However, it should be noted that there is a sharp decline in cellular adenosine triphosphate (ATP) content upon transition from the exponential to the stationary phase of growth [45]. Under such conditions, the ATP-dependent major cellular chaperone systems like DnaK-DnaJ-GrpE or GroEL-GroES [44] would be rendered ineffective. The stationary phase-inducible chaperone Hsp31, whose activity is negatively regulated by ATP, can, however, continue to act as an effective holdase in the starved cells [46,47]. Our present studies suggest that the chaperoning activity of the translationally suppressed ribosome might also provide an additional energetically inexpensive support towards maintaining an active cellular proteome.

Our earlier and present observations are summarized in the model shown in Fig. 5B. Earlier studies had demonstrated that the outcomes of the ribosome-unfolded protein interaction distinctly depend upon the unfolded protein concentration. (a) At stoichiometric ribosome: protein ratio of 1 : 1, the empty ribosome acts as a protein folding modulator and the binding of the unfolded protein and its subsequent release leads to high BCaII reactivation yields {1}. (b) However, when a 5-fold excess amount of uBCaII is present with respect to the empty ribosome, the increase in stable association between 50S and unfolded protein leads to lowered reactivation yields {2} and the manifestation of 50S antiassociation activity of unfolded protein. The stable dissociation of empty ribosome into its subunits leads to their vulnerability towards degradation by cellular nucleases {3}. Our studies suggest that in the presence of stationary phase-associated factors HPF or YfiA, the *E. coli* 70S ribosome retains the PTC-mediated protein folding activity and the ability to suppress protein aggregation {4}. Further, the presence of these factors renders the 70S ribosome resistant to unfolded protein-mediated subunit dissociation {5}.

Based on an earlier study, in which the BCaII protein structure was docked on domain V (RNA2 region) of the 50S ribosomal subunit of *T. thermophilus* ribosome [25], (Protein Data Bank: 4V8H) [48], it was proposed that the destabilization of the central inter-subunit bridge B2a (formed between helix 69 of the 23S rRNA and helix 44 of the 16S rRNA) [49] might underlie the unfolded protein-mediated dissociation of ribosomal subunits. It is possible that upon binding at the mRNA channel (head and body junction of the inter-subunit interface) of the small subunit, the hibernating factors apparently restrict the free movement of the subunits in such a way that the unfolded protein-mediated ribosome disassembly gets

arrested. The mechanism underlying the resistance of the hibernating factor-bound ribosome to such dissociation needs further investigation. In addition, such resistance of the factor-bound ribosome towards dissociation prevents its subsequent degradation by cellular nucleases {6}. The 100S ribosome isolated from *E. coli* displays chaperoning activity and can assist in refolding of unfolded protein and suppress aggregation of the mBCAII {7}. The dimeric ribosomes also exhibited resistance towards uBCAII-mediated dissociation {8} and subsequent degradation by cellular RNases {9}. Preliminary studies performed with 70S and 100S ribosomes isolated from Gram-positive *S. aureus* also revealed that (i) the 100S ribosome was relatively more resistant towards unfolded protein-mediated subunit dissociation and (ii) both the 70S and 100S ribosomes exhibited chaperoning activity.

Earlier studies on unfolded protein–ribosome interaction [17–19] imply that a direct link might exist between the accumulation of unfolded proteins during cellular stress and the increased probability of ribosome subunit dissociation and subsequent degradation. The resistance of the hibernating ribosome (70S_{Ec}-HPF or 70S_{Ec}-YfiA complexes or the 100S_{Ec} or 100S_{Sa} ribosomes) towards such dissociation might explain why their formation is necessary for the stabilization of the ribosomal population during the stationary phase. Further it should be noted that the molecular chaperoning activities were conventionally considered to be performed uniquely by the proteins themselves. However, several recent studies have recognized that RNA possesses protein folding ability which can indeed be more effective than the known chaperone proteins in facilitating protein folding and preventing protein aggregation [38–40]. The ribosome and its component 23S rRNA have been reported to behave like molecular chaperones *in vitro* in a *trans*-acting mode, although their relevance to *de novo* protein folding *in vivo* still remains to be further characterized. The inability of P-site tRNA bound ribosomes to act as a chaperone essentially demarcates the population of ribosomes involved in active translation from those involved in chaperoning activity. The hibernating translational machinery which is formed from the necessity of translation suppression under stress conditions would therefore be available for performing the noncanonical chaperoning activity. The biological significance of the formation of the hibernating ribosomes and their correlation with bacterial resilience under stress condition is not completely understood. Taken together, our studies provide further insights into how the hibernating ribosomes might contribute towards survival in a broad spectrum of cellular stress

conditions like stationary phase and dormant persister cell states [50] that are of clinical relevance.

Materials and methods

Reagents

The DreamTaq DNA polymerase and dNTPs were purchased from ThermoScientific™, Thermo Fisher Scientific (Waltham, MA, USA). The primers, antibiotics Kanamycin and BLS, antiprion drug 6AP, protein BCAII, guanidine hydrochloride (GuHCl), GTP as well as the chemicals used for preparing buffers, were purchased from Sigma-Aldrich (St. Louis, MO, USA). Genomic DNA isolation from *E. coli* MG1655 (for use as template in PCR) and 70S_{Ec} ribosome purification from *E. coli* MRE600 cells were performed as reported earlier [21,24]. Ni²⁺-NTA agarose was purchased from QIAGEN (Hilden, Germany). 100S_{Ec} ribosomes were prepared from the *E. coli* BW25113Δ*yfiA* cells which were purchased from the Keio Knockout Collection of the Coli Genetic Stock Centre, Yale University, USA [51]. 70S_{Sa} and 100S_{Sa} ribosomes were isolated from *S. aureus* MTCC 3160 cells obtained from Microbial Type Culture Collection and Gene Bank, MTCC, CSIR Institute of Microbial Technology, Chandigarh, India. The Luria Broth, Tryptic Soy Broth (TSB) and skimmed milk powder were purchased from Himedia Laboratories Pvt. Limited (Mumbai, Maharashtra, India). DNase I (RNase-free) enzyme was purchased from Fermentas, Thermo Fisher Scientific. Amicon Ultra centrifugal filters, polyvinylidene difluoride (PVDF) membrane and immobilized western chemiluminescence horseradish peroxidase (HRP) substrate were purchased from Millipore (Billerica, MA, USA). Zeba™ Spin desalting columns were purchased from ThermoScientific™, Thermo Fisher Scientific. CAII rabbit polyclonal IgG, His-probe rabbit polyclonal IgG and goat anti-rabbit IgG-HRP secondary antibodies were purchased from Santa Cruz Biotechnology (Dallas, TX, USA). All other chemicals were local products of analytical grade. Experimental data analysis was performed using ORIGINPRO 8 (OriginLab Corp., Northampton, MA, USA) and SIGMAPLOT 13 (Systat Software Inc., San Jose, CA, USA) softwares. Structural illustrations have been made using PYMOL 2008 (De Lano Scientific, Palo Alto, CA, USA).

Cloning and Purification of HPF and YfiA

The DNA corresponding to the stationary phase factors HPF and YfiA was PCR amplified using *E. coli* genomic DNA, extracted from *E. coli* (MG1655) cells, as template, DreamTaq DNA Polymerase and appropriate primers. The PCR amplified products were cloned into the pET-28a (+) (NOVAGEN; Merck-Millipore) expression vector. The gene now contained a T7 promoter upstream of a ribosome binding site with the ‘epsilon sequence’ originating from

bacteriophage T7 promoter, followed by a Shine–Dalgarno sequence. The *E. coli* BL21-DE3 cells, transformed with the recombinant plasmids, were grown in the presence of Kanamycin ($50 \mu\text{g}\cdot\text{mL}^{-1}$) for 7 h without induction. The induction step was avoided as it resulted in significant loss in cell mass. The cells were harvested by centrifugation at $11,400 g$ for 6 min at 4°C . Cell pellet was washed using wash buffer containing 20 mM Tris/HCl (pH 7.5), 10 mM $\text{Mg}(\text{OAc})_2$, 100 mM NH_4Cl and 5 mM β -mercaptoethanol and disrupted by sonication. Cell debris was pelleted by centrifugation for 45 min at $17,100 g$. The supernatant was loaded on a Ni^{+2} -NTA affinity flow column and eluted with a linear gradient of imidazole (50–200 mM) in wash buffer (50 mM phosphate buffer pH 8, 300 mM NaCl with different amounts of imidazole) ([24] with minor modifications). Eluted fractions (corresponding to different imidazole washes) were subjected to SDS/PAGE with appropriate protein ladder. Selected fractions corresponding to HPF or YfiA were pooled separately, subjected to centrifugal ultrafiltration using Amicon Ultra 3 KDa molecular weight cut-off filters, and protein concentration was estimated by measuring the absorbance at 280 nm. The residual imidazole from the protein was removed using 7 KDa desalting column. The purification of HflX protein was performed as reported earlier [52].

Purification and Enrichment of 70S and 100S ribosomes

Ribosomes used in this study were purified from both *E. coli* (Gram-negative bacteria) and *S. aureus* (Gram-positive bacteria). The *E. coli* 70S_{Ec} ribosomes were purified from MRE600 cells [53], and the purification was performed as reported earlier. *E. coli* MRE600 cells were grown in LB medium supplemented with 0.1% glucose until the $A_{600 \text{ nm}}$ was ~ 0.8 . Cells were then slowly cooled to 4°C to produce run-off ribosomes [21,24] and harvested in 20 mM Tris/HCl pH 7.5, 10 mM MgCl_2 , 100 mM NH_4Cl and 5 mM β -mercaptoethanol. Frozen cells were lysed in the same buffer containing $2 \mu\text{g}\cdot\text{mL}^{-1}$ DNase I, using French Pressure lysis cell. Cell debris was removed by centrifuging the suspension twice at $12\,000 g$ for 30 min in a Sigma 12158-H rotor. The supernatant was centrifuged at $1\,54\,000 g$ for 2 h in a Beckman Ti50 rotor (Beckman Coulter Life Sciences, Indianapolis, IN, USA), and the pellet containing ribosomes were resuspended in TMA-10 buffer (20 mM Tris/HCl pH 7.5, 10 mM MgCl_2 , 30 mM NH_4Cl , 5 mM β -mercaptoethanol [21,24]. One molar NH_4Cl was added, and the suspension was kept at 0°C for 1 h. The ribosomal preparation was clarified by centrifugation at $12\,000 g$ for 20 min in a Sigma 12158-H rotor. The supernatant was centrifuged at $1\,54\,000 g$ for 2 h in a Beckman Ti50 rotor (Beckman Coulter Life Sciences, Indianapolis, IN, USA), and the pellet was resuspended in TMA-10. About $75 A_{260 \text{ nm}}$ units (one $A_{260 \text{ nm}}$

unit is the amount of material that, when contained in 1 mL of solution, gives an absorbance value of 1 at 260 nm, in a 1 cm path-length cell) of this ribosomal preparation was loaded on top of a 5–30% linear sucrose (RNase-free) gradient in the same buffer and centrifuged at $1,39,065 g$ for 90 min in a Beckman SW40.1 rotor (Beckman Coulter Life Sciences, Indianapolis, IN, USA) at 4°C . The gradient was monitored at 260 nm, and appropriate fractions containing 70S_{Ec} particles were pooled. The pooled fractions containing the purified 70S_{Ec} ribosome particles were concentrated using Amicon Ultra 10K filters, and the sucrose from the fractions was removed by centrifugation filtration using the same filters and TMA-10 buffer at 4°C . The concentrated 70S_{Ec} ribosomes were stored in -80°C until further use [21,24].

The *E. coli* 100S_{Ec} ribosomes were purified from the BW25113 Δ yfiA cells, and the purification was performed as reported earlier with minor modifications [27]. *E. coli* BW25113 Δ yfiA cells were grown in M9 minimal media (33.7 mM Na_2HPO_4 , 22 mM KH_2PO_4 , 8.55 mM NaCl, 9.35 mM NH_4Cl , 1 mM MgSO_4 , 0.3 mM CaCl_2 complemented with 0.4% D-glucose) for 33 h [27] and then allowed to cool to 4°C to produce run-off ribosomes. The cells were then harvested in B100S buffer (25 mM HEPES-KOH pH 7.5, 100 mM KOAc, 15 mM $\text{Mg}(\text{OAc})_2$, 1 mM DTT) through centrifugation at $5000 g$ for 15 min at 4°C . The frozen cells were resuspended in B100S buffer containing $2 \mu\text{g}\cdot\text{mL}^{-1}$ DNase I and lysed using the French Pressure cell. The cell lysate was cleared of debris by centrifuging the suspension twice at $12\,000 g$ for 30 min in a Sigma 12158-H rotor. The crude ribosome was pelleted through a 25% w/v sucrose cushion (in B100S buffer supplemented with 0.01% Triton-X-100) by centrifugation at $2,88,350 g$ for 4 h (using Beckman Ti70 rotor, Beckman Coulter Life Sciences, Indianapolis, IN, USA). The pellet was resuspended in B100S buffer [27]. The 100S_{Ec} ribosomes were next enriched by loading on a 10–60% linear sucrose gradient in Buffer G (10 mM Tris/HCl pH 7.5, 50 mM KCl, 10 mM NH_4Cl , 25 mM MgCl_2) and centrifugation at $1\,55\,000 g$ for 3 h in a MLS 50 rotor (Beckmann Coulter Life sciences, Indianapolis, IN, USA) ([54,55] with minor modifications). The gradient was monitored at 260 nm, and appropriate fractions containing the 100S_{Ec} particles were pooled. Sucrose was removed from the pooled fractions using Amicon Ultra 10 KDa filters, and the fractions were concentrated using the same Buffer G with 25 mM MgCl_2 (10 mM Tris/HCl pH 7.5, 50 mM KCl, 10 mM NH_4Cl and 25 mM MgCl_2) ([54,55] with minor modifications) at 4°C . These concentrated fractions were subjected to repeated rounds of such centrifugation until substantially purified, and enriched fractions of 100S_{Ec} ribosomes were obtained. These were stored at -80°C until further use.

In case of *S. aureus*, both 70S_{Sa} and 100S_{Sa} ribosomes were purified and enriched using similar method as that for

100S_{Ec}. *S. aureus* MTCC 3160 cells were grown in TSB media for 4 h [30], with minor modifications, and the cells were harvested in the same manner as described earlier. The subsequent steps used were identical to those used for 100S_{Ec} purification. In this case, during enrichment, appropriate fractions for both 70S_{Sa} and 100S_{Sa} particles were pooled and processed in a similar manner to obtain enriched and purified 70S_{Sa} and 100S_{Sa} particles, which were stored in -80°C until further use.

Ribosome–antibiotic complex preparation

Ribosome-bound antibiotic complexes were prepared by incubating $0.3\ \mu\text{M}$ ribosome (either 70S_{Ec}-free or $A_{260\ \text{nm}}$ units equivalent concentration of 100S_{Ec} or 70S_{Ec}-HPF or 70S_{Ec}-YfiA) with different stoichiometric concentrations of BLS ($0\text{--}10\ \mu\text{M}$, as indicated in the figure legends) in BLS binding buffer (100 mM Tris-Cl pH 7.2, 10 mM MgCl₂, 100 mM NH₄Cl, 6 mM β -mercaptoethanol), at 37°C for 20 min, then at 20°C for 15 min and finally kept on ice for 5 min [21]. The final volume for binding was maintained at $50\text{--}100\ \mu\text{L}$ ($50\ \mu\text{L}$ for 70S_{Ec}-free and 100S_{Ec} and $100\ \mu\text{L}$ for 70S_{Ec}-HPF and 70S_{Ec}-YfiA). After incubation, $250\text{--}200\ \mu\text{L}$ of BCAII refolding buffer (50 mM Tris-Cl pH 7.5, 100 mM NaCl and specified concentrations of MgCl₂) [21,24] or Buffer G (10 mM Tris-Cl pH 7.5, 50 mM KCl, 10 mM NH₄Cl and specified concentrations of MgCl₂; as indicated in the figure legends; [55] with minor modifications) was added to the mix, and then, these ribosome-bound antibiotic complexes were used for BCAII reactivation studies.

Ribosome-HPF or YfiA complex preparation

Ribosome-bound HPF and YfiA complexes were prepared by incubating 0.1 or $0.3\ \mu\text{M}$ ribosome (70S_{Ec}-free) with different stoichiometric concentrations of HPF and YfiA ($1x$, $3x$ and $10x$, $x = 0.1$ or $0.3\ \mu\text{M}$, as indicated in the figure legends) in HPF or YfiA binding buffer (5 mM Tris/HCl pH 7.5, 50 mM KCl, 10 mM NH₄Cl, 7.5 or 10 mM MgCl₂ as indicated in figure legends) at 37°C for 30 min with a final binding volume of 50 or $80\ \mu\text{L}$ [11]. After incubation, $150\ \mu\text{L}$ (for light scattering studies) or $220\ \mu\text{L}$ (for refolding assay) of BCAII refolding buffer or Buffer G was added to the reaction mixture, and then, these HPF or YfiA bound ribosome complexes were used for BCAII reactivation as well as ribosomal subunit dissociation studies. For dissociation studies, the MgCl₂ concentration was 7.5 mM in HPF or YfiA binding buffer, refolding buffer and Buffer G. However, for dissociation of HPF or YfiA bound 70S_{Ec} in 1 mM MgCl₂, the binding of the factors with 70S_{Ec} was performed in HPF or YfiA binding buffer with 7.5 mM MgCl₂ (binding volume: $50\ \mu\text{L}$) as described above, and then added to refolding buffer with 1 mM

MgCl₂ ($150\ \mu\text{L}$). The reaction mixture was analysed both by SDGC and light scattering analysis. For SDGC, the reaction mix was incubated for 300 s and layered on a $17\text{--}25\%$ sucrose density gradient prepared in refolding buffer with 1 mM MgCl₂. For light scattering studies, the change in light scattering intensity at 350 nm of the reaction mixture was immediately measured for a period of 300 s. The complexes were also used for refolding studies where recovery of enzymatic activity was assayed by adding 500 mM para-nitro-phenyl acetate (PNPA) to the refolding mixture and measuring the increase in absorbance of para-nitro-phenol (PNP) at 420 nm over a period of 120 s [21].

Ribosome-6AP complex preparation

Ribosome-bound 6AP complexes were prepared by incubating 0.1 or $0.3\ \mu\text{M}$ ribosome (either 70S_{Ec}-free or $A_{260\ \text{nm}}$ units equivalent concentration of 100S_{Ec} or 70S_{Ec}-HPF or 70S_{Ec}-YfiA) with different stoichiometric concentrations of 6AP ($100\text{--}500\ \mu\text{M}$, as indicated in the figure legends) in refolding buffer (50 mM Tris/HCl pH 7.5, 100 mM NaCl, 7.5 mM MgCl₂; for 70S_{Ec}-free or HPF or YfiA bound 70S_{Ec}) [21,24] or in Buffer G (10 mM Tris/HCl pH 7.5, 50 mM KCl, 10 mM NH₄Cl, 7.5 mM MgCl₂, 1 mM DTT; for 100S_{Ec}) ([55] with minor modifications) at 29°C for 10 min [56]. The final volume of binding was maintained at $50\ \mu\text{L}$ for 70S_{Ec}-free and 100S_{Ec} and $100\ \mu\text{L}$ for factor-bound 70S_{Ec}. After incubation, 250 or $200\ \mu\text{L}$ of BCAII refolding buffer or Buffer G (as indicated in the figure legends) was added to the reaction mixture, and then, these ribosome complexes were used for BCAII reactivation.

Unfolding and refolding studies of BCAII

Bovine carbonic anhydrase II was unfolded with 6 M GuHCl in the presence of 3.5 mM EDTA for 3 h, refolded in BCAII refolding buffer or Buffer G (as indicated in the figure legends), and recovery of enzymatic activity was assayed as described earlier [18,19]. BCAII (Sigma-Aldrich) ($30\ \mu\text{M}$) was denatured to equilibrium with 6 M GuHCl and 3.5 mM EDTA at 29°C for 3 h, and refolding was initiated by 100-fold dilution in refolding buffer in the presence of equimolar concentration of chaperone. The volume of the refolding mix was $300\ \mu\text{L}$. BCAII and the ribosome (or its complexes) were each present at concentration of $0.3\ \mu\text{M}$ (or $A_{260\ \text{nm}}$ units equivalent to $0.3\ \mu\text{M}$). The refolding mix was incubated at 29°C for a period of 30 min as reported earlier [57,21,24]. Recovery of enzymatic activity was assayed by adding 500 mM PNPA to the refolding mixture and measuring the increase in absorbance of PNP at 420 nm with time (over a period of 120 s) [57,21,24]. Control experiments were performed in which BCAII was allowed to refold, in the absence of any chaperone under the various buffer conditions stated in figure legends. The

results obtained are referred to as 'uBCAII self' in this study. The refolding of BCAII was unaffected under the conditions used in our studies. The refolding of 0.3 μM uBCAII was performed in the presence and absence of 0.3 μM 70S_{Ec}-free, 70S_{Ec} bound to the antibiotic BLS (present in different concentrations of 0–10 μM , as indicated in figure legends) [21]. Similar refolding studies were also performed in the presence and absence of 70S_{Ec} bound to stationary phase factors HPF and YfiA, 70S_{Ec} bound to either of the factors and BLS, 70S_{Ec} bound to 6-AP (present in different concentrations of 0–500 μM) [56] and 70S_{Ec} bound to either of the factors and 6AP. Refolding studies with 0.3 μM uBCAII were also performed with A_{260 nm} units equivalent of 0.3 μM of 100S_{Ec} as well as 70S_{Sa} and 100S_{Sa}. Care was taken to ensure that in each case—control experiments of unassisted (self) folding and the 70S_{Ec}-free or 70S_{Sa}-free ribosome-assisted folding were performed under the same salt and buffer conditions. Control experiments were also performed to ensure that the factors or antibiotics themselves do not affect self-folding of BCAII under the conditions used in our study. Aggregation of mBCAII (0.9 μM) was monitored by turbidity measurements in Hitachi Spectrophotometer (U-1900). The effect of 70S_{Ec}-free (0.9 μM), HPF and YfiA (9 μM) bound 70S_{Ec} (HPF and YfiA in 10-fold excess concentration of that used for ribosome), 100S_{Ec} (0.9 μM equivalent A_{260 nm} units), 70S_{Sa}-free (0.9 μM equivalent A_{260 nm} units) and 100S_{Sa} (0.9 μM equivalent A_{260 nm} units) on mBCAII aggregation was monitored at 450 nm over a period of 1200 s [24].

Aggregation of reduced-denatured lysozyme

Lysozyme (2 μM) was reduced and denatured for 3 h at room temperature using 6 M GuHCl and 100 mM DTT [24]. Aggregation of R/D Lyso (2 μM) was monitored by turbidity measurements in Hitachi Spectrophotometer (U-1900). The effect of 70S_{Ec}-free (2 μM), HPF or YfiA (20 μM) bound 70S_{Ec} (HPF and YfiA in 10-fold excess concentration of that used for ribosome) on R/D Lyso aggregation was monitored at 450 nm over a period of 720 s [24].

Dissociation of ribosomal subunits: Light scattering studies

Dissociation of 70S_{Ec}-free or 70S_{Ec} ribosome bound to stationary phase factors HPF or YfiA or 100S_{Ec} ribosomes, in the presence of unfolded proteins or HflX, was measured by following ribosomal light scattering (Hitachi F-2700 fluorescence spectrophotometer, Tokyo, Japan; excitation: 5 mm slit; emission: 5 mm slit; wavelength at 350 nm at 90° angle) at 16 °C temperatures. Buffers used for 70S_{Ec}-free, 70S_{Ec}-HPF and 70S_{Ec}-YfiA dissociation were Refolding Buffer: 50 mM Tris/HCl (pH 7.5), 100 mM NaCl,

MgCl₂ concentration was 7.5 mM or as stated in the figure legends and that for 100S_{Ec} dissociation was Buffer G: 10 mM Tris/HCl pH 7.5, 50 mM KCl, 10 mM NH₄Cl, 7.5 mM MgCl₂, 1 mM DTT; unfolded BCAII or HflX was mixed in stoichiometric amounts, as specified in the figure legends. For studies with HflX, 1 μM HflX was incubated with 100 μM GTP for 30 s in Buffer G with 7.5 mM MgCl₂ at room temperature ([58], with minor modifications). 0.1 μM 70S_{Ec}-free, or the 70S_{Ec} ribosome (0.1 μM) prebound to factors (1 μM), or equivalent A_{260 nm} units of 100S_{Ec} was rapidly added to the mixture, and the change in light scattering intensity was measured at 350 nm for 300 s. For studies with uBCAII, 0.1 μM 70S_{Ec}-free or the 70S_{Ec} ribosome (0.1 μM) prebound to factors (1 μM) or the 100S_{Ec} (A_{260 nm} units equivalent to 0.1 μM) ribosome was added first to the reaction mixture followed by rapid addition of uBCAII and the change in light scattering intensity was measured at 350 nm for 300 s. Conditions used for light scattering studies were followed as reported previously [19]. Similar studies were also performed with 70S_{Sa}-free and 100S_{Sa} ribosomes where dissociation of the subunits in the presence of uBCAII and in Buffer G with 7.5 mM MgCl₂ was measured under similar experimental conditions as stated above.

Sucrose density gradient centrifugation

0.5 μM uBCAII was incubated with 0.1 μM of 70S_{Ec}-free or 70S_{Ec}-HPF or 70S_{Ec}-YfiA or 100S_{Ec} ribosome (0.1 μM equivalent A_{260 nm} units) or similar concentrations of 70S_{Sa}-free or 100S_{Sa} ribosomes or in Refolding buffer or Buffer G (with 7.5 mM MgCl₂) for 5 min. After incubation, 100 μL of reaction mixtures was applied on 5 mL of a 17–25% sucrose gradient (for 70S_{Ec}-free or 70S_{Ec}-HPF or 70S_{Ec}-YfiA) prepared in the Refolding buffer and 5 mL of 10–60% sucrose gradient (for 100S_{Ec} or 70S_{Sa}-free or 100S_{Sa}) prepared in Buffer G containing MgCl₂ concentrations as mentioned in the figure legends. Samples were centrifuged at 1 98 000 *g* for 2.5 h at 4 °C for 70S_{Ec}-free, 70S_{Ec}-HPF and 70S_{Ec}-YfiA. Samples were centrifuged at 1 55 000 *g* for 3 h at 4 °C for 100S_{Ec}, 70S_{Sa}-free and 100S_{Sa} ([54], with minor modifications). The rotor used for ultracentrifugation of both gradients was MLS 50. Fractions were collected (200 μL for 17–25% sucrose gradient or 100 μL for 10–60% sucrose gradient) from the top to the bottom of the tube, and absorbance at 260 nm was measured using a UV-visible spectrophotometer. For studies with HflX, 1 μM HflX was incubated with 100 μM GTP for 30 s in Buffer G with 7.5 mM MgCl₂ at room temperature ([58] with minor modifications). 0.1 μM 70S_{Ec}-free or equivalent A_{260 nm} units of 100S_{Ec} was rapidly added to the mixture and layered on a 10–60% sucrose density gradient and the subsequent steps followed were as described above.

Ultrafiltration and dot blot analysis

Hundred microlitre of reaction mix containing 0.1 μM 70S_{Ec}-free or HPF or YfiA bound 70S_{Ec} was incubated with uBCAII (0.5 μM) at 29 °C for 10 min and then loaded on an Amicon Ultra 100 K filter. The column was washed thrice with one part of refolding buffer and three parts of HPF or YfiA binding buffer. The retained fraction was eluted by centrifuging the inverted column at 13 860 *g* for 2 min and used for dot blot. In the dot blot analysis, the PVDF membrane was soaked in methanol for 15 s followed by 1 \times PBST for 15 min before dotting the samples. Each sample was divided into two 20 μL aliquots which were dotted on two separate PVDF membranes, and the membranes were allowed to dry for 1 h at room temperature. The membranes were then blocked with 5% skimmed milk prepared in 1 \times PBST for 1 h. One membrane was then incubated with primary antibody CAII rabbit polyclonal IgG; 1 : 5000 dilution for detecting bound BCAII. The other membrane was probed with His-probe rabbit polyclonal IgG; 1 : 1000 dilution for detecting bound HPF or YfiA. Both membranes were incubated with the respective primary antibodies at 4 °C overnight. The membranes were then washed five to six times (15-min intervals) with 1 \times PBST and then incubated with secondary antibody (goat anti-rabbit IgG HRP-conjugated; 1 : 10 000 dilution) for 1.5 h at room temperature. Then, the membranes were washed with 1 \times PBST five times and incubated with chemiluminescent HRP substrate and the signal was recorded using photographic plates [19].

Preparation of cell-free extract

Escherichia coli MG1655 cells were grown, pelleted and lysed using a French press as reported earlier ([34], with minor modifications). The lysate was centrifuged at 8630 *g* for 20 min to remove the cell debris. The resulting supernatant was centrifuged at 1 40 992 *g* for 2 h at 4 °C. The pellet was discarded, and the supernatant was again centrifuged for 3 h at 4 °C, and the ribosome-deficient supernatant was stored at –80 °C [19].

Ribosome degradation experiment

The binding of HPF and YfiA to 70S_{Ec} was performed as described above, but with a 5-fold excess concentration of the factors and the ribosome. The bound complexes were then added to refolding buffer such that a 5-fold dilution occurs. Thus, the final concentrations of the factors and the ribosome were maintained at 1 and 0.1 μM , respectively, to which 0.5 μM uBCAII was added such that the final reaction volume was 10 μL . The reaction mixtures were incubated with 90 μL of cell-free extract (prepared as stated above) for 90 min at 37 °C [19,34]. Following this, the reaction mixtures were loaded on to a 17–25% sucrose

gradient (for the 70S_{Ec}-free, 70S_{Ec}-HPF and 70S_{Ec}-YfiA samples) in refolding buffer and on to a 10–60% sucrose gradient (for 100S_{Ec} samples) in Buffer G containing 7.5 mM MgCl₂. The fractions (200 μL for the 17–25% gradient and 100 μL for the 10–60% gradient) were collected from the top to the bottom, and absorbance values were measured at 260 nm using a UV-visible spectrophotometer.

Acknowledgements

We are sincerely grateful for the experimental support received from the laboratory of Dr. Sagarmoy Ghosh, Department of Microbiology, University of Calcutta. We are also grateful to Dr. Nilansu Das, Surendranath College, Kolkata, Mr. Sayan Bhakta, IICB, Kolkata and Ms. Jayshree Singh, Department of Biotechnology, St. Xavier's College (Autonomous), Kolkata, for their assistance. The research work was supported by grants from the Department of Biotechnology, West Bengal (WB-DBT) [Grant Number: 65(Sanc.)-BT/(Estt.)/RD-51/2015] and Science and Engineering Research Board, Department of Science and Technology, India (SERB-DST, India) [Grant number: EMR/2017/001101].

Conflict of interest

The authors declare no conflict of interest.

Author contributions

CB, SB and SF conceived and designed the experiments. SF and SB performed the experiments. SF, SB and CB analysed the data. JS and BKP involved in structural illustrations. SF, SB, BKP, JS and CB wrote the paper.

References

- 1 Starosta AL, Lassak J, Jung K & Wilson DN (2014) The bacterial translation stress response. *FEMS Microbiol Rev* **38**, 1172–1201.
- 2 Matzov D, Bashan A, Yap MNF & Yonath A (2019) Stress response as implemented by hibernating ribosomes: a structural overview. *FEBS J* **286**, 3558–3565.
- 3 Wilson DN & Nierhaus KH (2007) The weird and wonderful world of bacterial ribosome regulation. *Crit Rev Biochem Mol Biol* **42**, 187–219.
- 4 Prossliner T, Skovbo Winther K, Sørensen MA & Gerdes K (2018) Ribosome hibernation. *Annu Rev Genet* **52**, 321–348.
- 5 Vila-Sanjurjo A, Schuwirth BS, Hau CW & Cate JHD (2004) Structural basis for the control of translation

- initiation during stress. *Nat Struct Mol Biol* **11**, 1054–1059.
- 6 Agafonov DE, Kolb VA, Nazimov IV & Spirin AS (1999) A protein residing at the subunit interface of the bacterial ribosome. *Proc Natl Acad Sci USA* **96**, 12345–12349.
- 7 Ueta M, Yoshida H, Wada C, Baba T, Mori H & Wada A (2005) Ribosome binding proteins YhbH and YfiA have opposite functions during 100S formation in the stationary phase of *Escherichia coli*. *Genes Cells* **10**, 1103–1112.
- 8 Durfee T, Hansen AM, Zhi H, Blattner FR & Ding JJ (2008) Transcription profiling of the stringent response in *Escherichia coli*. *J Bacteriol* **190**, 1084–1096.
- 9 Gohara DW & Yap MNF (2018) Survival of the drowsiest: the hibernating 100S ribosome in bacterial stress management. *Curr Genet* **64**, 753–760.
- 10 Yamagishi M, Matsushima H, Wada A, Sakagami M, Fujita N & Ishihama A (1993) Regulation of the *Escherichia coli* RMF gene encoding the ribosome modulation factor: growth phase- and growth rate-dependent control. *EMBO J* **12**, 625–630.
- 11 Basu A & Yap MNF (2016) Ribosome hibernation factor promotes Staphylococcal survival and differentially represses translation. *Nucleic Acids Res* **44**, 4881–4893.
- 12 Deutscher MP (2003) Degradation of stable RNA in bacteria. *J Biol Chem* **278**, 45041–45044.
- 13 Deutscher MP (2009) Chapter 9 maturation and degradation of ribosomal RNA in bacteria. *Prog Mol Biol Transl Sci* **85**, 369–391.
- 14 El-Sharoud WM (2004) Ribosome inactivation for preservation: concepts and reservations. *Sci Prog* **87**, 137–152.
- 15 Piir K, Paier A, Liiv A, Tenson T & Maiväli Ü (2011) Ribosome degradation in growing bacteria. *EMBO Rep* **12**, 458–462.
- 16 Basu A, Shields KE, Eickhoff CS, Hoft DF & Yap MNF (2018) Thermal and nutritional regulation of ribosome hibernation in *Staphylococcus aureus*. *J Bacteriol* **200**, e00426–18.
- 17 Basu A, Samanta D, Bhattacharya A, Das A, Das D & DasGupta C (2008) Protein folding following synthesis *in vitro* and *in vivo*: association of newly synthesized protein with 50S subunit of *E. coli* ribosome. *Biochem Biophys Res Commun* **366**, 592–597.
- 18 Basu A, Samanta D, Das D, Chowdhury S, Bhattacharya A, Ghosh J, Das A & DasGupta C (2008) *In vitro* protein folding by *E. coli* ribosome: unfolded protein splitting 70S to interact with 50S subunit. *Biochem Biophys Res Commun* **366**, 598–603.
- 19 Pathak BK, Banerjee S, Mondal S, Chakraborty B, Sengupta J & Barat C (2017) Unfolded protein exhibits antiassociation activity toward the 50S subunit facilitating 70S ribosome dissociation. *FEBS J* **284**, 3915–3930.
- 20 Das D, Das A, Samanta D, Ghosh J, Dasgupta S, Bhattacharya A, Basu A, Sanyal S & DasGupta C (2008) Role of the ribosome in protein folding. *Biotechnol J* **3**, 999–1009.
- 21 Mondal S, Pathak BK, Ray S & Barat C (2014) Impact of P-Site tRNA and antibiotics on ribosome mediated protein folding: studies using the *Escherichia coli* ribosome. *PLoS One* **9**, e101293.
- 22 Chattopadhyay S, Das B & Dasgupta C (1996) Reactivation of denatured proteins by 23S ribosomal RNA: role of domain V. *Proc Natl Acad Sci USA* **93**, 8284–8287.
- 23 Kudlicki W, Coffman A, Kramer G & Hardesty B (1997) Ribosomes and ribosomal RNA as chaperones for folding of proteins. *Fold Des* **2**, 101–108.
- 24 Pathak BK, Mondal S, Ghosh AN & Barat C (2014) The ribosome can prevent aggregation of partially folded protein intermediates: studies using the *Escherichia coli* ribosome. *PLoS One* **9**, e96425.
- 25 Polikanov YS, Blaha GM & Steitz TA (2012) How hibernation factors RMF, HPF, and YfiA turn off protein synthesis. *Science* **336**, 915–918.
- 26 Pang Y, Kurella S, Voisset C, Samanta D, Banerjee D, Schabe A, Das Gupta C, Galons H, Blondel M & Sanyal S (2013) The antiprion compound 6-aminophenanthridine inhibits the protein folding activity of the ribosome by direct competition. *J Biol Chem* **288**, 19081–19089.
- 27 Beckert B, Turk M, Czech A, Berninghausen O, Beckmann R, Ignatova Z, Plitzko JM & Wilson DN (2018) Structure of a hibernating 100S ribosome reveals an inactive conformation of the ribosomal protein S1. *Nat Microbiol* **3**, 1115–1121.
- 28 Maki Y, Yoshida H & Wada A (2000) Two proteins, YfiA and YhbH, associated with resting ribosomes in stationary phase *Escherichia coli*. *Genes Cells* **5**, 965–974.
- 29 Basu A & Yap MNF (2017) Disassembly of the *Staphylococcus aureus* hibernating 100S ribosome by an evolutionarily conserved GTPase. *Proc Natl Acad Sci USA* **114**, E8165–E8173.
- 30 Ueta M, Wada C & Wada A (2010) Formation of 100S ribosomes in *Staphylococcus aureus* by the hibernation promoting factor homolog SaHPF. *Genes Cells* **15**, 43–58.
- 31 Nierhaus KH (2014) Mg²⁺, K⁺, and the ribosome. *J Bacteriol* **196**, 3817–3819.
- 32 Kiel MC, Kaji H & Kaji A (2007) Ribosome recycling: an essential process of protein synthesis. *Biochem Mol Biol Educ* **35**, 40–44.
- 33 Zhang Y, Mandava CS, Cao W, Li X, Zhang D, Li N, Zhang Y, Zhang X, Qin Y, Mi K *et al.* (2015) HflX is

- a ribosome-splitting factor rescuing stalled ribosomes under stress conditions. *Nat Struct Mol Biol* **22**, 906.
- 34 Zundel MA, Basturea GN & Deutscher MP (2009) Initiation of ribosome degradation during starvation in *Escherichia coli*. *RNA* **15**, 977–983.
- 35 Nguyen VT, Morange M & Bensaude O (1989) Protein denaturation during heat shock and related stress. *Escherichia coli* β -galactosidase and *Photinus pyralis* luciferase inactivation in mouse cells. *J Biol Chem* **264**, 10487–10492.
- 36 Shcherbakova K, Nakayama H & Shimamoto N (2015) Role of 100S ribosomes in bacterial decay period. *Genes Cells* **20**, 789–801.
- 37 Franken LE, Oostergetel GT, Pijning T, Puri P, Arkhipova V, Boekema EJ, Poolman B & Guskov A (2017) A general mechanism of ribosome dimerization revealed by single-particle cryo-electron microscopy. *Nat Commun* **8**, 1–11.
- 38 Docter BE, Horowitz S, Gray MJ, Jakob U & Bardwell JCA (2016) Do nucleic acids moonlight as molecular chaperones? *Nucleic Acids Res* **44**, 4835–4845.
- 39 Seong IC, Ryu K & Seong BL (2009) RNA-mediated chaperone type for *de novo* protein folding. *RNA Biol* **6**, 21–24.
- 40 Horowitz S & Bardwell JCA (2016) RNAs as chaperones. *RNA Biol* **13**, 1228–1231.
- 41 Kovachev PS, Banerjee D, Rangel LP, Eriksson J, Pedrote MM, Martins-Dinis MMDC, Edwards K, Cordeiro Y, Silva JL & Sanyal S (2017) Distinct modulatory role of RNA in the aggregation of the tumor suppressor protein p53 core domain. *J Biol Chem* **292**, 9345–9357.
- 42 Son A, Il Choi S, Han G & Seong BL (2015) M1 RNA is important for the in-cell solubility of its cognate C5 protein: implications for RNA-mediated protein folding. *RNA Biol* **12**, 1198–1208.
- 43 Vendruscolo M (2012) Proteome folding and aggregation. *Curr Opin Struct Biol* **22**, 138–143.
- 44 Saibil H (2013) Chaperone machines for protein folding, unfolding and disaggregation. *Nat Rev Mol Cell Biol* **14**, 630–642.
- 45 Tran QH & Uden G (1998) Changes in the proton potential and the cellular energetics of *Escherichia coli* during growth by aerobic and anaerobic respiration or by fermentation. *Eur J Biochem* **251**, 538–543.
- 46 Mujacic M & Baneyx F (2006) Regulation of *Escherichia coli* hchA, a stress-inducible gene encoding molecular chaperone Hsp31. *Mol Microbiol* **60**, 1576–1589.
- 47 Tsai CJ, Aslam K, Drendel HM, Asiago JM, Goode KM, Paul LN, Rochet JC & Hazbun TR (2015) Hsp31 is a stress response chaperone that intervenes in the protein misfolding process. *J Biol Chem* **290**, 24816–24834.
- 48 Chakraborty B, Bhakta S & Sengupta J (2016) Disassembly of yeast 80S ribosomes into subunits is a concerted action of ribosome-assisted folding of denatured protein. *Biochem Biophys Res Commun* **469**, 923–929.
- 49 Liu Q & Fredrick K (2016) Intersubunit bridges of the bacterial ribosome. *J Mol Biol* **428**, 2146–2164.
- 50 McKay SL & Portnoy DA (2015) Ribosome hibernation facilitates tolerance of stationary-phase bacteria to aminoglycosides. *Antimicrob Agents Chemother* **59**, 6992–6999.
- 51 Baba T, Ara T, Hasegawa M, Takai Y, Okumura Y, Baba M, Datsenko KA, Tomita M, Wanner BL & Mori H (2006) Construction of *Escherichia coli* K-12 in-frame, single-gene knockout mutants: the Keio collection. *Mol Syst Biol* **2**, 2006.0008. <https://doi.org/10.1038/msb4100050>
- 52 Dey S, Biswas C & Sengupta J (2018) The universally conserved GTPase HflX is an RNA helicase that restores heat-damaged *Escherichia coli* ribosomes. *J Cell Biol* **217**, 2519–2529.
- 53 Das B, Chattopadhyay S, Bera AK & Dasgupta C (1996) *In vitro* protein folding by ribosomes from *Escherichia coli*, wheat germ and rat liver: the role of the 50S particle and its 23S rRNA. *Eur J Biochem* **235**, 613–621.
- 54 Beckert B, Abdelshahid M, Schäfer H, Steinchen W, Arenz S, Berninghausen O, Beckmann R, Bange G, Turgay K & Wilson DN (2017) Structure of the *Bacillus subtilis* hibernating 100S ribosome reveals the basis for 70S dimerization. *EMBO J* **36**, 2061–2072.
- 55 Khusainov I, Vicens Q, Ayupov R, Usachev K, Myasnikov A, Simonetti A, Validov S, Kieffer B, Yusupova G, Yusupov M *et al.* (2017) Structures and dynamics of hibernating ribosomes from *Staphylococcus aureus* mediated by intermolecular interactions of HPF. *EMBO J* **36**, 2073–2087.
- 56 Dos Reis S, Pang Y, Vishnu N, Voisset C, Galons H, Blondel M & Sanyal S (2011) Mode of action of the antiprion drugs 6AP and GA on ribosome assisted protein folding. *Biochimie* **93**, 1047–1054.
- 57 Pal S, Chandra S, Chowdhury S, Sarkar D, Ghosh AN & Das Gupta C (1999) Complementary role of two fragments of domain V of 23 S ribosomal RNA in protein folding. *J Biol Chem* **274**, 32771–32777.
- 58 Coatham ML, Brandon HE, Fischer JJ, Schümmer T & Wieden HJ (2015) The conserved GTPase HflX is a ribosome splitting factor that binds to the E-site of the bacterial ribosome. *Nucleic Acids Res* **44**, 1952–1961.

OPEN

Tau protein- induced sequestration of the eukaryotic ribosome: Implications in neurodegenerative disease

Senjuti Banerjee¹, Sehnaz Ferdosh¹, Amar Nath Ghosh² & Chandana Barat^{1*}

The human tau is a microtubule-associated intrinsically unstructured protein that forms intraneuronal cytotoxic deposits in neurodegenerative diseases, like tauopathies. Recent studies indicate that in Alzheimer's disease, ribosomal dysfunction might be a crucial event in the disease pathology. Our earlier studies had demonstrated that amorphous protein aggregation in the presence of ribosome can lead to sequestration of the ribosomal components. The present study aims at determining the effect of incubation of the full-length tau protein (Ht40) and its microtubule binding 4-repeat domain (K18) on the eukaryotic ribosome. Our *in vitro* studies show that incubation of Ht40 and the K18 tau variants with isolated non-translating yeast ribosome can induce a loss of ribosome physical integrity resulting in formation of tau-rRNA-ribosomal protein aggregates. Incubation with the tau protein variants also led to a disappearance of the peak indicating the ribosome profile of the HeLa cell lysate and suppression of translation in the human *in vitro* translation system. The incubation of tau protein with the ribosomal RNA leads to the formation of tau-rRNA aggregates. The effect of K18 on the yeast ribosome can be mitigated in the presence of cellular polyanions like heparin and tRNA, thereby indicating the electrostatic nature of the aggregation process.

Protein aggregate formation and their intracellular accumulation are associated with a wide range of neurodegenerative proteinopathies. The Alzheimer's disease (AD) is a neurodegenerative disease characterised by formation of neurofibrillary tangles (NFTs) that are composed of hyperphosphorylated tau proteins¹. In addition to Alzheimer's disease, abnormal aggregation of the tau protein has been linked to the pathogenesis of more than 20 other neurodegenerative disorders, collectively termed as tauopathies¹. Although a link between pathological tau aggregation and cognitive impairment has been established, the mechanism by which tau aggregation causes neuronal dysfunction is unclear.

Several lines of evidence suggest that the ribosome is a cellular interacting partner of the tau protein. Earlier immunohistochemical studies using tau specific antibody have demonstrated that, there is an association of the tau protein with both, the microtubule and the ribosome in the neuronal cells². More recent studies of the human tau interactome have also revealed a robust association of the tau protein with the ribonucleoproteome and these studies have indicated at the preferential association of the full-length tau protein Ht40 to the 80S ribosome³. Although aggregation of the tau protein is the primary event in AD, it has also been demonstrated that the impairment of cellular translation and ribosome dysfunction, due to tau-ribosome interaction, is an early event in the disease. Such disruption of protein synthesis machinery might contribute towards the neuronal loss which characterises the disease⁴. This is also in agreement with earlier studies which noted that a decline in protein synthesis and ribosome function is initiated during mild cognitive impairment (MCI) that develops into AD^{5,6}. Although a profound loss in the ribosomal complexes in the affected regions of the brain have been shown to occur in parallel to the progression of the disease⁷, the reasons underlying the disappearance of the ribosomal peaks is not completely understood.

The tau protein is a microtubule associated protein that promotes the assembly and stabilization of the microtubule structure⁸. Hence, tau mediated neurodegeneration might arise due to either the loss of physiological

¹Department of Biotechnology, St. Xavier's College, Park Street, Kolkata, 700016, West Bengal, India. ²National Institute of Cholera and Enteric Diseases P-33, C.I.T. Road, Scheme XM, Belehghata, India. *email: chandanasgb@yahoo.com

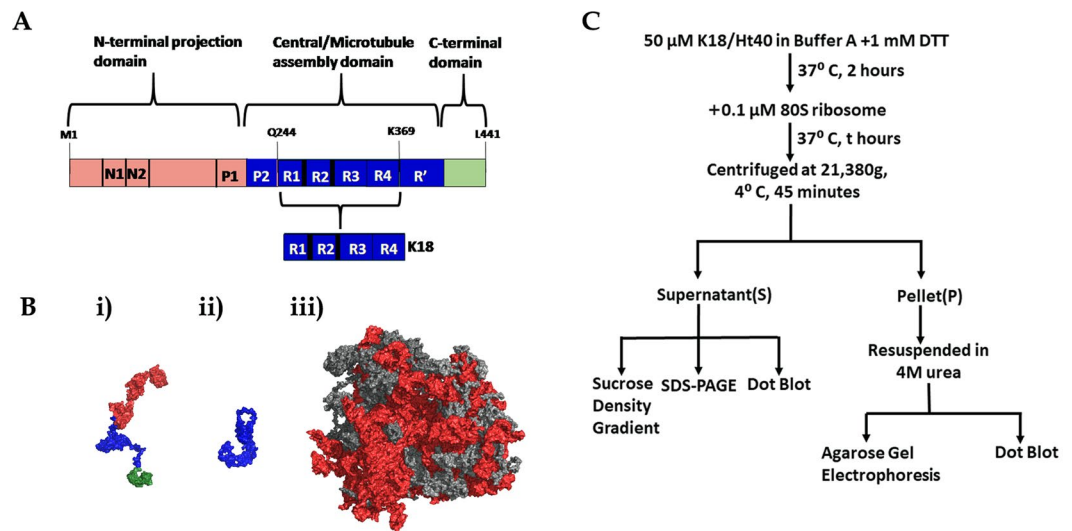


Figure 1. Structure of human full-length Tau and the yeast ribosome. **(A)** A schematic representation of the Tau protein: Schematic diagram of the human full-length tau protein Ht40 and its microtubule binding repeat domain K18, highlighting the functional and electrostatic differences between its domains. The “N terminal domain” has a calculated net negative charge of -14.9 (red), the “Central domain” has a calculated net positive charge of $+20.1$ (blue) and the “C-terminal domain” has a nominal negative charge of -3.1 (green). The R1, R2, R3 and R4 sequences constitute the K18 protein (blue) which has calculated a net charge of $+10$. All charges are calculated at pH 7.5 using PROTEIN CALCULATOR v3.4. **(B)** Surface representation of the Ht40 and K18 model structures obtained using *i*-TASSER and *Saccharomyces Cerevisiae* ribosome (PDB ID: 3Z22 and 3O58) [using PYMOL 2008 (De Lano Scientific, Palo Alto, CA, USA, available at: <http://www.pymol.org>]. The models of Ht40 (Radius of gyration: 6.5 ± 0.3 nm; Mylonas *et al.*, Biochemistry, 2008) and K18 (Radius of gyration: 3.8 ± 0.3 nm; Mylonas *et al.*, Biochemistry, 2008) displayed here were chosen based on the C-score. (i) Ht40 model: The N terminal domain has been represented in red, the positively charged central domain is represented in blue and the C terminal domain is represented in green (The colour coding is same as in A); (ii) Model of K18; (iii) Solvent exposed surface of the yeast 80S ribosome subunit (PDB ID: 3Z22 and 3O58). The rRNA is represented in red and the ribosomal proteins are represented in gray. **(C)** An outline of the experimental procedures followed in this study is depicted in the form of a flowchart.

function or the gain of toxic function. Tau aggregation would abolish its microtubule stabilizing function and hence, impair neuronal transport. However, the absence of significant neuronal abnormalities in tau knock-out mice⁹ have suggested that the loss of tau function may be less critical and the gain of toxic function in the process of tau aggregate formation might be the key factor in neurodegeneration. Several recent evidences also suggest that sequestration of cellular interacting partners (proteins or RNA) by protein aggregates could contribute to pathogenesis in a wide spectrum of neurodegenerative diseases¹⁰. The fact, that the intrinsically unstructured tau protein is capable of interacting with polyanionic cofactors like heparin¹¹ and cellular RNAs¹², raises the possibility that the tau protein is also capable of interacting with highly charged macromolecular complexes such as the ribosome. Our earlier studies had shown that the partial unfolding or amorphous aggregation of lysozyme and Bovine Carbonic Anhydrase II (BCAII), in the presence of empty non-translating prokaryotic or eukaryotic ribosome, could induce aggregation of ribosomal components¹³. Hence, based on these observations, the present study aims at determining the effect of incubation of the tau protein on the physical integrity of the eukaryotic 80S ribosome.

Our *in vitro* experiments demonstrate that the incubation of tau variants (K18 and Ht40) with the eukaryotic yeast 80S ribosome leads to a dose dependent and progressive loss of ribosomal peak, that is indicative of the loss of ribosome population. A disappearance of the ribosome peak and decline in *in vitro* translation ability of the HeLa cell lysate containing the human ribosome is also observed upon incubation with the tau variants, indicating a similar loss of physical integrity of the human ribosome. The incubation of the tau variants with isolated yeast ribosomal RNA leads to the formation of large tau-rRNA containing aggregates. Studies have also been performed on the effect of the cellular polyanions like heparin and tRNA (that are known tau protein interactors) on the outcome of Ht40- and K18- ribosome co-aggregation.

Results

Structure and electrostatics of human tau protein and yeast ribosome. Electrostatics have been shown to play a major role in determining the interactions of tau with its cellular partners¹⁴. Intrinsically unstructured proteins are also known to engage in non-native electrostatic interactions with their cognate cellular partners¹⁵. The electrostatic features of the tau protein variants used in our study and the ribosomes, which therefore might play a major role in the tau-ribosome interaction, is highlighted in Fig. 1. Figure 1A shows the full-length isoform of the tau protein Ht40 and its subdomain K18, whose effect on the ribosome forms the subject of this

study. The longest isoform of human Tau, 2N4R or Ht40, is divided into 3 functional domains: (a) the projection domain consisting of the N-terminal acidic region and proline rich domains, (b) the central microtubule assembly domain containing the pseudo-repeat regions and (c) the C terminal domain¹¹. The full length tau protein has been colour coded based on the predominant charges of its corresponding domains and highlights that the Ht40 is a dipole with oppositely charged domains. The wide variability in the pI of the domains results in a considerable difference in their net charge at physiological pH¹⁶. This renders the N-terminal domain acidic (red), the central domain basic (blue) and the C-terminal domain neutral (green) as shown in Fig. 1A. The positively charged K18 tau variant, that corresponds to the central microtubule binding repeat domains (R1, R2, R3 and R4), is represented in blue. The conformation of the two tau variants, Ht40 and K18 as predicted by the I-TASSER server^{17–19}, is shown in Fig. 1Bi,Bii and the colour coding of the domains based on the net charge is the same as in Fig. 1A. The ribosomal RNA (rRNA) present in the solvent exposed surfaces of the yeast 80S ribosome has been highlighted in red (Fig. 1Biii). Electrostatic calculations have indeed revealed that the ribosome surface is predominantly negatively charged²⁰ and the rRNA has a major contribution in negative electrostatic potential of the ribosome²¹. A flowchart denoting the basic procedure of the *in vitro* experiments performed in the study discussed below is shown in Fig. 1C and detailed in the “Materials and methods section”.

Effect of Tau on eukaryotic ribosomes. As stated in the introduction section, the effect of incubation of the tau protein on the eukaryotic 80S ribosome is the principal objective of the present study. As stated earlier, the flowchart in Fig. 1C outlines the basic procedures that have been followed, in which 50 μM of reduced tau variants (Ht40 and K18) were incubated with 0.1 μM of purified yeast 80S ribosome under physiological conditions, (37 °C and pH 7.5: materials and methods). The conditions of the experiments with respect to concentrations of the tau variants and the salt concentrations used, were optimum for tau aggregation²². However, no additional cellular polyanions that are necessary for inducing tau aggregation were present during the incubation. The centrifugal speed used in our study differs from the speed used earlier in polyA RNA induced tau aggregation studies²³, for separation of monomeric tau from tau-RNA aggregates. At this speed (1,00,000 g), the ribosome or rRNA alone is pelleted irrespective of the presence of the tau proteins. Hence, at the centrifugal speed used in our studies (21,380 g), the larger aggregates would form the pellet (P) while the supernatant (S) might be constituted of the residual ribosomes and smaller aggregates. In our initial experiments the tau variants were incubated with the ribosome for 6 hours. The supernatant fractions obtained after Ht40-80S and K18-80S incubation were analysed by sucrose density gradient centrifugation (SDGC) and the $A_{260\text{ nm}}$ profile obtained was compared to the profile of equivalent amount of untreated yeast 80S ribosome. As shown in Fig. 2Ai, a significant reduction in the ribosomal peak and a simultaneous appearance of peaks of ribonucleoprotein particles with lower sedimentation coefficients was observed when the ribosome was incubated with the tau protein variants. The disappearance of the ribosome peak might thereby indicate a global disassembly of the 80S ribosome and aggregation of its components that is also suggested by the experiments discussed in the next section.

The constituents of the pellet and supernatant fractions were also analysed using electrophoretic methods. Agarose gel electrophoretic analysis of the pellet fractions (Fig. 2Aii) showed that the aggregates in the pellet [that were formed in the presence of the tau variants (Ht40 and K18)] constituted of a major proportion of the ribosomal RNA. The method used for agarose gel electrophoresis is as described in the “Materials and methods” section. This method enables us to visualise the total rRNA present in the ribosome as a single consolidated band, as has been used in previous studies on tau-rRNA interactions²⁴. In the presence of suitable controls, this method has also been used in our earlier studies as a semi-quantitative technique for following protein-ribosome aggregation process¹³. Similarly, analysis of the protein components of the pellet and the supernatant fractions by denaturing SDS-PAGE was also done which showed that upon incubation of the 80S ribosome with the tau variants K18 and Ht40 (for 6 hours), the presence of ribosomal proteins was observed, both in the supernatant as well as in the pellet (Fig. 2Aiii). Control experiments were performed in which the yeast ribosome (0.1 μM) was incubated in the presence of the native bovine carbonic anhydrase II (nBCAII) protein (50 μM), under similar conditions, and centrifugation was performed as stated earlier. As shown in Fig. 2Aii, insignificant amount of ribosomal RNA was observed in the pellet, thereby indicating that the large rRNA containing aggregates were formed, specifically when the ribosome is incubated with the tau proteins. Also, upon incubation of 80S ribosome with native BCAII under similar conditions, all the ribosomal proteins were retained in the supernatant fraction (Fig. 2Aiii), thus reaffirming that aggregation of ribosomal components is subject to the specific presence of the tau protein variants. Additional experiments performed, showed that the 80S ribosome was retained in the supernatant when incubated alone or with DTT under similar conditions as stated above (Fig. S1A). Further control experiments were performed to verify whether a contaminant that co-purified during recombinant expression and purification of the tau protein might have led to ribosome aggregation. As described in the “materials and methods” section, the *E. coli* cells expressing the tau protein variants were lysed using the “direct boiling method” and the cellular extract obtained ($A_{280\text{ nm}}$ units equivalent to 50 μM of K18) was incubated with 0.1 μM yeast 80S ribosome for 6 hours and centrifuged. As shown in Fig. S1B, no ribosomal proteins were present in the pellet fraction at the speed of centrifugation used in our studies thus confirming that the aggregation of ribosomal components was specific to the presence of tau protein variants and not caused by any contaminant contributed by the cell extract.

Surprisingly, it was noted from the SDS PAGE profile that both K18 and Ht40 appeared to be present in the supernatant fraction (Fig. 2Aiii). This might be due to the limited period (6 hrs) for which the tau protein had been incubated with the ribosome during which all the tau protein had not been included in the large aggregates, which constitute the pellet. Hence, the time period of tau-ribosome incubation was extended to 24 hours, in order for the process to reach completion, and centrifuged. The presence of K18 and Ht40 in the supernatant and the pellet was analysed by dot-blot analysis using K18 and Ht40 specific monoclonal antibodies (materials and methods). The total rRNA content of the supernatant was also estimated using $A_{260\text{ nm}}$ values. As shown in

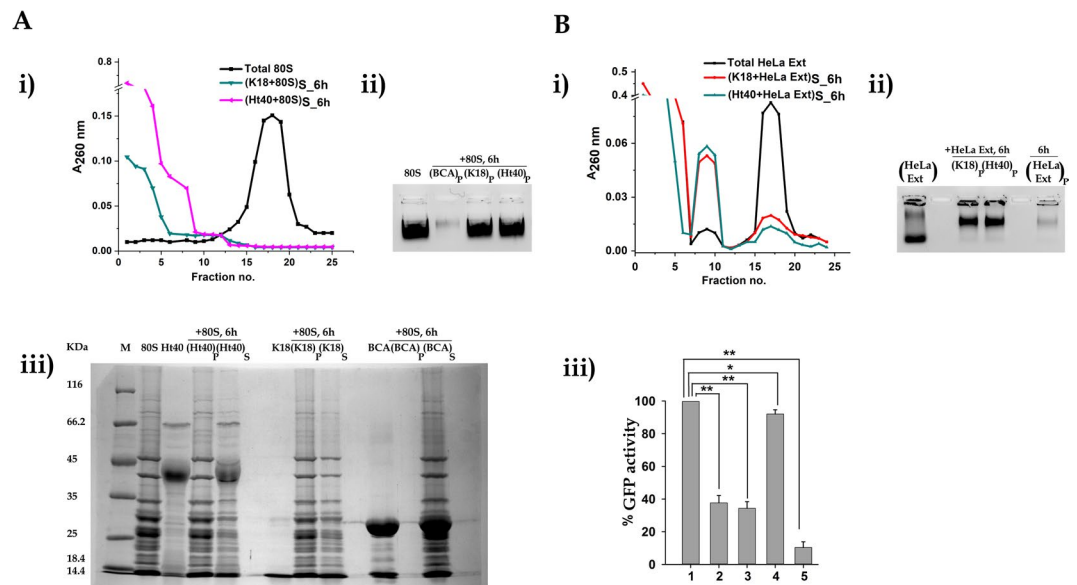


Figure 2. Effect of tau on eukaryotic ribosome. Effect of tau variants K18 or Ht40 on eukaryotic ribosome was studied using the procedure outlined schematically in Figure 1C. Briefly, 0.1 μM purified yeast 80S ribosome was incubated with 50 μM tau variant for 6 hours at 37 $^{\circ}\text{C}$ in Buffer A (25 mM Tris-HCl pH 7.5, 50 mM NaCl, 5 mM MgCl_2) and the resultant reaction mixture was centrifuged. The supernatant fractions were analysed using sucrose density gradient centrifugation (SDGC). The sedimentation profile of the ribosome in the supernatant fraction was obtained by plotting $A_{260\text{ nm}}$ against the fraction number (“S” in the subscript indicates the supernatant fraction and the number indicates the time of incubation in hours). Disappearance of the ribosomal peak was observed when the 80S ribosome was incubated with K18 or Ht40 (Ai). The pellet fractions (indicated by “P” in the subscript along with appropriate time of incubation denoted in hours) were resuspended in 4 M Urea containing Buffer A and analysed for the presence of Aii) ribosomal RNA (using 0.8% agarose gel electrophoresis) and for Aiii) ribosomal protein (using 12% SDS PAGE: materials and methods). Control experiments were performed where yeast 80S ribosome was similarly incubated in presence of native BCAII (BCA), centrifuged and analysed using electrophoretic methods (Aii, Aiii). **(A) Effect of tau variants on purified yeast 80S ribosome.** (i) Sedimentation profile of the supernatant: (1) Total 80S ribosome (■), (2) (K18 + 80S)_{S_6h} (▼), (3) (Ht40 + 80S)_{S_6h} (◄). (ii) Agarose gel electrophoretic analysis of pellet for the presence of ribosomal RNA; lanes from left to right contain: (1) Total 80S, (2) (BCA + 80S)_{P_6h}, (3) (K18 + 80S)_{P_6h}, (4) (Ht40 + 80S)_{P_6h}. (iii) SDS PAGE analysis of the pellet and supernatant for the presence of ribosomal proteins; lanes from left to right contain: (1) Molecular weight marker, (2) Total 80S, (3) Ht40 total protein, (4) (Ht40 + 80S)_{P_6h}, (5) (Ht40 + 80S)_{S_6h}, (6) Blank, (7) K18 total protein, (8) (K18 + 80S)_{P_6h}, (9) (K18 + 80S)_{S_6h}, (10) Blank, (11) BCAII total protein, (12) (nBCAII + 80S)_{P_6h}, (13) (nBCAII + 80S)_{S_6h}, (14) Blank. **(B) Effect of tau variants on human 80S ribosomes present in HeLa cell lysate.** The HeLa cell lysate or extract (ext) used in our experiments is a component of the human IVT kit. (i) Equivalent $A_{260\text{ nm}}$ units (to 0.1 μM of yeast 80S ribosome) of HeLa cell lysate was incubated in the presence of 50 μM K18 or Ht40 for 6 hours, under reducing conditions, at 37 $^{\circ}\text{C}$ and the resultant reaction mixture was analysed as stated in materials and methods. (i) Sedimentation profile of HeLa extract (ext) in the supernatant fraction; Total HeLa ext (■), (K18 + HeLa ext)_{S_6h} (●), (Ht40 + HeLa ext)_{S_6h} (▲). (ii) Agarose gel electrophoretic analysis of pellet for the presence of RNA; Lanes from left to right contain: (1) Total HeLa ext, (2) Blank, (3) (K18 + HeLa ext)_{P_6h}, (4) (Ht40 + HeLa ext)_{P_6h}, (5) Blank, (6) (HeLa ext)_{P_6h}. (iii) *In vitro* transcription-translation assay using human coupled IVT kit and tau variants. 50 μM K18 or Ht40 or nBCAII was added to the reaction mixture of human *in vitro* translation system and incubated at 30 $^{\circ}\text{C}$ for 6 hours (as prescribed by the manufacturer). Bar graphs show the percentage GFP activity in the presence and absence of tau protein variants. The GFP fluorescence activity observed in the reaction mix containing the plasmid and neither of the tau variants is considered as 100%. (1) + GFP plasmid, (2) 50 μM K18 + GFP plasmid, (3) 50 μM Ht40 + GFP plasmid, (4) 50 μM nBCAII + GFP plasmid, (5) - GFP plasmid. The experiment has been repeated thrice and the data are presented as means \pm SEM; *P < 0.05 or **P < 0.001 in one-way ANOVA (N = 3).

Fig. S1Ci,ii, both K18 and Ht40 are present in the pellet as well as in the supernatant and a significant proportion of the total rRNA is also retained in the supernatant (Fig. S1Ciii). Electron microscopy of an aliquot of the supernatant obtained by centrifugation after 24 hours of K18–80S incubation also showed the presence of aggregates (Fig. S1Civ), lending support to the fact that at the centrifugal speed used in our experiments, a proportion of ribosome-tau aggregates is still retained in the supernatant fraction. Thus, it is possible that the supernatant contains small co-aggregates of tau and ribosomal components. Taken together, these studies do however establish that the Tau protein is the initiator of ribosome disassembly and aggregation of ribosomal components. Further experiments were performed to study the dependence of tau-ribosome aggregation on the concentration of the

tau protein present. As shown in Fig. S1Di,ii,S1Ei,ii, the dose dependent reduction of the 80S ribosome peak and increase in appearance of the ribosomal RNA in the insoluble fraction occurs in presence of increasing concentration of both variants of the tau protein (K18 and Ht40) and the ribosome. Therefore, it could be implied that upon increasing the concentration of the tau protein (condition that promotes tau aggregation), the extent of tau induced ribosome aggregation is also increased.

It should be noted that the tau protein is a major protein of the human neuronal cells. Hence, whether this protein has a similar effect on the human ribosome as well, needed to be addressed. In order to study the effect of the tau protein on human ribosomes, the tau variants were incubated with the cell lysate obtained from the HeLa cell line (Materials and Methods). This cell lysate represents a heterogeneous system that includes the translational machinery as one of its significant components and the $A_{260\text{ nm}}$ profile obtained by sucrose density centrifugation can reflect the total ribosomal population present in the lysate. Hence, in our subsequent experiment, the HeLa cell lysate containing $0.1\ \mu\text{M}$ equivalent $A_{260\text{ nm}}$ units was incubated with $50\ \mu\text{M}$ of tau proteins K18 or Ht40 for 6 hours, centrifuged and the $A_{260\text{ nm}}$ profile (obtained by SDGC) of the supernatant was compared to that of the untreated lysate. A significant alteration of the $A_{260\text{ nm}}$ profile (Fig. 2Bi) and an accumulation of sub-ribonucleoprotein particles was observed upon incubation of the lysate with the tau protein. The pellet obtained after centrifugation of the aggregation mix contained a significant amount of the RNA (a substantial proportion of which is rRNA²⁵) (Fig. 2Bii) and of proteins present in the cell extract (Fig. S1Fi). In presence of the tau variants, a concomitant reduction of cellular RNA is observed in the supernatant fraction as analysed using agarose gel electrophoresis (Fig. S1Fii). However, the additional peak in the SDGC profile (Fig. 2Bi) and the shift in the mobilities of the RNA (Fig. 2Bii) that is observed only in the presence of the tau proteins need to be further investigated. The effect of the tau proteins on the translational ability of the HeLa cell lysate was also analysed. In this study, GFP was used as a reporter gene (Materials and methods). As shown in Fig. 2Biii, the fluorescence activity of the GFP reporter protein, measured 6 hours after the initiation of translation, was significantly reduced in the presence of the ($50\ \mu\text{M}$) tau protein variants. No significant change in GFP activity was observed in presence of equivalent amounts of the native BCAL1 protein. Earlier studies had also indicated that the tau protein might possess the ability to modulate the translation process^{4,26}. Hence the translational suppression in presence of the tau protein variants implies that the loss of physical integrity of the ribosomal population (as observed by change in $A_{260\text{ nm}}$ profile in Fig. 2Bi) is also reflected in the loss of functional integrity of the ribosome.

Although, further *in vitro* and *in vivo* experiments need to be performed with purified human ribosomes and disease affected neurons respectively, our studies imply that tau-ribosome interaction could underlie the change in ribosome profile observed in diseased neurons. Further, based on the observed similarity in the effect of tau variants on both yeast and human ribosomes and the fact that yeast is established as a model system for studies of neurodegenerative diseases²⁷, all subsequent experiments in this study were performed with purified yeast 80S ribosome.

Time course of tau induced ribosome aggregation. In order to explore the time course followed by the tau-ribosome aggregation process, the tau-variants ($50\ \mu\text{M}$) were incubated with the ribosome ($0.1\ \mu\text{M}$) for different time periods and centrifuged. The supernatant and pellet fractions were analysed by SDGC and gel electrophoresis. The sucrose density gradient profiles of the supernatants in Fig. 3Ai,Aii show that for increasing periods of K18–80S and Ht40–80S incubation, a progressive disappearance of the ribosomal peak with the appearance of small ribonucleoprotein particles is observed. Agarose gel electrophoresis of the corresponding pellets also showed an increase in intensity of the rRNA band, upon increasing the time of tau-ribosome incubation for both K18 (Fig. 3Bi) and Ht40 (Fig. 3Bii). The supernatant and pellet fractions obtained at selected time points after initiation of tau-ribosome incubation, were also analysed using denaturing SDS-PAGE in order to determine the presence of ribosomal proteins. A time dependant appearance of the overall ribosomal proteins in the pellet with their reduction in the supernatant is observed (Fig. S2Ai,ii). These observations indicate that at a high tau:80S ratio of 500:1, a process of global disassembly of the 80S ribosome might be initiated with the formation small and large aggregates constituted of tau and ribosomal components. The tau- ribosome aggregation process, visualized by low resolution electron microscopy (materials and methods), also shows the formation of large heterogeneous aggregates at 24 hours of tau-ribosome incubation (Fig. S2B,C) while no such aggregation was apparent when the tau variants were incubated alone in the absence of ribosome (Fig. S2D). Our preliminary studies, as stated above, shows that the tau protein, which initiates the process of disassembly and aggregation of the ribosomal components, is present both in the supernatant and pellet. However, further studies need to be performed in order to analyse the (a) partitioning of the tau, rRNA and ribosomal proteins into large and small aggregates, (b) aggregation status of the tau proteins and (c) its association with the ribosomal components.

At each time point of incubation, the area under the 80S peak in the supernatant and the intensity of the rRNA band in the pellet provides a semi-quantitative measure for following the tau-ribosome aggregation process. Hence, the experiments in Fig. 3Ai,Aii,3Bi and 3Bii were performed multiple times and the relative intensities of the rRNA in the pellet and area under the 80S peak in the SDGC profile of the supernatant are represented in the form of a bar diagram (Fig. 3Ci,Cii). In this representation, the intensity of the rRNA pellet band obtained upon 24 hours incubation of the tau variants with the ribosome was considered as 100%. This was done on basis of the observation that a substantial proportion of the rRNA is still retained in the supernatant (as sub-ribonucleoprotein particles) even after 24 hours of tau-ribosome incubation (Figs. S1Biii, 3A,ii). As shown in the Fig. 3Ci, a sharp rise in rRNA in the pellet fraction was observed with a concomitant decrease of the ribosomal peak in the supernatant between 1.5 to 4 hours of K18–80S incubation. Ht40 induced 80S aggregation, however, showed a drastic increase between 4 to 8 hours (Fig. 3Cii). These experiments were indicative of a cooperative nature of the tau-ribosome aggregation process and were further investigated by performing the seeding experiments as stated below.

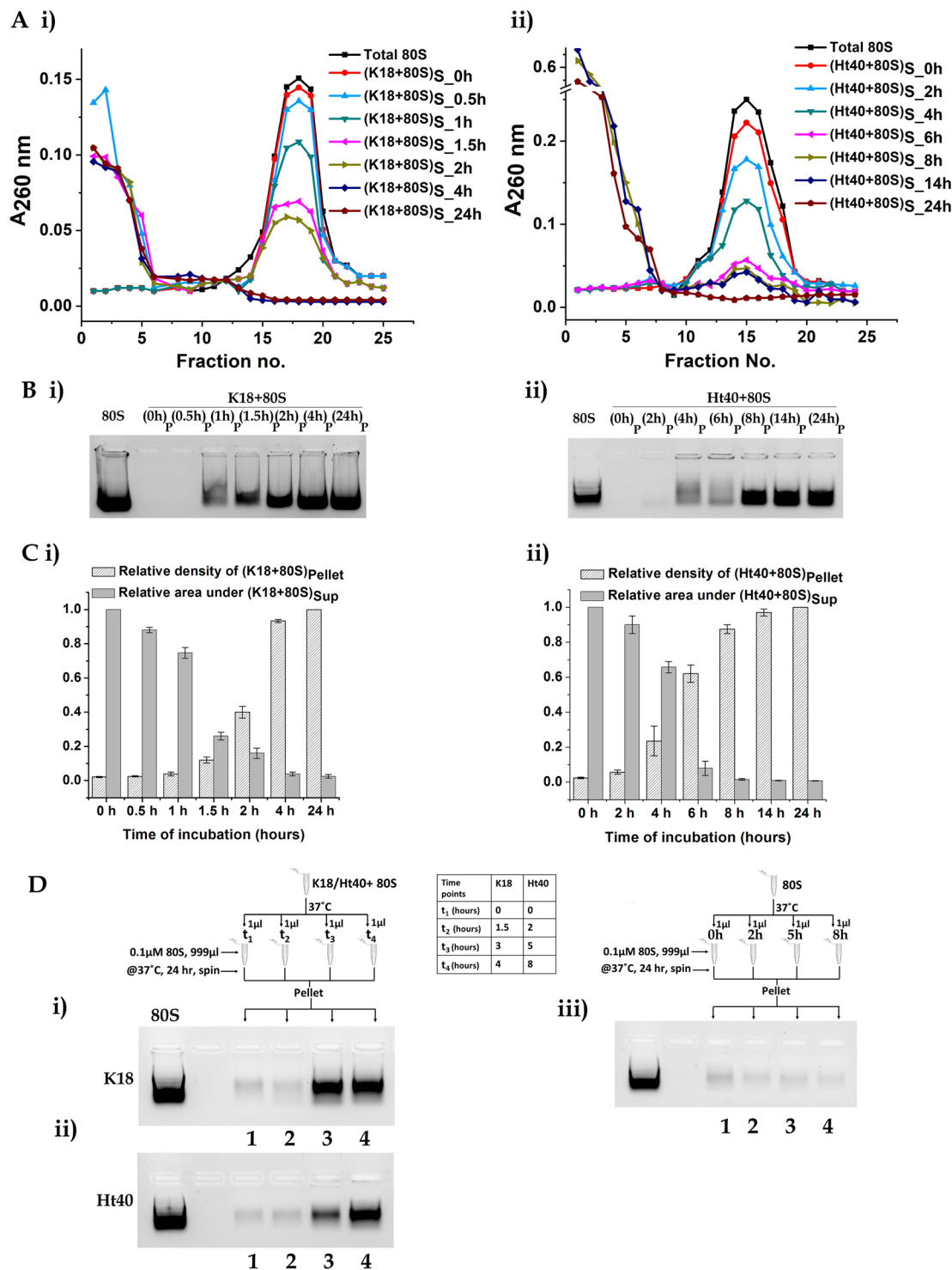


Figure 3. Time dependence of tau induced yeast 80S ribosome aggregation, The yeast 80S ribosome (0.1 μ M) was incubated with the tau variants (50 μ M) for different time intervals, centrifuged and the supernatant and pellet fractions were analysed as stated in materials and methods. **(A)** (i) Sedimentation profile of the supernatant obtained at different time intervals for K18-80S aggregation: Total 80S ribosome (■), (K18 + 80S)_{S_0h} (●), (K18 + 80S)_{S_0.5h} (▲), (K18 + 80S)_{S_1h} (▼), (K18 + 80S)_{S_1.5h} (◆), (K18 + 80S)_{S_2h} (▶), (K18 + 80S)_{S_4h} (◈) and (K18 + 80S)_{S_24h} (◉). (ii) Sedimentation profile of the supernatant obtained at different time intervals for Ht40-80S aggregation: Total 80S ribosome (■), (Ht40 + 80S)_{S_0h} (●), (Ht40 + 80S)_{S_2h} (▲), (Ht40 + 80S)_{S_4h} (▼), (Ht40 + 80S)_{S_6h} (◆), (Ht40 + 80S)_{S_8h} (▶), (Ht40 + 80S)_{S_14h} (◈) and (Ht40 + 80S)_{S_24h} (◉). **(B)** (i) Agarose gel electrophoretic analysis of pellet obtained at different time intervals for K18-80S aggregation for the presence of ribosomal RNA: Lanes from left to right contain; (1) Total 80S ribosome, (2) (0h)_P (3) (0.5h)_P (4) (1h)_P (5) (1.5h)_P (6) (2h)_P (7) (4h)_P (8) (24h)_P (ii) Agarose gel electrophoretic analysis pellet obtained at different time intervals for Ht40-80S aggregation for the presence of ribosomal RNA: Lanes from left to right contain; (1) Total

80S ribosome, (2) (0h)_p, (3) (2h)_p, (4) (4h)_p, (5) (6h)_p, (6) (8h)_p, (7) (14h)_p, (8) (24h)_p. (C) (i) *Area under 80S peak in supernatant and densitometry of rRNA in pellet for K18-80S aggregation*: Bar graphs representing the relative intensity obtained after densitometric scanning of the rRNA bands in the pellet fraction on agarose gel electrophoresis and relative area under the peak of 80S ribosome in the soluble fraction at different time intervals of K18-80S aggregation. [(K18 + 80S)_{p,24h} assumed as 1 for densitometry calculations whereas the area under the 80S peak at 0h has been assumed as 1 for area under the 80S peak calculations]. (ii) *Area under 80S peak in supernatant and densitometry of rRNA in pellet for Ht40-80S aggregation*: Bar graphs representing the relative intensity obtained after densitometric scanning of the rRNA bands in the pellet fraction on agarose gel electrophoresis and relative area under the peak of 80S ribosome (profile in SDGC)/ in the soluble fraction at different time intervals of Ht40-80S aggregation. [(Ht40 + 80S)_{p,24h} assumed as 1 for densitometry calculations whereas the area under the 80S peak at 0h has been assumed as 1 for area under the 80S peak calculations]. (D) *Ability of tau ribosome aggregates to induce aggregation of untreated ribosome*: Seeding experiments with tau-ribosome aggregates were performed as stated in materials and methods. Briefly, 0.1 μM 80S ribosome was incubated with 50 μM K18 or Ht40 at 37 °C. 1 μl aliquots were withdrawn from the reaction mixtures at specified time points and added to 999 μl of fresh 80S ribosome, which was then incubated for 24 hours, centrifuged and the pellet analysed using agarose gel electrophoresis. A schematic representation of the seeding experiments is included in the Figure. Aliquots drawn at respective time points are indicated as (t)_{al}. *Agarose gel electrophoresis of rRNA in the pellet when 0.1 μM 80S was incubated with aliquots of Tau-80S aggregation mix withdrawn at different time points*: (i) For K18 + 80S induced aggregation, lanes from left to right contain: (1) Total 80S, (2) Blank and 80S ribosome incubated with aliquots withdrawn at (3) 0h, (4) 1.5h, (5) 3h, (6) 4h (ii) For Ht40 + 80S induced aggregation lanes from left to right contain: (1) Total 80S, (2) Blank and 80S ribosome incubated with aliquots withdrawn at (3) 0h, (4) 2h, (5) 5h, (6) 8h (iii) Control experiments show that 80S ribosome which was not previously incubated with K18 or Ht40 was incapable of inducing ribosome aggregation. Lanes 3-6 (numbered as 1-4) are 80S ribosome incubated with aliquots of untreated ribosome withdrawn at 0h, 2h, 5h and 8h respectively.

In the seeding experiments aliquots from the reaction mixture containing the ribosome and tau variants (K18 or Ht40) were withdrawn at different time points (as indicated in the Fig. 3D) and added to a thousand-fold excess of fresh (untreated) 0.1 μM 80S ribosome (materials and methods). These mixtures were incubated for 24 hours at 37 °C, centrifuged and the insoluble pellet fractions were analysed using agarose gel electrophoresis. A schematic representation of the experiments performed is included in the Figure (Fig. 3D). It was observed that, the aliquot, when withdrawn after the 3hrs of K18- ribosome incubation and 5 hrs of Ht40-ribosome incubation, was sufficient to induce significant aggregation of the new 80S ribosome that had not previously been incubated with the tau protein (Fig. 3Di,Dii respectively). Appropriate control experiments were performed which showed that the aliquots drawn from 0.1 μM 80S incubated under similar conditions in the absence of any tau protein variant for the above mentioned time points (0h, 2h, 5h and 8h), could not induce the aggregation of fresh 80S ribosome (Fig. 3Diii). This study implicates a self-perpetuating nature of the ribosome aggregation process once it is initiated by the tau- ribosome interaction. Whether the aggregated ribosomes or a component formed due to tau-induced ribosome disassembly and co-aggregation has provided this potential to self-perpetuate their own aggregation needs to be further studied.

Yeast ribosomal RNA as an inducer for tau aggregation. Since the ribosome is a complex multi-component ribonucleoprotein particle, the question arises as to whether a particular component is primarily responsible for the tau-ribosome aggregation process. As stated in the introduction section, the natural tendency of the tau protein to interact with cellular polyanions presents the anionic surface of the ribosome, largely constituted of rRNA (Fig. 1), as a potential candidate for tau-ribosome aggregation. Previous studies have shown that tau aggregate formation can also be induced upon incubation with cytoplasmic RNA, a major proportion of which is rRNA²⁵. Several studies have also shown that RNA can influence the aggregation of prion proteins^{28,29}. Interestingly, cytoplasmic RNA has been detected in pathological lesions associated with diverse neurodegenerative diseases³⁰.

Hence, subsequent studies were performed on the effect of incubation of tau variants with rRNA isolated from the yeast 80S ribosome. In this study 1 μM of extracted 80S rRNA (as described in materials and methods) was incubated with 50 μM of K18 or Ht40 for 48 hours at 37 °C and the change in light scattering intensity at 450 nm was measured. As shown in Fig. 4A, a significant increase in light scattering intensity was observed when K18 and Ht40 were incubated with 80S rRNA, in comparison to when the tau variants and the rRNA were incubated alone.

In order to further analyse the aggregates formed, the reaction mixture was centrifuged and the pellet and supernatant fractions were analysed using agarose gel electrophoresis and dot blot analysis (materials and methods). As shown in Fig. 4Bi, for K18-rRNA incubation, the rRNA indeed forms a major component of the pellet fraction, although a portion of it is still retained in the supernatant fraction. Dot blot analysis of the soluble and insoluble fractions obtained upon K18-rRNA incubation (materials and methods) showed that almost the entire amount of K18 protein is present in the pellet fraction, in presence of rRNA (Fig. 4Bii). Similar observations were made in the agarose gel (Fig. 4Ci) and dot blot analysis (Fig. 4Cii) of the supernatant and pellet obtained upon Ht40-rRNA incubation. Whether the rRNA:tau ratio of 1:50, unlike the 80S ribosome:tau ratio of 1:500 and the extended period of tau-rRNA incubation (48h) are responsible for the presence of tau entirely in the pellet needs to be further analysed. Electron microscopy of the aggregates obtained upon incubating both K18 and Ht40 with rRNA at 37 °C for 48 hours showed the formation of intertwined fibrils (Fig. 4Di,Dii respectively), having appearance similar to that observed upon incubation with ribosome. These experiments, were performed with

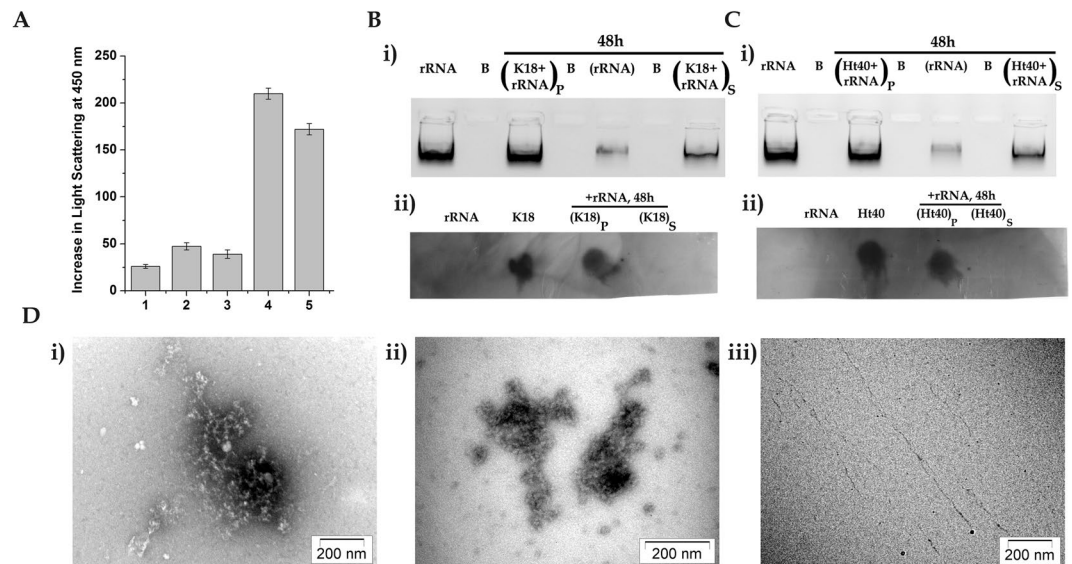


Figure 4. Yeast ribosomal RNA can lead to the formation of rRNA-tau coaggregates. 50 μ M K18 or Ht40 was incubated in the absence and presence of 1 μ M 80SrRNA for 48 hours at 37 $^{\circ}$ C as described in “Materials and Methods”. The aggregation was monitored by change in light scattering intensity and substantial increase in scattering was observed after 48 hours of tau-rRNA incubation. The reaction mixture was centrifuged, the supernatant and pellet fractions were analysed using dot blot and agarose gel electrophoresis. **(A)** *Light Scattering studies*: Bar graphs representing change in light scattering intensity at 450 nm after 48 hours of incubating K18 or Ht40 (50 μ M) in the presence of 80SrRNA (1 μ M) (Materials and Methods): (1) rRNA alone, (2) K18 alone (3) Ht40 alone, (4) K18 + 80SrRNA, (5) Ht40 + 80SrRNA. **(B)** Analysis of supernatant and pellet obtained from K18-80SrRNA aggregation i) *Agarose gel electrophoresis analysis*: Lanes from left to right indicate; (1) Total 80SrRNA, (2) Blank, (3) (K18 + rRNA)_{P, 48h}, (4) Blank, (5) (rRNA)_{P, 48h}, (6) Blank, (7) (K18 + rRNA)_{S, 48h} ii) *Dot blot analysis using anti-K18 monoclonal IgG antibody*: Dots from left to right indicate; Total 80SrRNA, Total K18, (K18 + rRNA)_{P, 48h}, (K18 + rRNA)_{S, 48h}. The full-length dot-blot image is shown in Fig. S4Bi. **(C)** Analysis of supernatant and pellet obtained from Ht40-80SrRNA aggregation i) *Agarose gel electrophoresis analysis*: Lanes from left to right indicate; (1) Total 80SrRNA, (2) Blank, (3) (Ht40 + rRNA)_{P, 48h}, (4) Blank, (5) (rRNA)_{P, 48h}, (6) Blank, (7) (Ht40 + rRNA)_{S, 48h} ii) *Dot blot analysis using anti-Ht40 monoclonal antibody*: Dots from left to right indicate; Total 80SrRNA, Total Ht40, (Ht40 + rRNA)_{P, 48h}, (Ht40 + rRNA)_{S, 48h}. The full-length dot-blot image is shown in Fig. S4Bii. **(D)** *Transmission electron microscopic analysis of tau-rRNA aggregates*: Micrographs were prepared from samples withdrawn at 48 hours from the initiation of incubation of 1 μ M 80SrRNA with or without 50 μ M of K18 or Ht40 (materials and methods): Micrographs of (i) (K18 + 80SrRNA)_{48h}, (ii) (Ht40 + 80SrRNA)_{48h}, (iii) (80SrRNA)_{48h}.

the total 80SrRNA and the contribution of specific rRNA (28S and 18S) requires further analysis. In the control experiment, the incubation of the rRNA alone under similar conditions showed no apparent aggregate formation (Fig. 4Diii).

In this context, it should be noted that recent studies show that RNA can influence aggregation of disease-associated proteins^{28,31}. A recent study with recombinant prion protein (rPrP) has showed that depending upon the protein: RNA stoichiometric ratio, the RNA is capable of inhibiting or stimulating protein aggregation. At a high protein: RNA ratio, rPrP aggregation²⁸ like tau aggregation in our study, is stimulated, also leading to its co-aggregation with the RNA. Our experiments also collectively indicate that the rRNA component of the ribosome could play a significant role in the ribosome-tau aggregation phenomenon observed here.

Effect of cellular anions on tau-ribosome aggregation. Earlier studies have demonstrated the importance of electrostatic interactions in determining the interaction of tau with its cellular partners and that the behaviour of the tau protein can be modulated in presence of cellular polyanions¹⁴. Hence, further studies were performed to investigate the possibility of inhibition of tau initiated ribosome aggregation by electrostatic shielding agents in the form of competitor polyanions like heparin and tRNA. In these experiments the tau variants were incubated with the ribosome in presence of increasing concentrations (0x, 1x, 5x, 10x; x = 0.1 μ M) of tRNA or heparin, centrifuged and the aggregation process was followed by agarose gel electrophoresis of rRNA present in the insoluble tau-ribosome aggregates. The highest concentrations of tRNA and heparin used in these experiments were 10-fold higher than that of the 80S ribosome, as was used in our earlier studies¹³. Also, as reported in literature, the cellular stoichiometric ratio of tRNA with respect to the ribosome in yeast is approximately 10-fold³².

As shown in Fig. 5, increasing concentrations of heparin could significantly inhibit K18-ribosome aggregation, that is reflected as a reduced formation of insoluble rRNA containing aggregates (Fig. 5Ai–iii). No such inhibition of Ht40 induced ribosome aggregation was observed (Fig. 5Ai and represented in the bar diagram

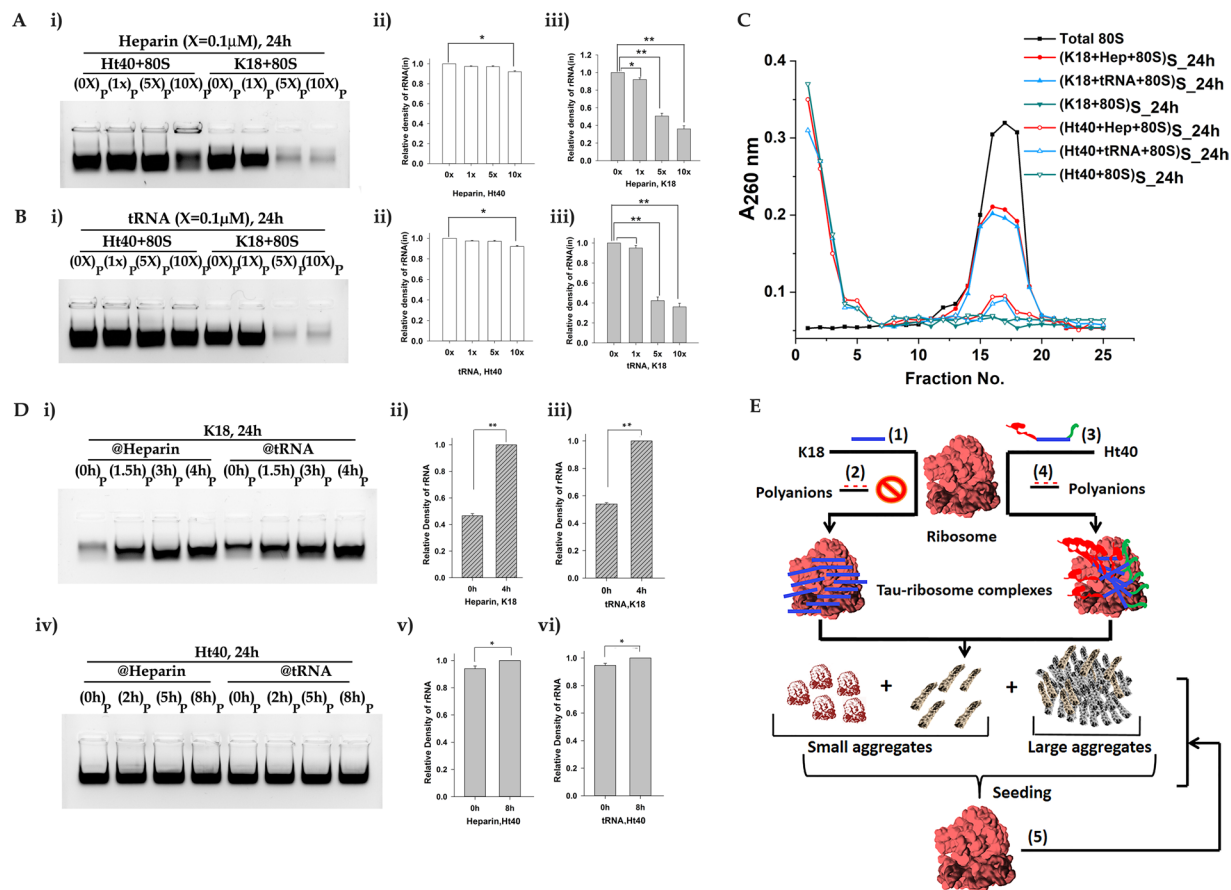


Figure 5. Effect of polyanions on Tau induced 80S aggregation. 0.1 μM of 80S ribosome was incubated with 50 μM K18 or Ht40 in presence of increasing concentrations (0x, 1x, 5x and 10x; $\times = 0.1 \mu\text{M}$) of heparin (hep) or yeast phenylalanine tRNA for 24 hours (Materials and Methods). The reaction mixture was centrifuged, the pellet and supernatant were analysed as described before. (A,B) Agarose gel electrophoretic analysis of rRNA in the pellet. (A). Effect of heparin: (i) Lanes from left to right contain: (1) (Ht40 + 0x hep+80S)_p, (2) (Ht40 + 1x hep+80S)_p, (3) (Ht40 + 5x hep+80S)_p, (4) (Ht40 + 10x hep+80S)_p, (5) (K18 + 0x hep+80S)_p, (6) (K18 + 1x hep+80S)_p, (7) (K18 + 5x hep+80S)_p, (8) (K18 + 10x hep+80S)_p; (ii) Bar graphs depicting the densitometric analysis of rRNA band intensities show no suppression of aggregation in presence of heparin for Ht40-80S aggregation. (Ht40 + 0x heparin+80S)_{p,24h} assumed as 1 for calculations; (iii) Bar graphs depicting the densitometric analysis of rRNA band intensities show suppression of K18-80S aggregation in presence of heparin; (K18 + 0x heparin+80S)_{p,24h} assumed as 1 for calculations. The experiments were repeated thrice and the data are presented as means \pm SEM; * $P < 0.05$ or ** $P < 0.001$ in one-way ANOVA (N = 3). (B). Effect of tRNA: (i) Lanes from left to right contain: (1) (Ht40 + 0x tRNA+80S)_p, (2) (Ht40 + 1x tRNA+80S)_p, (3) (Ht40 + 5x tRNA+80S)_p, (4) (Ht40 + 10x tRNA+80S)_p, (5) (K18 + 0x tRNA+80S)_p, (6) (K18 + 1x tRNA+80S)_p, (7) (K18 + 5x tRNA+80S)_p, (8) (K18 + 10x tRNA+80S)_p; Bar graphs were plotted as in (A) and depicts the densitometric analysis of rRNA band intensities. Bar graphs (Bii) [(Ht40 + 0x tRNA+80S)_p assumed as 1] and (Biii) [(K18 + 0x tRNA+80S)_p assumed as 1] shows selective suppression of aggregation K18-80S aggregation but no suppression of Ht40-80S aggregation in presence of tRNA. The experiments were repeated thrice and the data are presented as means \pm SEM; * $P < 0.05$ or ** $P < 0.001$ in one-way ANOVA (N = 3). (C). Sedimentation profile of supernatant fraction: 80S was incubated with K18 or Ht40 in presence of 10x ($x = 0.1 \mu\text{M}$) heparin or tRNA and the sedimentation profile was observed for; (1) Total 80S (■), (2) (K18 + hep+80S)_{S,24h} (●), (3) (K18 + tRNA+80S)_{S,24h} (▲), (4) (K18 + 80S)_{S,24h} (▼), (5) (Ht40+hep+80S)_{S,24h} (○), (6) (Ht40+tRNA+80S)_{S,24h} (△), (7) (Ht40 + 80S)_{S,24h} (▽). Retention of 80S peak was observed with heparin and tRNA selectively in case of K18-80S aggregation. (D). Effect of delayed addition of heparin and tRNA: 0.1 μM 80S was incubated with 50 μM of Tau variants (K18 or Ht40) and 1 μM (10x) heparin or tRNA was added to the reaction mixture at different time points from the initiation of incubation (Materials and Methods). The reaction mixture was further incubated till 24 hours, centrifuged and rRNA in the pellet was analysed using agarose gel electrophoresis. (i) K18-80S aggregation for delayed addition of heparin and tRNA: Lanes from left to right contain pellets for K18-80S aggregation when heparin was added at: (1) 0 h, (2) 1.5 h, (3) 3 h, (4) 4 h and when tRNA was added at (5) 0 h, (6) 1.5 h, (7) 3 h, (8) 4 h. Bar graphs (ii) and (iii) depicting the densitometric analysis of relative intensities of rRNA bands (Intensity of pellet band for 4 h assumed as 1) in the pellets for Di show that delayed addition of heparin and tRNA shows no effective of suppression in case of K18-80S aggregation. (iv) Ht40-80S aggregation for delayed addition of heparin and tRNA: Lanes from left to right contain pellets for Ht40-80S aggregation when heparin was added at: (1) 0 h, (2) 2 h, (3) 5 h, (4) 8 h and when tRNA was added at (5) 0 h, (6) 2 h, (7) 5 h,

(8) 8 h. Bar graphs (v) and (vi) shows the densitometric analysis of relative intensities of rRNA bands (Intensity of pellet band for 8 h assumed as 1) that revealed the lack of any effect of the time of heparin or tRNA addition on the Ht40-80S aggregation process. The experiments were repeated thrice and the data are presented as means \pm SEM; * $P < 0.05$ or ** $P < 0.001$ in one-way ANOVA ($N = 3$). (E) A model showing the fate of the ribosome upon encountering the Ht40 and K18 Tau variants. The tau protein variants Ht40 and K18 associate with the RNA rich polyanionic ribosome surface. The possible aggregation of tau on the exposed rRNA initiates the process of co-aggregation of tau and ribosomal components leading to a time dependent formation of small and large RNA protein co-aggregates. The highly positively charged K18 variants associates with the ribosome surface predominantly via electrostatic interactions (1), that is effectively inhibited in presence of cellular polyanions like tRNA and heparin (2). The full-length tau variant Ht40 having an additional large unstructured N-terminal domain associates with the ribosome via electrostatic and additional interactions (3) which is not effectively shielded in the presence of added polyanions (4). The tau (K18 and Ht40) ribosome aggregates are capable of seeding aggregation of fresh untreated ribosomes (5). This cartoon representation has been created using Adobe Photoshop CS 8.0.

Fig. 5Aii,Aiii). Selective inhibition of K18-80S aggregation was also observed in presence of yeast tRNA, under the conditions used in our experiment (Fig. 5Bi and represented in the bar diagram Fig. 5Bii,Biii). The sucrose density gradient profile of the soluble fraction also showed a significant retention of the 80S peak in the presence of the highest concentration of polyanions for K18 induced ribosome aggregation. No such protective effect of the polyanions was observed on the ribosomal peak for Ht40 induced 80S aggregation (Fig. 5C). Control experiments were performed to verify whether the heparin and tRNA concentrations used in our experiments could themselves lead to tau or ribosome aggregation. When the ribosome was also incubated with these polyanions for 24 hours in absence of the Tau protein variants, no significant appearance of rRNA was observed in the insoluble pellet (Fig. S3A), confirming that the polyanions themselves do not induce ribosome aggregation. Also, in control experiments, K18 or Ht40 were incubated with different concentrations of heparin and tRNA (used in our above stated experiments), for 24 hours, centrifuged and the insoluble pellet was analysed on SDS-PAGE (Fig. S3Bi,ii). It was observed that, the polyanions even at their highest concentrations (1 μ M) could not themselves induce aggregation of the ribosome or the tau variants.

We also analysed whether the time of addition of these polyanions could affect tau induced ribosome aggregation. As shown in Fig. 5D(i-iii), presence of these polyanions from the initiation ($t = 0$ h of ribosome-tau incubation) of the aggregation process was necessary for effective suppression of ribosome aggregation induced by K18. Also, as expected from the above observations (Fig. 5B), the time of inducer addition showed no such effect in case of Ht40 induced 80S aggregation (Fig. 5Div-vi).

From the selective effect of the polyanions, it can be concluded that under our experimental conditions, electrostatics plays a major role in determining the outcome of K18-80S aggregation process. Further reasons that might underlie the difference between K18 and Ht40-80S aggregation are discussed below and is depicted in the model (Fig. 5E).

Discussion

As stated in the introduction section, a significant change in the 80S ribosome profile occurs in the neurons of individuals afflicted with Alzheimer's disease and a gradual decrease in the neuronal ribosome population is observed with the progression of the disease^{6,7}. Our *in vitro* studies show that when full length tau protein (Ht40) and the K18 tau variants were incubated *in vitro* with isolated non-translating yeast ribosome under conditions that are conducive to tau aggregation (but in absence of polyanionic inducer), the aggregation of ribosomal components was induced. The tau protein variants had a similar effect on the ribosome profile of the HeLa cell lysate and suppression of translation by the human *in vitro* translation system was also observed in presence of the tau protein variants. The concentration and time dependence of tau mediated ribosome aggregation and the ineffectiveness of BCAII protein to induce 80S ribosome aggregation are indicative of a ribosome aggregation process that is subject to the specific presence of the tau proteins. Further *in vivo* experiments need to be performed with the disease affected neurons to confirm our observations made *in vitro*. Our studies imply that the tau proteins alone might mediate the change in ribosomal profiles observed in neurons of the Alzheimer's affected regions of human brain⁷, which might be a vital determinant of tau aggregation toxicity.

The ability of tau-ribosome co-aggregates to seed the aggregation of ribosomes is another surprising phenomenon observed in this study. This study implies that the tau-ribosome aggregates formed can successfully propagate the aggregation of new ribosomes without requiring the presence of freshly added tau proteins. It might be noted that earlier studies have shown that when the K18 variant of the tau protein, rPrP and the p53 proteins were incubated with RNA, protein-RNA aggregates formed could act as seeds to nucleate *de novo* protein aggregation^{23,28,31}. Since the eukaryotic ribosome is a large ribonucleoprotein particle, a large amount of tau- rRNA and tau-ribosomal protein aggregates are formed during the tau-ribosome aggregation process. As RNA molecules have been observed to contribute to the seeding behaviour of RNA-protein aggregates (as stated earlier), it might be suggested that the ribosome, majorly consisting of rRNA molecules, might rely on the rRNA component for this seeding behaviour. In addition, the large number of ribosomal proteins with intrinsically disordered regions can also play a significant role. Hence, further studies need to be performed to identify the component formed due to tau-ribosome co-aggregation that possesses the potential to self-perpetuate the ribosome aggregation process.

Another question that arises is what forms the basis for the tau-ribosome interaction that eventually culminates into the co-aggregation process reported in this study. Several recent studies have highlighted that the electrostatic interactions between the unfolded nascent polypeptide chain and the ribosome have diverse effects

on translation rate³³ and co-translational protein folding³⁴. Interestingly, an unrelated study has also implicated that the ribosome surface properties may limit the mobility of positively charged variants of recombinant GFP in *E. coli*²¹. The formation of aggregates upon incubation of the purified ribosomes with the positively charged GFP variant indicates at the tendency of a positively charged protein to induce ribosome aggregation. Our earlier studies have also suggested that electrostatics plays a role during co-aggregation of lysozyme (which has a net positive charge at physiological pH) with the ribosome¹³. However, the contribution of net charge on a protein towards its ability to bring about ribosome aggregation needs further investigation. Recent studies have demonstrated that the disease associated intrinsically disordered proteins are highly charged and often rely on non-native electrostatic interactions for associating even with their appropriate cellular binding partners^{35,36}. Such a tendency of engaging in promiscuous interactions might also lead to cytotoxicity. Indeed, it has been demonstrated that electrostatic interaction of the tau protein with anionic lipid membranes can induce tau aggregation and that the resultant membrane permeabilization may serve as a pathway by which tau protein aggregates exert their toxicity^{37,38}. Earlier studies had demonstrated that cellular RNA (a major portion of which is rRNA) can induce tau fibrillization²⁷ and RNA modulated prion aggregation is also widely reported in literature^{28,29}.

Our studies also show that the incubation of the tau variants with the rRNA isolated from the 80S ribosome could lead to the formation of tau-rRNA aggregates. The ability of the rRNA to induce rRNA-Tau aggregation implicated that the rRNA component of the ribosome plays a dominant role in this process, although, the participation of ribosomal proteins containing regions of intrinsic disorder³⁹, in the tau-ribosome aggregation process, also requires to be further investigated. However, in light of present studies and taking into account the relative size and concentration of the eukaryotic ribosome and the tau variants, it is possible that the anionic surface of the ribosome, that is predominantly composed of rRNA, could present itself as a potential surface on which multiple tau molecules can associate (Fig. 5E). Such associations could induce tau aggregation by either screening of the intermolecular electrostatic repulsions between tau proteins or by increasing the local tau concentration. Since the rRNA acts as an architectural scaffold for the ribosome, such tau-rRNA interactions and aggregation of tau on the ribosome surface could lead to disruption of the ribosome structure. Such tau-targeted structural destabilization of the translational machinery could lead to cytotoxicity, although this model (Fig. 5E) needs to be further verified. Intriguingly, recent studies have also indicated that ribosomes are especially susceptible to the protein aggregates that are formed either due to abnormal protein stoichiometry during aneuploidy or due to protein aggregation in aged brains^{40,41}. Our recent and earlier¹³ studies suggest that the ribosome when placed in the vicinity of protein aggregate formation have a tendency to co-aggregate, thereby providing a plausible explanation to the predominance of ribosomal proteins in the aggregates observed in these studies^{40,41}. The inhibition of tau-ribosome electrostatic interactions in the presence of added polyanions, like heparin and tRNA, indeed could inhibit K18 induced tau aggregation. However, the lack of inhibition of Ht40 mediated ribosome aggregation in presence of the polyanions might be either due to the difference in the net positive charge of K18 and Ht40 at physiological pH (Fig. 1) or because of additional interactions between the large unstructured N-terminus of the full-length tau protein and the ribosome. It should be noted here that, the specific interactions between the chemically unfolded protein and the ribosomal RNA, that forms the basis of the ability of the ribosome to act as a protein folding modulator, has been widely reported in literature⁴² and the references therein). Whether such tau-ribosome interactions play a role in the observed co-aggregation of the tau proteins with the ribosome needs to be investigated.

The question also arises about whether such tau-ribosome interactions would become more probable under pathological conditions and whether such interactions are a cause or consequence of the AD pathology. Such a probability of aberrant non-translating ribosome-tau interactions might increase in AD, in which the mutated tau proteins (P301L tau mutant)³ and the differentially truncated forms of tau lose their affinity for microtubules, thus altering their subcellular localization and increasing the cytosolic tau concentration^{43–45}. Studies on the abilities of other tau isoforms to initiate the tau-ribosome aggregation process also need to be performed. Preliminary studies conducted with the 3-repeat domain containing tau variant (K19) show that similar to K18 variant, K19 is able to aggregate the ribosome (Fig. S3C), although further experiments are necessary to characterize the K19-tau mediated ribosome aggregation process. Earlier studies also suggest that there exists a correlation between the glycosylation and phosphorylation status of the tau protein and AD. However, it should be noted that our studies have been conducted with tau proteins expressed in bacterial cells and hence lack any such post-translational modification. Further investigations are also necessary to determine the effects of such disease associated changes in post-translational modifications on the ability of tau protein to induce ribosome aggregation⁴⁶. The age dependent decline in both protein translation⁴⁷ and cellular chaperone⁴⁸ levels might further increase the possibility of promiscuous tau-ribosome interactions. The interference in biological functions of the tau protein as discussed above and its increased aggregation propensity are the early events in AD. Although, the tau-ribosome aggregation is likely to be a consequence rather than a cause for AD, our present studies indicate that the disruption of cellular translation machinery might provide important insights into the processes that lead to Alzheimer's disease pathology.

Materials and Methods

Materials. Bovine Carbonic Anhydrase II (BCAII), NaCl, MgCl₂, DTT, Tris-base, SP sepharose were purchased from Sigma Aldrich. Tau 4RD (K18), Tau 3RD (K19) and Ht40 clones were obtained as kind gifts from Dr. Jayant B. Udgaonkar's Laboratory (NCBS). Polyallomer ultracentrifuge tubes were purchased from Beckman Coulter. Nitrocellulose filter was purchased from Bio-Rad, PVDF membrane was purchased from Millipore, mouse monoclonal anti-human Tau 4RD antibody was purchased from EMD Millipore (primary antibody for K18) [Anti-Tau (4-repeat isoform RD4) Antibody, clone 1E1/A6; Catalogue no.: 05–804], mouse monoclonal anti-mouse D8 antibody (primary antibody for Ht40) [Tau Antibody (D8), Catalogue no.: sc-166060] and the goat-anti-mouse HRP conjugated antibody (Secondary antibody) were purchased from Santa-Cruz

Biotechnology. The western chemiluminescence HRP substrate was purchased from Millipore (Immobilon). Yeast phenylalanine tRNA was purchased from Sigma-Aldrich. All other chemicals were local products of analytical grade. Experimental data analysis was performed using OriginPro8 (Origin Corp., Northampton, MA, USA), QuantityOne Bio-Rad and SIGMA-PLOT 14 (Systat Software, Inc., San Jose, CA, USA) software. PYMOL 2008 (De Lano Scientific, Palo Alto, CA, USA) was used to display the Protein Data Bank files. Net charge calculations of human full-length tau (Ht40) and K18 were performed using PROTEIN CALCULATOR v3.4.

Buffers. Buffers used in this study were: Buffer A for aggregation reactions: 25 mM Tris-HCl pH 7.5, 50 mM NaCl, 5 mM MgCl₂ (with minor modifications from Ramachandran *et al.*, 22); Buffer B for cell lysis: 50 mM PIPES NaOH pH 6.9, 20 mM NaCl, 1 mM EDTA, 5 mM DTT, 1 mM PMSF²²; Buffer C for protein purification²²: 50 mM PIPES NaOH pH 6.9, 20 mM NaCl; Buffer D for protein purification²²: 50 mM PIPES NaOH, pH 6.9 500 mM NaCl; Buffer E for final buffer exchange and protein storage²²: 25 mM Tris-HCl pH 7.5.

Purification of Tau K18, K19, Ht40 and yeast 80S ribosome. Yeast *Saccharomyces cerevisiae* ribosome (80S) was purified according to Chakraborty *et al.*⁴⁹. Yeast 80S rRNA was extracted as mentioned in Piir *et al.*⁵⁰. Tau K18 and Ht40 were purified using a two-step purification method: direct-boiling method^{51,52} and cation-exchange purification method²². The *E. coli* BL21(DE3) cells were transformed with Tau k18, k19, ht40 plasmids and cells were harvested for large scale purification by centrifugation. The cell pellets were resuspended and boiled in Buffer B for 20 minutes with gentle agitation after every 5 minutes. The boiled cell suspension was immediately chilled on ice for 15 minutes before centrifuging it at 4 °C and 16,000 g for 20 minutes. The supernatant was retained and incubated with SP sepharose for cation exchange chromatography and washed with increasing concentrations of NaCl (obtained by mixing Buffer C and Buffer D)²². Fractions containing pure protein were pooled together, concentrated and finally buffer exchanged into Buffer E and frozen at -80 °C until further use. The protein concentration was determined as mentioned in Ramachandran *et al.*²².

Tau-ribosome aggregation. The tau aggregation procedure and buffer composition were followed from Ramachandran *et al.*²² with minor modifications. 50 μM Tau K18 or Ht40 was reduced in presence of 1 mM DTT for 2 hours at 37 °C in Buffer A, at the end of which 0.1 μM 80S or 1 μM 80S rRNA or 1 μM heparin or 1 μM tRNA or A_{260 nm} units equivalent to 0.1 μM 80S (7.9 A_{260 nm} units) HeLa cell lysate was added and incubated for 6 hours at 37 °C or as mentioned. For aggregation reactions with increasing concentrations of tau, 10 μM, 25 μM and 50 μM of K18 and Ht40 was used. In control experiments 50 μM native BCAII (nBCAII) was incubated with 0.1 μM 80S for 6 hours at 37 °C. 80S (0.1 μM) was also incubated in the presence and absence of 1 mM DTT for 6 hours in buffer A and centrifuged. Aggregation reactions were centrifuged at 21,380 g for 45 minutes at 4 °C and the pellet and supernatant fractions separated. It should be noted that the centrifugal speed used in earlier studies on polyA RNA induced tau aggregation²³ to separate monomeric tau and tau-RNA aggregates was 1,00,000 g which could not be used for our studies, since at this centrifugal speed the ribosome or rRNA alone is pelleted irrespective of the presence of the tau proteins. Hence, at the centrifugal speed of 21,380 g¹³, the larger aggregates formed the pellet (P), while the supernatant (S) constituted of the residual ribosomes or smaller aggregates. The constituents of the pellet fractions were analysed using 12% SDS-PAGE or 0.8% agarose gel electrophoresis and the supernatant fractions by sucrose density gradient centrifugation or SDS-PAGE after TCA precipitation. The SDS-PAGE were stained using Coomassie Brilliant Blue at 37 °C and the agarose gels were stained using ethidium bromide.

Gel electrophoretic analysis of insoluble aggregates. Aggregation samples were centrifuged at 21,380 g for 45 minutes at 4 °C. The pellets and supernatant were analysed for their total rRNA content in a non-denaturing 0.8% agarose gel, using a procedure used earlier to study interaction of tau with cellular RNA (with minor modifications)²⁴. Briefly, the pellets had to be treated with 4 M urea and incubated for 20 minutes at room temperature (a treatment that was necessary to enable the RNA in the large aggregates to enter the gel), before loading on a 0.8% agarose gel for electrophoresis. The electrophoresis was performed in 1xTAE at 65 V for 10 min before visualizing under ultraviolet light using the GelDoc imaging system (MEGA BIO-PRINT 1100/20M). In this experiment, the total RNA runs as a single band, in which the intensities of the rRNA bands were compared by densitometric analysis (QuantityOne Bio-Rad). This procedure had also been used in our earlier studies to follow the lysozyme ribosome co-aggregation process¹³. The total ribosome or rRNA used in the experiment was treated similarly and analysed. For the analysis of the protein constituents, the protein in the supernatant was TCA precipitated and the pellets were resuspended in Laemmli buffer containing 4 M urea and boiled before loading onto a 12% SDS-PAGE.

Sucrose density gradient centrifugation. Aggregation reactions were centrifuged at 21,380 g for 45 minutes at 4 °C and the supernatant fraction was layered on a 17–25% sucrose gradient. The gradient was centrifuged at 1,98,000 g (MLS-50 rotor, Beckman Coulter) for 2.5 hours at 4 °C and 200 μl fraction volumes were collected from top to bottom and absorbance at 260 nm was measured for analysing the 80S ribosome profile.

Dot blot analysis for tau-ribosome aggregation. 50 μM K18 or Ht40 was reduced in 1 mM DTT at 37 °C for 2 hours after which 0.1 μM 80S was added to it. The resultant reaction mixture was incubated at 37 °C for 24 hours and centrifuged at 21,380 g, 4 °C for 45 minutes. The supernatant and the resuspended (in 1 M Urea) pellet fractions were dotted on PVDF membrane. The membrane was blocked with 5% skimmed milk for 1.5 hours and then washed three times (3 minutes intervals) with 1x PBST and incubated with specific primary antibody (Anti-Tau 4RD antibody monoclonal IgG; 1:250 dilution for K18 and D8-anti tau monoclonal IgG; 1:1000 dilution for Ht40) at 4 °C for overnight. The membrane was then washed eight times (15 minutes intervals) with 1x PBST and then incubated with secondary antibody (goat anti-mouse IgG HRP conjugated; 1:10,000 dilution) for

1.5 hours at room temperature. Then the membrane was washed with 1x PBST for eight times and incubated with chemiluminescent HRP substrate and the signal was recorded using photographic plates.

Human *in vitro* transcription-translation assay. The *in vitro* translation assay was done using 1-Step Human Coupled IVT Kit – DNA; 88881, ThermoFisher Scientific. K18 and Ht40 were added to the prescribed reaction mix to a final concentration of 50 μM . The positive control set contained no tau proteins and the negative control set did not contain the GFP (reporter gene) plasmid. All the reaction sets were incubated till 6 hours at 30 $^{\circ}\text{C}$ (as prescribed) and GFP (reporter gene) fluorescence was monitored at ex/em: 482/512 nm. The experiment was repeated three times.

Electron microscopy. 50 μM K18 or Ht40 was reduced at 37 $^{\circ}\text{C}$ for 2 hours after which 0.1 μM 80S was added. The resultant reaction mixture was incubated for 2 and 24 hours at 37 $^{\circ}\text{C}$. For studies with rRNA, 1 μM 80S rRNA was incubated for 48 hours with 50 μM K18 or Ht40 reduced in 1 mM DTT as described above. Imaging of aggregation in the samples was done by using a transmission electron microscope (FEI Tecnai12BioTwin) with an acceleration voltage of 120 kV. Aliquots (5 μl) containing the aggregation mixture were placed on the copper grid coated with carbon film (300 meshes) and one drop of 2% uranyl acetate was placed on the grid. The excess water was removed carefully with filter paper and the grid was left to dry in air.

Time course study of aggregation. 50 μM K18 or Ht40 was reduced at 37 $^{\circ}\text{C}$ for 2 hours after which 0.1 μM 80S was added. The resultant reaction mix was centrifuged at 21,380 g for 45 minutes at 4 $^{\circ}\text{C}$ after 0 h, 0.5 h, 1 h, 1.5 h, 2 h, 4 h and 24 h of incubation for K18 and 0 h, 2 h, 4 h, 6 h, 8 h, 14 h and 24 h of incubation at 37 $^{\circ}\text{C}$. The supernatant fractions were analysed using a 17–25% sucrose density gradient (as described below) and the pellets obtained were analysed using 0.8% agarose gel (as described below). The supernatant and pellet fractions obtained at 0.5 h, 2 h, 6 h and 24 h were also analysed using 12% SDS-PAGE as described above.

Seeding assay for tau induced 80S aggregation. 50 μM K18 was reduced in Buffer A for 2 hours at 37 $^{\circ}\text{C}$, after which 0.1 μM 80S was added to it. 1 μl aliquots were drawn from this reaction mixture after 0, 1.5, 3, 4 hours of incubation (for K18 induced 80S aggregation) and 0, 2, 5, 8 hours of incubation (for Ht40 induced aggregation) added to 999 μl of fresh 0.1 μM 80S in Buffer A. This new reaction mixture was then incubated for 24 hours at 37 $^{\circ}\text{C}$ and then centrifuged at 21,380 g at 4 $^{\circ}\text{C}$ for 45 minutes. The insoluble fraction was resuspended in 4 M urea containing Buffer A and analysed using a 0.8% agarose gel electrophoresis.

Dot-blot analysis for Tau-rRNA aggregation. 50 μM K18 or Ht40 was reduced in 1 mM DTT at 37 $^{\circ}\text{C}$ for 2 hours after which 1 μM 80S was added to it. The resultant reaction mixture was incubated at 37 $^{\circ}\text{C}$ for 48 hours and centrifuged at 21,380 g, 4 $^{\circ}\text{C}$ for 45 minutes. The most commonly used Tau aggregation inducer for *in vitro* studies is heparin. In the presence of heparin at an appropriate stoichiometry the K18 aggregates much faster (24 hours)²² as compared to Ht40 (48–144 hours)⁵³. Hence, the reaction was allowed to proceed till 48 hours in order for it to reach saturation. The supernatant and the resuspended (in 1 M Urea for 30 minutes at 37 $^{\circ}\text{C}$) pellet fractions were dotted on PVDF membrane and the dot blot analysis was carried on as described above.

Light scattering study. 50 μM of K18 or Ht40 was reduced in Buffer A with 1 mM DTT for 2 hours at 37 $^{\circ}\text{C}$ after which 1 μM of LiCl extracted 80SrRNA was added to the reaction mixture (t = 0 h) and further incubated for 48 hours at 37 $^{\circ}\text{C}$. The light scattering of the solutions was measured at t = 0 h and t = 48 h and the increase was plotted in the form of bar diagrams. For control, the rRNA alone, K18 alone and Ht40 alone reaction sets were similarly incubated and the increase in their light scattering was measured at 48 hours. Before measuring the light scattering intensity, all the solutions were pipetted three times. The intensity was measured at excitation: 450 nm and emission: 450 nm in Hitachi F-2700 spectrofluorometer.

Delayed heparin/tRNA addition assay for tau induced 80S aggregation. 50 μM K18 was reduced in Buffer A for 2 hours at 37 $^{\circ}\text{C}$ in presence of 1 mM DTT, after which 0.1 μM 80S was added to it. 1 μM heparin or tRNA was added after 0, 1.5, 3 and 4 hours of addition of the ribosome in case of K18 and after 0, 2, 5 and 8 hours of addition of the ribosome in case of Ht40. The resultant reaction mixture was further incubated for 24 hours at 37 $^{\circ}\text{C}$ and centrifuged at 21,380 g at 4 $^{\circ}\text{C}$ for 45 minutes. The insoluble fraction was resuspended in 4 M urea containing Buffer A and analysed using a 0.8% agarose gel electrophoresis.

Received: 23 September 2019; Accepted: 28 February 2020;

Published online: 23 March 2020

References

- Ballatore, C., Lee, V. M. Y. & Trojanowski, J. Q. Tau-mediated neurodegeneration in Alzheimer's disease and related disorders. *Nature Reviews Neuroscience* **8**, 663–672, <https://doi.org/10.1038/nrn2194> (2007).
- Binder, L. I., Frankfurter, A. & Rebhun, L. I. The distribution of tau in the mammalian central nervous system. *J. Cell Biol.* **101**, 1371–1378, <https://doi.org/10.1083/jcb.101.4.1371> (1985).
- Gunawardana, C. G. *et al.* The human tau interactome: Binding to the ribonucleoproteome, and impaired binding of the proline-to-leucine mutant at position 301 (P301L) to chaperones and the proteasome. *Mol. Cell. Proteomics* **14**, 3000–3014, <https://doi.org/10.1074/mcp.M115.050724> (2015).
- Meier, S. *et al.* Pathological tau promotes neuronal damage by impairing ribosomal function and decreasing protein synthesis. *J. Neurosci.* **36**, 1001–1007, <https://doi.org/10.1523/JNEUROSCI.3029-15.2016> (2016).
- Kelley, B. J. & Petersen, R. C. Alzheimer's disease and mild cognitive impairment. *Neurologic clinics* **25**, 577–609 (2007).
- Ding, Q., Dimayuga, E. & Keller, J. N. Oxidative damage, protein synthesis, and protein degradation in Alzheimer's disease. *Current Alzheimer Research* **4**, 73–79 (2007).

7. Ding, Q., Markesbery, W. R., Cekarini, V. & Keller, J. N. Decreased RNA, and increased RNA oxidation, in ribosomes from early Alzheimer's disease. *Neurochem. Res.* **31**, 705–710, <https://doi.org/10.1007/s11064-006-9071-5> (2006).
8. Weingarten, M. D., Lockwood, A. H., Hwo, S. Y. & Kirschner, M. W. A protein factor essential for microtubule assembly. *Proc. Natl. Acad. Sci. USA* **72**, 1858–1862, <https://doi.org/10.1073/pnas.72.5.1858> (1975).
9. Honson, N. S. & Kuret, J. Tau aggregation and toxicity in tauopathic neurodegenerative diseases. *Journal of Alzheimer's Disease* **14**, 417–422, <https://doi.org/10.3233/JAD-2008-14409> (2008).
10. Yang, H. & Hu, H. Y. Sequestration of cellular interacting partners by protein aggregates: implication in a loss-of-function pathology. *FEBS Journal* **283**, 3705–3717, <https://doi.org/10.1111/febs.13722> (2016).
11. Ramachandran, G. & Udgaonkar, J. B. Mechanistic studies unravel the complexity inherent in tau aggregation leading to Alzheimer's disease and the tauopathies. *Biochemistry* **52**, 4107–4126, <https://doi.org/10.1021/bi400209z> (2013).
12. Fichou, Y. *et al.* Cofactors are essential constituents of stable and seeding-active tau fibrils. *Proc. Natl. Acad. Sci. USA* **115**, 13234–13239, <https://doi.org/10.1073/pnas.1810058115> (2018).
13. Pathak, B. K., Mondal, S., Banerjee, S., Ghosh, A. N. & Barat, C. Sequestration of Ribosome during Protein Aggregate Formation: Contribution of ribosomal. *RNA. Sci. Rep.* **7**, 42017, <https://doi.org/10.1038/srep42017> (2017).
14. Castro, T. G., Munteanu, F. D. & Cavaco-Paulo, A. Electrostatics of Tau Protein by Molecular Dynamics. *Biomolecules* **9**, 116, <https://doi.org/10.3390/biom9030116> (2019).
15. Chu, W. T., Clarke, J., Shammass, S. L. & Wang, J. Role of non-native electrostatic interactions in the coupled folding and binding of PUMA with Mcl-1. *PLoS Comput. Biol.* **13**, e1005468, <https://doi.org/10.1371/journal.pcbi.1005468> (2017).
16. Kolarova, M., Garcia-Sierra, F., Bartos, A., Riczny, J. & Ripova, D. Structure and pathology of tau protein in Alzheimer disease. *International Journal of Alzheimer's Disease.*, <https://doi.org/10.1155/2012/731526> (2012).
17. Yang, J. *et al.* The I-TASSER suite: Protein structure and function prediction. *Nature Methods* **12**, 7, <https://doi.org/10.1038/nmeth.3213> (2014).
18. Roy, A., Kucukural, A. & Zhang, Y. I-TASSER: A unified platform for automated protein structure and function prediction. *Nat. Protoc.* **5**, 725, <https://doi.org/10.1038/nprot.2010.5> (2010).
19. Zhang, Y. I-TASSER server for protein 3D structure prediction. *BMC Bioinformatics* **9**, 40, <https://doi.org/10.1186/1471-2105-9-40> (2008).
20. Baker, N. A., Sept, D., Joseph, S., Holst, M. J. & McCammon, J. A. Electrostatics of nanosystems: Application to microtubules and the ribosome. *Proc. Natl. Acad. Sci. USA* **98**, 10037–10041, <https://doi.org/10.1073/pnas.181342398> (2001).
21. Schavemaker, P. E., Śmigiel, W. M. & Poolman, B. Ribosome surface properties may impose limits on the nature of the cytoplasmic proteome. *Elife* **6**, e30084, <https://doi.org/10.7554/eLife.30084> (2017).
22. Ramachandran, G. & Udgaonkar, J. B. Understanding the kinetic roles of the inducer heparin and of rod-like protofibrils during amyloid fibril formation by tau protein. *J. Biol. Chem.* **286**, 38948–38959, <https://doi.org/10.1074/jbc.M111.271874> (2011).
23. Dinkel, P. D., Holden, M. R., Matin, N. & Margittai, M. RNA Binds to Tau Fibrils and Sustains Template-Assisted Growth. *Biochemistry* **54**, 4731–4740, <https://doi.org/10.1021/acs.biochem.5b00453> (2015).
24. Wang, X. S. *et al.* The Proline-Rich Domain and the Microtubule Binding Domain of Protein Tau Acting as RNA Binding Domains. *Protein Pept. Lett.* **13**, 679–685, <https://doi.org/10.2174/092986606777790566> (2006).
25. Kampers, T., Friedhoff, P., Biernat, J., Mandelkow, E. M. & Mandelkow, E. RNA stimulates aggregation of microtubule-associated protein tau into Alzheimer-like paired helical filaments. *FEBS Lett.* **399**, 344–349, [https://doi.org/10.1016/S0014-5793\(96\)01386-5](https://doi.org/10.1016/S0014-5793(96)01386-5) (1996).
26. Koren, S. A. *et al.* Tau drives translational selectivity by interacting with ribosomal proteins. *Acta Neuropathol.* **137**, 571–583, <https://doi.org/10.1007/s00401-019-01970-9> (2019).
27. Tenreiro, S. & Outeiro, T. F. Simple is good: Yeast models of neurodegeneration. *FEMS Yeast Research* **10**, 970–979, <https://doi.org/10.1111/j.1567-1364.2010.00649.x> (2010).
28. Kovachev, P. S. *et al.* RNA modulates aggregation of the recombinant mammalian prion protein by direct interaction. *Scientific reports* **9**, 1–12, <https://doi.org/10.1038/s41598-019-48883-x> (2019).
29. Silva, J. L. & Cordeiro, Y. The 'Jekyll and Hyde' actions of nucleic acids on the prion-like aggregation of proteins. *Journal of Biological Chemistry* **291**, 15482–15490, <https://doi.org/10.1074/jbc.R116.733428> (2016).
30. Ginsberg, S. D. *et al.* RNA sequestration to pathological lesions of neurodegenerative diseases. *Acta Neuropathol.* **96**, 487–494, <https://doi.org/10.1007/s004010050923> (1998).
31. Kovachev, P. S. *et al.* Distinct modulatory role of RNA in the aggregation of the tumor suppressor protein p53 core domain. *J. Biol. Chem.* **292**, 9345–9357, <https://doi.org/10.1074/jbc.M116.762096> (2017).
32. Waldron, C. & Lacroute, F. Effect of growth rate on the amounts of ribosomal and transfer ribonucleic acids in yeast. *J. Bacteriol.* **122**, 855–865 (1975).
33. Wruck, F., Katranidis, A., Nierhaus, K. H., Büldt, G. & Hegner, M. Translation and folding of single proteins in real time. *Proc. Natl. Acad. Sci. USA* **114**, E4399–E4407, <https://doi.org/10.1073/pnas.1617873114> (2017).
34. Waudby, C. A., Dobson, C. M., & Christodoulou, J. Nature and Regulation of Protein Folding on the Ribosome. *Trends in biochemical sciences*, <https://doi.org/10.1016/j.tibs.2019.06.008> (2019).
35. Ganguly, D. *et al.* Electrostatically accelerated coupled binding and folding of intrinsically disordered proteins. *J. Mol. Biol.* **422**, 674–684, <https://doi.org/10.1016/j.jmb.2012.06.019> (2012).
36. Kim, J. Y., Meng, F., Yoo, J. & Chung, H. S. Diffusion-limited association of disordered protein by non-native electrostatic interactions. *Nat. Commun.* **9**, 1–10, <https://doi.org/10.1038/s41467-018-06866-y> (2018).
37. Jones, E. M. *et al.* Interaction of Tau protein with model lipid membranes induces tau structural compaction and membrane disruption. *Biochemistry* **51**, 2539–2550, <https://doi.org/10.1021/bi201857v> (2012).
38. Elbaum-Garfinkle, S., Ramlall, T. & Rhoades, E. The role of the lipid bilayer in tau aggregation. *Biophys. J.* **98**, 2722–2730, <https://doi.org/10.1016/j.bpj.2010.03.013> (2010).
39. Peng, Z. *et al.* A creature with a hundred waggly tails: Intrinsically disordered proteins in the ribosome. *Cell. Mol. Life Sci.* **71**, 1477–1504, <https://doi.org/10.1007/s00018-013-1446-6> (2014).
40. Samant, R. S., Masto, V. B. & Frydman, J. Dosage compensation plans: protein aggregation provides additional insurance against aneuploidy. *Genes & Development* **33**, 1027–1030, <https://doi.org/10.1101/gad.329383.119> (2019).
41. Sacramento, E. K. *et al.* Reduced proteasome activity in the aging brain results in ribosome stoichiometry loss and aggregation. *BioRxiv* 577478, <https://doi.org/10.1101/577478> (2019).
42. Das, D. *et al.* Role of the ribosome in protein folding. *Biotechnology journal* **3**, 999–1009, <https://doi.org/10.1002/biot.200800098> (2008).
43. Götz, J., Xia, D., Leinenga, G., Chew, Y. L. & Nicholas, H. R. What renders TAU toxic. *Frontiers in Neurology* **4**, 72, <https://doi.org/10.3389/fneur.2013.00072> (2013).
44. Medina, M., Hernández, F. & Avila, J. New features about tau function and dysfunction. *Biomolecules* **6**, 21, <https://doi.org/10.3390/biom6020021> (2016).
45. Khatoun, S., Grundke-Iqbal, I. & Iqbal, K. Brain Levels of Microtubule-Associated Protein τ Are Elevated in Alzheimer's Disease: A Radioimmuno-Slot-Blot Assay for Nanograms of the Protein. *J. Neurochem.* **59**, 750–753, <https://doi.org/10.1111/j.1471-4159.1992.tb09432.x> (1992).

46. Martin, L., Latypova, X. & Terro, F. Post-translational modifications of tau protein: Implications for Alzheimer's disease. *Neurochemistry International* **58**, 458–471, <https://doi.org/10.1016/j.neuint.2010.12.023> (2011).
47. Gonskikh, Y. & Polacek, N. Alterations of the translation apparatus during aging and stress response. *Mechanisms of Ageing and Development* **168**, 30–36, <https://doi.org/10.1016/j.mad.2017.04.003> (2017).
48. Jinwal, U. K. *et al.* Hsc70 rapidly engages tau after microtubule destabilization. *J. Biol. Chem.* **285**, 16798–16805, <https://doi.org/10.1074/jbc.M110.113753> (2010).
49. Chakraborty, B., Bhakta, S. & Sengupta, J. Disassembly of yeast 80S ribosomes into subunits is a concerted action of ribosome-assisted folding of denatured protein. *Biochem. Biophys. Res. Commun.* **469**, 923–929, <https://doi.org/10.1016/j.bbrc.2015.12.107> (2016).
50. Piir, K., Tamm, T., Kisly, I., Tammsalu, T. & Remme, J. Stepwise splitting of ribosomal proteins from yeast ribosomes by LiCl. *PLoS One* **9** <https://doi.org/10.1371/journal.pone.0101561> (2014).
51. Barghorn, S., Biernat, J. & Mandelkow, E. Purification of recombinant tau protein and preparation of alzheimer-paired helical filaments *in vitro*. *Methods in Molecular Biology* **299**, 35–51, <https://doi.org/10.1385/1-59259-874-9-035> (2005).
52. KrishnaKumar, V. G. & Gupta, S. Simplified method to obtain enhanced expression of tau protein from *E. coli* and one-step purification by direct boiling. *Prep. Biochem. Biotechnol.* **47**, 530–538, <https://doi.org/10.1080/10826068.2016.1275012> (2017).
53. Flach, K. *et al.* Tau oligomers impair artificial membrane integrity and cellular viability. *J. Biol. Chem.* **287**, 43223–43233, <https://doi.org/10.1074/jbc.M112.396176> (2012).

Acknowledgements

We are sincerely grateful to Dr. Jayati Sengupta (CSIR-Indian Institute of Chemical Biology) and Dr. Sagarmoy Ghosh, University of Calcutta (Department of Microbiology) for extending their laboratory facilities to us. The contribution of Mr. Sayan Bhakta, CSIR-IICB in obtaining images from Pymol is acknowledged. This work has been supported entirely by the grant received from the Department of Science & Technology, Government of India (Science & Engineering Research Board) [EMR/2017/001101] and the contribution is being sincerely acknowledged. The fellowships of Ms. Senjuti Banerjee and Ms. Sehnaz Ferdosh have been provided by the Council of Scientific & Industrial Research, Government of India [08/548(0004)2015-EMR-I] and Department of Biotechnology, Government of West Bengal, [953(Sanc)/BT(Estt)/RD-51/2015] respectively.

Author contributions

Conceptualization: C.B. Methodology: C.B., S.B. and S.F. Investigation: S.B., S.F. and C.B. Analyzed the data: S.B., S.F. and C.B. Writing-Original Draft: C.B. Prepared figures: S.B. and S.F. Contributed reagents/materials/analysis tools: C.B. and A.N.G. Supervision: C.B.

Competing interests

The authors declare no competing interests.

Additional information

Supplementary information is available for this paper at <https://doi.org/10.1038/s41598-020-61777-7>.

Correspondence and requests for materials should be addressed to C.B.

Reprints and permissions information is available at www.nature.com/reprints.

Publisher's note Springer Nature remains neutral with regard to jurisdictional claims in published maps and institutional affiliations.



Open Access This article is licensed under a Creative Commons Attribution 4.0 International License, which permits use, sharing, adaptation, distribution and reproduction in any medium or format, as long as you give appropriate credit to the original author(s) and the source, provide a link to the Creative Commons license, and indicate if changes were made. The images or other third party material in this article are included in the article's Creative Commons license, unless indicated otherwise in a credit line to the material. If material is not included in the article's Creative Commons license and your intended use is not permitted by statutory regulation or exceeds the permitted use, you will need to obtain permission directly from the copyright holder. To view a copy of this license, visit <http://creativecommons.org/licenses/by/4.0/>.

© The Author(s) 2020